



INTERNATIONAL ENERGY AGENCY

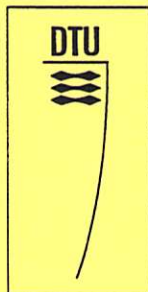
**Implementing Agreement for Co-operation in the
Research and Development of Wind Turbine Systems
ANNEX XI**

28th Meeting of Experts

State of the Art of Aerolastic Codes for Wind Turbine Calculations

Lyngby, April 11-12, 1996

Organized by : The Technical University of Denmark



Scientific Coordination :

B. Maribo Pedersen
Dept. of Fluid Mechanics
Technical University of Denmark



INTERNATIONAL ENERGY AGENCY

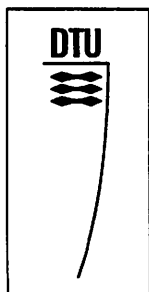
**Implementing Agreement for Co-operation in the
Research and Development of Wind Turbine Systems
ANNEX XI**

28th Meeting of Experts

State of the Art of Aerolastic Codes for Wind Turbine Calculations

Lyngby, April 11-12, 1996

Organized by : The Technical University of Denmark



Scientific Coordination :

**B. Maribo Pedersen
Dept. of Fluid Mechanics
Technical University of Denmark**

I

CONTENTS

	page
B.MARIBO PEDERSEN Introductory Note	1
D.C.QUARTON Calculation of Wind Turbine Aeroelastic Behaviour The Garrad Hassan Approach	3
C. LINDENBURG Results of the PHATAS-III Development	13
ALAN D. WRIGHT Aeroelastic Code Development Activities in the United States	25
L.N.FREEMAN and R.E.WILSON The FAST Code	37
G.GIANNAKIDIS and J.M.R.GRAHAM Prediction of H.A.W.T. Blade Stall and Performance	57
STIG ØYE FLEX 4, Simulation of Wind Turbine Dynamics	71
HANS GANANDER The VIDYN - Story	77
M.B.ANDERSON Numerical Techniques for the Improved Performance of a Finite Element Approach to Wind Turbine Aeroelastics	91
MARKUS REES, ARNE VOLLAND An Aeroelastic Code for Coupled Fixed-Rotating Structures	97
DAVID INFIELD Aeroelastic Modelling without the Need for Excessive Computing Power	105
ALLAN KRETZ Windane-12 Windturbine	115
JØRGEN THIRSTRUP PETERSEN The Aeroelastic Code HawC - Model and Comparisons	129

II

GUNNER LARSEN and POUL SØRENSEN Design Basis 2	137
W. KUIK The Wind Turbine Response Program called FKA_12 of Stentec, the Netherlands	147
B. VISSER The Aeroelastic Code FLEXLAST	161
T. VRONSKY Practical Aspects of a Flexible Wind Turbine Blade Design	167
IAN FLETCHER How Compromised is Design?	169
F. KIESSLING, M. RIPPL On the Aeroelasticity and Dynamics of Wind Turbines	173
DAVID SHARPE Notes from Round-Table Discussion	201
B.MARIBO PEDERSEN Summary of the Meeting	207
LIST OF PARTICIPANTS	209
IEA R&D WIND - ANNEX XI List of Previous Meetings of Experts	213

28th IEA Experts Meeting**STATE OF THE ART OF AEROELASTIC CODES
FOR WIND TURBINE CALCULATIONS**

April 11.-12. 1996, Technical University of Denmark

INTRODUCTORY NOTE

The technological development of modern wind turbines has been dependent on the parallel development of the computational skills of the designers. The combination of the calculation of the flow field around the wind turbine rotor - both far field and near field - and the calculation of the response of the wind turbine structure to the resulting, non-stationary air loads, also known as aero-elastic calculations have now reached a reasonable degree of maturity.

Computer codes to carry out such calculations have been developed in many countries, and it now appears appropriate to try to get an overview of the state of the art.

Since all these calculations have to be based on more or less simplified, physical models of the real world and on mathematical models as basis for the numerical computations, it is obvious that many variants exist to different degrees of sophistication.

At this expert meeting it is the intention to bring together as many as possible of the researchers, who have developed such codes for thorough exposition and discussion of the merits and also the shortcomings of their work.

This means that such issues as how the external and local flow field is modeled, in what way is instationary inflow, turbulence, tower shadow etc. treated, how detailed is the local flow field around the blade modeled, how are instationarities and non-linearities dealt with.

On the structural side, how detailed is the blade, tower, coupling to gear-box and generator etc. modeled. and finally, to what degree have the results been validated by comparison with measurements.

It is hoped that through open and frank discussions of these issues, two main points may be clarified.

- To what level of accuracy can we now determine the behaviour of the different elements of a wind turbine, i.e. how well are we able to compute deflections, fluctuating loads and power output.
- Which are the main outstanding areas upon which our next research efforts should be focused.

11.01.96 bmp

Calculation of Wind Turbine Aeroelastic Behaviour The Garrad Hassan Approach

IEA Experts Meeting: "State of the Art Aeroelastic Codes for Wind Turbine Calculations", 11 - 12 April 1996, Technical University of Denmark

D C Quarton, Garrad Hassan and Partners Ltd, Bristol, UK

Background

The Garrad Hassan approach to the prediction of wind turbine loading and response has been developed over the last decade. The goal of this development has been to produce calculation methods that contain realistic representation of the wind, include sensible aerodynamic and dynamic models of the turbine and can be used to predict fatigue and extreme loads for design purposes.

The Garrad Hassan calculation method [1] is based on a suite of four key computer programs:

- WIND3D for generation of the turbulent wind field
- EIGEN for modal analysis of the rotor and support structure
- BLADED for time domain calculation of the structural loads
- SIGNAL for post-processing of the BLADED predictions

The interaction of these computer programs is illustrated in Figure 1. A description of the main elements of the calculation method will be presented.

Wind Field

Until relatively recently, calculations of the loading and behaviour of wind turbines were based on simplified models of the wind. It was common to assume a representation based solely on a steady wind speed, a constant power or logarithmic law model of wind shear and a constant yaw misalignment. Although such input taken together with representation of the tower shadow effect enables a satisfactory calculation of the periodic loading, it provides no basis for evaluating the random loads due to wind turbulence.

A model of the turbulent wind field suitable for loading calculations requires correct representation of both the temporal and spatial structure of the longitudinal wind speed fluctuations. Calculations based on a turbulence simulation which assumes a fully coherent cross-wind spatial structure will not take into account the crucially important 'eddy slicing' transfer of rotor load from low frequencies to those associated with the rotational speed and its harmonics. This 'eddy slicing', associated with the rotating blades slicing through the turbulent structure of the wind, is a significant source of fatigue loading.

The wind simulation method adopted by Garrad Hassan is based on that described by Veers [2] and encoded in the computer program WIND3D. The rotor plane is covered by a rectangular grid of points, and a separate time history of wind speed is generated for each of these points in such a way that each time history has the correct single-point wind turbulence spectral

characteristics, and each pair of time histories has the correct cross-spectral or coherence characteristics.

The wind speed time histories may, in principle, be generated from any user-specified auto-spectral density and spatial cross-correlation characteristics. The von Karman model, defined in [3], is generally accepted to be the best analytical representation of isotropic turbulence and forms the basis of the simulation provided by WIND3D.

In addition to wind turbulence simulation based solely on the longitudinal component of turbulence, WIND3D also has the capability to generate a wind field based on the three orthogonal components of turbulent wind speed. The three component wind turbulence model is again based on the von Karman representation [3].

The complete wind field is obtained by superposing the simulated wind turbulence on the deterministic spatial variations of wind speed. The Garrad Hassan computer analysis allows the specification of three forms of deterministic spatial variation of wind speed:

- Wind shear
- Tower shadow
- The wake of an upwind turbine

Wind shear may be specified by means of either a power law or a logarithmic law profile.

Tower shadow may be specified by means of a potential flow dipole model (for an upwind turbine) or an empirical tower wake model [6] (for a downwind turbine). The empirical model gives a cosine shaped velocity deficit behind the tower.

For a turbine operating in the wake of another, a Gaussian wake profile can be specified. The wake centreline may be offset laterally to allow for the case of partial wake immersion.

Finally, in addition to the turbulence model described above, two further forms of temporal variations in the wind field may be specified:

- A user-specified time history of wind speed and direction which is coherent over the whole rotor.
- Independent sinusoidal or half-sinusoidal transients in wind speed, wind direction, vertical wind shear and horizontal wind shear as specified in the IEC 1400-1 design standard [6].

In all cases, deterministic wind upflow and yaw misalignment angles may also be specified.

Aerodynamics

The blade aerodynamics are solved in the BLADED code using standard blade element theory [4]. The apparent wind speed vector is determined at each blade element and each point in time by means of a three dimensional interpolation of the incident wind field with appropriate superposition of the blade rotational and structural velocities. The induced axial and tangential flow may be determined using equilibrium, frozen or dynamic wake models. A tip loss model due to Prandtl [5] is provided.

The BLADED code also incorporates a treatment of dynamic stall due to Beddoes [7].

Structural Dynamics

The structural dynamics of the wind turbine are modelled by means of a modal representation. The modal characteristics of the rotor and support structure are determined from finite element analyses of the two components using the code EIGEN. Coupling of the modal dynamics of the rotor and support structure is incorporated in the equations of motion. The analysis takes account of the centrifugal stiffening of the blade structure due to its rotation.

The dynamic response of the wind turbine is calculated by time-marching integration of the modal equations of motion and appropriate superposition of the modal solutions. The aeroelastic behaviour of the rotor is taken into account by consideration of the interaction of the structural dynamics with the aerodynamics along each blade.

Power Train

A selection of models of the drive train and generator are included in BLADED. The equations of motion allow additional degrees of freedom (if required) to model drive-train torsion, flexible mountings, and generator dynamics.

The drive train may be modelled as either stiff or flexible, in which case the torsional stiffness of the low and high speed shafts may be specified. Additionally, a torsionally flexible drive train mounting may be specified as either a flexible gearbox mounting, or as a flexible pallet mounting with the gearbox and generator mounted rigidly to the pallet. In each case the flexibility of the mounting is specified in terms of a torsional spring and damper. A shaft brake may be mounted at either end of the low speed or high speed shaft.

For a fixed speed machine an induction generator model is supplied, which relates electrical torque to slip speed by means of a first order response. For a variable speed turbine, a first order model of the torque response of the generator and frequency converter system is supplied. Generator losses may be modelled as a function of shaft power.

Controller

BLADED incorporates a comprehensive range of controller options, including fixed and variable speed operation, and pitch or stall regulation. The blades may be modelled with full or partial span pitch control, or with control provided by ailerons or spoilers.

A pitch regulated turbine may pitch towards feather or towards stall, and the pitch actuator response is specified by a first order model relating pitch demand to pitch angle, with rate limits. A proportional plus integral (PI) controller regulates the pitch angle, in response to electrical power in the case of a fixed speed turbine, or generator speed in the case of a variable speed turbine.

For a variable speed turbine, the generator torque is controlled below rated such that the turbine will maintain a chosen tip speed ratio as long as it remains within the allowed speed limits. When the speed limit is reached, PI control of torque is used to maintain the desired speed.

The gain of all PI controllers may be scheduled as a function of one of several variables, and all controllers have integral wind-up prevention.

Time constants may be specified for the power or speed transducers.

Parameters may also be specified to define the supervisory control associated with start-up and normal and emergency stop sequences for the turbine. These sequences all assume constant pitch rates. For the emergency stop, pitching and brake application may occur immediately (as in a grid loss situation) or at defined rotor overspeeds.

Post-Processing

Post-processing of the output from the aeroelastic code BLADED is provided by the program SIGNAL. The following analyses can be carried out:

- Basic statistics of output signals (minimum, maximum, mean, standard deviation)
- Fourier harmonics
- Extraction of periodic and random components
- Auto-spectral and cross-spectral analysis
- Probability distribution analysis
- Peak value and level crossing analysis
- Channel combination
- Rainflow cycle counting
- Fatigue damage analysis
- Extreme value analysis
- Annual energy capture

Validation

Garrad Hassan have undertaken extensive validation of the computer programs described above in order to provide confidence in the accuracy of the calculations. The computer programs have been validated against measurements on a number of different wind turbines covering a wide range of sizes and configurations:

- WEG MS-1, Orkney, UK, 1991
- Howden HWP300 and HWP330, USA, 1993
- ECN 25m HAT, Netherlands, 1993
- Newinco 500 kW, Netherlands, 1993
- Nordex 26m, Denmark, 1993
- Nibe A, Denmark, 1993
- Holec WPS-30, Holland, 1993
- Nordtank 300 kW, Denmark, 1993
- Riva Calzoni M30, Italy, 1993
- Tjaerborg 2 MW, Denmark, 1994
- WindMaster 750kW, Holland, 1994
- Zond Z-40, USA, 1994
- Nordtank 500kW, Wales, 1995
- Vestas V27, Greece, 1995
- Danwin 200 kW, Sweden, 1995
- Carter 300 kW, UK, 1995
- NedWind 1 MW, Holland, 1995

BLADED for Windows

Over the last three years Garrad Hassan have been developing the Wind Turbine Design Tool under Joule contract to the CEC. The Design Tool, known as BLADED for Windows, is based on the validated computer programs referred to above but with an extremely user-friendly, Windows based user interface. The user interface is designed to allow the user to enter the relevant data to describe the turbine and the required calculations in a rapid and straightforward way, with graphical aids available on the screen where appropriate to ensure clarity. Example data entry screens are given in Figures 2, 3, 4 and 5.

References

1. Quarton D C, Wastling M A, Garrad A D and Hassan U, "The calculation of wind turbine loads - a frequency or time domain problem?", Proceedings of British Wind Energy Conference, Nottingham, 1992.
2. Veers P S, "Three dimensional wind simulation", SAND88 - 0152, Sandia National Laboratories, March 1988.
3. Engineering Sciences Data Unit, "Characteristics of atmospheric turbulence near the ground. Part II: Single point data for strong winds", ESDU 74031, 1974.
4. Wilson R E and Lissaman P B, "Aerodynamic performance of wind turbines", Oregon State University, June 1976.
5. Prandtl L and Tietjens O G, "Applied Hydro- and Aeromechanics", Dover Publications Inc., 1957.
6. IEC 1400-1, Wind turbine generator systems - Part1: Safety requirements, First edition, 1994-12.
7. Leishman J G and Beddoes T S, "A semi-empirical model for dynamic stall", Journal of the American Helicopter Society, July 1989.

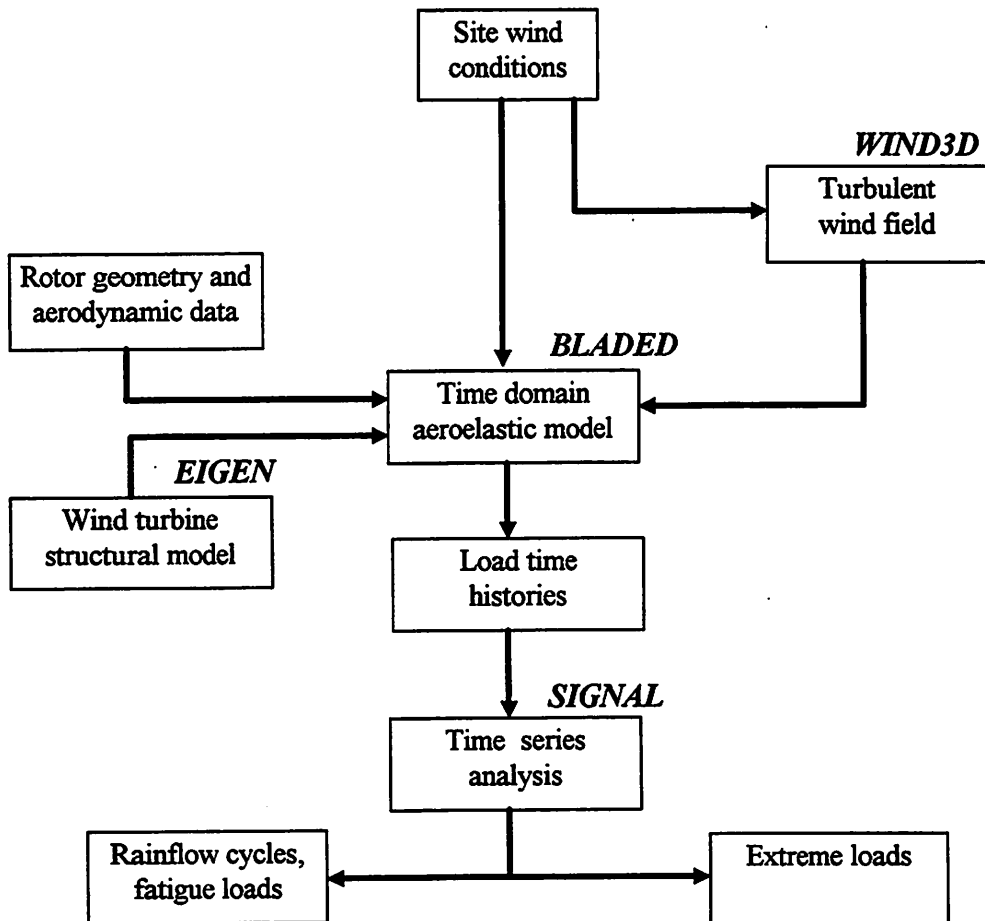


Figure 1 Garrad Hassan Analysis of Wind Turbine Loads

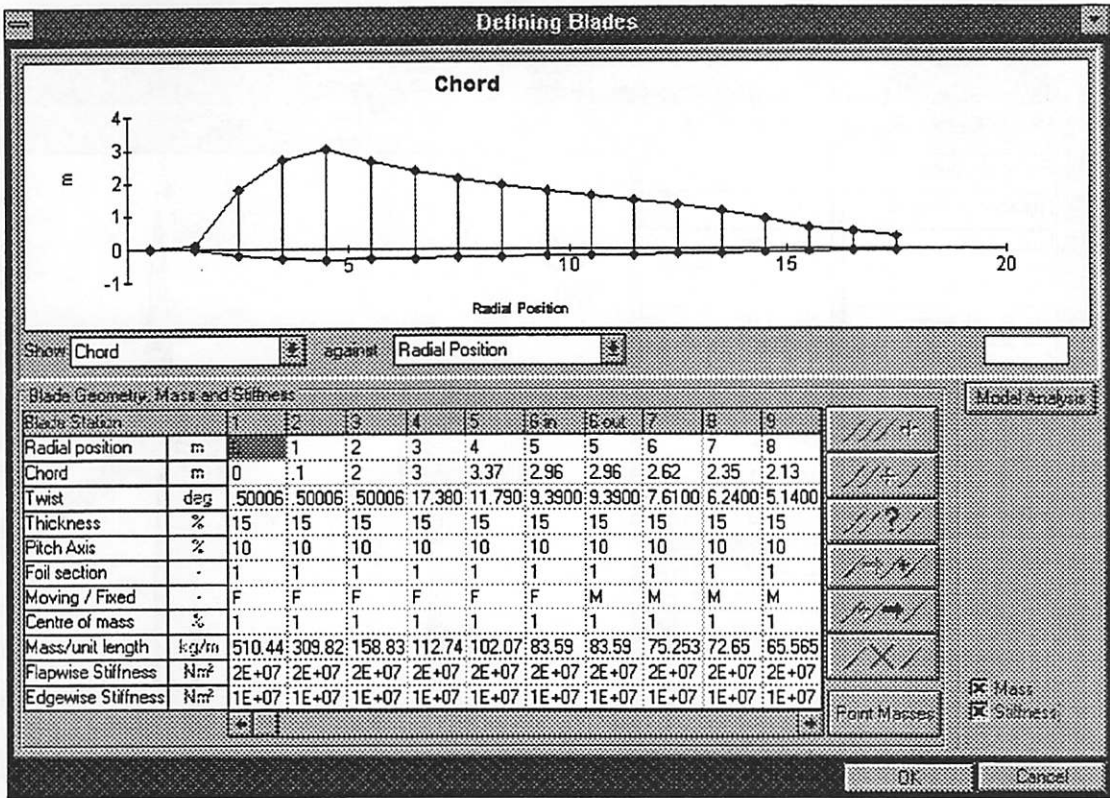


Figure 2 Blade Data Entry Screen

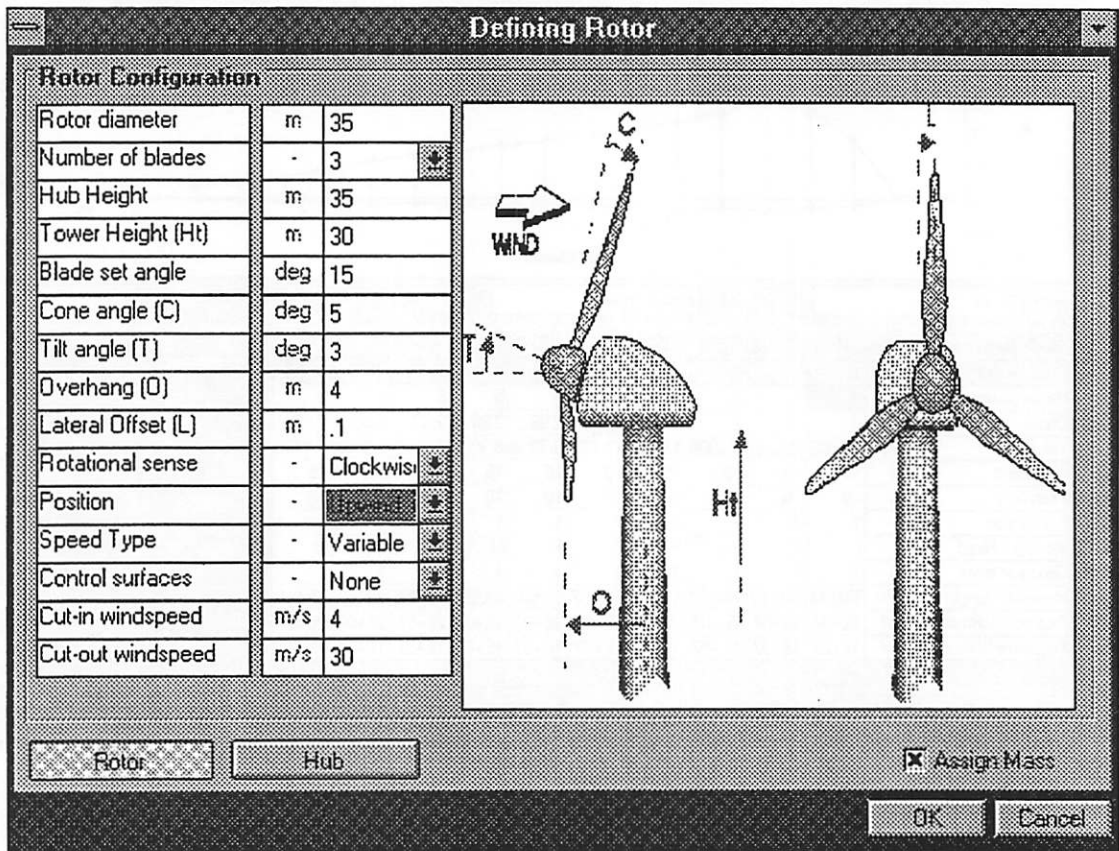


Figure 3 Rotor Data Entry Screen

Define Power Train

Transmission **Mounting** Generator Losses

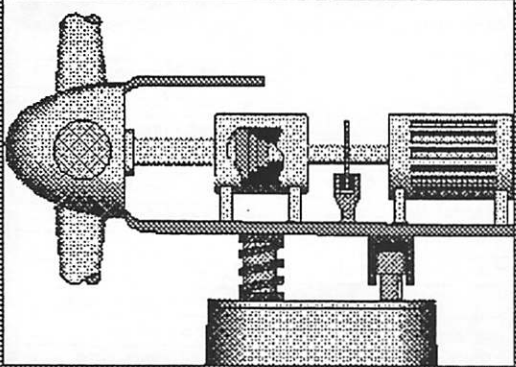
Rigid
No additional data required

Flexible drive train/pallet - rotational spring / damper

Pallet mount stiffness	Nm/rad	0
Pallet mount damping	Nm/rad	0
Moment of inertia of pallet + components	kgm ²	0

Flexible gearbox mount - rotational spring / damper

Gearbox mount stiffness	Nm/rad	10000
Gearbox mount damping	Nm/rad	10000
Moment of inertia of gearbox	kgm ²	1E+07



OK Cancel

Figure 4 Power Train Mounting Data Entry Screen

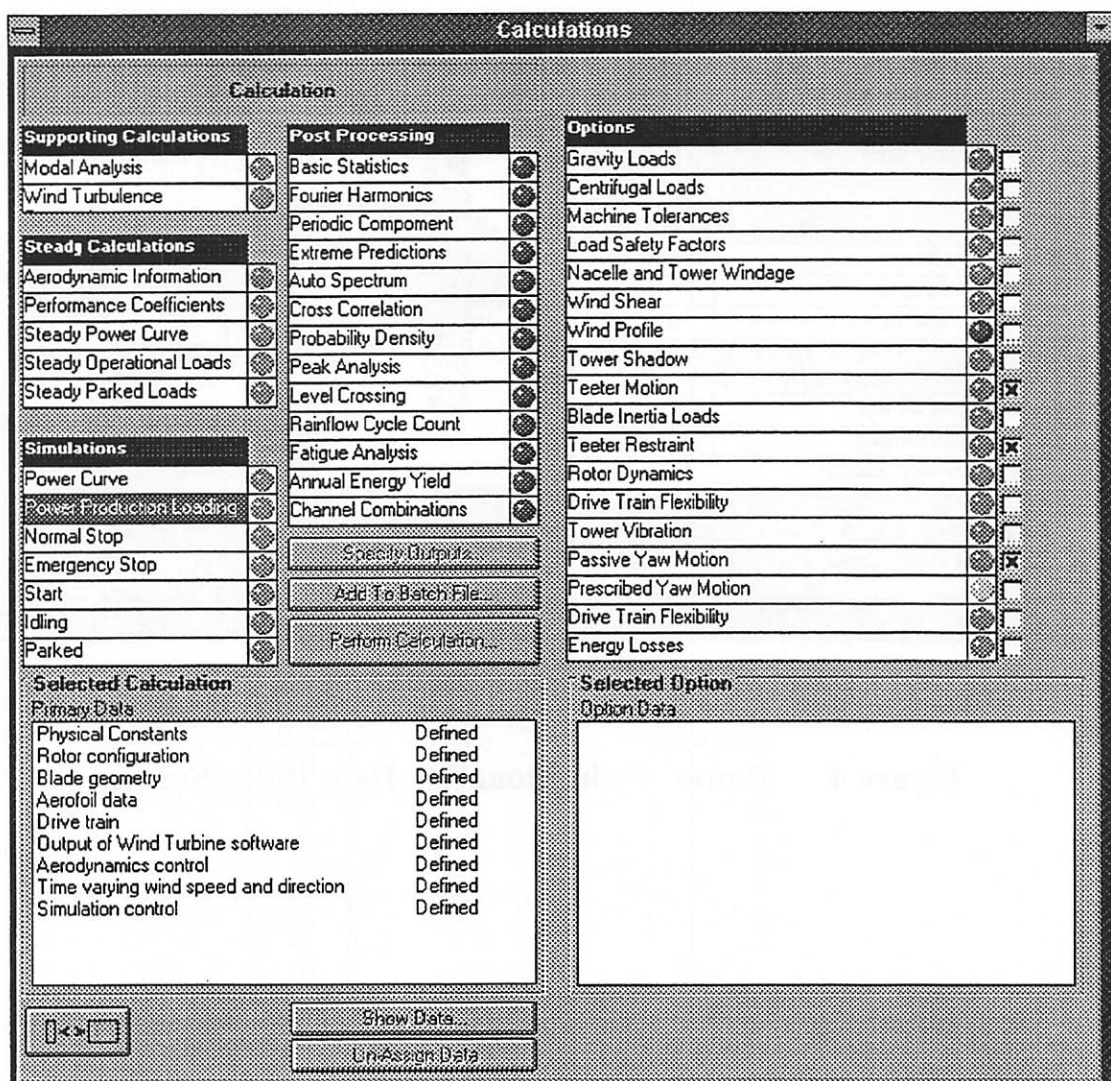


Figure 5 Calculations Menu

Results of the PHATAS-III development

C. Lindenburg

Netherlands Energy Research Foundation ECN
Unit Renewable Energy
p.o. box 1,
1755 ZG Petten

Introduction

The computer program PHATAS-III –Program for Horizontal Axis wind Turbine Analysis and Simulation version III– is developed for the calculation of the non-linear dynamic behaviour and the corresponding loads in the main components of a horizontal axis wind turbine in time domain. The basis of PHATAS-III is the PHATAS-II code. Both these codes are developed at ECN unit Renewable Energy while the development of PHATAS-III is mainly funded by NOVEM B.V.

Thanks to the application of PHATAS in national and international benchmark exercises and in research projects the program has developed to an accurate and flexible tool for dynamic load prediction. The reliability of PHATAS as design and analysis tool for wind turbines is assured by an intensive verification and documentation for each release. For PHATAS-III this documentation is updated with a status document [1], a user's manual [2] and a model description [3].

Structural dynamic modelling

The solution model in PHATAS is characterised by a large number of optional structural dynamic degrees of freedom of which all mutual interactions and the interactions with the aerodynamic loads are described. An example of a turbine as modelled in PHATAS is given in figure 1 showing the FLEX-TEETER turbine. The structural dynamic degrees of freedom include:

Continuous flatwise blade bending This description includes the radial displacements due to geometric non-linear effects of strong deformation such that Coriolis loads and the resulting shaft torque variations are described.

Continuous edgewise blade bending implemented in a similar way as flapwise deformation.

Passive or controlled pitch for full span or partial span.

Blade flapping hinges with a spanwise location, viscous damping, hinge stiffness and bumper stiffness.

Teetered hub with δ_3 orientation, eccentricity along the rotor shaft -'underslung'- stiffness and damping. It has been shown that using a high stiffness this degree of freedom can be used to model shaft bending.

Generator characteristics ; synchronous, asynchronous or user-defined. The models for synchronous and asynchronous characteristics include one elementary terms for dynamic behaviour.

Drive train with shaft torsional flexibility and torsional flexibility and damping in the gearbox support. The layout of the drive train model in PHATAS-III is shown in figure 2.

Tower torsion as single degree of freedom. Using zero torsional stiffness and the appropriate viscous damping and friction the free yawing behaviour can be modelled.

Tower bending with one degree of freedom in the two perpendicular directions. Here the fore-aft bending is modelled as translation of the nacelle. The sideways bending includes rotation 'naying' of the nacelle such that interactions with tower bending and drive train dynamics is fully described.

Control Algorithms for pitch control, yaw actions and/or transient states of operation can be added to the code by writing them in reserved (FORTRAN-) subroutines.

Part of the PHATAS output is a table with system frequencies as function of the rotor speed. With this table a Campbell diagram can be plotted, see figure 3.

Aerodynamic modelling

The solution of the rotor aerodynamics of PHATAS-II is based on the Blade Element Momentum theory and the assumption of a stationary (equilibrium) wake. The flow around the blade tips is described using the tip loss factor of Prandtl.

The relative airflow –with which the aerodynamic loads are calculated– is evaluated for the position of the deformed blade and includes the motions due to the rate of change of all deformations and degrees of freedom. This means that aerodynamic damping is implicitly included in the structural dynamic behaviour. Also the local direction vector of the deformed blade is included in the calculation of the relative wind velocity vector.

Additional specifications of the aerodynamic model of PHATAS-III compared with that of PHATAS-II are:

3D correction on airfoil data for the spanwise pressure gradient and the centrifugal loads on the boundary layer. This correction follows the rule of Snel, Houwink and Bosschers [4]. For a good implementation of dynamic stall a correction based on the delay of the physical stall behaviour is desirable.

Figure 4 shows the coefficients of an airfoil with and without the two means of 3D correction for a local chord/span ratio of 0.342.

Dynamic wake model Within the European project "Joint Investigation of Dynamic Inflow Effects and Implementation of an Engineering Method" a model is developed for the instationary effects of the wake and for oblique inflow, known as the "ECN differential equation model", see [5] appendix L. This model has been implemented in PHATAS-III and tested for the cases from the European project and for consistency with regard to turbine dimension and time step size.

The instationary wake effects are modelled by including the time derivative of the induced velocity in the momentum equation. The results for verification of instationary wake effects are shown in figure 5.

The effects of oblique inflow are described by a difference of the induced velocity on the upwind side and on the downwind side of the rotor plane, in terms of a sinusoidal function of the rotor azimuth.

In PHATAS one of the following wind loadings can be applied:

- Using models for shear, gust, wind direction and turbulence.
- Reading wind data from an ASCII file (e.g. from measurements).
- Reading wind data from a file with a (3D-) stochastic wind field as generated with SWIFT [6].

The reading of the SWIFT wind loading on the rotor and the application of the dynamic inflow model are implemented with respect to the plane in which the rotor blade rotate. This means that the tilted and the teetered position of the rotor is taken into account.

Verification

Using the program PHATAS-II ECN has participated in a number of joint European and National research projects in which the dynamic loads calculated with PHATAS have been compared with loads from other codes and with measured loads. Among these projects are:

WTBE-ML 'Wind Turbine Benchmark Exercise on Mechanical Loads' [7].

KRH 'Kwalificatie Rekenprogrammas Horizontale as turbines' [8] (Dutch).

REFSTRESS European 'Reference Procedure to Establish Fatigue Stresses for large size Wind Turbines' [9].

Dynamic Loads in Wind Farms I & II [10]

With regard to teetered rotor configurations some joint investigations are carried out within the FLEXHAT project. Here the dynamic loads calculated with FLEXLAST (SPE) and PHATAS are compared mutually and with measured loads. These investigations dealt with passive pitch regulated- and with stall operation.

Current developments

Computational Steering A graphic interface for PHATAS-III has been built recently by which the external conditions (wind) and the properties of the turbine (stiffnesses, damping values up to tower height) can be adjusted while the dynamic behaviour is being calculated. An plot of this graphical interface is shown in figure 6 showing wind loading and the deformed rotor geometry in different views. The scale for displaying the deformations is also variable.

Dynamic Stall models In cooperation with NLR the ONERA model has been implemented in a "garage" version of PHATAS-II.

Within the TIDIS project a model is developed for the dynamic airfoil behaviour in 3D stall. This model is about to be finished in the spring of 1996.

Modular tower model The current model for tower deformation has only one degree of freedom for bending in each of the two perpendicular

directions. For towers that are relatively flexible –either by design or due to the fact that they are large and material efficient– the second bending frequency is of the order of the rotor frequencies. Because there is limited interaction between the tower dynamics and the rotor dynamics it is possible to develop a model for tower dynamics with a well defined interface to the aeroelastic rotor code at the location of the yaw bearing. This makes it possible to generate a model for dynamics of the tower with tools similar to those used for finite element code based packages.

Actual shortcomings

Dynamics for complex towers The modelling of the dynamics of large towers or platforms, see figure 7, becomes possible when the modular model for tower bending is generated.

Detailed rotor aerodynamics In 1995 a proposal is sent to the European Community for the development of a vortex description of the free wake that should deal with instationary effects, interaction between blade element aerodynamics, oblique inflow, tip loss and so forth. Many researchers supported this development without success.

Dynamic stall Several models for dynamic stall are available in garage versions that will soon be suitable for engineering environment. These models are more or less empirical.

Besides it appears to be difficult to obtain representative airfoil coefficients (including 3D effects) for large angles of attack.

Blade torsion In the past the equations for blade torsion have been derived and added in an early PHATAS-II version. Because this blade torsion was never validated and because blade torsion is seldom required the terms for blade torsion were commented inactive in the code.

Reasons for recovering the model for blade torsional dynamics are:

- Manufacturers want to know the loss of energy due to elastic blade deformation.
- With the availability of dynamic stall models and with the more detailed models for wind loading and dynamic stall it is useful to consider all dynamics that interact with instationary aerodynamic loads.

System requirements

SUN version

The program PHATAS-III is developed on a SUN SPARC workstation under SUN-OS 4.1.1. (the upgrades SUN-OS 4.1.x are compatible) and is compiled with the SUN FORTRAN 1.4 compiler.

The system requirements for the SUN version are:

- A SUN SPARC IPC workstation;
- At least 4Mb of RAM memory (12Mb to 16Mb is recommended);
- When a specific control routine is to be linked to PHATAS-III , the SUN FORTRAN 1.4 compiler (or later) must be available.
- The binary datafiles, generated as output of PHATAS use about 300 bytes of disk space for each time step of which the solution is written. To store these files and other files with time series for the design or analysis of wind turbines a free hard disk capacity of 300Mb or more is recommended.

DOS version

The program PHATAS-III release "MAR-1995" is also available for a PC compiled with the MS FORTRAN PowerStation compiler.

The system requirements for the DOS version are:

- A computer with a 386 + 387, a 486DX or a Pentium processor;
- At least 4Mb of RAM memory (7Mb or more is recommended);
- The operating system DOS 3.3 or later;
- When a specific control routine is to be linked to PHATAS, the MS FORTRAN PowerStation compiler must be available which needs DOS 5.0 and MS Windows 3.1 (or later versions);
- A hard disk with at least 300Mb free space is recommended (as for the SUN version).

REFERENCES

- [1] Lindenburg, C. and Schepers, J.G. ;
STATUS OF PHATAS-III RELEASE "MAR-1995", SUN and DOS version. ECN-R--95-015, Petten, April 1996.
- [2] Lindenburg, C. ;
PHATAS-III USER'S MANUAL, Program for Horizontal Axis wind Turbine Analysis and Simulation version III.
ECN-C--95-040, Petten, April 1996.
- [3] Lindenburg, C. and Schepers, J.G.;
PHATAS-III AEROELASTIC MODELLING, Program for Horizontal Axis wind Turbine Analysis and Simulation version III.
ECN-C--96-025, Petten, May 1996.
- [4] Snel, H., Houwink, R. and Bosschers J. ;
SECTIONAL PREDICTION OF LIFT COEFFICIENTS ON ROTATING WIND TURBINE BLADES IN STALL.
ECN-C--93-052, Petten, December 1994.
- [5] Snel, H. and Schepers, J.G. ;
JOINT INVESTIGATION OF DYNAMIC INFLOW EFFECTS AND IMPLEMENTATION OF AN ENGINEERING METHOD'.
ECN-C--94-107, Petten, April 1995.
- [6] Winkelaar, D. ;
SWIFT, PROGRAM FOR THREE DIMENSIONAL WIND SIMULATION, Part 1: Model description and program verification.
ECN-R--92-013, Petten, December 1992.
- [7] Grol, H.J. van, Snel, H. and Schepers, J.G. ;
WIND TURBINE BENCHMARK EXERCISE ON MECHANICAL LOADS, A State of the Art Report, Volume I, part A and B.
ECN-C--91-030 and ECN-C--91-031, Petten, May 1991.
- [8] Schepers, J.G., and Snel, H.;
KWALIFICATIE HORIZONTALE AS TURBINES (KRH).
ECN-89-96, Petten, June 1989.
- [9] Grol, H.J. van and Bulder, B.H. ;
REFERENCE PROCEURE TO ESTABLISH FATIGUE STRESSES FOR LARGE SIZE WIND TURBINES, A State of the Art Report.
ECN-C--94-013 and ECN-C--94-014, Petten, February 1994.
- [10] Tindall, A.J. et al ;
DYNAMIC LOADS IN WIND FARMS. Final report of Joule project JOUR 0084-c, 1993.

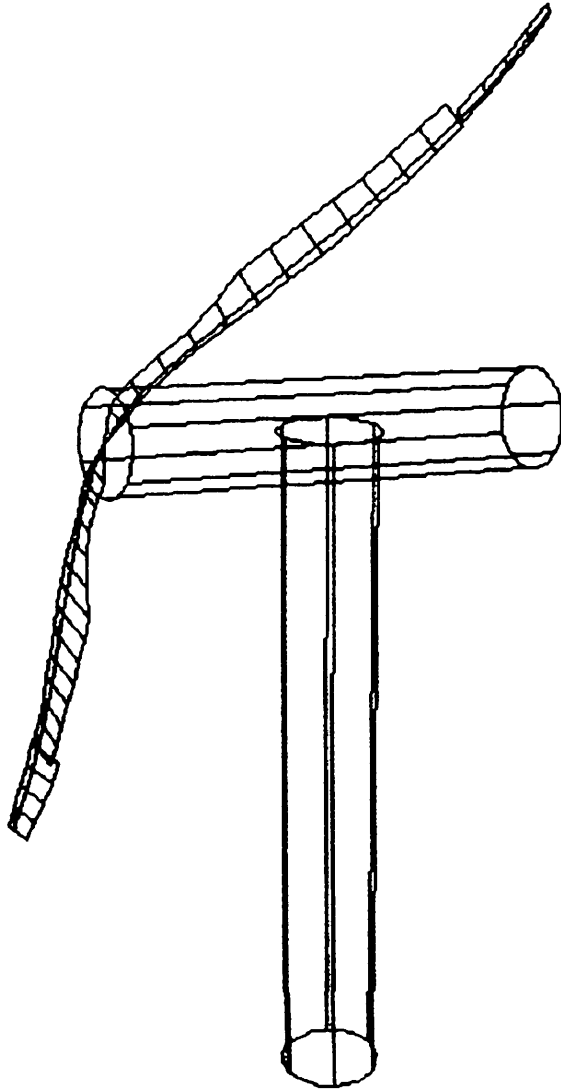


Figure 1. Deformed FLEXTEETER rotor geometry as modelled in PHATAS

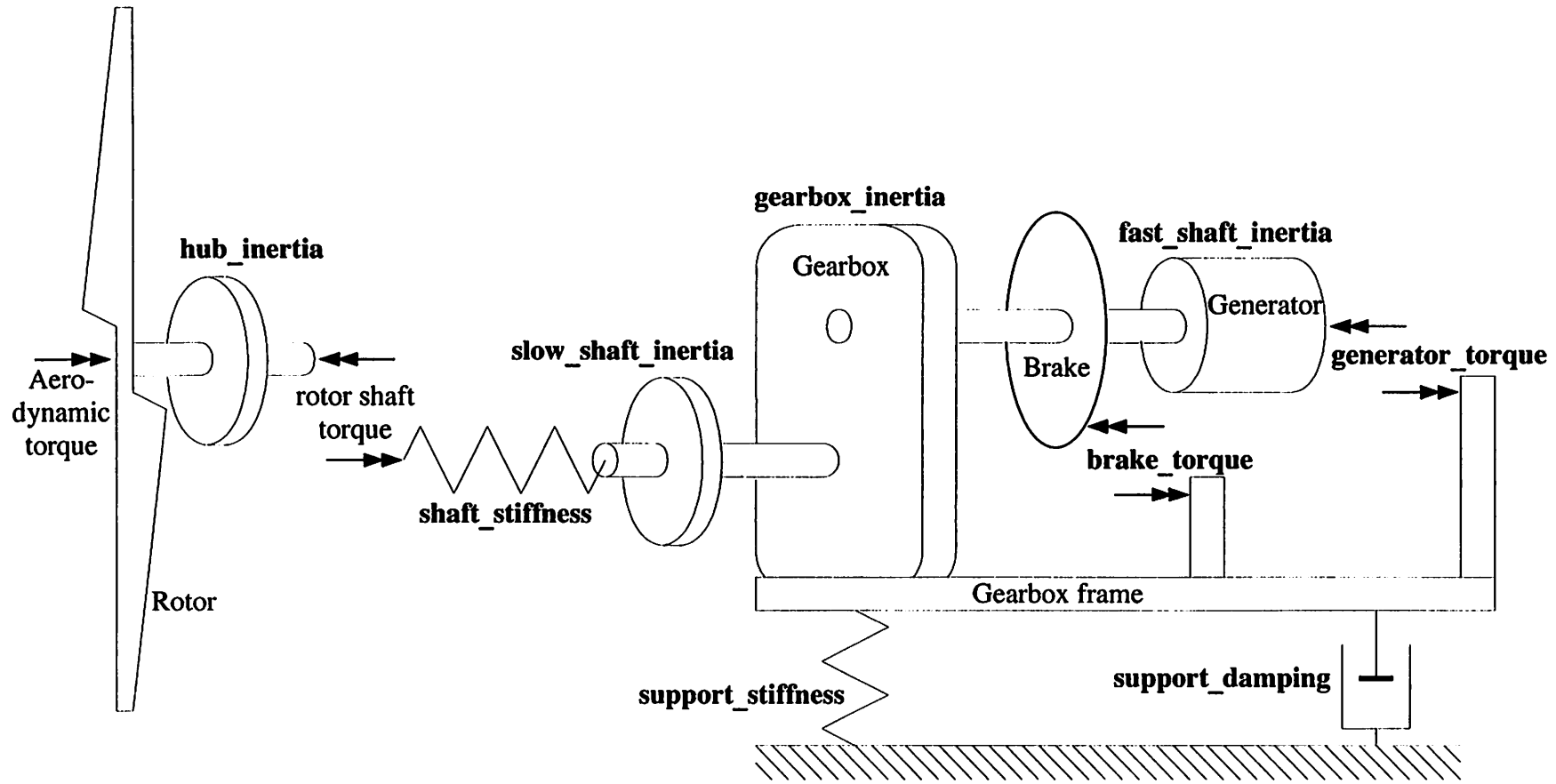


Figure 2. Drive train layout as modelled in PHATAS-III.

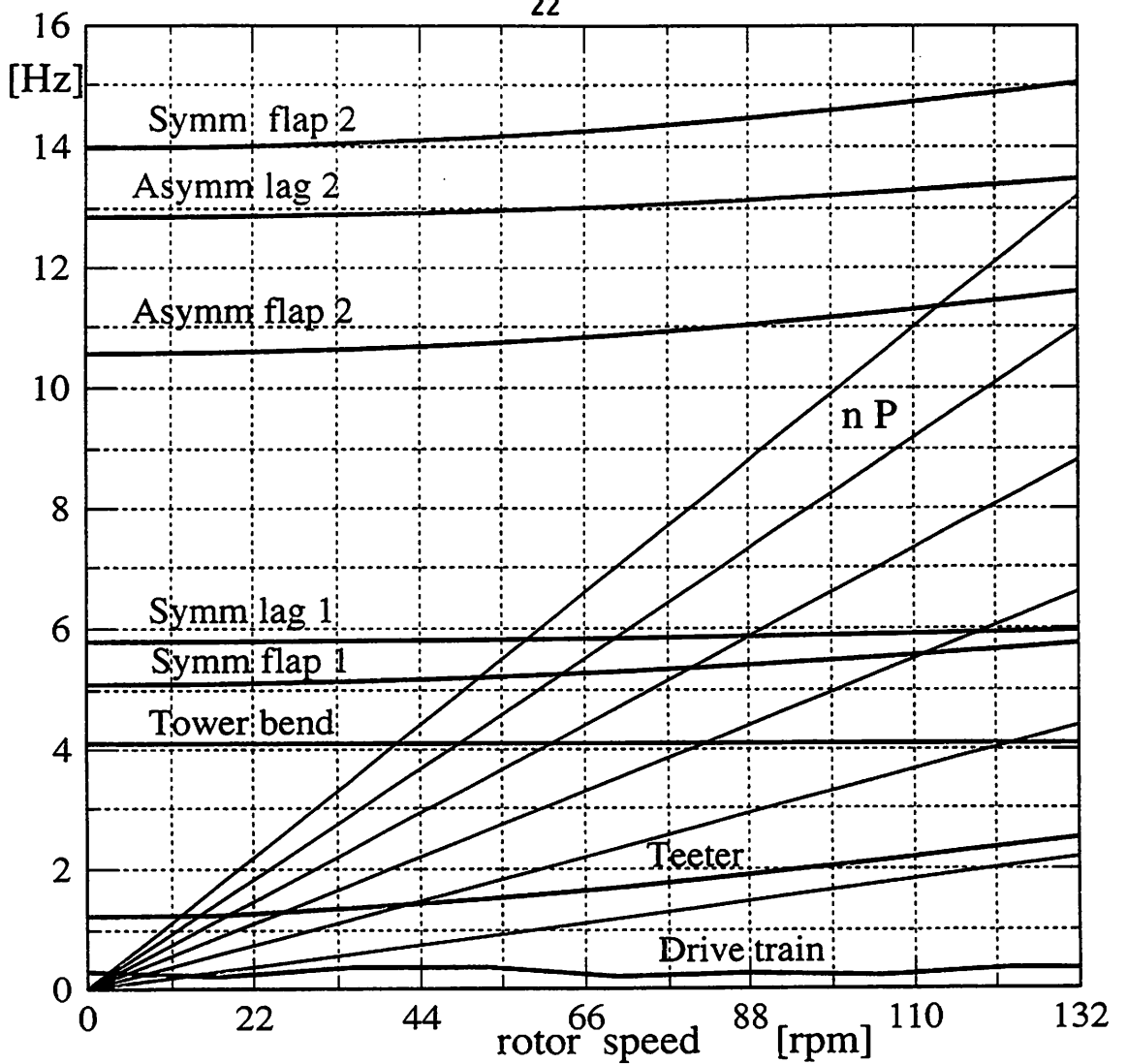


Figure 3. Campbell diagram for the WEG MS-1 wind turbine

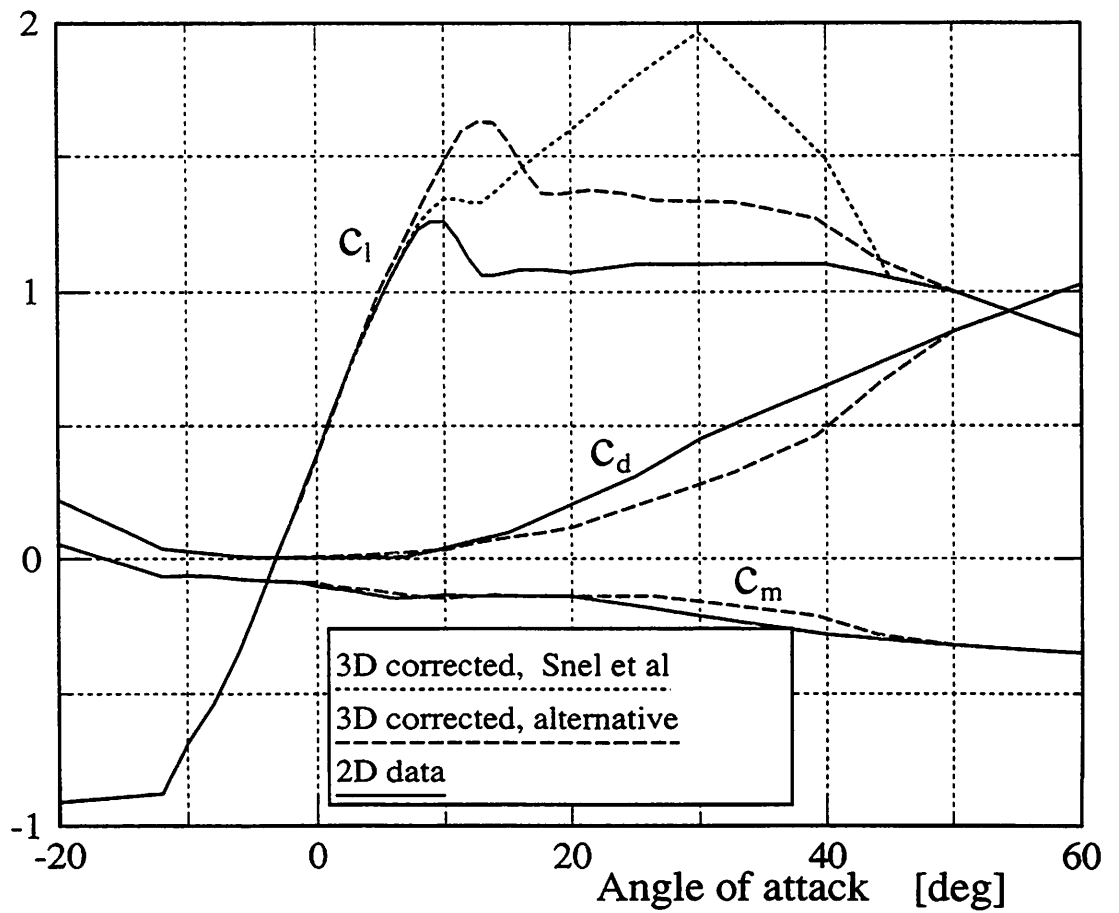


Figure 4. NACA63-621 airfoil coefficients for $c/r = 0.342$.

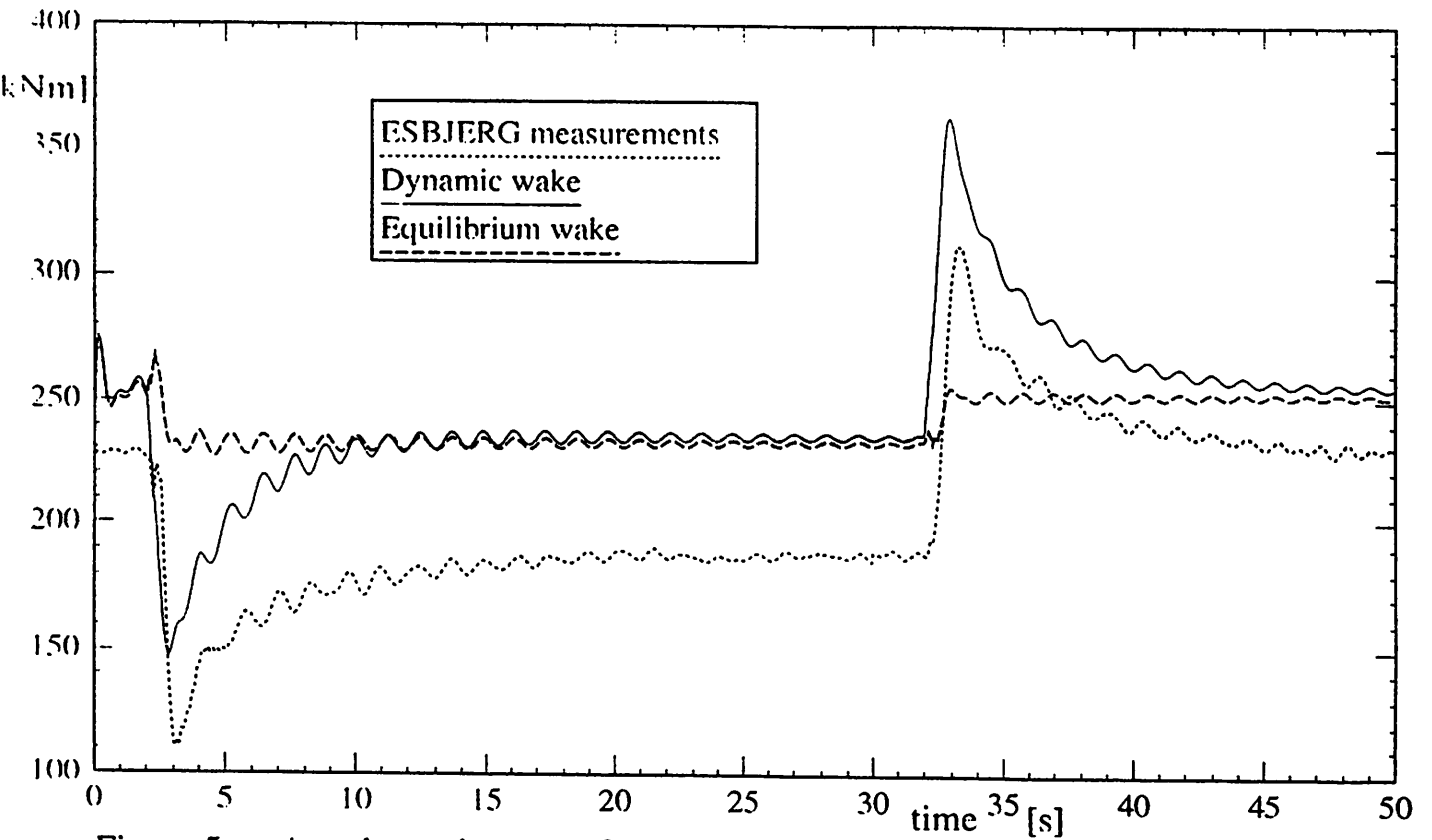


Figure 5.a. Aerodynamic torque for steps in pitch angle; 8.7 m/s wind.

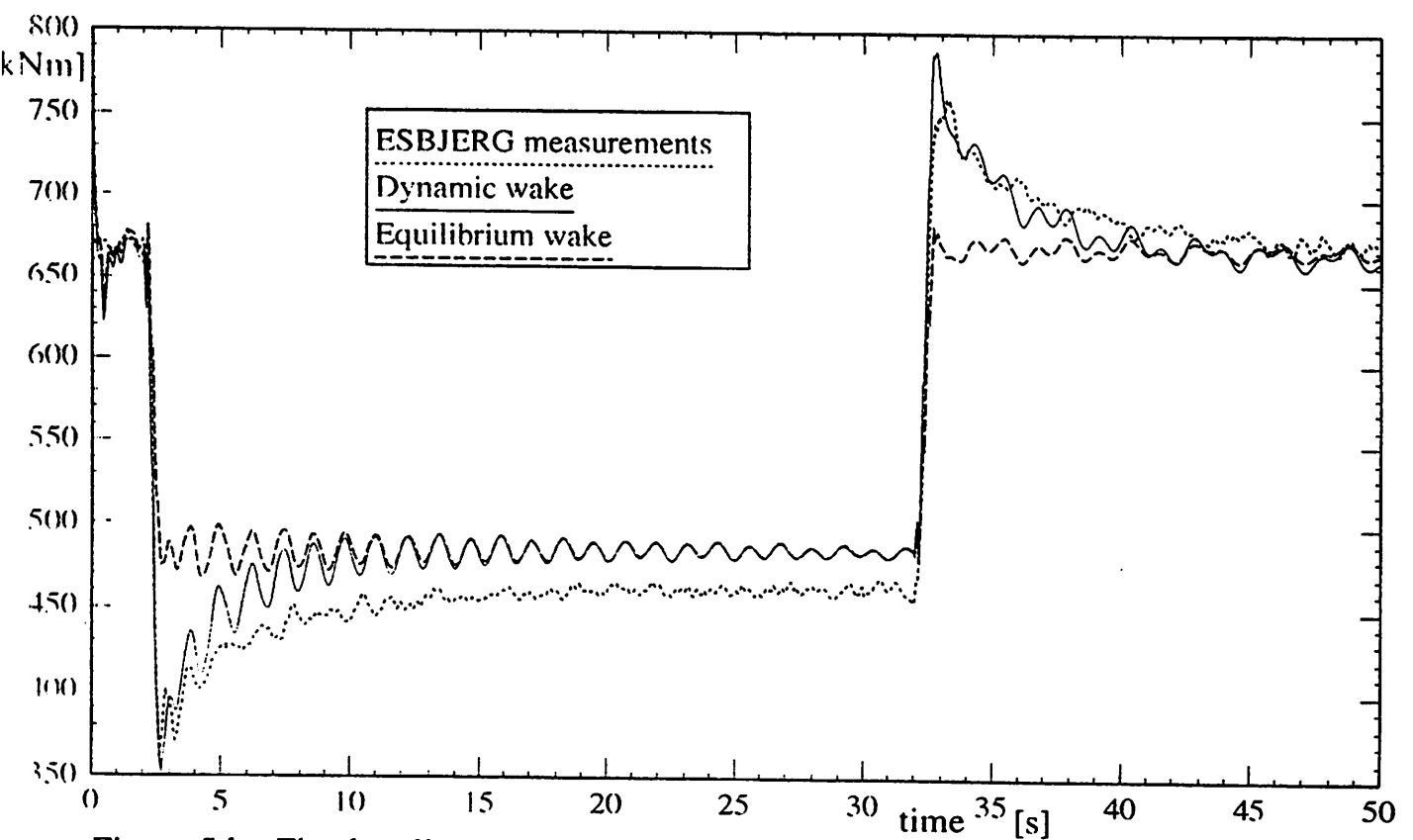
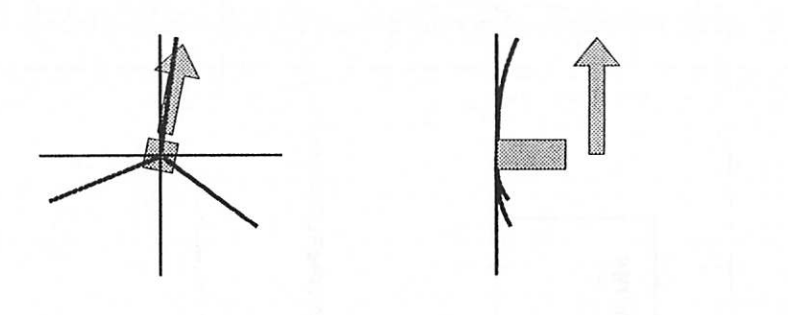
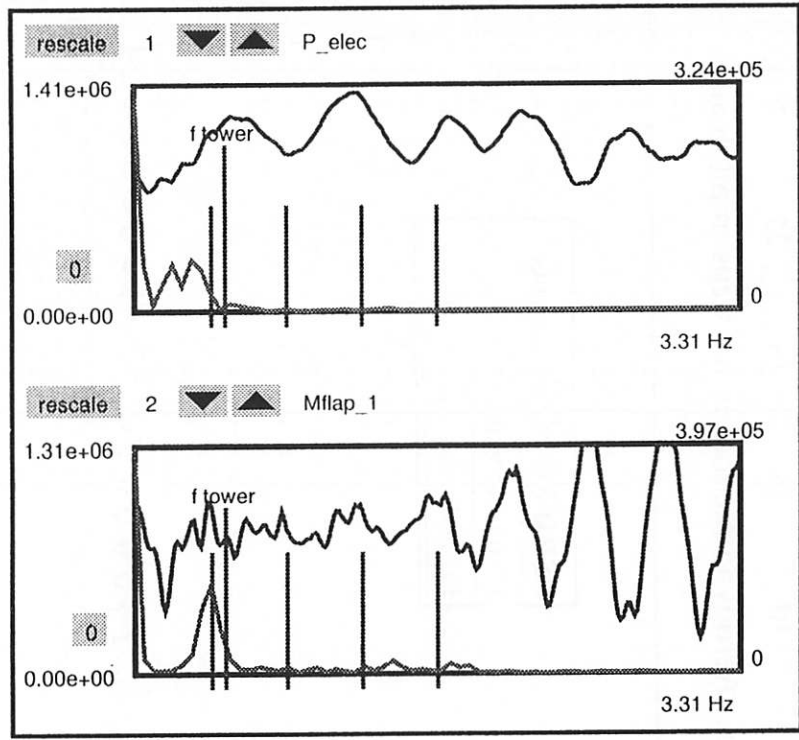
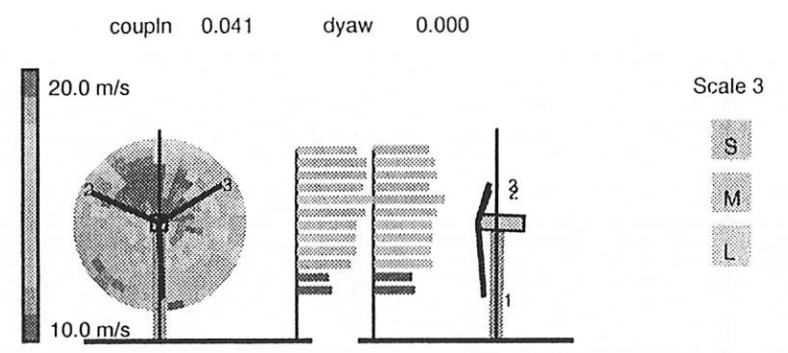
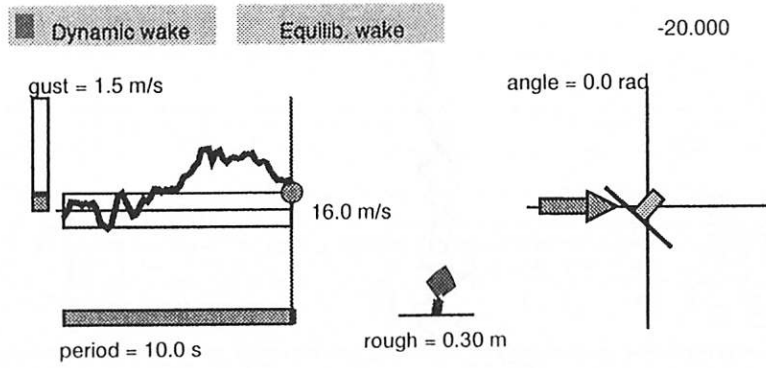
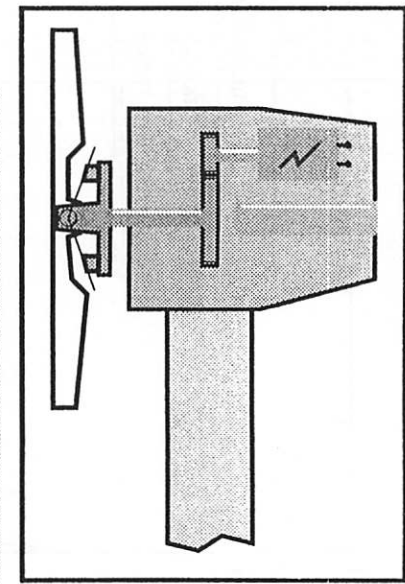


Figure 5.b. Flap bending moments for steps in pitch angle; 8.7 m/s wind.



Edgewise damping	1.50 %
Flatwise damping	1.51 %
Hinge stiffness	2.09e+08 Nm/rad
Hinge damping	5.90e+05 Nm/(rad/s)
Bumper angle	5.73 deg
Bumper stiffness	0.00e+00 Nm/rad
Shaft stiffness	1.0e+07 Nm/rad
Gearbox stiffness	1e+08 Nm/rad
Gearbox damping	2e+05 Nm/(rad/s)
Nominal slip	1.67 %
Generator time constant	0.000 s
Height	40.400 m
Tower frequency	0.486 Hz
Tower damping	0.50 %



Interactive Phatas
ECN 1996

Time 93.150 s
delta T 0.025 s
facor 1.000
faconv 1.000

Figure 6 Graphical interface for Computational Steering on PHATAS III

AEROELASTIC CODE DEVELOPMENT ACTIVITIES IN THE UNITED STATES

Alan D. Wright

National Renewable Energy Laboratory

Golden, Colorado

phone: (303)-384-6928

fax: (303)-384-6999

email: alan_wright@nrel.gov

ABSTRACT

Designing wind turbines to be fatigue resistant and to have long lifetimes at minimal cost is a major goal of the federal wind program and the wind industry in the United States. To achieve this goal, we must be able to predict critical loads for a wide variety of different wind turbines operating under extreme conditions. The codes used for wind turbine dynamic analysis must be able to analyze a wide range of different wind turbine configurations as well as rapidly predict the loads due to turbulent wind inflow with a minimal set of degrees of freedom.

Code development activities in the US have taken a two-pronged approach in order to satisfy both of these criteria: 1) development of a multi-purpose code which can be used to analyze a wide variety of wind turbine configurations without having to develop new equations of motion with each configuration change, and 2) development of specialized codes with minimal sets of specific degrees of freedom for analysis of two- and three-bladed horizontal axis wind turbines and calculation of machine loads due to turbulent inflow. In the first method we have adapted a commercial multi-body dynamics simulation package for wind turbine analysis. In the second approach we are developing specialized codes with limited degrees of freedom, usually specified in the modal domain.

This paper will summarize progress to date in the development, validation, and application of these codes.

INTRODUCTION

The development of modern horizontal axis wind turbines (HAWTs) has necessitated the development of wind turbine aeroelastic codes for analysis of wind turbine loads and response. The demands placed on these computer codes have been severe. They must account for the following effects: interaction between the blades and non-steady airflow, the yaw motion of the nacelle, pitch control of the blades, teetering rotors, the interaction between the rotor and supporting tower, starting and braking sequences, and various machine control schemes. Each of these aspects has its own mathematical difficulties and approximations have usually been sought in their solution.

The strengths and weaknesses of some of the various wind turbine computer codes developed here in the U. S. and in Europe was reported in (Malcolm, 1994). Because of these limitations the U. S. National Renewable Energy Laboratory (NREL) decided to focus code development activities along two main approaches: 1) adaptation of a existing commercial multi-body dynamics package for wind turbine use, in order to model wind turbines of different configurations without having to derive and validate complex equations of motion, and 2) development of a wind turbine code with several important system degrees of freedom, but which is more specialized than the multi-purpose code. Such a code would represent machine

degrees of freedom in the modal domain, thus obtaining faster runtimes than the multi-body codes, which discretize components into several rigid body masses connected by springs or beams.

The general purpose program selected was the Automatic Dynamic Analysis of Mechanical Systems (ADAMS®) program available from Mechanical Dynamics, Inc. of Ann Arbor Michigan.

In the second approach, a streamlined code is under development and refinement through a subcontract between NREL and Oregon State University. This code is called FAST (Fatigue, Aerodynamics, Structures, and Turbulence) and can be used to model both two- and three-bladed wind turbines. The two-bladed version is called FAST2 and the three-bladed version is FAST3.

In addition, the National Renewable Energy Laboratory has supported the continued validation and refinement of a code with just a few degrees of freedom, namely blade flap and machine yaw, called YawDyn (Hansen, 1992). An aerodynamic subroutine package, once solely contained in the YawDyn code, has been made a stand-alone package for inclusion into other structural dynamics codes (Hansen, 1995). This subroutine package is now a part of the ADAMS/WT software package (Elliott, 1994) and is used to supply the ADAMS engine with aerodynamic forces for the blades.

We envision using each of these codes for a different purpose: simple codes such as YawDyn can be used to obtain quick estimates of preliminary design loads. The ADAMS code is intended for final detailed loads calculations in the final design stage, when the design is nearly completed. The FAST code can be used to obtain loads estimates for intermediate design studies.

In this paper we will describe these different codes and show validation and application results.

CODE DESCRIPTION

ADAMS is a general-purpose, multibody system analysis code. It models systems as groups of rigid mass PARTS² connected by joints and forces that correspond to physical components. A variety of linearly elastic elements is available, ranging from simple spring dampers to BEAMS and FIELDS. The difference between BEAMS and FIELDS is described in (Mechanical Dynamics, Inc., 1995).

If the engineer decides to add another PART and add an additional degree of freedom, he or she does not have to derive and debug the equations. The ADAMS software seems to have the necessary ingredients to allow one to model many different

¹ADAMS is a registered trademark of Mechanical Dynamics, Inc.

² Words that are all caps in a san serif font are ADAMS keywords.

types of wind turbine configurations operating under various conditions (Elliott, 1994).

We have found that the capability of being able to model subcomponents of the turbine separately, such as blades, drive-trains, hubs, and towers to be helpful in the model validation process. After development and validation of these submodels, we can go on to combine these submodels into a total wind turbine systems model with more confidence.

One of the biggest disadvantages of ADAMS is the long runtimes for a wind turbine model. For calculation of loads due to turbulent inflow conditions, one needs to simulate at least ten minutes of the operating turbine. A typical run-time on a UNIX Workstation is about 7-10 hours for such a simulation. Use of the ADAMS software for performing a large multitude of such runs is prohibitive, such as in a machine's preliminary and intermediate design stages. Thus a code having a faster run-time, and with fewer degrees of freedom is needed for such calculations.

We have developed the FAST2 and FAST3 codes with this goal (two- and three-bladed versions of FAST). Unlike the multi-body dynamics approach, which discretizes a flexible component by dividing it into a number of rigid body masses, the FAST code models flexible bodies via modal coordinates and mode shapes. Thus, a blade may be modeled with just a few degrees of freedom, such as two flap modes and one lag mode. A similar blade modeled with ADAMS is typically divided into about ten rigid body masses, each having six degrees of freedom for a total of sixty. A complete wind turbine can be modeled in FAST with less than 15 degrees of freedom, while a similar model using ADAMS might contain more than 100 degrees of freedom. Typical runtimes with FAST2 take about one-sixth the time required for a similar ADAMS run for a similar turbine model.

The dynamic response of a two-bladed, horizontal-axis wind turbine is modeled by the FAST2 code as six rigid bodies and four flexible bodies. The six rigid bodies are the earth, nacelle, tower top base plate, armature, hub, and gears. The flexible bodies include blades, tower, and drive shaft. The model connects these bodies with several degrees of freedom, including tower flexibility (in the fore-aft and side-side directions, two modes each); rotor teeter; blade flexibility (two flap modes per blade; and one lag mode); nacelle yaw; variable rotor speed; and drive shaft torsion flexibility. The three-bladed rigid hub version of FAST (FAST3) contains all of these degrees of freedom except rotor teeter.

FAST uses equations of motion based on Kane dynamics (Wilson, 1995). Kane's method is used to set up equations of motion that can be solved by numerical integration. This method greatly simplifies the equations of motion by directly using the generalized coordinates and eliminating the need for separate constraint equations. These equations are easier to solve than those developed using methods of Newton or Lagrange and have fewer terms, reducing computation time. For more information on FAST code theory and formulation, see (Harman, 1995).

Aerodynamic forces are determined using Blade Element Momentum Theory. Lift and drag forces on the blades are determined by table look-up of the blade's lift and drag coefficients C_l and C_d . At NREL, we are using two versions of FAST: a version with the original Oregon State University aerodynamic subroutines and a version with the University of Utah AeroDyn subroutines. We set the goal of having the University of Utah develop a stand-alone aerodynamic subroutine package for inclusion into any wind turbine

structural dynamics code (Hansen, 1995). This package includes the effects of dynamic stall, dynamic inflow, table look-up of C_l and C_d data, and input of 3-D turbulence.

We now show the progress made over the past few years in the validation and application of these codes.

VALIDATION AND APPLICATION OF ADAMS

A particular two-bladed, teetering-hub, horizontal-axis wind turbine prototype, developed under NREL's Turbine Development Program, has shown response at normal operating speed, involving blade symmetric edge-bending and nacelle and tower top tilt motion. This response has not been seen in production versions of this machine. This interaction is seen as a 7-per-revolution response in the blade root-edgewise bending moments, and as a 6- and 8-per-revolution response in the nacelle and tower. These responses can be seen in Figure 1.

To assist us in understanding this system interaction, we used the ADAMS dynamics software to model this prototype. We ran the ADAMS code using the University of Utah AeroDyn package (Hansen, 1995) to supply aerodynamic forces to the model. First, however, we developed an ADAMS blade submodel and compared predicted blade modes and frequencies to isolated blade modal test data. We used a submodule of ADAMS named ADAMS/Linear to give us predicted blade modal information for a nonrotating blade. Of great importance in this blade modeling was the inclusion of significant coupling between blade flap and edge degrees of freedom caused by the blade's pretwist and principal axis orientation. In general, the principal axes were oriented differently than the section chordline at each blade radial station.

We then expanded the blade model to include the rotor hub, drive-train shaft bending, nacelle yaw, and tower subassemblies. Validation of this model was done by comparing ADAMS/Linear results for the static machine to modal test results. In addition, various operating machine loads measurements were compared to model predictions, such as blade root flap-, edge-bending moments, and nacelle pitching accelerations.

We found the comparison of ADAMS/Linear predictions to modal test data crucial in helping to identify the cause of this machine interaction. Early in the modeling process we did not have accurate blade or system modal information from which to check the accuracy of our model. We made numerous ADAMS runs, only to find that the amount of 7-per-revolution response in the blade root-edgewise bending moment was greatly underpredicted. Identifying the important modes involved in this interaction and validating them with modal test data greatly accelerated our progress, although some uncertainty still exists regarding correct tower-top and machine bedplate stiffness, which has not been resolved at this time.

Table 1 shows comparisons between ADAMS/Linear predictions and test data for modes involving rotor symmetric edgewise motion and symmetric flapwise response for the blades both vertical and horizontal. Except for the first one, these modes were all in the 6-8 Hz category. In this table, the plus sign indicates that the two components of this mode are in phase, while the minus sign indicates that they are 180 degrees out of phase.

Mode 1, shown in Figure 2, is dominated by rotor symmetric edgewise bending and low-speed shaft-bending. In this mode, the hub end of the nacelle moves in phase with the blade tips. Figure 3 shows Mode 2. The rotor's symmetric edge mode is now reacting against the machine's yaw inertia instead of the shaft and tower top, showing the difference in frequency of this

mode compared to the previous one. Mode 3 (not shown) is the same for the blades vertical and horizontal. We found very little tower or nacelle participation in this mode; however, its proximity to mode 4 was probably important. Mode 4, shown in Figure 4, involves nacelle participation in the opposite sense to mode 1. When the blade tips move up, the hub end of the nacelle moves down, 180 degrees out of phase with the blade tips. This mode seemed to be the key for tuning our ADAMS model to get good agreement with test data.

Somewhere in this system there is extra compliance that causes this mode to be lower than previously thought. Tuning the ADAMS turbine model to agree with these stationary modes does give us good results. It is possible that compliance could be added in other locations and similar results obtained.

We made in-depth studies of the effects of various turbine parameters on the operating loads of this machine, using the "tuned" ADAMS model. We studied the effects of such parameters as blade edgewise and flapwise stiffness, tower top

TABLE 1. COMPARISON OF INITIAL PREDICTED MACHINE FREQUENCIES TO MODAL TEST DATA

Mode Number and Shape	Blades Horizontal		Blades Vertical	
	Measured (Hz)	Predicted (Hz)	Measured (Hz)	Predicted (Hz)
1. edge symm. + nacelle pitch	4.3	4.8	n/a	n/a
2. edge symm. + yaw	n/a	n/a	6.6	6.6
3. flap symm. + (tower long.)	7.2	7.2	7.2	7.3
4. edge symm. - nacelle pitch	7.4	8.1	n/a	n/a

Input of our initial tower properties resulted in a prediction of 8.1 Hz for this mode, as seen in Table 1. The cause of this overprediction is still unknown, but we had to arbitrarily soften the upper tower elements by at least 50% in order to lower the frequency of this mode to its measured value of 7.4 Hz, which is critical to predicting the response of this system. This "tuning" of the inputs was necessary to obtain predictions which were realistic as we now show.

In Figure 5 we compare ADAMS predicted loads versus measured results for the blade root edgewise bending moments. We show results for both our original tower top properties ("stiff tower top") in which the frequency of mode 4 was 8.1 Hz as well as the modified one ("soft tower top"), in which that frequency was tuned to 7.4 Hz. The difference in predicted response is readily seen. Tuning mode 4 to its measured value was very important to obtaining realistic predictions.

We show similar results for the nacelle pitch acceleration in Figure 6. The nacelle acceleration was also very sensitive to the frequency of mode 4. For the stiff tower case, the predictions didn't even begin to match the test data. The soft tower case matched better, although there was some underprediction of the peaks in the response.

Figure 7 shows the blade's root flapwise bending moment comparison. This parameter was not as sensitive to the frequency of Mode 4. The cyclic 8 per revolution response is somewhat overpredicted.

We investigated the effects of varying turbine and aerodynamic input parameters on the predicted behavior of these loads. One parameter we found to be of particular importance was tower shadow velocity deficit. We ran cases where we varied the amount of deficit from 10% to 50%. Figure 8 shows these results. It seems that the tower shadow, felt by the rotor to some extent during every rotor revolution, acts as a triggering mechanism for this response.

One of the main uncertainties we still face is why Mode 4 lies at 7.4 Hz instead of our original estimate of 8.1 Hz. We carefully input the tower top, bedplate, and shaft properties from our best available knowledge of the turbine's properties.

stiffness, blade tip-brake mass, low-speed shaft stiffness, nacelle mass moments of inertia, and rotor speed. We showed which parameters can be varied in order to make the turbine less responsive to such atmospheric inputs as wind shear and tower shadow. We then gave designers a set of "design guidelines" in order to show how these machines can be designed to be less responsive to these inputs.

We again ran the ADAMS code using the University of Utah AeroDyn package (Hansen, 1995) to supply aerodynamic forces to the model. We ran the aerodynamics package using steady winds as inputs, with dynamic stall and dynamic inflow included, as well as tower shadow having a 50% velocity deficit in a rectangular shaped region and also a small amount of vertical wind shear (.05 power law wind shear coefficient). The wind speed for these cases was approximately 12 m/s. Only steady state responses of the machine were analyzed, the effects of stochastic fluctuations in loads and responses due to turbulent inflow conditions were not included in this study.

From examination of the mode shapes involving rotor symmetric lag motion, shown previously, we see that several parameters may affect the rotor's symmetric lag mode. With the rotor parked horizontally, this mode involves bending of the blades (mostly in edgewise bending), low-speed shaft bending, and tower top bending. When the rotor is parked vertically, this mode involves blade bending, low-speed shaft bending, and nacelle yaw motion. The features of these modes give us a clue as to the most important turbine parameters that can be adjusted to affect these modes, which in turn affect the rotor's symmetric lag response to atmospheric inputs. We showed that by moving the frequency of these modes closer to or away from certain harmonics of the rotor speed, the rotor response is increased or decreased.

Figures 9 and 10 show the effects of variations in these parameters: 1) blade edgewise stiffness distribution, and 2) tower top stiffness. In each case we started with the baseline value, shown as solid black in each figure. We then varied each parameter from the baseline value, reran the code, and computed

and plotted the predicted content in each harmonic of the edgewise-bending moments.

Changes were made to the blade's stiffness distribution by modifying the entire distribution without changing the shape of the distribution. The tower's stiffness was modified by changing only the last two beam stiffnesses near the tower top.

We see that decreasing the stiffness from its baseline value dramatically changes the 7P harmonic of the blade's root edgewise bending. The effect of changing this parameter is to effectively change the frequency of the rotor symmetric lag mode. At the baseline value, the machine's nonrotating rotor symmetric lag frequency is at 7.1 Hz, which is slightly above 7P. For the operating machine, this frequency will be even higher, because of the effects of centrifugal stiffening. When we increase the blade's edgewise stiffness by 30%, the machine's nonrotating rotor symmetric lag mode increases to 7.8P, and decreases to 6.6P with a 15% decrease from the baseline value. We see the resonant behavior of this response, as the symmetric lag frequency changes from its highest value of 7.8P (at the baseline +30% stiffness) to 6.6P for the lowest value of stiffness (baseline -30% stiffness).

Figure 10 shows the effects of variations in the tower's top stiffness on predicted bending moments. We changed the tower's stiffness incrementally from its baseline value. This parameter has a dramatic effect on the frequency of the rotor symmetric lag mode, decreasing it when the tower top stiffness is decreased. The amplitude of the 7P harmonic response increases as we lower the tower top stiffness. Again, we can see the resonant behavior of the rotor symmetric lag response, as the symmetric lag frequency decreases and moves through 7P.

We studied other parameters that affect the frequency of the rotor's symmetric lag mode and the results are very similar to the results we have just shown, as described in (Wright, 1995). We saw very similar behavior when we varied the blade's tip-brake mass, which we do not show but just mention here. Again, the 7P response shows a resonant character because changing the blade's tip-brake mass affects the rotor's symmetric lag natural frequency.

We went on in (Wright, 1995) to give designers a few guidelines to follow in order to attempt to avoid these resonance conditions. We advised designers to design their machines so that the rotor's symmetric lag modes do not coincide with odd harmonics of the rotor speed. The other guideline is to design a machine such that symmetric flap modes do not lie at even harmonics of the rotorspeed.

We have seen how the ADAMS dynamics code was used to investigate the cause of a system resonance condition in a two-bladed teetering hub downwind turbine. We also saw its use in investigating the effects of various parameters on predicted behavior.

Our other goal is to develop a code which can be used for fast calculation of loads and responses due to turbulence inflow, for intermediate design purposes. Such a code is called FAST.

VALIDATION AND APPLICATION OF FAST

We modeled a similar two-bladed teetering hub wind turbine, this time using the FAST2 code for two-bladed rotors. The machine under study was a free-yaw, downwind turbine,

developed under the Turbine Development Program at NREL. We wanted to test how well FAST could predict loads and responses during a long simulation of the operating turbine, with input of turbulent inflow conditions.

The machine we used for comparison purposes was tested in Tehachapi, California. Several channels of data were recorded at 40 Hz, including rotor azimuth, blade root flapwise- and edgewise-bending moments, shaft bending in two directions, as well as rotor torque, nacelle vertical acceleration, rotor teeter, one hub-height wind speed, and various other channels. The fact that only one anemometer of wind speed data was recorded meant that information about vertical and horizontal wind shear was missing. This prevented the FAST code from being run in a simple deterministic manner for validation of loads caused by deterministic inputs such as tower shadow, gravity, and wind shear. We obtained three different 10-minute sets of operating turbine data at different wind speeds, sampled at 40 Hz. We analyzed these data using the General Postprocessor (GPP) written by M. Buhl of NREL (Buhl, 1995), performing such functions as statistical analyses, power spectral density calculations, rainflow counting, and histograms. The three data sets spanned wind speeds from 11 to 20 m/s, as shown in Table 2.

For all cases shown here, the rotor speed was assumed to be constant and prescribed, so that the rotor rotation was not a degree of freedom for these runs. For the induction generator on this machine, constant rotor speed was assumed. We neglected drive-train torsion and tower fore-aft and side-to-side bending degrees of freedom. The principle degrees of freedom we used in these runs were the blade first and second flap modes, rotor teeter, and nacelle yaw.

Although this machine is not located in the middle of a multi-row wind park in San Geronio, California, it is situated at the top of a hill, near other turbines. Therefore, flow modeled as occurring over smooth and homogeneous terrain will give inaccurate results, as we show later.

The turbulent inflows for each of the three case studies were generated with the NREL version of the SNLWIND-3D turbulence simulation code (Kelley, 1992). This code is an expansion of the SNLWIND code developed by Veers (Veers, 1988) for simulating the longitudinal component of the inflow. In contrast to Veers' original version, SNLWIND-3D generates the full wind vector in Cartesian space. In its latest form, it provides a wide range of turbulence simulations, including conditions seen over smooth, homogeneous terrain, at the upwind row of a multi-row wind park, and within the wind park at two row-to-row spacing. The code also provides simulations using either the Kaimal or von Karman neutral-flow spectral models specified in the IEC-TC88 Draft Document, "Safety of Wind Turbine Generator Systems." In this study, we generated simulated inflows that a turbine would characteristically encounter when operating individually in smooth, homogeneous terrain and within a large wind park in San Geronio Pass with a row-to-row spacing of 7 rotor diameters. We also created simulated inflows using the Kaimal spectral model specified by the IEC-TC88 Draft Document. For most cases, we used a 6x6 turbulence grid density. We compared predictions using a 6x6 grid density and 12x12 grid density for data set Case 2.

TABLE 2. Dataset characteristics.

Mean wind-speed (m/s)	Standard deviation (m/s)	Date of Data	Time of Data	Weather Conditions
Case 1 11.10	1.89	4/19/94	16:22	clear, humid, 67 deg.
Case 2 13.56	2.03	4/21/94	14:24	sunny, 58 deg.
Case 3 19.64	2.16	6/6/94	9:41	clear, 50 deg.

The boundary conditions available with the three observed data sets were very sparse and were limited to the hub-height mean wind speed, the turbulence intensity, and the time-of-day. Furthermore, the turbine from which the measurements were derived was located within a wind park in the Tehachapi Pass and not San Gorgonio. Our approach was to use the time-of-day and the magnitude of the mean wind speed to estimate a stability condition; i.e., whether conditions were stable or unstable and to what degree as expressed by an estimate of the Richardson number stability parameter.³ For the smooth terrain simulations, we attempted to match the simulated turbulence intensities (or wind speed standard deviations) to the observed values by adjusting some of the critical boundary layer scaling parameters such as the mixed layer depth⁴, z_i , and friction velocity⁵, u_* . The simulations generated in concert with the

IEC-TC88 specifications used only the hub mean wind speed as a parameter because all other boundary conditions are designated.

Table 3 summarizes the boundary conditions used for each case and the measured turbulence parameters derived from the simulation at hub height. For the San Gorgonio simulations, no attempt was made to make the simulated turbulence intensity or wind speed standard deviation agree with the observed value. This is because the higher density of turbines at the San Gorgonio location produce much higher values than are seen elsewhere. In two instances, it was necessary to make adjustments in the simulation boundary conditions to achieve better agreement between the modeled and observed turbine dynamics, as described below.

Figure 11 is a comparison of predicted and measured blade

TABLE 3. Turbulence simulation boundary conditions summary

Case	Observed Hub Mean Wind Speed (m/s)	Observed Hub Turbulence Intensity	Estimated Richardson number stability parameter, Ri	Estimated surface roughness length, z_0 (m)	Estimated Power Law Exponent	Estimated Mixed Layer Depth, z_i (m)	Simulated Friction Velocity, u_* (m/s)	Simulated Turbulence Intensity
1, Smooth	11.10	0.17	+0.010	0.010	0.143	n.a.	0.658	0.17
1, IEC	11.10	0.17	0.0	0.003	0.200	n.a.	0.123	0.17
1, San Gor	11.10	0.17	+0.010	0.263	0.125	n.a.	1.381	0.25
1B, San Gor	11.10	0.17	+0.007	0.263	0.125	n.a.	1.409	0.25
2, Smooth	13.56	0.15	-0.250	0.010	0.143	1596	0.981	0.15
2B, Smooth	13.56	0.15	-0.010	0.010	0.143	1596	0.882	0.14
2, IEC	13.56	0.15	0.0	0.003	0.200	n.a.	0.445	0.17
2, San Gor	13.56	0.15	-0.010	0.213	0.115	3300	1.360	0.18
3, Smooth	19.64	0.11	-0.010	0.010	0.125	3000	0.941	0.11
3, IEC	19.64	0.11	0.0	0.003	0.200	n.a.	0.424	0.17
3, San Gor	19.64	0.11	-0.002	0.225	0.110	3840	2.130	0.14

³ A non-dimensional number representing the ratio of turbulence generation by buoyancy to shear. Negative values correspond to unstable flows, positive ones to stable conditions, and zero to neutral (turbulence generation by shearing alone).

⁴ The depth of the planetary boundary layer or PBL. The region of the atmosphere where the vertical exchange of momentum, heat, and moisture with the surface takes place. An important scaling height during the daytime hours when unstable conditions exist.

⁵ A critical boundary layer turbulence scaling parameter derived from $(u'w')^{1/2}$ where u' and w' are the fluctuating (zero mean) longitudinal and vertical wind components.

root flapwise bending moment rainflow counts for Case 1. The figure shows the predicted results using each turbulent inflow regime listed in Table 3. We see that use of the San Gorgonio turbulence data (both the Case 1, San Gor and the Case 1B, San Gor) give us the best results. Use of either the smooth or IEC inputs causes underprediction of the rainflow counted flapwise bending moments. Both the Smooth turbulence and the IEC turbulence are for smooth terrain. The only difference between these two inputs is that the Smooth case allows one to model non-neutral stability conditions. The IEC case assumes neutral conditions. In any event, the use of turbulence that is typical inside a wind park gives the most realistic results.

We used two different San Gorgonio turbulence inputs for this case (Case 1, San Gor and Case 1B, San Gor). By lowering the Richardson number stability parameter from +0.010 to +0.007 (destabilizing the flow) in the San Gorgonio simulation, we improved the comparison between modeled and observed behavior (Case 1B, San Gor).

Figure 12 is a histogram of rotor teeter for data set Case 1. These results show that the use of San Gorgonio turbulence data gives the best results. The use of IEC and Smooth turbulence creates a teeter histogram that is too tall and narrow compared to the test data.

Figure 13 is a comparison of rainflow counts of predicted and measured blade root flapwise bending moments for the second data set. Again, the San Gorgonio turbulence data give the best results, while use of both IEC and Smooth turbulence gives rainflow counts that decrease much more rapidly than do the measured data.

For San Gorgonio turbulence, we compared results using both a 6x6 and a 12x12 grid size and found that the 12x12 grid shows somewhat better behavior. For this case and for this turbine rotor diameter, the increase in turbulence grid size from 6x6 to 12x12 did not seem to greatly change the predictions. We intend to study this effect further on larger size rotors and for other wind speed conditions. Only upon completing such a study can we draw conclusions about the effect of grid size on stochastic loads predictions.

Figure 14 shows a histogram of rotor teeter. Our first choice of a stability value for Case 2, Smooth, proved too unstable (it created an excess of large, convective eddies). We were able to improve the correlation with the observed results by increasing the stability (R_i) from -0.250 to -0.010, seen in Figure 14 as Case 2B, Smooth. The IEC and Smooth cases produce histograms that again are narrower and taller than the measured results. The San Gorgonio case follows the measured results quite accurately, following the tails of this histogram distribution and estimating the height better than any of the other cases.

We believe it is important to perform an ensemble of turbulence simulations when comparing model results with an observed data set and a given set of boundary conditions. Each turbulence simulation represents a single realization or sample from an infinite number of potential outcomes. It is impossible to accurately quantify the degree of uncertainty between the observed and modeled results with a single realization. Our present objective is to establish the best estimate of the loads spectra derived from a simulated turbulent inflow to compare with the observed. To that end we have chosen to use 31 simulations for a given set of atmospheric boundary conditions as our ensemble. This number of simulations is the minimum required to apply large-sample statistics in quantifying the uncertainty of the results. We then applied a robust smoothing technique known as *locally weighted regression* or LOESS (Cleveland, 1979) to the ensemble results to obtain a smoothed estimate of the 31-sample aggregate. We showed those results in (Wright, 1996).

The results of case 3 comparisons were also discussed in (Wright, 1996) and follow the same general trends that we found for comparison cases 1 and 2. In general we found that we had to input turbulence characteristic of that found within a multi-row windpark to even approach agreement with the measured results.

CONCLUSIONS

We have described wind turbine aeroelastic code development activities during the past several years here in the United States. We have developed wind turbine codes along two general paths: 1) development of a multi-purpose code for analysis of a wide range of wind turbine configurations operating under extreme conditions, and 2) development of specialized wind turbine codes containing a few of the most important turbine degrees of freedom. The former code is for detailed analysis of machine loads and responses in the final design stage, while the latter code is for analysis of preliminary and intermediate design loads and responses when a large multitude of code runs must be made including the effects of turbulent inflow.

Future code development activities will be the development of techniques for predicting an operating turbines modal and stability characteristics. This type of analysis will become more important as machines become lighter and more flexible.

In addition we plan to incorporate the effects of wind turbine control systems into our aeroelastic codes in order to predict the effects of controls on wind turbine loads and response.

ACKNOWLEDGMENTS

This work has been supported by the US Department of Energy under contract number DE-AC36-83CH10093.

REFERENCES

- Malcom, D. J., Wright, A. D., 1994. "The Use of ADAMS to Model the AWT-26 Prototype." Presented at the 1994 Energy-sources Technology Conference and Exhibition, *Wind Energy-1994, SED-Vol. 15*, New Orleans, Louisiana.
- Hansen, A. C., 1992, "Yaw Dynamics of Horizontal Axis Wind Turbines," NREL/TP-442-4822, National Renewable Energy Laboratory, Golden, Colorado.
- Hansen, A. C., 1995, "USER'S GUIDE to the Wind Turbine Dynamics Computer Programs YawDyn and AeroDyn for ADAMS," Program date and version YawDyn 9.3, prepared for the National Renewable Energy Laboratory under Subcontract No. XAF-4-14076-02.
- Elliott, A. S., and Wright, A. D., 1994, "ADAMS/WT: An Industry-Specific Interactive Modeling Interface for Wind Turbine Analysis," Presented at the 1994 ASME Wind Energy Symposium, *Wind Energy-1994, SED-Vol. 15*, New Orleans, LA.
- Mechanical Dynamics, Inc., 1995, *ADAMS User's Guide* (ver 8.1).
- Veers, P. S., 1988, "Three-Dimensional Wind Simulation," SAND 88-0152, Sandia National Laboratories Albuquerque, NM.
- Kelley, N. D., 1992, "Full Vector (3-D) Inflow Simulation in Natural and Wind Farm Environments Using an Expanded Version of the SNLWIND (Veer's) Turbulence Code," NREL/TP-442-5225, National Renewable Energy Laboratory, Golden, CO.
- Wilson, R. E., Freeman, L. N., and Walker, S. N., 1995 "FAST2 Code Validation." presented at the 1995 ASME Wind Energy Symposium, Houston, TX.
- Harman, C. R., Wilson, R. E., Freeman, L. N., and Walker, S. N., 1995, "FAST Advanced Dynamics Code, Two-blade

Teetered Hub Version 2.1, User's Manual." Draft Report, National Renewable Energy Laboratory, Golden, CO.

Buhl, M. L., Jr., 1995, "GPP User's Guide, A General-Purpose Postprocessor for Wind Turbine Data Analysis," NREL/TP-442-7111, National Renewable Energy Laboratory, Golden, CO.

Wright, A. D., Bir, G. S., and Butterfield, C. P., 1995, "Guidelines for Reducing Dynamic Loads in Two-Bladed

Teetering-Hub Downwind Wind Turbines," NREL/TP-442-7812, National renewable Energy Laboratory, Golden, CO.

Wright, A. D., Kelley, N. D., and Bir, G. S., 1996, "Application of the FAST2 Code to Prediction of Fatigue Loads for Two-Bladed Teetering Hub Wind Turbines." presented at the 1996 ASME Wind Energy Symposium, Houston, TX.

Cleveland, W.S., 1979, "Robust Locally Weighted Regression and Smoothing Scatterplots," *J. American Statistical Assoc.*, Vol. 74, 368, pp. 829-836.

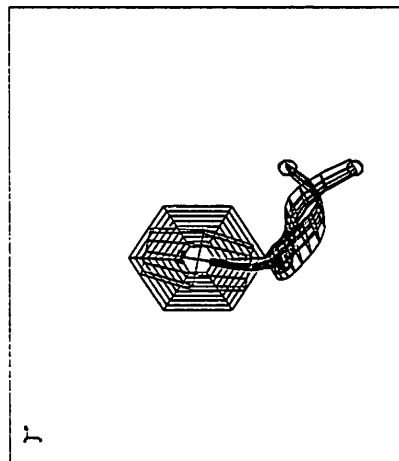
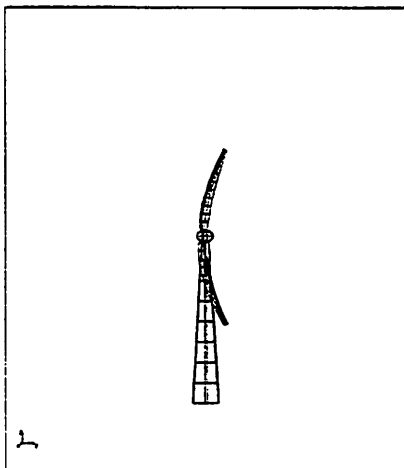
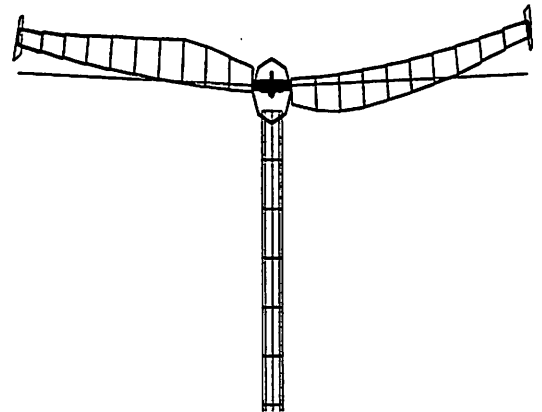
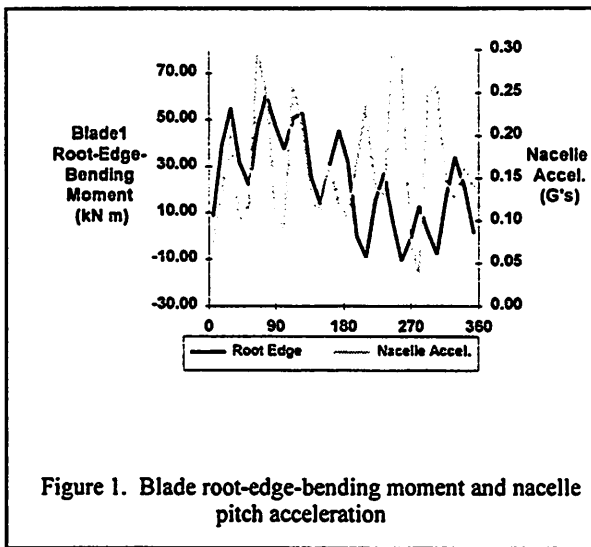


Figure 3. MODE 2: Rotor symmetric lag mode, rotor parked vertically

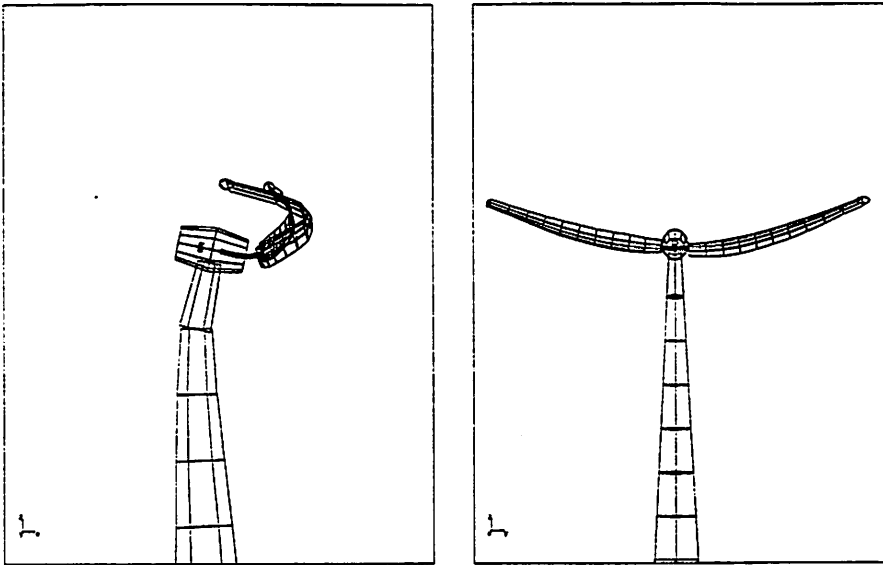
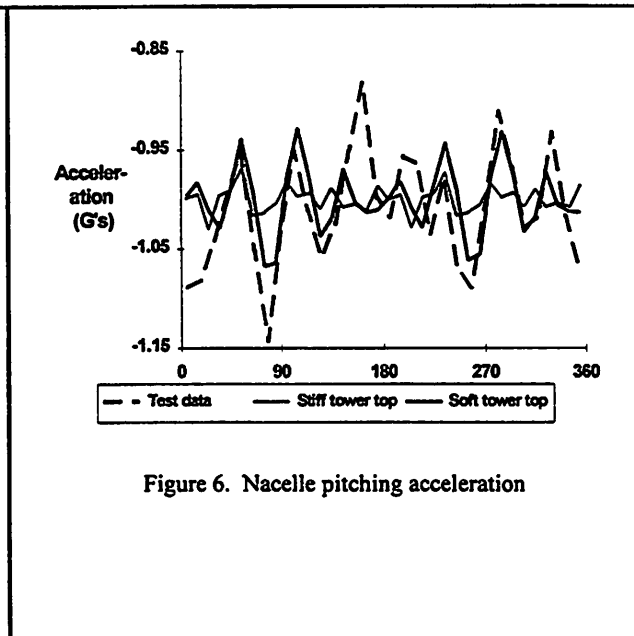
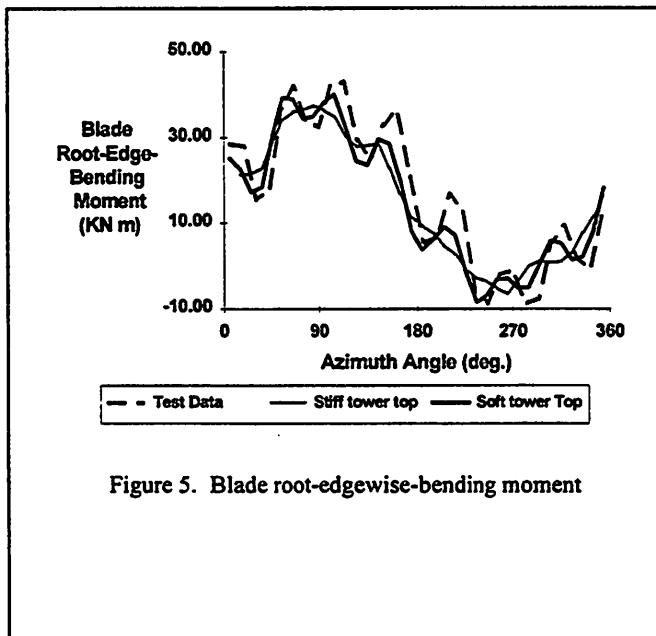
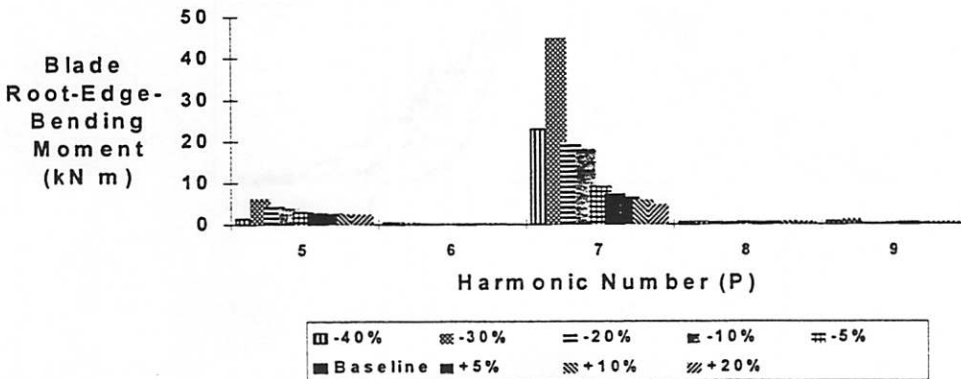
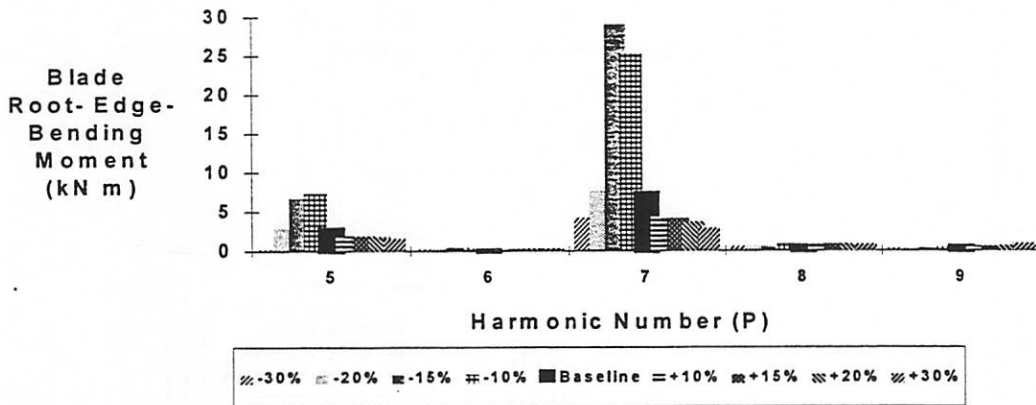
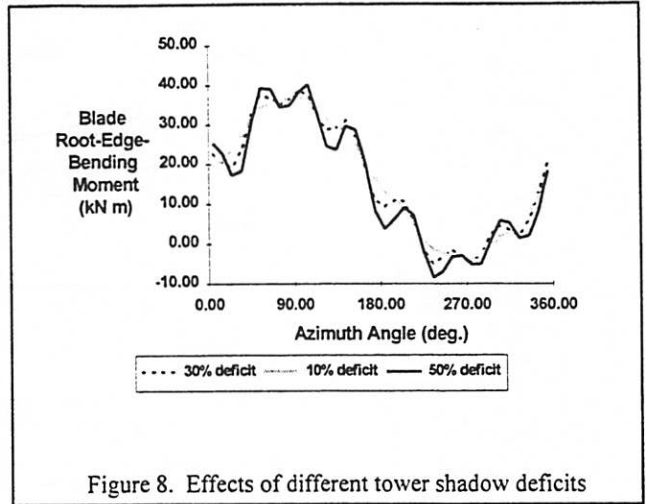
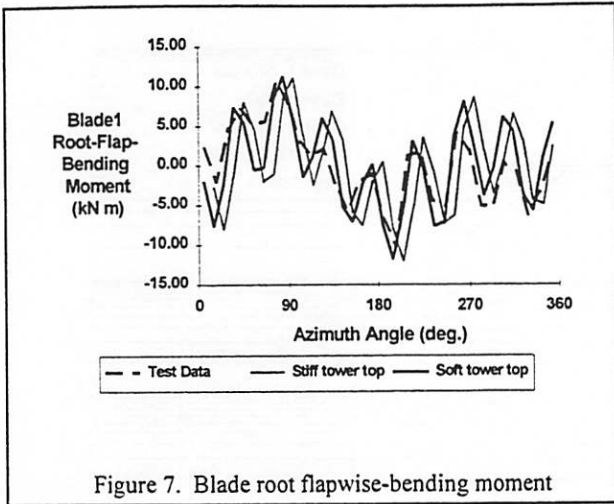


Figure 4. MODE 3: Rotor symmetric lag mode, rotor parked horizontally





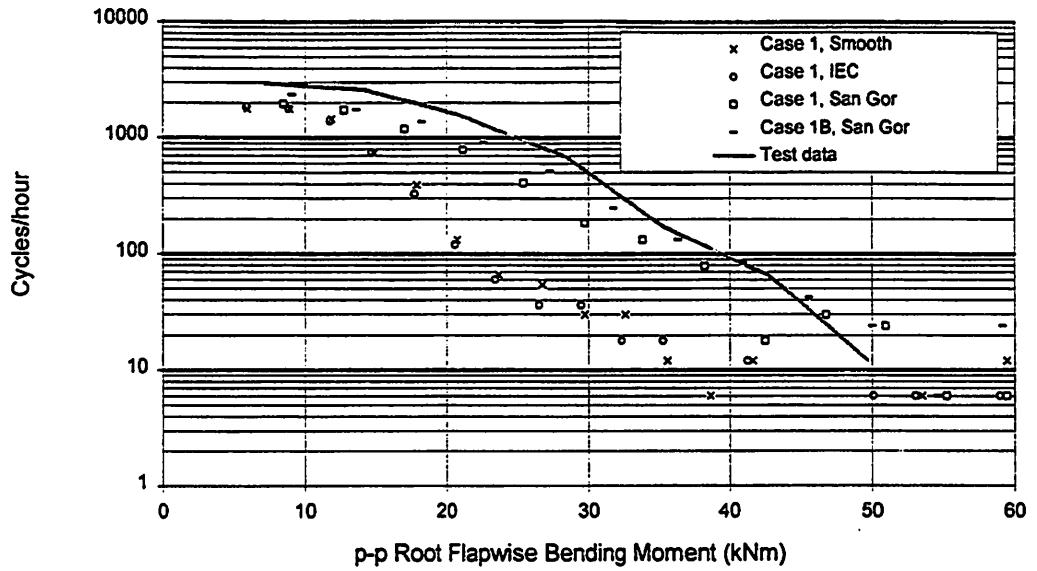


Figure 11. Rainflow counts for blade root flapwise-bending moments for Case 1.

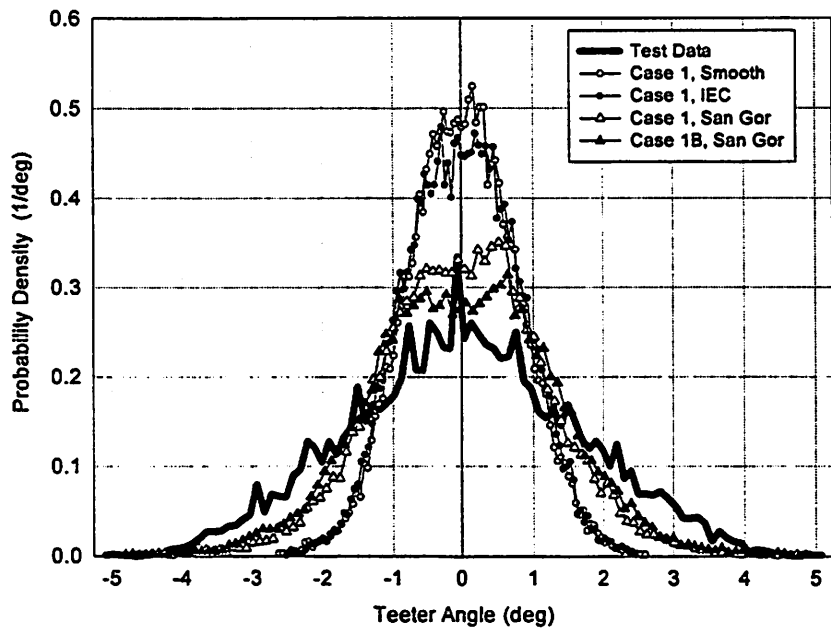


Figure 12. Histogram of rotor teeter for Case 1.

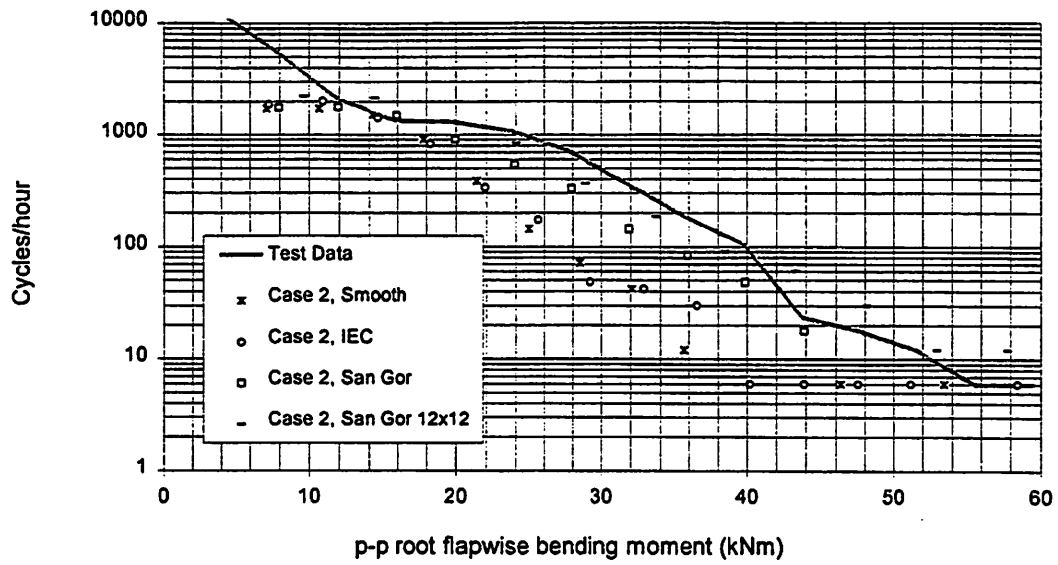


Figure 13. Rainflow counts for blade root flapwise-bending moments for Case 2.

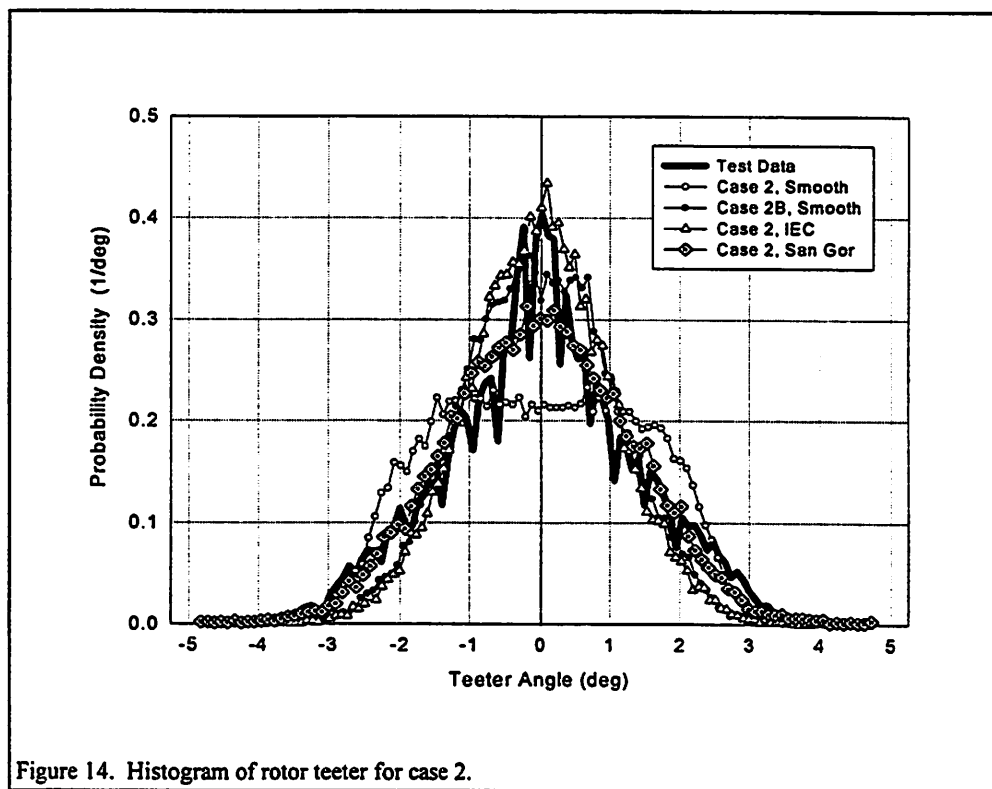


Figure 14. Histogram of rotor teeter for case 2.

THE FAST CODE

L.N. Freeman and R.E. Wilson

Department of Mechanical Engineering
Oregon State University
Corvallis, OR 97331

ABSTRACT

The FAST Code which is capable of determining structural loads on a flexible, teetering, horizontal axis wind turbine is described and comparisons of calculated loads with test data are given at two wind speeds for the ESI-80. The FAST Code models a two-bladed HAWT with degrees of freedom for blade bending, teeter, drive train flexibility, yaw, and windwise and crosswind tower motion. The code allows blade dimensions, stiffnesses, and weights to differ and models tower shadow, wind shear, and turbulence. Additionally, dynamic stall is included as are delta-3 and an underslung rotor. Load comparisons are made with ESI-80 test data in the form of power spectral density, rainflow counting, occurrence histograms, and azimuth averaged bin plots. It is concluded that agreement between the FAST Code and test results is good.

SCOPE

A current topic of considerable interest relates to the improvement of the accuracy and the reduction of time and effort needed to determine stochastic loads is, "how simple or complex must the structural dynamics model be?" This study compares calculated loads to measured loads for a contemporary lightweight teetered wind turbine using a structural model that has been incorporated into a computer code, FAST (Fatigue, Aerodynamics, Structure, Turbulence).

Before the accuracy associated with different levels of structural model can be ascertained, any model or code must first be validated. The FAST code results will be compared to test data from a horizontal axis wind turbine.

The ESI-80 test results (Musial, 1985) represent a valuable data set based on the current existence of both the data tapes and the original test machine. Additionally, personnel associated with the tests are still active in the wind energy field. The original machine was at the University of Massachusetts during much of 1992 and 1993 where measurements were made on the rotor to determine the actual parameters of the test machine (Bywaters, 1992). By using the ESI-80 test data, the study relates most closely with ESI-80-like machines. The ESI-80 has a significant amount of excitation in the range from 6 per revolution to 8 per revolution.

FAST CODE

The dynamic response of a horizontal-axis wind turbine (HAWT) has been modeled using five rigid bodies and three flexible bodies. There are 14 degrees-of-freedom in the system. The model accounts for blade flexibility, tower flexibility, yaw motion of the nacelle, variations in both rotor and generator speed, blade teetering, and blade bending. By selecting various physical constants, a variety of different configurations may be modelled, including generator axis tilt, preconed blades, teetering with selected hinge locations, "delta-3" orientation, various restrictions on the teeter angle, selected drive-train flexibility and damping, and tower flexibility parameters.

The first four degrees-of-freedom arise from flapwise blade motion of each of the two blades. The model allows for full or partial blade pitch. The blade torsional degree of freedom is not modeled in this study.

The fifth degree-of-freedom accounts for teeter motion of the two blades about a pin located on the turbine hub. The intersection of the blades principal moment of inertia axes can be displaced by the teeter axis by an undersling length. Additionally, the model allows for blade precone and a delta-3 angle. A lumped hub mass can be included in the code at a specified distance from the teeter pin. Teeter motion can be unrestricted, restricted by teeter dampers or teeter springs, or a combination of both.

The sixth degree-of-freedom accounts for variations in rotor speed. This degree-of-freedom can model a motor for start-up, a brake for shutdown, an induction generator with slip, or a variable-speed generator.

The seventh degree-of-freedom models the drive train flexibility between the generator and the rotor. This flexibility was modeled using a lumped drive train torsional spring and a damper.

The eighth degree-of-freedom accounts for yaw motion of the nacelle and rotor. Yaw motion can be free or fixed with a torsional yaw spring and/or a yaw damper. A yaw tracking control model can be implemented with the fixed yaw version. The rotor can be either upwind or downwind. Aerodynamic nacelle loads are not currently modeled.

The ninth and tenth degrees-of-freedom are first mode tower motions. The ninth and tenth degrees-of-freedom are perpendicular to each other. The eleventh and twelfth degrees-of-freedom are the second mode tower motions. The eleventh and twelfth tower degrees-of-freedom are in the same direction as the ninth and tenth, respectively. Aerodynamic tower loads are not included. The last two degrees-of-freedom, 13 and 14, are edgewise motion of the blades.

The aerodynamic loading on the blades is determined using modified strip theory with nonlinear lift and drag characteristics. The aerodynamics is driven by a wind model that consists of a deterministic portion made up of mean wind, shear, and tower interference and a stochastic portion consisting of an atmospheric turbulence model including time varying wind direction.

The major loading on the wind turbine blades is due to the aerodynamic forces of lift and drag. The local relative wind speed contains contributions from the local wind, the rigid body motion of the blade due to rotation about the drive shaft, teeter and yaw axes, the flexible body motion of the blades and tower, and a contribution due to induction. The induced velocity is determined using strip theory wherein the local force on a blade element due to lift is equated to the momentum flux. The blade force is based on the flow relative to the blade and contains the induced velocity explicitly in the velocity squared term and also contains the induced velocity implicitly in the lift coefficient and in the various trigonometric functions that are used to obtain the component of the blade force in the direction of the momentum flux.

The momentum flux through a segment of the rotor disk is obtained using Glauert's Momentum Equation. Whereas the blade force involves the flow relative to the blade, the momentum flux is determined in an inertial reference frame. The induced velocity appears both explicitly and implicitly in the momentum flux as well as in the blade force so that the induction must be solved for using iteration. A significant amount of computing time is used to determine the local induction at each time step.

The iteration process neglects the effects of the tangential component of the induced velocity, as well as the effects of turbulence. The effects of turbulence are ignored during the iteration because it is assumed that turbulence does not have a fully developed wake and, therefore, does not contribute significantly to the induced velocity. Once the iteration process is completed, turbulence is used in determining the final aerodynamic coefficients.

The aerodynamic loads are calculated in the blade deformed position. The resulting nonlinear equations are solved in the time domain using a predictor-corrector method. Tower and blade loads are determined by integration along the blade.

Turbulence in the wind was accounted for by use of a turbulence model, the Sandia Three-Dimensional Wind Simulation (Veers, 1984). This gives a rotationally sampled longitudinal turbulence component for each blade at one point on the blade. Each value represents the change in wind velocity due to turbulence. These values are superimposed on the steady component of the wind which already includes the effects of tower shadow and wind shear.

The FAST Code was developed at Oregon State University under contract to the Wind Technology Branch of the National Renewable Energy Laboratory (NREL) (Wilson et al., 1994).

THE ESI-80 WIND TURBINE

The ESI-80 wind turbine was tested extensively (Musial et al., 1985) and has been selected to compare calculated results from the FAST Code to field data. The wind turbine, which has two 40-foot (12.19 m) teetering blades, is a fixed pitch, free yaw, downwind machine with wood epoxy composite blades. The rotor blades employ the NASA LS(1) airfoil section. The specifications for the ESI-80 are summarized in Table 1.

FIELD MEASUREMENTS

The ESI-80 test turbine was located in the Altamont Pass near Tracy, California. A 120 ft (37 m) meteorological tower was located 160 ft (50 m) to the west of the wind turbine in the prevailing wind direction.

Table 2 lists the items that were measured during the test program and subsequently digitized at 50 Hz by the Solar Energy Research Institute (now NREL).

Table 1. ESI-80 Turbine Specifications

Rated Power	250 kW
Rated Wind Speed	20.3 ms (45 mph)
Rotor Diameter	24.2 m (80 feet)
Rotor Type	Teetered — Underslung
Rotor Orientation	Downwind
Blade Construction	Wood-Epoxy
Rotor Airfoil	NASA LS(1) 04xx
Tip Speed	77.9 m/s (173 mph)
Cut-In Wind Speed	5.9 m/s (13 mph)
Rotor rpm	60 rpm
Generator Type	300 kW, Induction
Gearbox	Planetary, 30:1
Hub Height	24.9 m (81.5 feet)
Tower	Open — Truss
Pitch	Fixed
Yaw	Passive
Overspeed Control	Tip Vanes
Total System Weight	9750 kg (21,500 lb)
Coning	7°
Natural Frequencies	
Teeter	1 Hz
Tower	1.31 Hz
First Flapwise	2.05 Hz
Second Flapwise	6.91 Hz
Edgewise	7.70 Hz

Table 2. Measured Parameters for the ESI-80 Test Turbine

Channel	Description
1	Wind Speed @ 31.5 m (120 ft)
2	Wind Direction @ 31.5 m (120 ft)
3	Wind Speed @ 24.5 m (80 ft)
4	Wind Direction @ 24.5 m (80 ft)
5	Wind Speed @ 12.2 m (40 ft)
6	Wind Direction @ 12.2 m (40 ft)
7	Rotor Azimuth Position
8	Teeter Angle
9	Yaw Angle
10	Blade Root Flap Bending
11	Blade Flap Bending @ 60% R
12	Low-Speed Shaft Torque

FAST RESULTS

Turbulence induced loads on the ESI-80 were examined using 10 minute records of wind conditions and loads measurements as reported by Wright and Butterfield (1992). The mean wind speed for Case 1 was 36.14 mph and turbulence intensity was 12.1%. For Case 2, the mean wind speed was 22.6 mph and the turbulence intensity was 9.7%.

The Sandia Three-Dimensional Wind Simulation (Veers, 1984), developed by Veers, was used for turbulent wind simulation. This code simulates the longitudinal component of the turbulence perpendicular to the rotor disk in non-yawed flow. The full three-component field of turbulence was not used.

The simulation method determines the "rotationally sampled" wind speed, although nonrotating wind speed can also be obtained from the model with minor modifications. The approach of this method is to simulate wind speed time series in a plane perpendicular to the mean wind direction and to propagate the time series in the mean wind direction at the mean wind speed. These signals are then rotationally sampled to prepare an input time series for the FAST Code.

In order to facilitate the calculation of blade loads, the FAST Code was run at constant rotor angular velocity. Further, the tower motion was limited to the first tower mode. Thus, ten degrees-of-freedom were employed; six degrees-of-freedom for the blade, teeter, yaw, and tower motion in two directions. Data on the configuration of the ESI-80 used for the tests was facilitated by measurements made at the University of Massachusetts. Of particular note is the presence of both teeter springs and teeter dampers.

COMPARISONS, 36.1 MPH

Histograms of test data and code calculations are shown below. Figure 1 shows a histogram for the 36.1 mph case for the blade root flatwise bending moment. Agreement between test data and code is good with a similar shape to both distributions. The test data mean was 26.34 kNm, while the FAST Code mean was 3.6 kNm lower. Figure 2 shows the flapwise bending moment histogram at a station 60% of the rotor radius. Again the data is higher than the code results, the mean for the data being 4.49 kNm and the mean for the code was 0.4 kNm lower. Since the mean acceleration of the blade in the flatwise direction is zero, the difference between test data and code must be from the mean aerodynamic loads, the mean centrifugal loads, or due to the data. Calculation of the mean blade root bending moment and comparison to test data shown in Figure 3 suggest that the calibration of the strain gages drift from test run to test run so that the code results shown in Figures 1 and 2 are felt to be within the range of experiment test error.

Figure 4 shows the teeter occurrence histogram at 36.1 mph. Several items may be mentioned concerning the data. First, the mean teeter angle from the test data is not zero being 0.24° . Second, the effects of the teeter springs/dampers can be seen in the data; the plateau above $+2^\circ$ and a similar plateau at about -1° . While the FAST Code results also exhibit "plateaus" in the region of $\pm 2^\circ$, the code has a mean teeter angle of zero and the calculations are more or less symmetrical about the origin. Third, shape of the distribution of teeter angle was found to be a result of including the yaw degree-of-freedom. McCoy (1992) had modeled the ESI-80 using a code without a yaw degree-of-freedom and obtained a teeter occurrence histogram similar to the distribution that would be obtained from a harmonic oscillator. Further improvement to the teeter histogram was obtained by use of the variable speed degree-of-freedom.

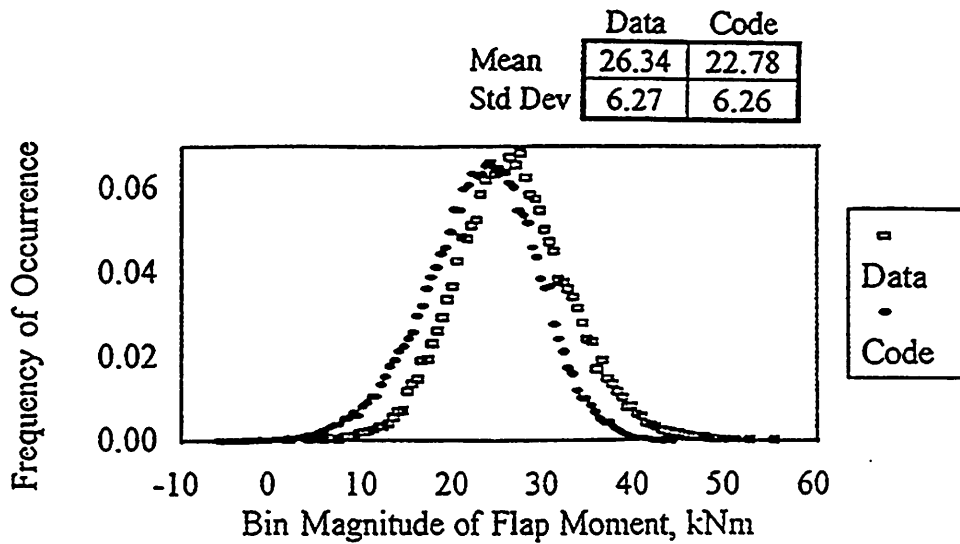


Figure 1. Occurrence Histogram of Blade Flap Moment at Root for ESI-80 Machine at 36 mph Wind Speed

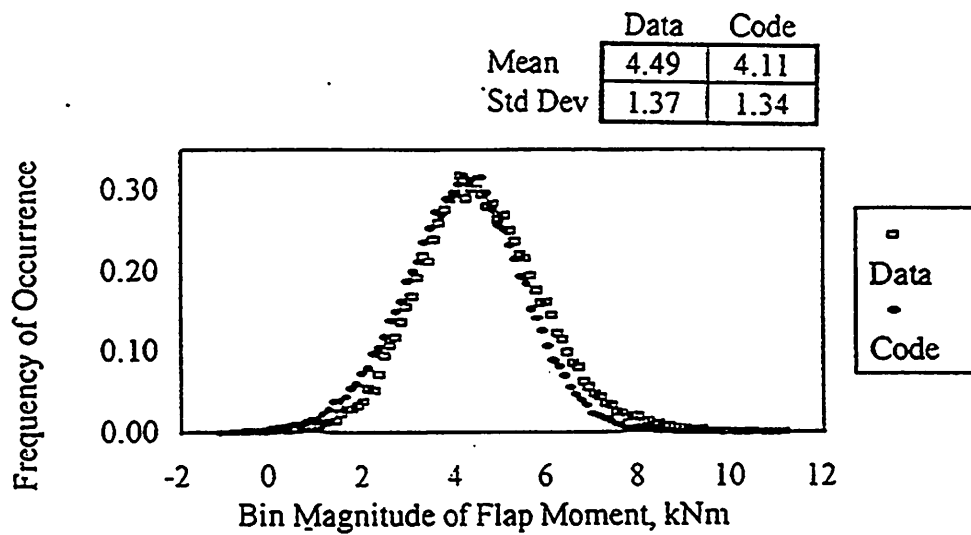


Figure 2. Occurrence Histogram of Blade Flap Moment at 60% Blade Station for ESI-80 Machine at 36 mph Wind Speed

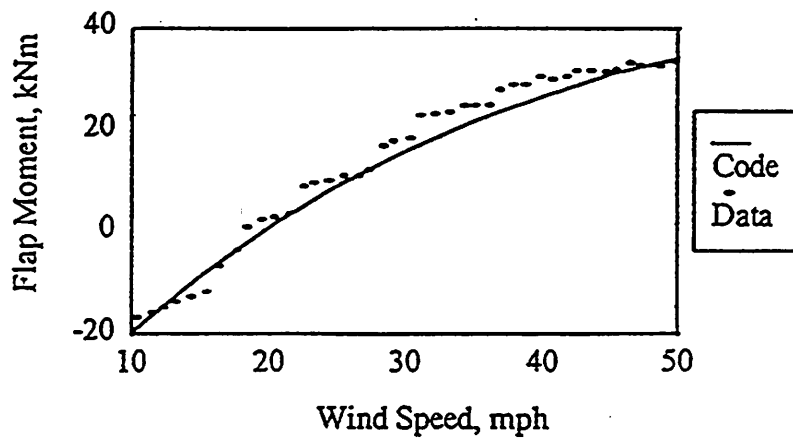


Figure 3. Mean Blade Flap Moment versus Mean Wind Speeds for the ESI-80 Machine

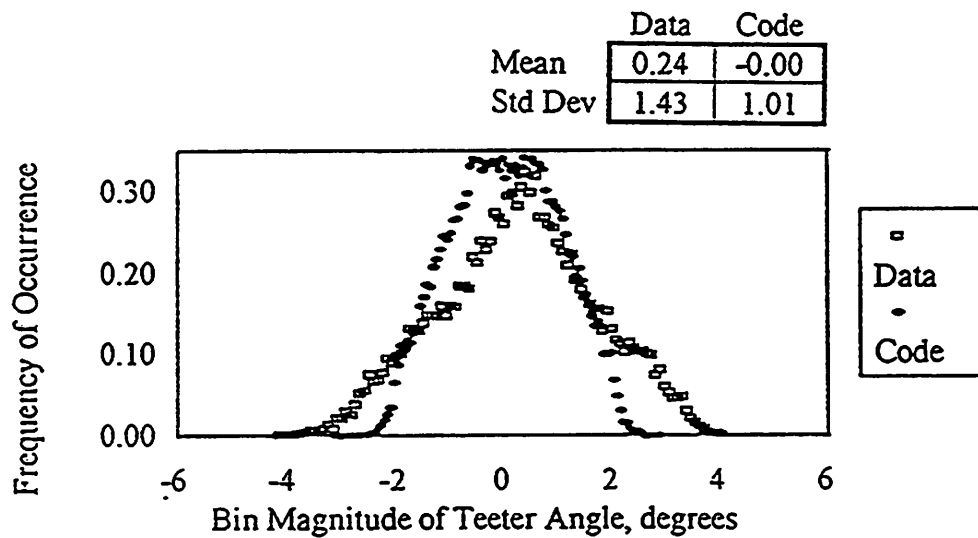


Figure 4. Occurrence Histogram of Teeter Angle for ESI-80 Machine at 36 mph Wind Speed

Azimuth averaged load plots are the second form of comparison between test data and FAST calculations. Figure 5 shows the azimuth binned blade root flatwise bending moment at 36.1 mph. Note that the load scale covers the range from 10 to 40 kNm. Agreement between FAST calculations is good as all fluctuations shown by the data are present in the calculations. The magnitude of the calculated moment between 90° and 135° (post tower shadow region) and between 270° and 315° has a maximum difference of 9 kNm below the test data.

Power Spectral Density of the root flatwise bending moment is shown in Figure 6 for a wind speed of 36.1 mph. Agreement between code and test data is good including the broadening in the region of 2 Hertz. The code failed to predict the broad plateau between 2 and 3 Hertz that appears in the test until the edgewise degrees-of-freedom were incorporated into the code.

Rainflow cycle counting is shown in Figure 7 for the 36.1 mph case. Agreement between FAST calculations and test data is good over the entire range. Code calculations shown in Figures 1 through 7 were made without dynamic stall. Calculations made with dynamic stall produced similar results to those produced without dynamic stall except for the low magnitude cycles.

COMPARISONS, 22.6 MPH

A histogram of the blade root flatwise bending moment is shown in Figure 8. Agreement between FAST2 calculation is very good as the mean, standard deviation, and distribution are all very close. The azimuth averaged flatwise blade bending moment shown in Figure 9 also shows good agreement between test data and calculations in magnitude, phase angle, and representation of major fluctuations. The power spectral density of the root flap moment is illustrated in Figure 10. While agreement between the test data and code is good, there appears to be a scale shift in the frequency, the data peaks occurring at slightly lower than integer values of the rotor angular velocity while the code peaks occur at values slightly above integer values of the rotor angular velocity. With the rotor angular velocity of

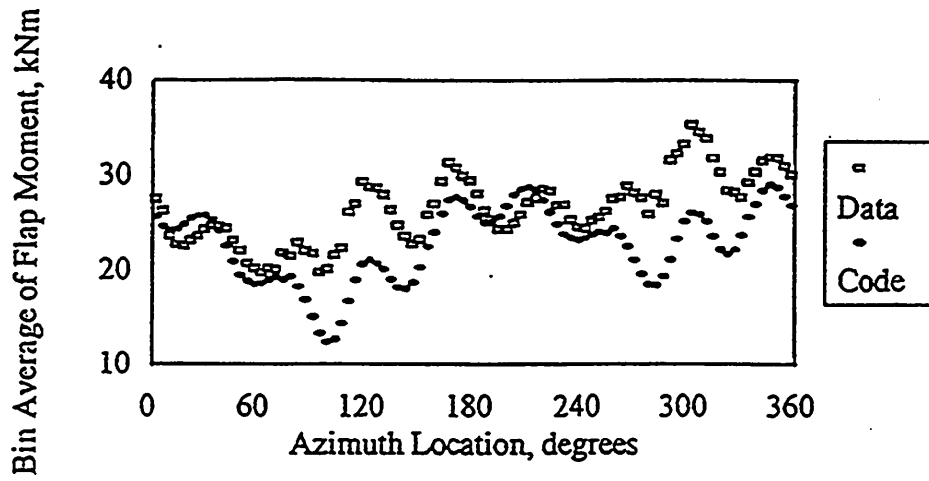


Figure 5. Azimuth Binning of Blade Flap Moment at Root for ESI-80 Machine at 36 mph Wind Speed

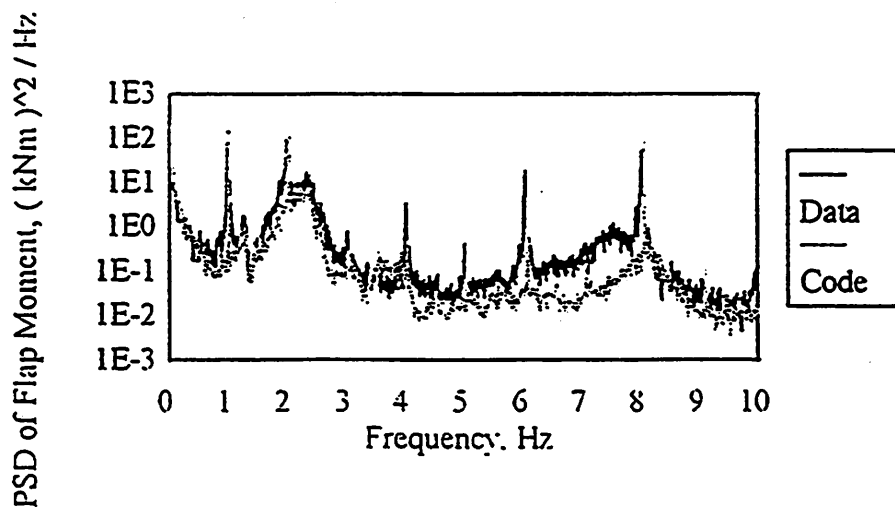


Figure 6. Power Spectral Density of Blade Flap Moment at Root for ESI-80 Machine at 36 mph Wind Speed

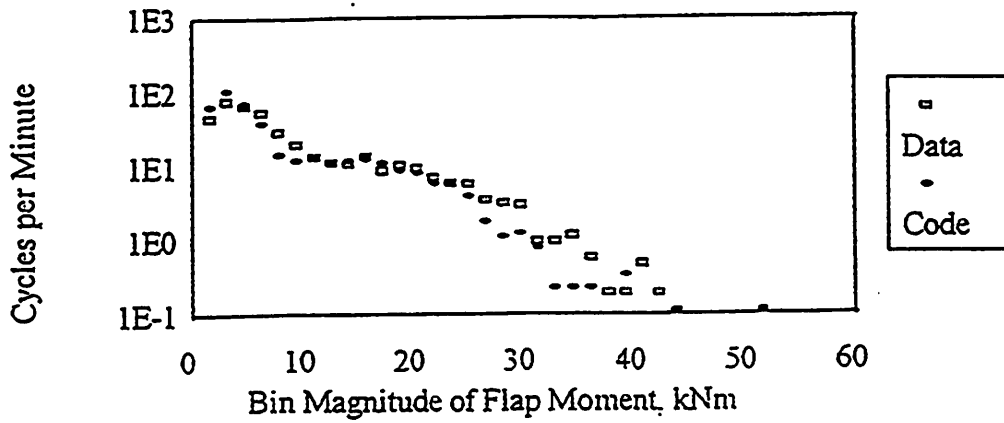


Figure 7. Rainflow Cycle Counting for the Blade Root Flap Moment for ESI-80 Machine at 36 mph Wind Speed

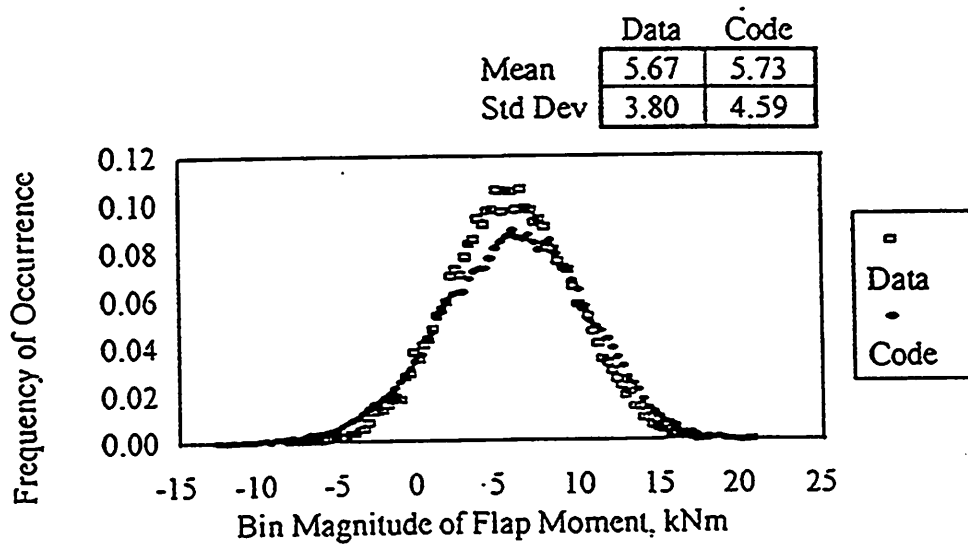


Figure 8. Occurrence Histogram of Blade Flap Moment at Root for ESI-80 Machine at 23 mph Wind Speed

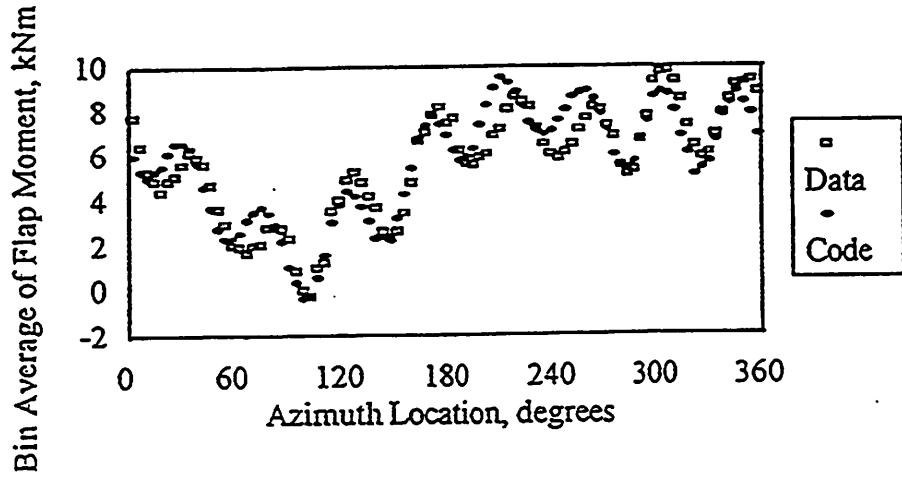


Figure 9. Azimuth Binning of Blade Flap Moment at Root for ESI-80 Machine at 23 mph Wind Speed

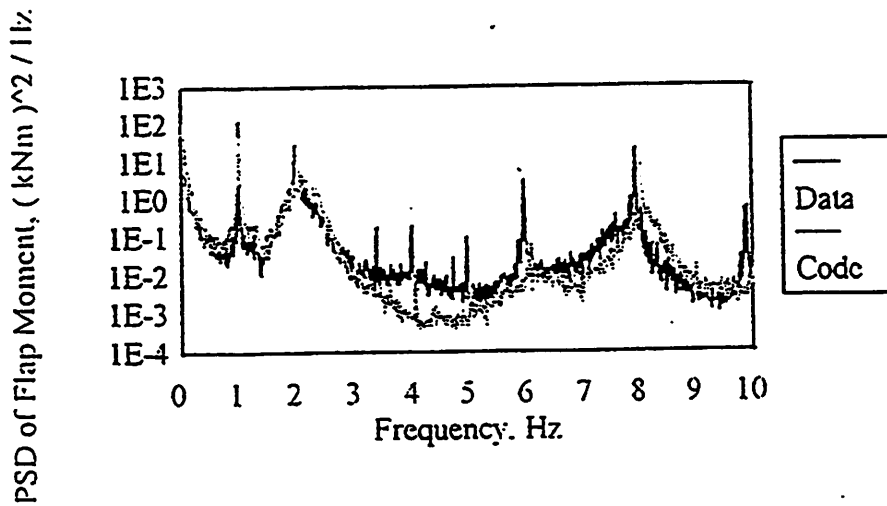


Figure 10. Power Spectral Density of Blade Flap Moment at Root for ESI-80 Machine at 23 mph Wind Speed

1.005 Hertz, the differences are believed to be associated with the digitization of the data from the analog tape (Wright, 1991).

Rainflow cycle counting is shown in Figure 11 where root flap cyclic moment count is shown at 22.6 mph. The results shown in this figure show as good agreement with the test data as the previous figures. The 60% blade station cyclic count is shown in Figure 12. Agreement between the code and test data is again good.

OTHER OUTPUT

In addition to the quantities previously illustrated, there are a number of variables of interest for which ESI-80 test data is not available. Paramount of these quantities is the blade edgewise bending moment. Figure 13 shows the blade root edgewise bending moment at 36.1 mph. Shown in Figure 13 are the rainflow cycle count for fixed speed operation. The code was run using both fixed and variable speed operation and the difference in calculated loads was found to be minor. The rainflow cycle count shows the characteristic behavior of a bi-modal distribution, the large number of low amplitude cycles being due to the gravity loads that occur once per rotor revolution. Figure 14 shows the distribution of the calculated angle-of-attack near the blade tip for both wind speeds. While comparison data is not available, such plots may be useful in determining the magnitude and the frequency of large angle-of-attack excursions.

Finally, Figures 15 and 16 show the calculated blade tip deflection, including the effects of blade teeter and elastic flatwise bending, at a wind speed of 36.1 mph. Again, while test data is not available for the tip deflection, such calculations would be of use to a wind turbine designer. Figure 15 shows the occurrence distribution of the tip deflection while Figure 16 shows the azimuth-binned distribution of tip deflection.

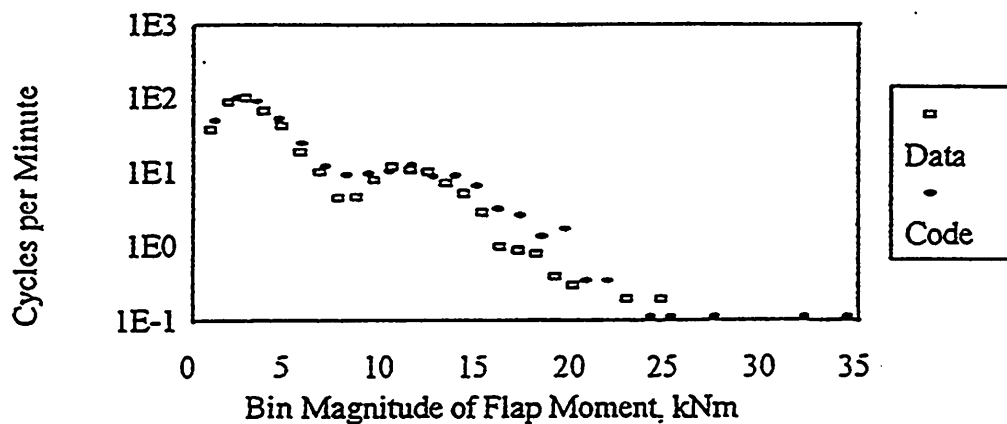


Figure 11. Rainflow Cycle Count of Blade Flap Moment at Root for ESI-80 Machine at 23 mph Wind Speed

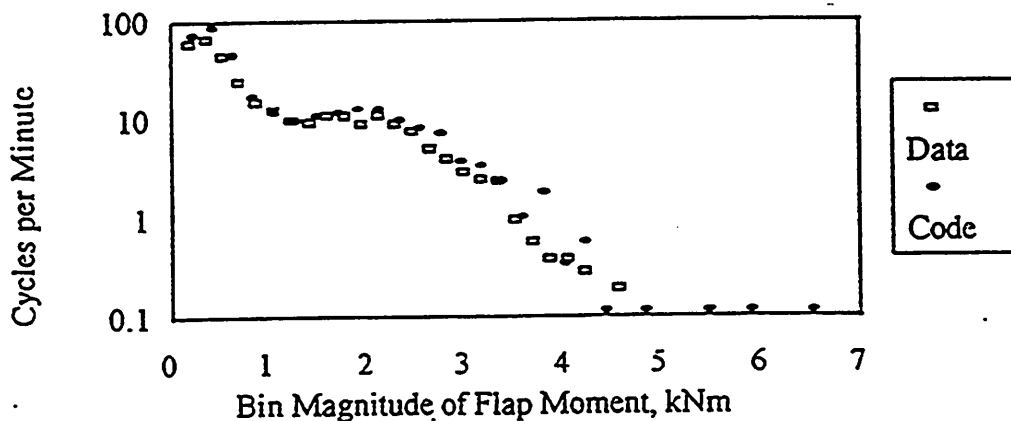


Figure 12. Rainflow Cycle Count of Blade Flap Moment at 60% Blade Station for ESI-80 Machine at 23 mph Wind Speed

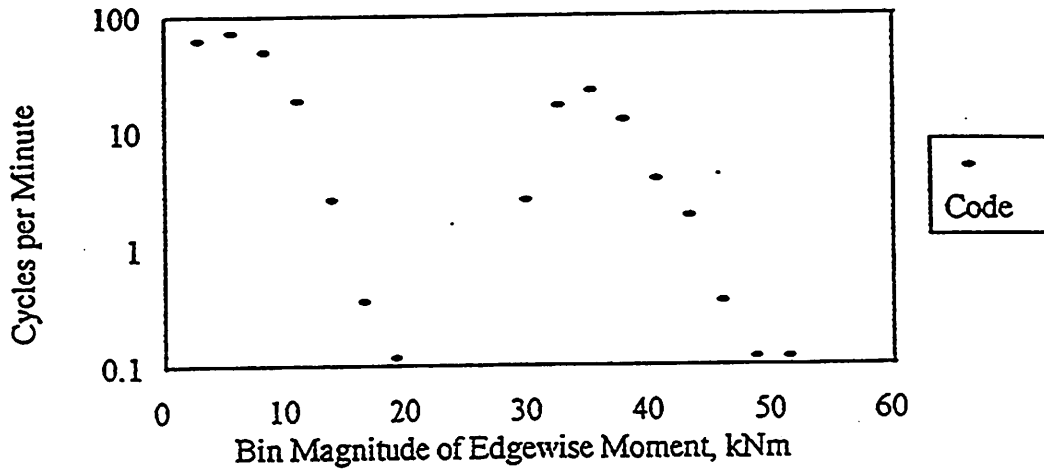


Figure 13. Calculated Rainflow Cycle Count for the Blade Root Edgewise Bending Moment at 36.1 mph

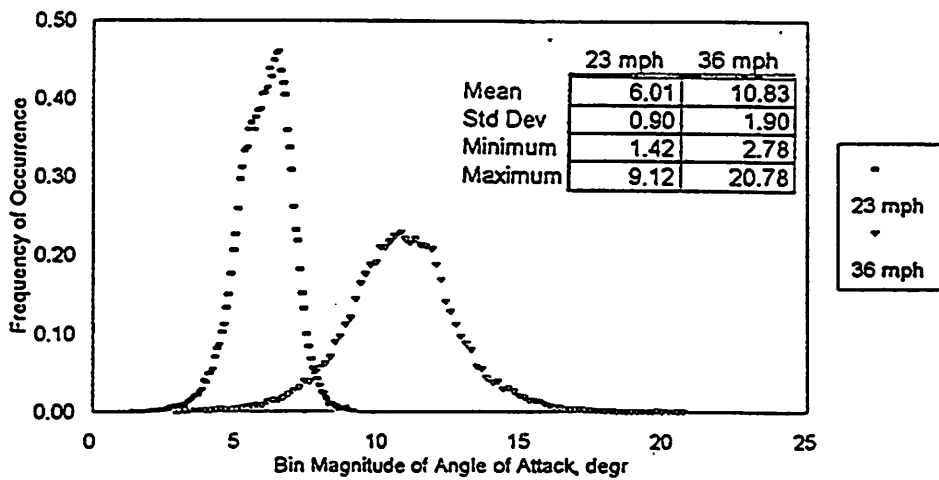


Figure 14. Calculated Frequency Distribution of the Angle-of-Attack Near the Blade Tip for the ESI-80

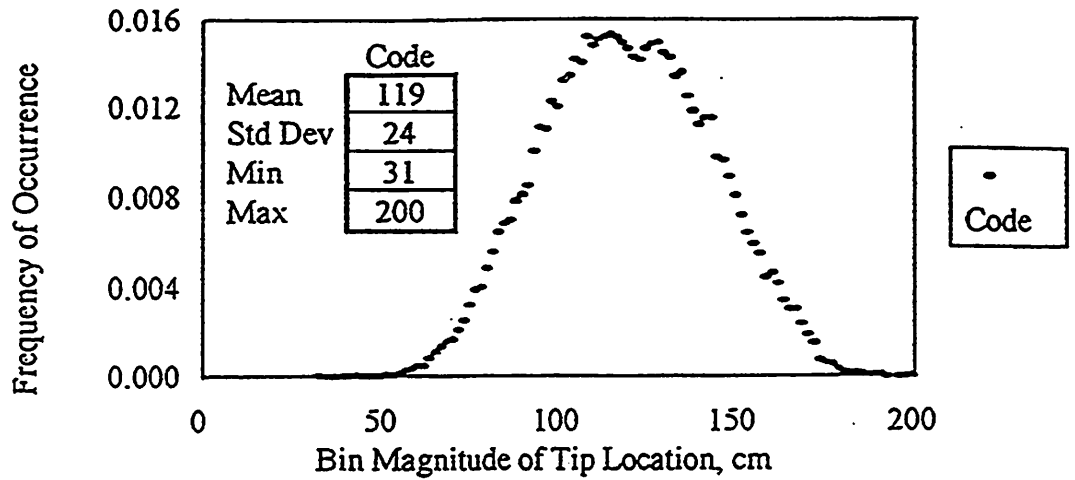


Figure 15. Calculation Frequency Distribution of the Blade Tip Deflection of the ESI-80 Operating at 36.1 mph

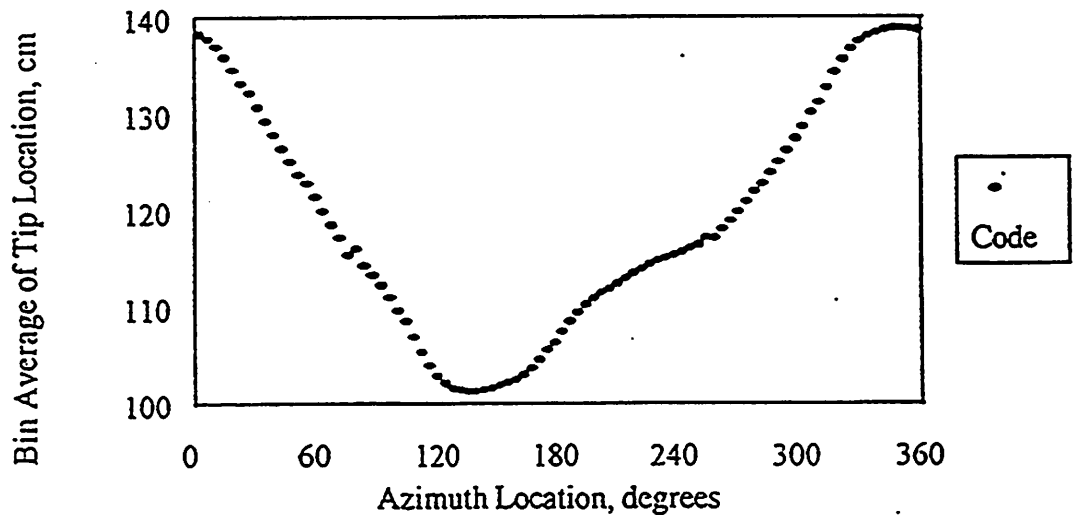


Figure 16. Calculated Azimuth-Binned Blade Tip Deflection of the ESI-80 Operating at 36.1 mph

CONCLUSIONS

Comparison of ESI-80 test results for the root flapwise bending moment have been made with calculations from the FAST Code. The comparisons have been made at mean wind speeds of 22.6 and 36.1 mph and cover occurrence histograms, azimuth averaged bin plots, power spectral density distributions, and rainflow counting. Based on the results shown in Figures 1 through 12 it is our opinion that the FAST Code is capable of good accuracy in the determination of stochastic blade bending loads on the ESI-80 wind turbine. Calculations have been made using both fixed and variable rotor angular velocity and it is concluded that the blade flatwise loads and teeter motion are adequately determined for the ESI-80 using a constant rotor angular velocity.

REFERENCES

Bywaters, G., October 1992, Personal Communication.

McCoy, T.J., January 1992, "Development of Stochastic Loads for the Design of an Advanced Wind Turbine," *Eleventh ASME Wind Energy Symposium Proceedings*, edited by Veers and Hock, ASME, New York.

Musial, W.D., Butterfield, C.P., and Handman, D., 1985, "ESI-80/EPRI Test Program," EPRI Research Project RP1996-A, Final Draft Report.

Veers, P.S., 1984, "Modeling Stochastic Wind Loads on Vertical Axis Wind Turbines," SAND83-1909, Sandia National Laboratory.

Wilson, R.E., Walker, S.N., and Freeman, L.N., July 1994, "Advanced Dynamics Code Development," OSU/NREL Report 94-01, Phase III Annual Technical Progress Report, Mechanical Engineering Department, Oregon State University, Corvallis, OR.

Wright, A.D., August 1991, Digitized ESI-80 Test Data, (unpublished), SERI.

Wright, A.D. and Butterfield, C.P., 1992, "The NREL Teetering Hub Rotor Code: Final Test Results and Conclusion," *Eleventh ASME Wind Energy Symposium Proceedings*, edited by Veers and Hack, ASME, New York.

“Prediction of H.A.W.T. blade stall and performance”

G. Giannakidis and J.M.R. Graham

Dept. of Aeronautics

Imperial College

London

tel: +44 171 5945043

Fax: +44 171 5848120

email: g.giannakidis@ic.ac.uk

m.graham@ic.ac.uk

Abstract

A model is being developed for the prediction of Horizontal Axis Wind Turbine blade stall and performance coupled with a simple aeroelastic analysis model. For the aerodynamic calculation a two dimensional unsteady Navier-Stokes solver on a sectional basis on the blade is coupled with a three dimensional vortex lattice wake. Pressure coefficient distributions are calculated from the two dimensional viscous flow in each blade section. The aerodynamic computations are coupled with a vibrating beam model in order to incorporate flapwise deformations of the blade.

1 Introduction

The majority of three dimensional computations for flow around HAWTs presented until today are inviscid (Hansen et al [6], Zervos et al [17], Simoes et al [13], de Vries [1], Wood [16], Pasmajoglou et al [11]). All the approaches use some kind of representation for the wake (vortex lattice, vortex particles, vortex lines) and calculate the three dimensional effects on the rotor blade. Dynamic stall, which is an important phenomenon in this kind of flow is usually treated by means of empirical methods. However a fully three dimensional viscous calculation would be extremely expensive in computational time.

Therefore the present approach was to compromise and use a two dimensional viscous calculation on sections of the rotating blade, since viscous effects are expected to be dominant in the vicinity of solid surfaces, coupled with a three dimensional vortex lattice model for the wake. The consideration of two dimensional sections on the blade is analogous to the blade element theory, that is commonly used for engineering calculations (de Vries [1]), but with a better wake

model. However it has been shown by experiments that three dimensional effects are important on the blade sections that are close to the rotor hub under stall conditions. Therefore the incorporation of the quasi-three dimensional approach by Sorensen et al [14] in the present model will be the next step. In the present model sections on only one blade of the wind turbine are modelled using the two dimensional Navier-Stokes approach due to the high computational cost involved. The other blades are modelled using the vortex lattice method developed by Pesmajoglou and Graham [11]. The aerodynamic computations are coupled with a simple one dimensional vibrating beam model for the incorporation of aeroelastic effects in the flapwise direction.

2 Solution of the two dimensional Navier-Stokes equations

2.1 Velocity - Vorticity formulation of the equations

On each blade section the velocity-vorticity formulation of the Navier-Stokes equations was considered on a rotating frame of reference (Speziale [15]). The two dimensional equations for the velocity and vorticity in vector form are written:

$$\nabla^2 \vec{u} = -\nabla \times \vec{\omega} \quad (1)$$

$$\frac{D\vec{\omega}}{Dt} = \nu \nabla^2 \vec{\omega} \quad (2)$$

For the numerical solution a time split approach is followed in which diffusion of vorticity is treated on an unstructured finite element mesh whereas convection is treated in an Lagrangian approach through the introduction of point vortices (see Graham [4], Graham and Cozens [5], Meneghini [8]).

At the beginning of the time step $n+1$ the velocity field is calculated through the two equations for the two components of velocity:

$$\frac{\partial^2 u}{\partial x^2} + \frac{\partial^2 u}{\partial y^2} = -\frac{\partial \omega}{\partial y} \quad (3)$$

$$\frac{\partial^2 v}{\partial x^2} + \frac{\partial^2 v}{\partial y^2} = \frac{\partial \omega}{\partial x} \quad (4)$$

These two Poisson's equations are discretised through a Galerkin formulation on an unstructured finite element mesh (Figure 1) generated by FELISA (see [10]).

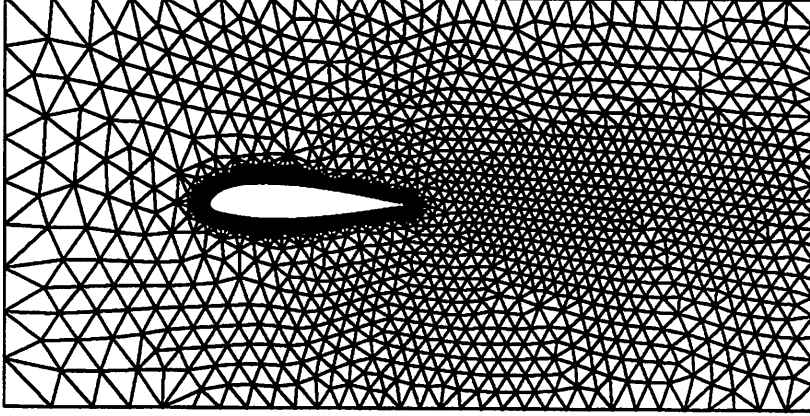
The main problems are the boundary conditions on a solid wall. In order to enforce the zero normal velocity condition a Neumann boundary condition was used as follows.

On the body surface the velocities are written as a function of a component u_n normal to the boundary segment and a component u_s tangential to it:

$$u = u_s \cos \theta - u_n \sin \theta$$

$$v = u_s \sin \theta + u_n \cos \theta$$

Figure 1: Two dimensional unstructured mesh



where $\cos \theta$ is the direction cosine of the boundary segment. Then

$$\frac{\partial u}{\partial n} = \frac{\partial u_s}{\partial n} \cos \theta - \frac{\partial u_n}{\partial n} \sin \theta$$

$$\frac{\partial v}{\partial n} = \frac{\partial u_s}{\partial n} \sin \theta + \frac{\partial u_n}{\partial n} \cos \theta.$$

Using continuity and the definition of ω :

$$\frac{\partial u_n}{\partial n} + \frac{\partial u_s}{\partial s} = 0$$

$$\omega = \frac{\partial u_n}{\partial s} - \frac{\partial u_s}{\partial n}$$

we can finally get

$$\frac{\partial u}{\partial n} = \left(\frac{\partial u_n}{\partial s} - \omega \right) \cos \theta + \frac{\partial u_s}{\partial s} \sin \theta \quad (5)$$

$$\frac{\partial v}{\partial n} = \left(\frac{\partial u_n}{\partial s} - \omega \right) \sin \theta - \frac{\partial u_s}{\partial s} \cos \theta \quad (6)$$

so that the normal derivatives of the two components of the velocity are expressed as tangential derivatives of the local components which can be calculated using a first order finite difference approximation.

Then the velocity at each node is forced to have a zero normal component through $\vec{u}^* = \vec{u}_i - \beta \vec{u}_{ni}$, where \vec{u}_{ni} is the normal velocity to node i and β is a relaxation factor usually taken $\beta = 1.5$. The velocity \vec{u}^* is then decomposed to u_n and u_s and used in equations 5, and 6. These Neumann boundary conditions

are enforced with equations 3 and 4. The value of the normal velocity at each node is checked after the solution and if it is greater than a prescribed accuracy the iteration continues.

Once the velocity field is calculated the calculation proceeds for the vorticity.

The vorticity equation is split into diffusion and convection. The diffusion equation is modelled as

$$\frac{\omega^{n+1} - \omega^n}{\Delta t} = \nu((1 - a) \nabla^2 \omega^n + a \nabla^2 \omega^{n+1}) \quad (7)$$

where for $a = 1$ the scheme is fully implicit in time while for $a = 0.5$ the Crank-Nicholson scheme is derived.

Following the Galerkin formulation for linear finite elements and discretising the vorticity as $\omega = \sum \omega_m N_m$ we get:

$$(a\nu[K] + \frac{1}{\Delta t}[L])[\Delta\omega]^{n+1} = -\nu[K][\omega]^n + [f]^n. \quad (8)$$

where the equation was modified so that at each time step the solution for the change in vorticity $\Delta\omega = \omega^{n+1} - \omega^n$ was obtained. This was done in order to increase the accuracy of the solution and to reduce the computational time needed to solve the system of equations iteratively.

For the solution of equation 8 the boundary condition used on the blade surface was that used by Koumoutsakos et al [7]. After the velocity field is calculated there is a slip velocity u_s on the solid surface which can be considered as a spurious vortex sheet. In order to satisfy the no-slip condition, vorticity must be shed into the flow. Then the circulation Γ in the flow field would be modified in the time interval $[t, t + \Delta t]$ as:

$$\oint u_s(s) ds = \int_t^{t+\Delta t} \frac{d\Gamma}{dt'} dt'. \quad (9)$$

where s is the arc length along the body surface. But Kelvin's theorem states that the rate of change of circulation in the flow field is

$$\frac{d\Gamma}{dt} = -\nu \oint \frac{\partial\omega}{\partial n}(s) ds. \quad (10)$$

so from the two equations above we get

$$\nu \int_t^{t+\Delta t} \frac{\partial\omega}{\partial n} dt = -u_s(s) \quad (11)$$

and considering $\partial\omega/\partial n$ to be constant over Δt we get

$$\frac{\partial\omega}{\partial n} = -\frac{u_s}{\nu\Delta t} \quad (12)$$

which gives a Neumann boundary condition on the solid wall. For the outer boundaries of the domain, ω was set to zero at inflow and $\vartheta\omega/\vartheta n = 0$ at outflow.

Once the change in ω at each node point is calculated it must be convected. At the first time step point vortices are introduced at nodes where there are changes in the vorticity, which have a strength $\Gamma_i = \omega_i A_i$ where A_i is an area associated with each node. In subsequent time steps the change in ω at each node is put back to the point vortices that contributed to that node in a way that conserves the total circulation.

The point vortices are then convected with the local velocity using a first order scheme:

$$x_k^{n+1} = x_k^n + u^{n+1}(x_k^n, y_k^n)\Delta t \quad (13)$$

$$y_k^{n+1} = y_k^n + v^{n+1}(x_k^n, y_k^n)\Delta t \quad (14)$$

The vorticity is then interpolated back onto the nodes using the shape functions of the finite element approach and the time stepping proceeds with the calculation of the velocity field again.

2.2 Pressure and Forces calculation

In the two dimensional domain the equation for pressure is written as

$$\nabla^2 p = -2\left(\frac{\vartheta u}{\vartheta y} \frac{\vartheta v}{\vartheta x} - \frac{\vartheta u}{\vartheta x} \frac{\vartheta v}{\vartheta y}\right) \quad (15)$$

This is also solved using the finite element approximation described in previous sections since it is another Poisson's equation. The boundary condition for pressure on a solid surface is

$$\frac{\vartheta p}{\vartheta n} = -\nu \frac{\vartheta \omega}{\vartheta s} \quad (16)$$

where $\vartheta\omega/\vartheta s$ is calculated using first order finite differences. On the inflow boundary and the upper and lower boundaries of the domain p is set to a constant reference value (usually zero). On the outflow boundary a traction free boundary condition (Donea et al [2], Mittal et al [9]) was enforced stating

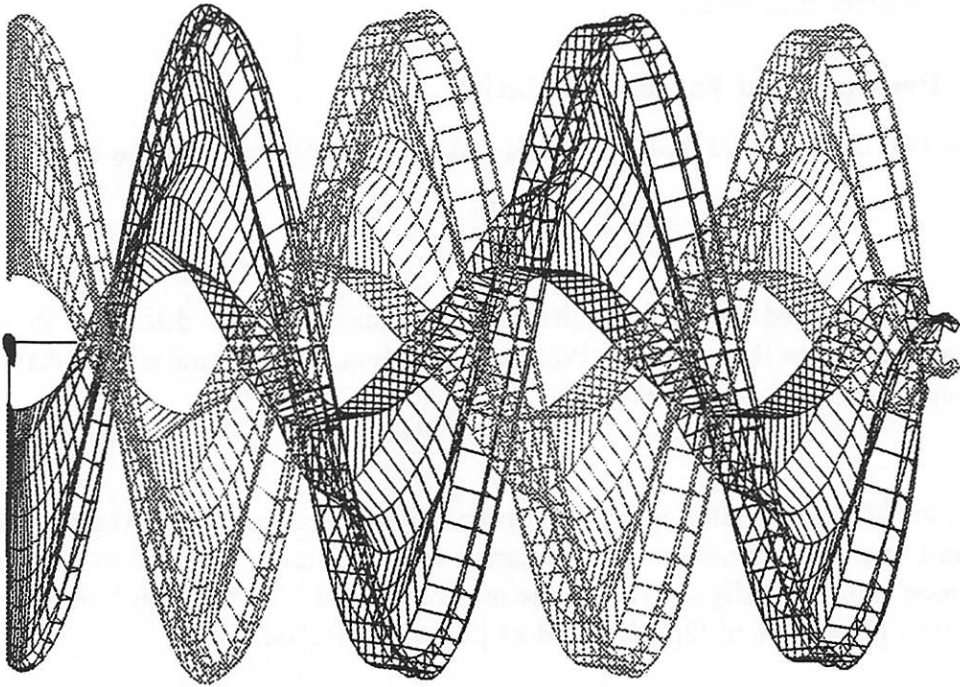
$$p = -2\nu \frac{du_s}{ds}$$

Once the pressure is calculated at the nodes on the body it can be integrated to give the forces on it. The frictional forces are simply calculated from the expression $\tau_w(s) = -\mu\omega(s)$.

3 The vortex lattice model

In order to model the wake of a H.A.W.T. an unsteady vortex lattice method is used (Pesmajoglou et al [11]). So the circulation produced in the viscous calculations described in Section 2 for one blade is shed into the wake using the coupling procedure described in Section 4. Once the circulation is shed into the wake it is treated as a three dimensional inviscid vortex lattice (Figure 2). The other blades of the wind turbine are modelled by an unsteady lattice. In each time step the new strength of each of these bound lattice is calculated using an equation of the form $\Gamma = A^{-1}U_n$, where U_n is the total velocity normal to the blade at the control point of each lattice and A^{-1} is the inverse matrix of influence coefficients. Then a lattice is shed in the wake equal in strength to the last bound lattice.

Figure 2: Vortex lattice wake of a two bladed rotor



Each node of a vortex line in the wake is then convected by the local velocity $\vec{U} = \vec{U}_\infty - \vec{\Omega} \times \vec{r} + \vec{U}_{ind}$, where \vec{U}_∞ is the free-stream velocity, $\vec{\Omega} \times \vec{r}$ is the velocity of the rotating frame of reference bound to the blade of the wind turbine and \vec{U}_{ind} is the velocity induced by all the lattice in the wake.

According to the Biot-Savart law the velocity induced at a point P by a three

dimensional vortex line extending from point A to point B is:

$$\vec{Q}_i = \frac{\Gamma}{4\pi} \vec{r}_A \times \vec{r}_B \left(\frac{1}{r_A} + \frac{1}{r_B} \frac{1}{r_A r_B + \vec{r}_A \vec{r}_B} \right) \quad (17)$$

So the total induced velocity would be $\vec{U}_{ind} = \sum_{i=1}^K \vec{Q}_i$ where K is the total number of vortex lines in the wake.

The main problem of this inviscid approach is the fact that when vortex lines approach each other, unrealistically high induced velocities appear. In order to overcome this a ‘‘vortex core’’ method (Scully [12], Simoes [13]) was applied (see also Pesmajoglou et al [11]). So the velocity induced at a field point by a vortex line of strength Γ was multiplied by:

$$\frac{r_h^2}{r_h^2 + r_c^2} \quad (18)$$

where r_h is the minimum distance between the vortex line and the field point and r_c is the vortex core radius. This is taken equal to:

$$r_c(t) = \sqrt{\frac{\kappa\Gamma}{\pi} \Delta t + r_0^2} \quad (19)$$

where $\kappa = 0.095$ is a constant and r_0 is the core radius at the beginning of the time step Δt . The core radius is taken to be zero when the vortex element is shed in order to model very approximately the effect of the viscous diffusion of vorticity in the wake.

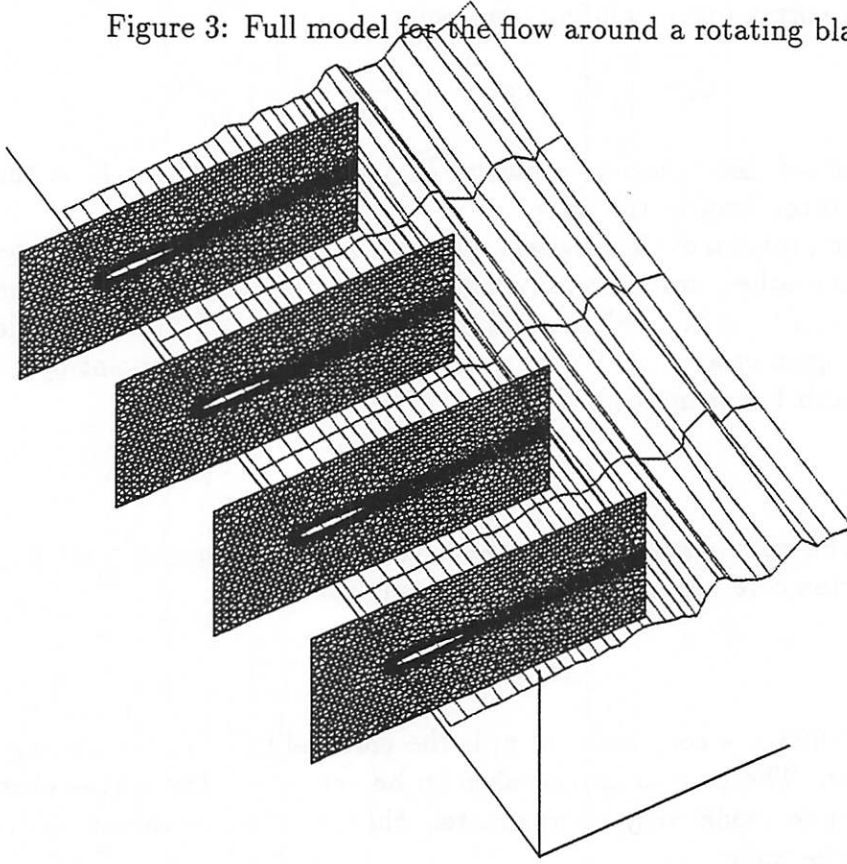
In order to reduce the computational effort the wake was frozen after one revolution of the rotor, and so was simply convected with the free stream velocity. Also an amalgamation procedure was used for the lattice in the wake which significantly reduced their number.

4 Coupling of blade and wake calculations

The final step in the implementation of the present method is the coupling of the approaches described in Sections 2 and 3. So the three dimensional blade is divided into a number of two dimensional sections (see Figure 3). On each of these sections the two dimensional Navier-Stokes equations, in the velocity-vorticity formulation, are solved. The vorticity that is created in the form of point vortices in each section is turned into a set of three dimensional vortex lines. In order to do this, the two dimensional domain is divided into a number of regions. In each region a vortex line is created of strength $\Gamma = \sum \Gamma_i$, where Γ_i is the strength of each point vortex in this region. This vortex line is placed at the ‘‘centre of vorticity’’:

$$x = \frac{\sum |\Gamma_i| x_i}{\sum |\Gamma_i|}, \quad y = \frac{\sum |\Gamma_i| y_i}{\sum |\Gamma_i|}. \quad (20)$$

Figure 3: Full model for the flow around a rotating blade.



Once these lines reach the outflow boundary of the finite element domain, they are released in the wake and they are treated as part of the three dimensional vortex lattice using the method described in Section 3.

The coupling between the two approaches is done through the boundary conditions on the outer boundaries of the finite element domain (see Egolf et al [3]). So the velocity at each boundary node is set equal to the free stream plus the velocity induced by the lattice in the wake. Also the effect of the lattice in the finite element domain on the external velocity field is taken into account.

The Navier Stokes equations in the rotating frame of reference bound to the blade do not need to be modified in this particular case. However the pressure has to be modified. So the equations of section 2.2 hold for the “modified pressure”:

$$P = p + \frac{1}{2}(\vec{\Omega} \cdot \vec{r})^2 - \frac{1}{2}\Omega^2 r^2 \quad (21)$$

where $\vec{\Omega}$ is the rotational velocity and \vec{r} is the position vector.

The following non-dimensionalisation is used for the quantities in the finite element domain at a section of spanwise position L_z and of chord c :

$$u' = \frac{u}{U}, \quad v' = \frac{v}{U}$$

$$\omega' = \frac{\omega c}{U}, \quad t' = \frac{tU}{c}$$

where $U = (|U_\infty|^2 + |\Omega L_z|^2)^{1/2}$ is the total external velocity for this section. The same non-dimensional time step is used for all the two dimensional sections, which is smaller than the time step used for the wake calculation.

For the pressure calculation in the finite element domain of each section the boundary conditions are given from the unsteady Bernoulli equation for the outer flow:

$$p = p_\infty + \frac{1}{2}(U^2 - q^2) - \frac{\partial \phi}{\partial t} \quad (22)$$

where q is the local velocity (including the effect of the wake lattice) and $\partial \phi / \partial t$ is the rate of change of the potential due to the unsteady motion of the wake lattice. The potential is calculated through the integration of the velocity around the boundary of the finite element domain. A reference value of zero is set for ϕ at the foremost point of the innermost section.

5 Aeroelastic model

A simple one dimensional finite element approach is taken for the study of the out of plane flapping motion of the blade. which is modelled as a cantilever beam of varying cross sectional area. So if $[y_d]$ is the vector of deformation the differential equation that governs the movement of the blade is:

$$[M][\ddot{y}_d] + ([K] + \Omega^2[K_2])[y_d] = [f], \quad (23)$$

where $[M]$ is the mass matrix, $[K]$ is the stiffness matrix, and Ω is the rotational velocity. The term $\Omega^2[K_2]$ is due to the centrifugal forces on the blade. Damping effects are neglected at this point. The distributed force vector $[f]$ is calculated from the aerodynamic part and is used as input to the aeroelastic computation.

Equation 23 is integrated in time using a Newmark method. The time step used for this calculation is smaller than the one used for the wake calculation.

The deformation and the speed of deformation is the output of the aeroelastic calculation and it is used as input for the aerodynamic calculation.

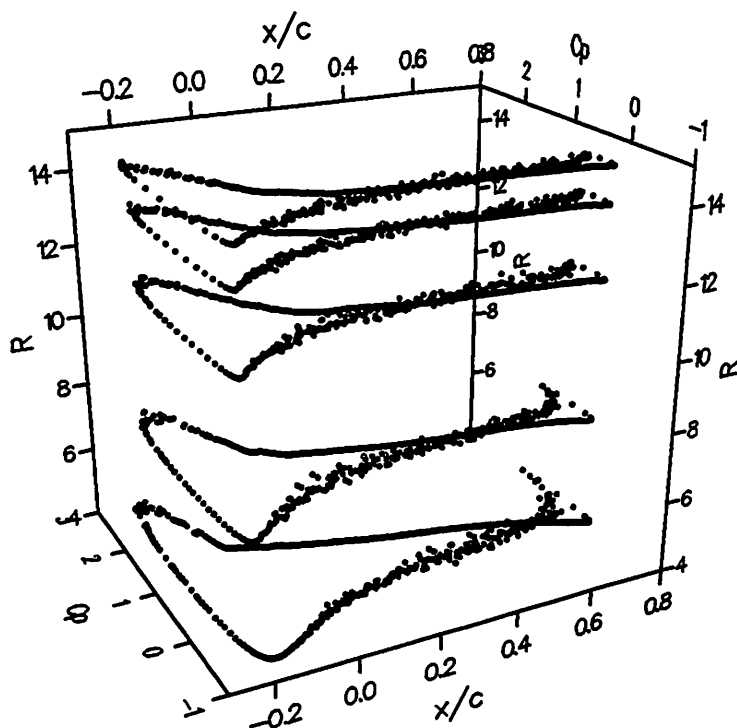
6 Some results

Some results are presented for the calculation of a HAWT with blades of 30 m diameter. The blade sections are of the NACA230xx family. Five sections were used on the first blade where the Navier-Stokes calculation was performed. The pressure distribution on these sections can be seen in Figure 4.

The wake in the case of vortex lattice computation only is shown in Figure 5 and the time variation of the force coefficients in Figure 6.

Pressure distribution

Figure 4: Pressure distribution



7 Further work

The pressure distribution on the rotating blade will be compared with experimental values in order to study the scale of the three dimensional effects on the flow.

The quasi three-dimensional approach by Sorensen [14] will be incorporated in the present scheme so that three dimensional effects on the viscous flow near the turbine blades will be taken into account as well and their effect on dynamic stall will be studied.

8 Acknowledgements

This work is supported by the European Commission, DG XII through the Human Capital and Mobility programme.

Figure 5: Wake with vibrating blades

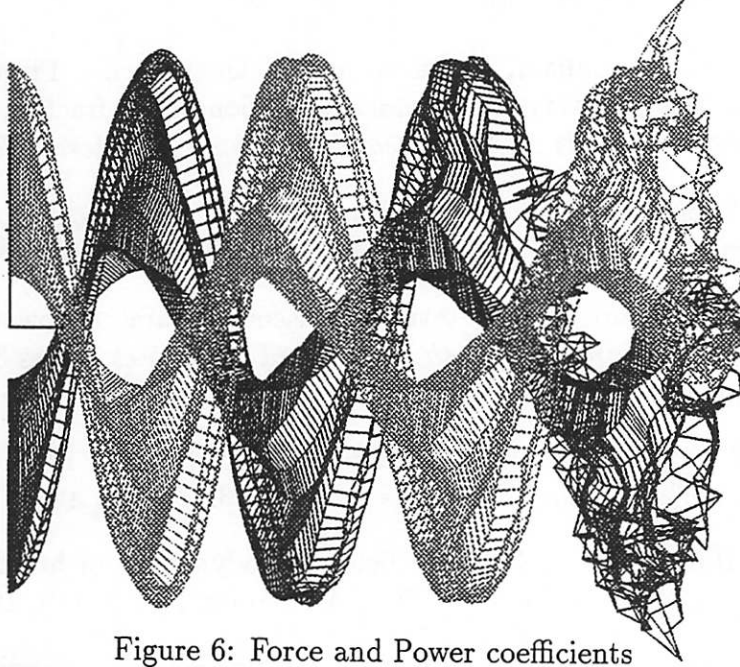
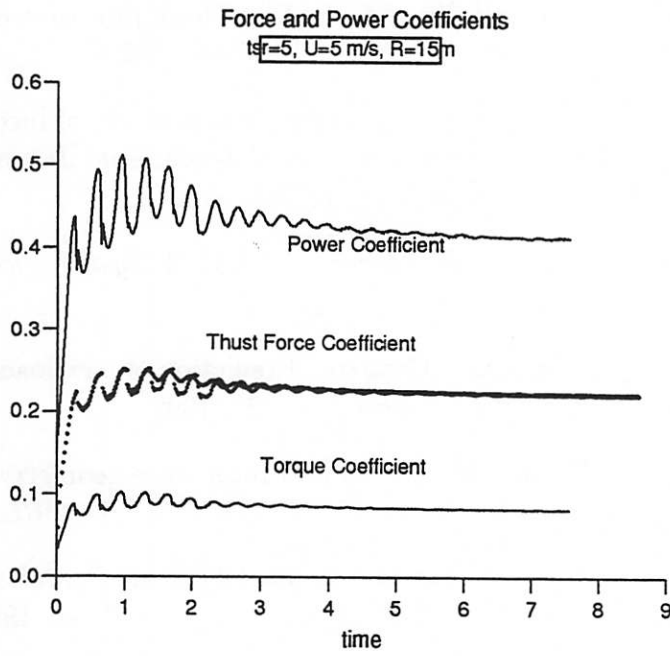


Figure 6: Force and Power coefficients



References

- [1] O. de Vries. On the theory of the horizontal axis wind turbine. *Annual Review of Fluid Mechanics*, 15:77–96, 1983.
- [2] J. Donea, S. Giuliani, H. Laval, and L. Quartapelle. Finite element solution of the unsteady navier-stokes equations by a fractional step method. *Computer methods in Applied mechanics and Engineering*, 30:53–73, 1982.
- [3] T.A. Egolf and S.P. Sparks. A full potential flow analysis with realistic wake influence for helicopter rotor airload prediction. CR 4007, NASA, 1987.
- [4] J.M.R. Graham. Computation of viscous separated flow using a particle method. In *Numerical Methods in Fluid Mechanics*, pages 310–317. Oxford University Press, 1988.
- [5] J.M.R. Graham and P.D. Cozens. Vortex shedding from edges including viscous effects. *Fluid Dynamics Research*, 3:111–114, 1988.
- [6] A.C. Hansen and C.P. Butterfield. Aerodynamics of horizontal axis wind turbines. *Annual Review of Fluid Mechanics*, 25:115–149, 1993.
- [7] P. Koumoutsakos, A. Leonard, and F. Pepin. Boundary conditions for viscous vortex methods. *Journal of Computational Physics*, 113:52–61, 1994.
- [8] J. Meneghini. *Numerical Simulation of bluff body flow control using a discrete vortex method*. PhD Thesis, Imperial College, 1993.
- [9] S. Mittal and T.E. Tezduyar. A finite element study of incompressible flows past oscillating cylinders and aerofoils. *International Journal for Numerical Methods in Fluids*, 15:1073–1118, 1992.
- [10] J. Peiro, J. Peireira, and K. Morgan. *FELISA System, Reference Manual*. 1994.
- [11] S. Pasmajoglou and J.M.R. Graham. Prediction of yaw loads on a horizontal axis wind turbine. *EWEC*, pages 420–423, 1993.
- [12] M.P. Scully. Computation of helicopter rotor wake geometry and its influence on rotor harmonic airloads. ASRL-TR 178-1, M.I.T., 1975.
- [13] F.J. Simoes. *A steady inviscid flow model for horizontal axis wind turbine rotors under high loading*. Phd thesis, Imperial College, 1991.
- [14] D.N. Sørensen, J.N. Sørensen, and P. Nygreen. Preliminary results of quasi-3D dynamic stall model. report -, Technical Univ. of Denmark, 1995.

- [15] C.G. Speziale. On the advantage of the vorticity-velocity formulation of the equations of Fluid Dynamics. *Journal of Computational Physics*, 73:476–480, 1987.
- [16] D.H. Wood. A three dimensional analysis of stall delay on a horizontal axis wind turbine. *Journal of wind engineering and Industrial aerodynamics*, 31:1–14, 1991.
- [17] A. Zervos, S. Huberson, and A. Hemon. Three dimensional free wake calculation of wind turbine wakes. *Journal of wind engineering and Industrial aerodynamics*, 27:65–76, 1988.

FLEX4

Simulation of Wind Turbine Dynamics.

Stig Øye
Department of Energy Engineering
Fluid Mechanics Section
Technical University of Denmark

Introduction.

The computer program FLEX4 has been developed at the Department of Fluid Mechanics at the Technical University of Denmark. Some highlights of the program are :

- Simulates the operation of wind turbines with 1 to 3 blades, fixed or variable speed, pitch or stall controlled.
- Simulates all major deflection modes of wind turbines, including large rotations from free yaw or teeter.
- Runs in the time-domain producing output files directly comparable to measured data.
- Simulated turbulence included in the wind input.
- Simulates transients like starts and stops by pitching or braking.
- Option for simulation of non-linear stiffness, e.g. in a teeter bearing.
- The program is developed directly for DOS-PC's using a highly efficient method giving ratios between computing time and simulated time of 1-2 on a Pentium-133 MHz PC.
- The program package includes programs for post-processing of data, i.e. interactive viewing on screen, plotting of timeseries, FFT-analysis and Rainflow-Count-routines.

Background.

The Department of Fluid Mechanics has been involved in the modelling of wind turbines since 1978. Although the work was mainly in the aerodynamics, it soon became clear that aeroelastic effects were important in load calculations for wind turbines. Therefore several aeroelastic computer codes were developed and used during design of large wind turbines.

However, these early codes either lacked generality or required excessive computer power and time. The experience with these codes and the experience from measurements obtained over the years has been used to design the FLEX4-code in a way which is believed to be much closer to optimum regarding the tradeoffs between computational efficiency and accuracy.

The result is a model with relatively few but important degrees of freedom combined with a fully nonlinear calculation of response and loads.

Aeroelastic code FLEX4, DTU

Wind model :

- mean wind and wind shear
- skewed inflow (horizontal and vertical)
- tower 'shadow'
- turbulence :
 - 3D-simulation with prescribed intensity, frequency spectrum and coherence of 3 components individually.

Rotor aerodynamics :

- Aerofoil data from tables
- Dynamic stall model (stall hysteresis)
- Induced velocities by standard strip theory + dynamic wake model

Structural model :

- Degrees of freedom :

tower	3	(2 bending, 1 torsion)
nacelle	1	(tilt)
shaft	4	(1 rotation, 2 bending, 1 torsion)
blades	3 (4)	(2 flap-, 1 (2) edgewise per blade)
total	17 (20)	(by 3 blades)
- nonlinear coupling of degrees of freedom

Dynamic calculation :

- time domain simulation
- method : integration of equations of motion for small time steps (Runge-Kutta-Nyström)

Calculation of section forces and moments :

- Fully nonlinear integration of external loads and inertia forces

Result :

- files with timeseries of loads etc. to be analyzed like measurements

Aeroelastic code FLEX4, DTU

Special features :

- Flexible generator model (nonlinear slip, variabel RPM etc.)
- Simulation of mechanical brake (at hub or generator)
- Simulation of pitch control (full span pitch incl. pitching of blade structure)
- Simulation of tip brakes (by pitching aerodynamics only)
- Simulation of control system (pitch, generator, brake, yaw)
- Simulation of teeter hub
- Simulation of nonlinear stiffnesses (gearbox/shaft torsion, teeter stops)
- Easy on/off-selection of DOF
- Well defined and low numerical damping
- Simulation of structural damping for each DOF (viscous)
- High computational efficiency (computing time to simulated time ratio less than 2 on a 133 MHz Pentium PC)

The following pages show examples of results from 3 simulations of the loads on a typical 37 m diameter 500 kW stall controlled wind turbine.

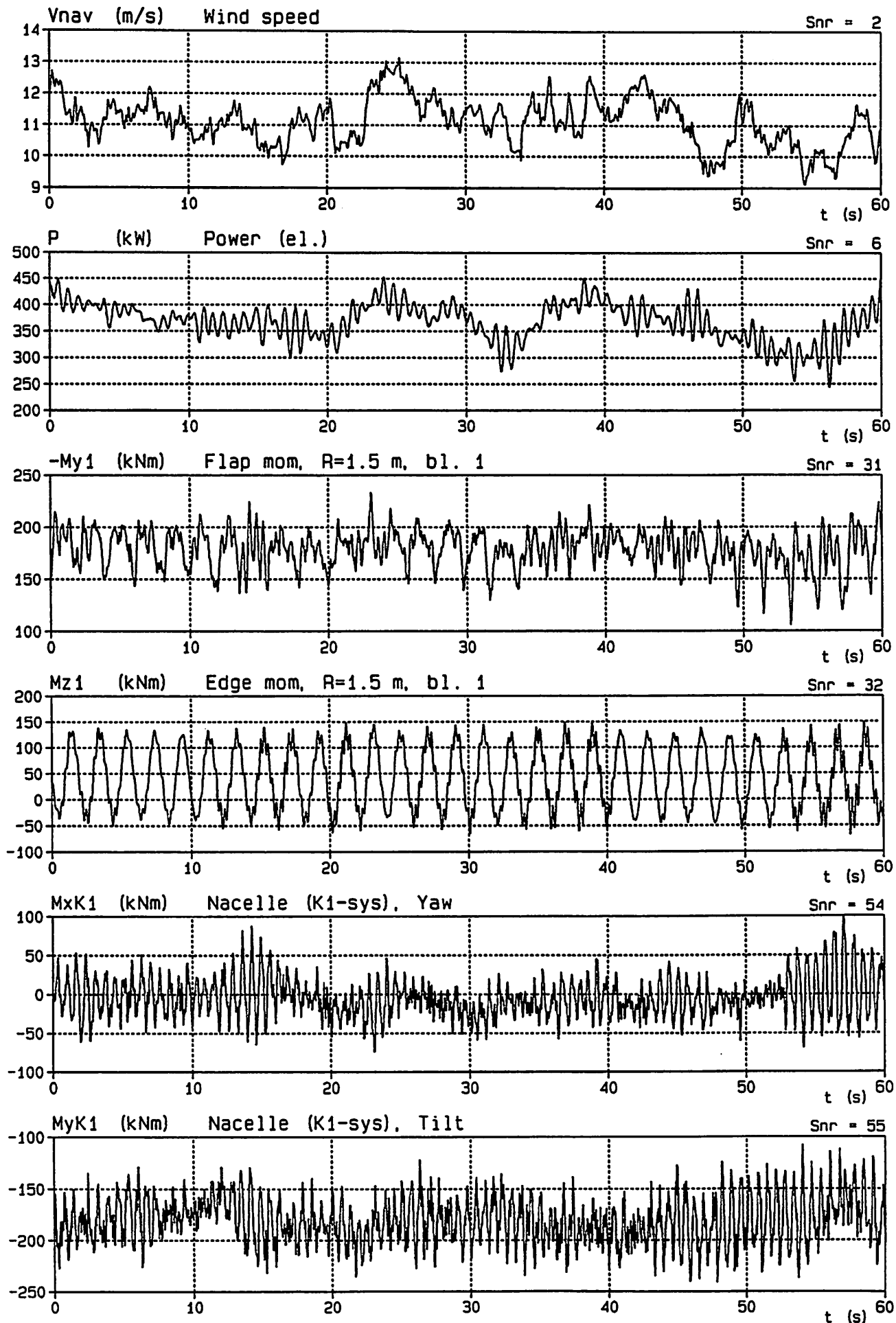
Example 1: Normal operation at 11 m/s mean wind speed and a turbulence intensity of 11%.

Example 2: Normal operation at 18 m/s (4 m/s above rated) with a turbulence intensity of 12%. The turbine shows signs of unstable edgewise vibrations.

Example 3: An example of simulation of transient operation. The generator load is lost which initiates braking on the high speed shaft and activation of the aerodynamic tip brakes.

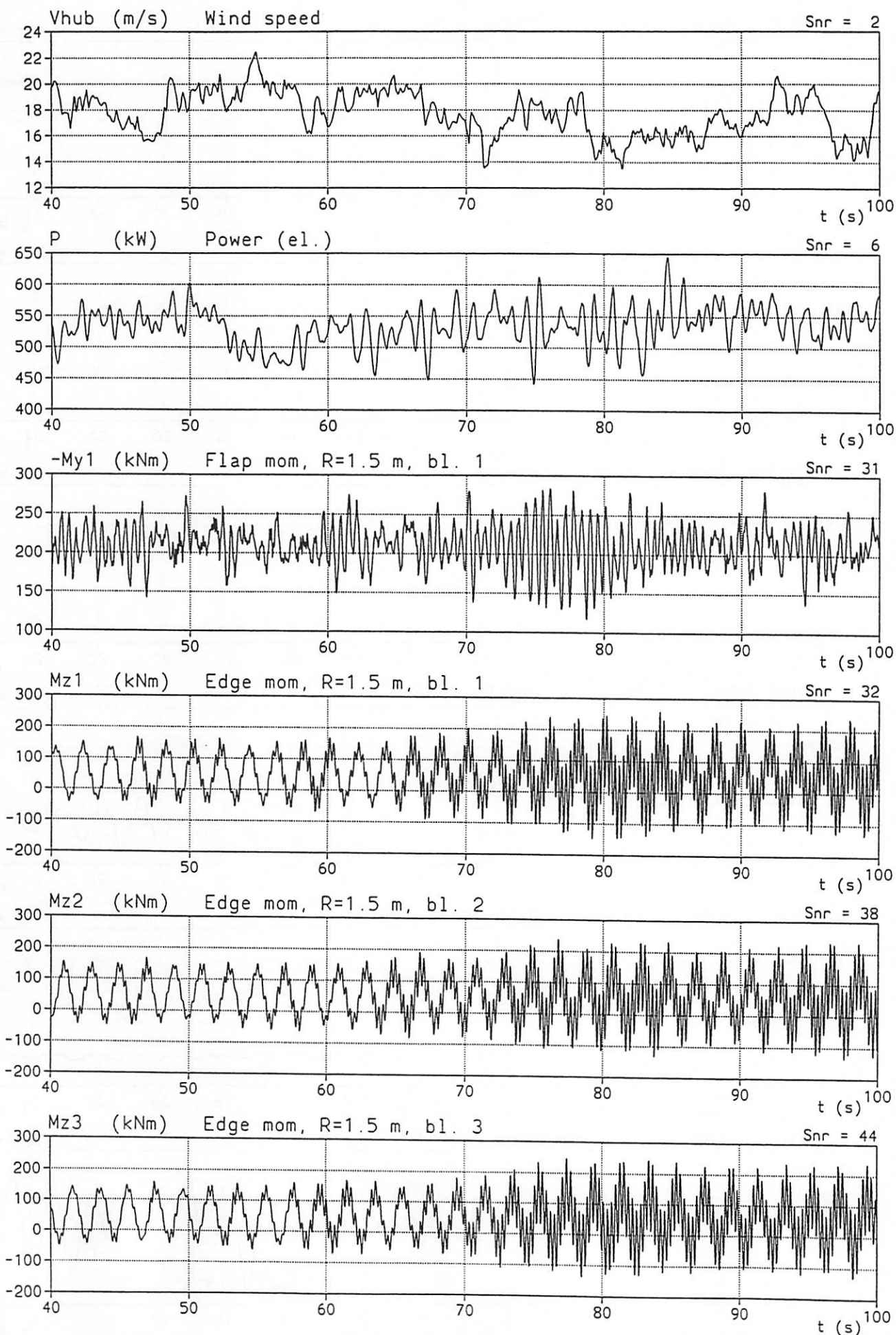
500kW/37m, V=11, Ti=0.1,

08.05.92 12:52



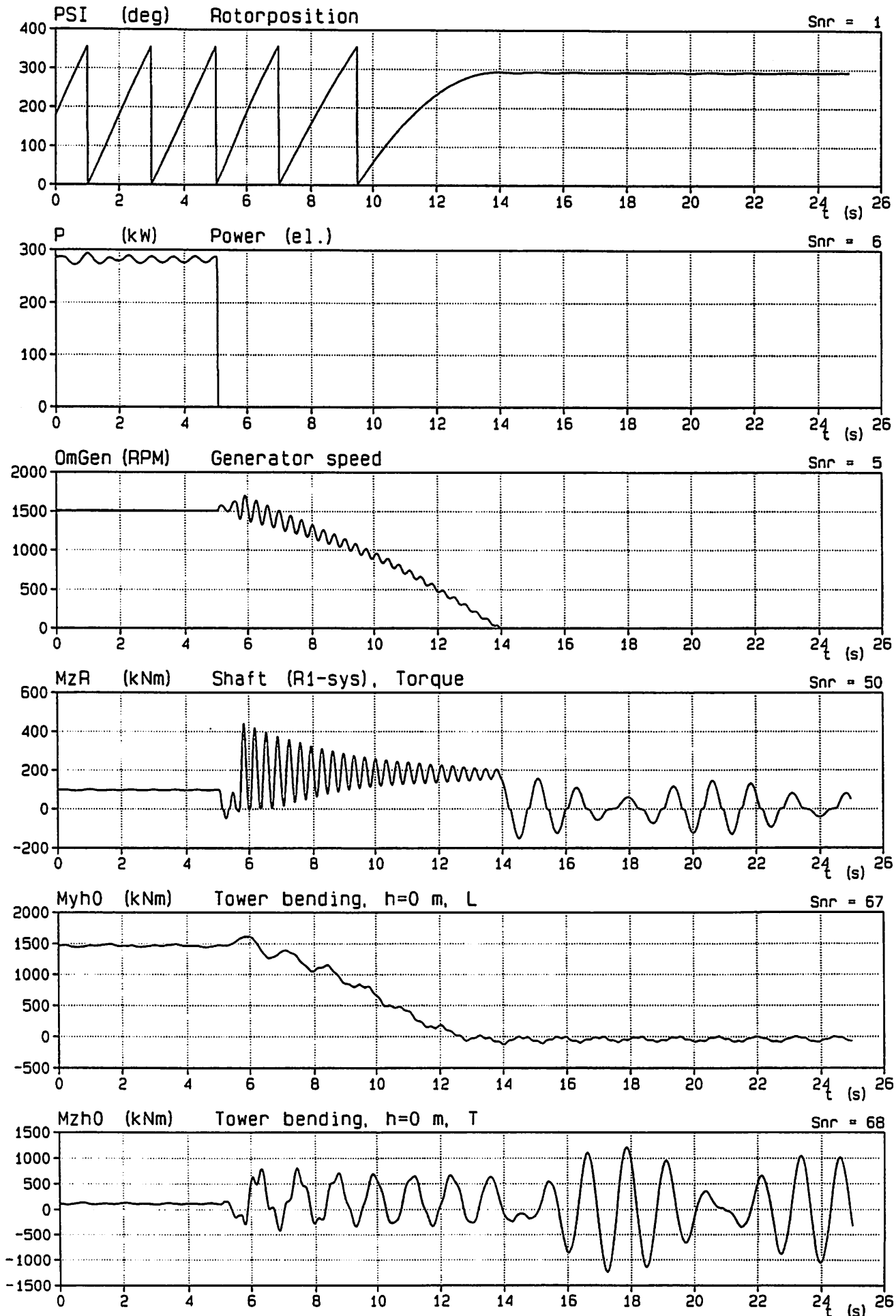
500kW/37m, V=18, ti=0.12, yaw=0

29.02.96 22:45



500kW/37m, V=10, ti=0, stop

12.03.95 18:02



Presentation at the 28:th IEA Experts Meeting,
April 11-12 1996 at DTU.

State of the Art of Aeroelastic Codes for Wind Turbine Calculations.

Hans Ganander
Teknikgruppen, Sollentuna, Sweden

The Vidyn - story.

- National wind energy R&D program (FFA, CTH and MIUU)
- 1983-87 Evaluation of the two large 2 bladed prototypes Maglarp and Näsudden
 - down/up wind
 - soft/stiff
- 1985-92 Joule projects
 - Wind Turbine Benchmark Exercise
 - Refstress
 - Dynamic Inflow

The Vidyn - story, cont'd

Verifications

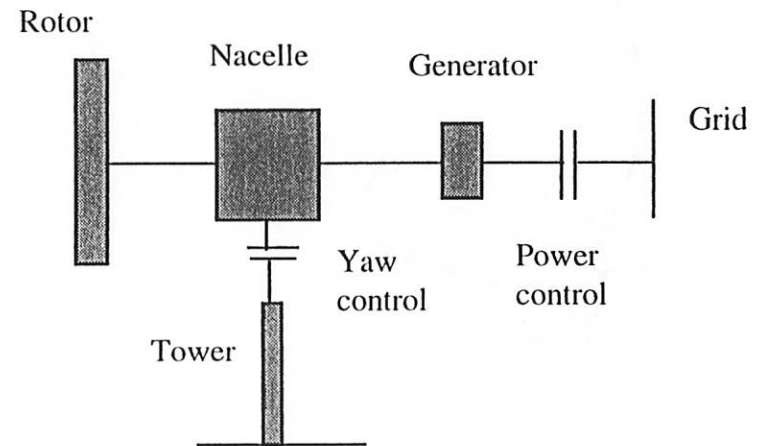
- Maglarp, 3MW, 80 m two bladed down wind, teetered, free yaw, cone 6, no tilt, soft
- Näsudden I, 2 MW, 75 m two bladed up wind, no cone, tilt 10, stiff
- Nibe B, 600 kW, 40 m three bladed up wind, yaw stability tests
- MS1, 20 m two bladed down wind, with/without teeter, flexible drive train
- Howden, 300 kW, 33 m three bladed up wind, yaw dynamics due to wake effects
- Tjaereborg, 2 MW, 60 m three bladed up wind
- Zephyr, 275 kW, 28 m two bladed individual flap hinges, partial pitch, passive control
- Hönö, 40 kW, 13.5 m two bladed up wind, variable teeter spring and cone angle. Used for teeter and yaw stability tests
- Alsvik, 180 kW, 23 m three bladed up wind, stall, wake studies
- Nordic 400, 400 kW, 35 m two bladed up wind teetered, variable speed and stall control
- Nordic 1000, 1MW, 56 m two bladed up wind teetered, variable speed and stall control

The Vidyn - story, continued

- Applications
 - Nordic 400
 - Nordic 1000
 - Zephyr 28/250
 - Näsudden II
 - Näsudden III
 - Joule projects

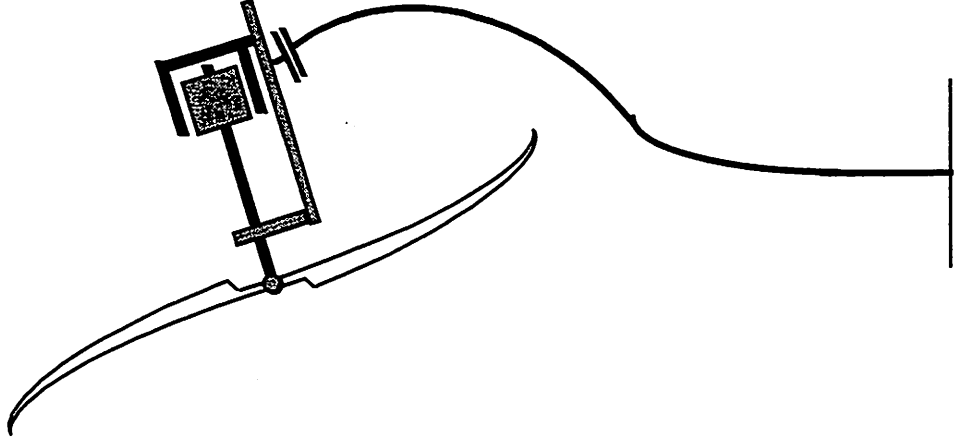
VIDYN - wind turbine simulation model

- Components
 - blade / rotor, flexible
 - nacelle, rigid
 - tower, flexible
 - drive train, flexible
 - control: pitch, rot. speed, yaw
- Some geometry parameters
 - cone angle
 - δ_3 angle
 - tilt angle
 - teeter position



VIDYN -wind turbine simulation model, cont'd

- Degrees of freedom
 - tower top translation and rotation in two horizontal directions
 - yaw angle
 - turbine and generator angles
 - teeter angle
 - flap and edge deflection modes



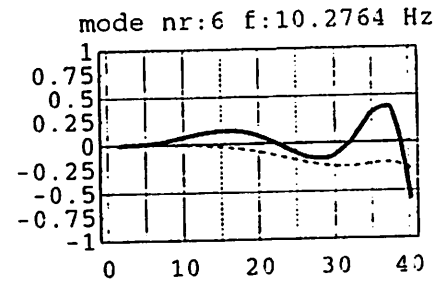
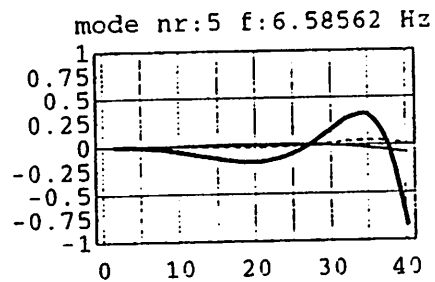
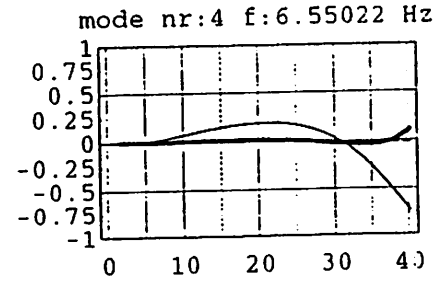
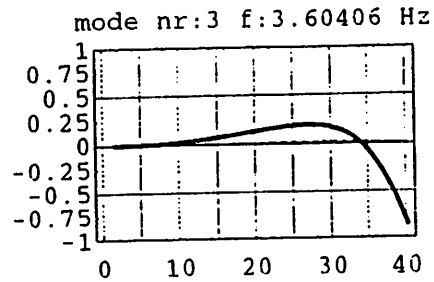
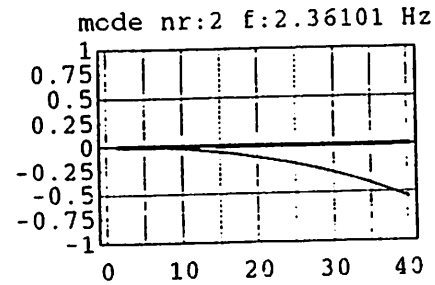
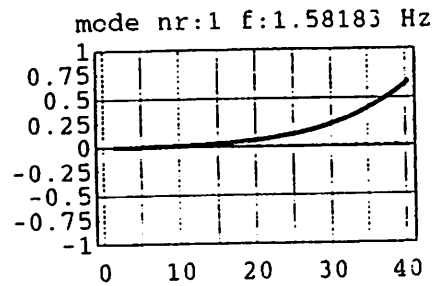
VIDYN - wind turbine simulation model, cont'd

- **Aerodynamics**
 - blade element momentum theory
 - FFA-version of Beddoe model for instationary aerodynamics
 - models for dynamic inflow phenomenas
 - tower shaddow: up/down wind, wind direction
- **Wind**
 - simple table:speed, direction and shear components (vert. and hor.)
 - measurements
 - simulated wind speed fields, with u- and v-componenets
- **Lagrange equations and numerical integration**

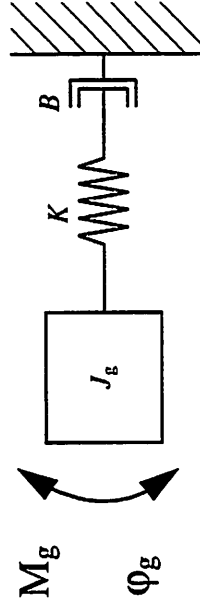
The VIDYN future

- Instationary aerodynamics
- Structure : blade / rotor, nacelle / tower
- Generator models
- Control algorithms
- Derivation of equations
- Integration methods

Extended blade mode description

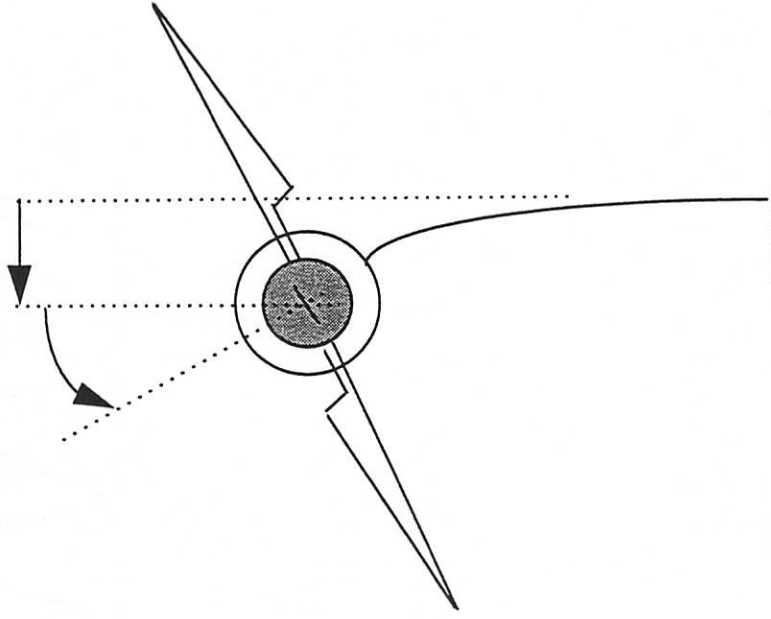


Model of induction generator



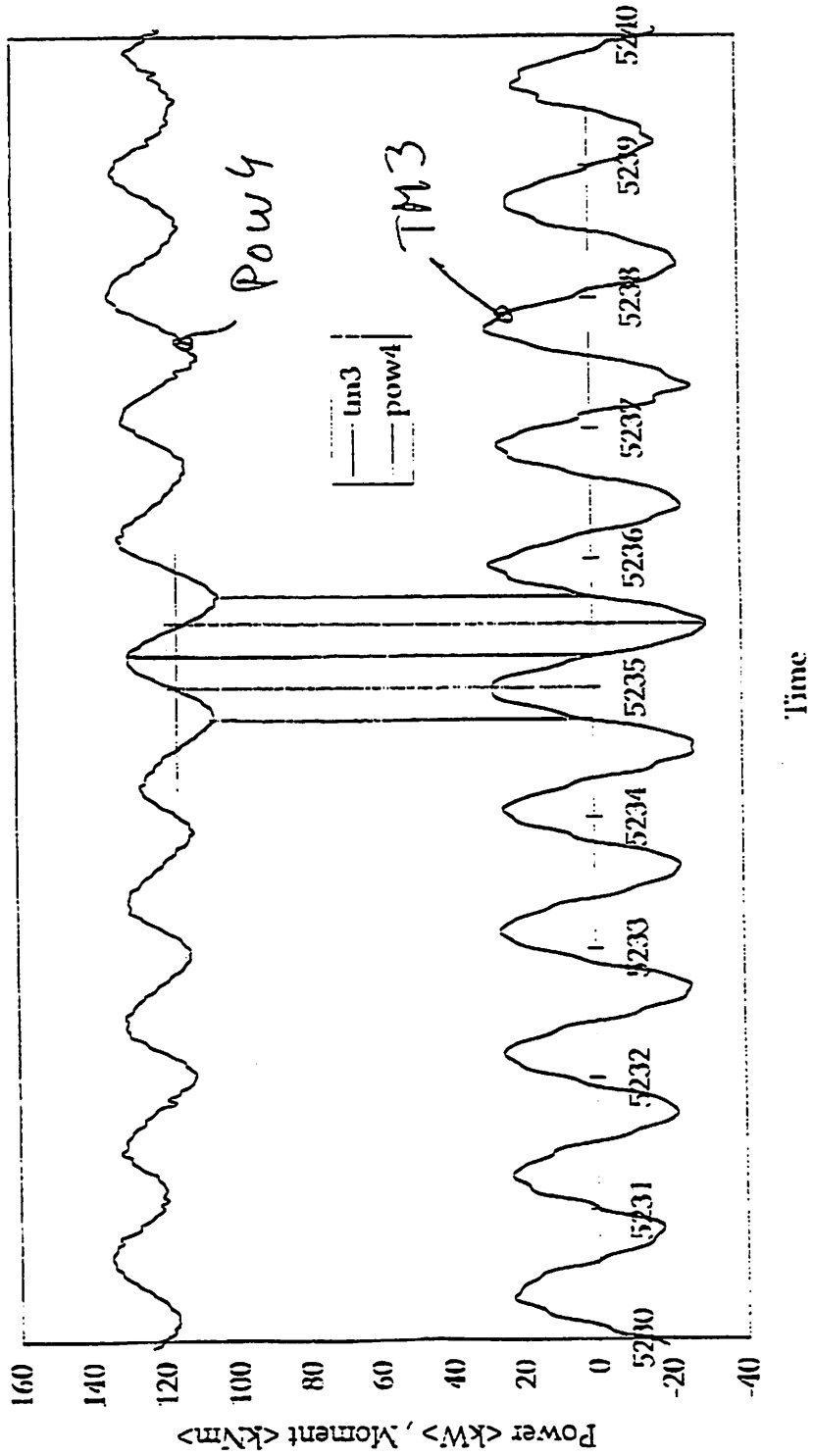
$$G_g(s) = \frac{\frac{K}{s + \frac{K}{B}}}{J_g \left(s^2 + s \frac{K}{B} + \frac{K}{J_g} \right)} = \frac{s \cdot \varphi_g}{M_g}$$

Coupling between generator and tower bending



- Tower top lateral motion ± 3 [mm]
- Corresponding angle ± 0.04 [dgr]
- Generator slip 2 % (42-42.8 rpm) at 180 kW
- Tower eigenfrequency 1.1 [hz]
- Power variation ± 10 [kW] at tower eigenfrequency
- Gear box characteristics
- Other couplings

Measured power and lateral tower bending moment



Accuracy aspects

- Design / Theory?
- Load => stress/strain => fatigue / ultimate
- Load specifications for components
- Wind and aerodynamics
- What do we need?

Need for improvements.

- **Soft designs:**
 - larger turbines
 - cost reduction
 - reduction of dependence of stiffnesses (prototype,)
- **Technical solutions which require more knowledge?**
 - stall
 - free yaw
 - variable speed
- **Structural behaviour at extremes**
- **Stability and flutter**

**NUMERICAL TECHNIQUES FOR THE IMPROVED PERFORMANCE
OF A FINITE ELEMENT APPROACH TO WIND TURBINE
AEROELASTICS**

**M.B.ANDERSON
RENEWABLE ENERGY SYSTEMS LTD
EATON COURT
MAYLANDS AVENUE
HEMEL HEMPSTEAD
UK**

**IEA R&D WIND ANNEX XI: 28th Topical Experts' Meeting
"STATE OF THE ART OF AEROELASTIC CODES FOR WIND TURBINE
CALCULATIONS"**

**TECHNICAL UNIVERSITY OF DENMARK
11 TO 12 APRIL 1996**

NUMERICAL TECHNIQUES FOR THE IMPROVED PERFORMANCE OF A FINITE ELEMENT APPROACH TO WIND TURBINE AEROELASTICS

1.0 EQUATIONS OF MOTION

The tower and rotor can be considered as separate sub-structures represented by the following equations of motion:

$$[M_T]\{\ddot{U}_T\} + [C_T]\{\dot{U}_T\} + [K_T]\{U_T\} = \{F_T\} \quad (1)$$

$$[M_R]\{\ddot{U}_R\} + [C_R + C_\Omega]\{\dot{U}_R\} + [K_R - S_\Omega]\{U_R\} = \{F_R\} \quad (2)$$

Here the subscripts refer to the tower and rotor systems respectively. The quantities C_R and C_Ω , which are derived from rotating co-ordinate effects, are the Coriolis and centrifugal softening matrices respectively. The stiffness matrix, K_R is complicated by the fact that it contains additional terms due to centrifugal stiffening.

Equations (1) and (2) can be combined into a single matrix equation as follows:

$$\begin{bmatrix} M_T & 0 \\ 0 & M_R \end{bmatrix} \begin{Bmatrix} \ddot{U}_T \\ \ddot{U}_R \end{Bmatrix} + \begin{bmatrix} C_T & 0 \\ 0 & C_R + C_\Omega \end{bmatrix} \begin{Bmatrix} \dot{U}_T \\ \dot{U}_R \end{Bmatrix} + \begin{bmatrix} K_T & 0 \\ 0 & K_R - S_\Omega \end{bmatrix} \begin{Bmatrix} U_T \\ U_R \end{Bmatrix} = \begin{Bmatrix} F_T \\ F_R \end{Bmatrix} \quad (3)$$

Denoting the time-dependent constraint relation which connects the rotor to the tower as $[T]$ then it is convenient to use a single vector $\{U\}$ to describe the displacements of the system as a whole, e.g.

$$\begin{Bmatrix} U_T \\ U_R \end{Bmatrix} = [T]\{U\} \quad (4)$$

Similar relationships can be derived for the velocities and accelerations:

$$\begin{Bmatrix} \dot{U}_T \\ \dot{U}_R \end{Bmatrix} = [\dot{T}]\{U\} + [T]\{\dot{U}\} \quad (5)$$

$$\begin{Bmatrix} \ddot{U}_T \\ \ddot{U}_R \end{Bmatrix} = [\ddot{T}]\{U\} + 2[\dot{T}]\{\dot{U}\} + [T]\{\ddot{U}\} \quad (6)$$

Substituting equations (4), (5) and (6) into (3) yields:

$$\begin{aligned} & ([T]^T [M][T])\{\ddot{U}\} + ([T]^T [C][T] + 2[T]^T [\dot{T}])\{\dot{U}\} \\ & + ([T]^T [K][T] + [T]^T [M][\ddot{T}] + [T]^T [C][\dot{T}])\{U\} = [T]^T \{F\} \end{aligned} \quad (7)$$

The vector $\{F\}$ will in general be a function of time and of the vector $\{U\}$ and its derivatives.

Through the introduction of the time dependent connection matrix $[T]$ the solution of this equation can be time consuming unless a number of simplifications are made

2.0 SIMPLIFICATIONS

As pointed out by Lobitz the connecting matrix, $[T]$ only modifies terms in the matrices associated with the tower or connection nodes, and by a judicious selection of the physical

modelling at these points certain terms in equation (7) can be simplified. For example, if the tower connection node possesses only lumped translational mass then the terms

$$[T]^T[M][T], [T]^T[M][\dot{T}] \quad \text{and} \quad [T]^T[M][\ddot{T}]$$

are time invariant and only need to be calculated once. Additionally if the tower connection node is not directly involved in any damping then also the term

$$[T]^T[C][T]$$

becomes time invariant and the term

$$[T]^T[C][\dot{T}]$$

and vanishes. Equation (7) hence simplifies to:

$$[M_o]\{\ddot{U}\} + [C_o]\{\dot{U}\} + ([K_o] + [T]^T[K][T]) = [T]^T\{F\} \quad (8)$$

and therefore the only term which requires to be calculated at each time step is

$$[T]^T[K][T]$$

3.0 INTEGRATION OF THE EQUATIONS OF MOTION

The loading vector $\{F\}$ will comprise deterministic (wind shear, tower shadow, gravity etc.) and stochastic (turbulence) components and therefore to obtain a statistically meaningful result a long integration time is required. Unless an integration scheme is used which is numerically fast and accurate then having a system with so many degrees of freedom would not be a tractable approach.

For equations of motion with constant coefficients implicit methods are unconditionally stable which allows for the arbitrary selection of the time step required to fully model the highest frequency of interest. However, the equations motion here are unfortunately contain coefficients which are time dependent and therefore unconditional stability can not always be guaranteed. An alternative approach would be through the use of a explicit integration scheme such as Runge-Kutta or a predictor corrector technique based on Gear's backward differentiation method. As the equations of motion are likely to be *stiff* then the time step required to maintain stability would be prohibitively short to allow a stochastic response to be analysed.

The technique which has been adopted here is based on the Newmark-Beta implicit integration scheme:

$${}^{t+\Delta}U = {}^tU + ((1-\delta) {}^t\ddot{U} + \delta {}^{t+\Delta}\ddot{U})\Delta t \quad (9)$$

$${}^{t+\Delta}\ddot{U} = {}^tU + {}^tU\Delta t + ((1/2 - \alpha) {}^t\ddot{U} + \alpha {}^{t+\Delta}\ddot{U})\Delta t^2 \quad (10)$$

To avoid confusion and for the sake of brevity the symbols of $[\]$ and $\{ \}$ representing matrices and vectors have been dropped.

In addition to equations (9) and (10) the equilibrium equation at time $t+\Delta t$ also requires solution:

$$M {}^{t+\Delta}\ddot{U} + C {}^{t+\Delta}\dot{U} + K {}^{t+\Delta}U = {}^{t+\Delta}R \quad (11)$$

The parameters α and δ can be determined to obtain integration accuracy and stability but are usually selected according to the equation:

$$\delta \geq 0.5; \quad \alpha \geq 0.25(0.5 + \delta)^2 \quad (12)$$

The following additional integration constants are also required:

$$a_0 = \frac{1}{\alpha \Delta t^2}; \quad a_1 = \frac{\delta}{\alpha \Delta t^2}; \quad a_2 = \frac{1}{\alpha \Delta t}; \quad a_3 = \frac{1}{2\alpha} - 1; \quad a_4 = \frac{\delta}{\alpha} - 1$$

$$a_5 = \frac{\Delta t}{2} \left(\frac{\delta}{\alpha} - 2 \right); \quad a_6 = \Delta t(1 - \delta); \quad a_7 = \delta \Delta t \quad (13)$$

At each time step the effective stiffness matrix and load is required:

$${}^{t+\Delta t} K_e = {}^{t+\Delta t} K + a_0 {}^{t+\Delta t} M + a_1 {}^{t+\Delta t} C \quad (14)$$

$${}^{t+\Delta t} R_e = {}^{t+\Delta t} R + {}^{t+\Delta t} M (a_0 {}^t U + a_2 {}^t \dot{U} + a_3 {}^t \ddot{U}) +$$

$${}^{t+\Delta t} C (a_4 {}^t U + a_5 {}^t \dot{U} + a_6 {}^t \ddot{U}) \quad (15)$$

From which the displacements can be calculated:

$${}^{t+\Delta t} K_e {}^{t+\Delta t} U = {}^{t+\Delta t} R_e \quad (16)$$

and the accelerations and velocities:

$${}^{t+\Delta t} \ddot{U} = a_0 ({}^{t+\Delta t} U - {}^t U) - a_2 {}^t \dot{U} - a_3 {}^t \ddot{U} \quad (17)$$

$${}^{t+\Delta t} \dot{U} = {}^t \dot{U} + a_6 {}^t \ddot{U} + a_7 {}^{t+\Delta t} \ddot{U} \quad (18)$$

Even though the application of this integration scheme allows for the possibility of selecting large integration steps the time dependent coefficients require that equation (16) be solved at each time step. If the system had not contained time dependent coefficients then it would have been possible to use LU decomposition with pivoting and back-substitution.

To avoid this problem recourse can be made to the fact that the effective stiffness matrix is *sparse* and only a small number of the matrix elements are varying with time. In this case the Woodbury formula which is a block-matrix version of the Sherman-Morison formula can be used.

Suppose that it is possible to write the matrix to be inverted as:

$$[A] \rightarrow [A] + \{u\} \otimes \{v\} \quad (19)$$

for some vectors $\{u\}$ and $\{v\}$. If u is a unit vector $\{e_i\}$ then equations (19) adds the components of v to the i th row. Similarly if $\{v\}$ is a unit vector $\{e_j\}$ then equation (19) adds the of U to the j th column. If both $\{u\}$ and $\{v\}$ proportional to unit vectors $\{e_i\}$ and $\{e_j\}$ respectively, then a term is added only to element a_{ij} .

The Sherman-Morrison formula gives the inverse as follows:

$$([A] + \{u\} \otimes \{v\})^{-1} = [A]^{-1} - \frac{([A]^{-1} \{u\}) \otimes (\{v\} [A]^{-1})}{(1 + \lambda)} \quad (20)$$

where $[A]$ is a N by N matrix and

$$\lambda \equiv \{v\}[A]^{-1}\{u\} \quad (21)$$

The whole procedure requires only $3N^2$ multiplies whereas standard methods require of the order of N^3 multiplies, a saving of a factor of N . The Woodbury formula extends the above to allow more than a single correction term, viz.

$$([A] + [U][V]^T)^{-1} = [A]^{-1} - ([A]^{-1}[U]([I] + [V]^T[A]^{-1}[U])^{-1}[V]^T[A]^{-1}) \quad (22)$$

where $[U]$ and $[V]$ are N by P matrices, with $P < N$. P is the number of correction terms. More often than not $[A]^{-1}$ is not explicitly kept or obtained and therefore we may use equation in the following manner:

$$\left([A] + \sum_{k=1}^P \{u_k\} \otimes \{v_k\} \right) \{x\} = \{b\} \quad (23)$$

First solve the P auxiliary equations, noting that the each vector $\{u\}$ contains only unity at the locations to be changed in the row in the k th column

$$\begin{aligned} [A]\{z_1\} &= \{u_1\} \\ [A]\{z_2\} &= \{u_2\} \\ &\dots \\ [A]\{z_k\} &= \{u_k\} \end{aligned} \quad (24)$$

and construct the matrix $[Z]$ by columns from the z 's obtained,

$$[Z] \equiv \{z_1\} \dots \{z_p\} \quad (25)$$

Next, do the P by P matrix inversion

$$[H] = ([I] + [V]^T[Z])^{-1} \quad (26)$$

Finally solve one further auxiliary problem

$$[A]\{y\} = \{b\} \quad (27)$$

In terms of the above quantities, the solution is given by

$$\{x\} = \{y\} - [Z]([H]([V]^T\{y\})) \quad (28)$$

4.0 RESULTS

Through the use of the above technique it is possible to compute the aeroelastic response of a horizontal axis wind turbine comprising:

- structural

rotor substructure	144 dof
tower substructure	48 dof
induction, synchronous or variable speed gearbox	

- aerodynamic
 - 3 blades (10 elements per blade)
 - dynamic stall
 - 6 different aerofoil types with combination of fixed or pitching elements
- control
 - stall or power regulation or speed control and shutdowns
- wind shear
- tower shadow
- turbulence
 - 8 radial points
 - 32 circumferential
 - 3 components

On a DEC Alpha Workstation the code will simulate the response in close to real-time.

5.0 LIMITATIONS

As the code is presently formulated deflections from the initial starting point have to be small and therefore its ability to fully analyse very flexible structures is limited.

GAROS, AN AEROELASTIC CODE FOR COUPLED FIXED-ROTATING STRUCTURES

Markus Rees¹⁾, Arne Vollan²⁾

¹⁾ *aerodyn* Energiesysteme GmbH

Provianthausstr. 9, D-24768 Rendsburg, Germany, Tel: ++49 - 4331 - 12750, Fax: ++49 - 4331 - 127555

²⁾ Pilatus Flugzeugwerke, CH-6370 Stans, Switzerland, Tel: ++41 - 41 - 6196677, Fax: ++41 - 41 - 6196452

1. INTRODUCTION

The GAROS (General Analysis of Rotating Structures) program system has been specially designed to calculate aeroelastic stability and dynamic response of horizontal axis wind energy converters. Nevertheless it is also suitable for the dynamic analysis of helicopter rotors and has been used in the analysis of car bodies taking account of rotating wheels. GAROS was developed over the last 17 years by Mr. Arne Vollan who kindly supported this presentation.

The rotor of the wind energy converter may have one, two or more blades. The blades may be rigidly attached to the hub or they may be fully articulated. The elastic properties of the blades as well as of the tower are taken into account. This means that the equations of motion have periodic coefficients and a stability analysis thus requires the Floquet method. The structure is divided in two substructures: a non-rotating supporting substructure and a rotating substructure.

In the rotating system we have Coriolis and centrifugal forces as additional inertia terms. Beside this we take into account the stationary tension force which leads to geometric stiffness terms. Forces from gravity are of course also included.

The aerodynamic forces may be divided into two parts. Wind dependent forces and unsteady forces which are induced by the elastic deformation and elastic velocities of the aerodynamic blade elements. The aerodynamic forces will be discussed in detail later.

The calculations are made in three steps. Finite element calculation are made for the non-rotating and the rotating structure. In the second step the generalised matrices are established with an reduced modal approach using the results from the FEM calculations. In the third step the stability analysis and the time response calculations are carried out.

Figure 1 shows a Flow-Chart of the GAROS analysis.

In the following I will discuss the mechanical and the aerodynamic model in detail. A short overview of the solution methods for the equation of motion in time and frequency domain will be given. After this one example for the FEM model of the rotor and tower will be discussed.

2. MECHANICAL MODEL

2.1 The Lagrange potential

In the dynamic analysis, the finite element method is used in order to model the two substructures. The equations of motion are found by applying the Lagrange equation to the energy expressions and the generalised forces of the structures. Denoting the kinetic energy by T and the potential energy by U , the Lagrange potential is

$$L = T - U \quad (2.1)$$

Further denoting the virtual work of the external forces by dW and the generalised co-ordinates by g , the Lagrange equation is

$$\frac{d}{dt} \left[\frac{dL}{dg} \right] - \frac{dL}{dg} = \frac{dW}{dg} \quad (2.2)$$

The kinetic energy is calculated for each mass point of the coupled structure yielding mass-, Coriolis- and centrifugal-matrices. The potential energy is the elastic energy of all elements in the two substructures which is calculated with the finite element program. In addition to this the gravity potential of all mass points are taken into account and calculated in GAROS. The external forces are the aerodynamic forces acting on the blade elements.

The calculation of the kinetic and the potential energy of the supporting structure with M mass points is straight forward and is, in fact, done by the finite element program. For the calculation of the kinetic energy of the rotating structure with N mass points the deflection and the rotation of the coupling point must be accounted for as well as the deflection and the velocity of the rotating structure. Since the calculation of the kinetic energy expression of the rotating substructure is one of the mayor parts for the equation of motion it will be discussed in more detail here.

2.2 Kinetic energy of the rotating substructure

We define the following 3 co-ordinate systems:

- S_0 is the inertia system attached to the coupling point of the supporting structure. The supporting structure is described in this co-ordinate system.

- S1 is S0 after an elastic translation defined by the vector $\underline{\rho}$ of the coupling point
- S2 is S1 after an elastic rotation defined by the vector $\underline{\alpha}$ of the coupling point. The angles are assumed to be small.
- S3 is S2 after a rigid body rotation about the z-axis by an (large) azimuth angle Ωt .

We also can define the following vectors:

- \underline{r} : undeformed position of a point in the rotor structure defined in S3
- $\underline{\rho}$: elastic deformation of a point in the rotor structure defined in S3
- $\underline{\sigma}$: translation of the coupling point defined in S0
- $\underline{\alpha}$: rotation of the coupling point defined in S0

The instantaneous deformed position \underline{r}_i of the mass point i of the rotating structure can be transformed to the inertial system S0 by the equation

$$\underline{r}_{i0} = \underline{\sigma} + (\underline{I} + \underline{A}) \underline{H} (\underline{r}_i + \underline{\rho}_i) \quad (2.3)$$

with the following matrices:

$$\underline{I} = \begin{bmatrix} 1 & 0 & 0 \\ 0 & 1 & 0 \\ 0 & 0 & 1 \end{bmatrix} \quad \underline{A} = \begin{bmatrix} 0 & -\alpha_z & \alpha_y \\ \alpha_z & 0 & -\alpha_x \\ -\alpha_y & \alpha_x & 0 \end{bmatrix} \quad (2.4)$$

$$\underline{H} = \begin{bmatrix} \cos \Omega t & -\sin \Omega t & 0 \\ \sin \Omega t & \cos \Omega t & 0 \\ 0 & 0 & 1 \end{bmatrix}$$

Denoting the mass of point i by m_i , the kinetic energy T_i for this point is:

$$T_i = \frac{m_i}{2} (\dot{\underline{r}}_{i0}^T \dot{\underline{r}}_{i0}) \quad (2.5)$$

After inserting (2.3) and some rather lengthy algebraic manipulations we finally obtain a suitable expression for the kinetic energy of the rotating structure which is then used in the Lagrange equation. The vectors $\underline{\rho}$, $\underline{\sigma}$ and $\underline{\alpha}$ are time dependent.

2.3 Equation of motion for one mass point of the rotor structure

We can define the generalised co-ordinate \underline{g}_i for the mass point i by

$$\underline{g}_i = \begin{bmatrix} \underline{\sigma} \\ \underline{\alpha} \\ \underline{\rho}_i \end{bmatrix} \quad (2.6)$$

After applying the Lagrange equation to the Lagrange potential L of the mass point i in the rotor structure we find the equation of motion for the coupled fixed-rotating structure in the following form:

$$\underline{M}_i \ddot{\underline{g}}_i + \left[2\Omega (\underline{C}_i + \underline{D}_i) \right] \dot{\underline{g}}_i + \left[\Omega^2 (\underline{Z}_i + \underline{K}_{\text{rot}}) + \underline{K}_i \right] \underline{g}_i = \underline{f}_i \quad (2.7)$$

With the matrices:

- \underline{M}_i : mass matrix of mass point i in the rotor structure (9 x 9)
- \underline{C}_i : Coriolis matrix of mass point i in the rotor structure (9 x 9)
- \underline{Z}_i : centrifugal matrix of mass point i in the rotor structure (9 x 9)
- \underline{K}_i : elastic stiffness matrix of mass point i in the rotor structure (9 x 9)
- $\underline{K}_{\text{rot}}$: geometric stiffness matrix of mass point i in the rotor structure (9 x 9)
- \underline{D}_i : damping matrix of mass point i in the rotor structure (9 x 9)

Each of these matrices consist of 5 terms

Non-periodic term	subscript 0
$\sin \Omega t$ term	subscript 1
$\cos \Omega t$ term	subscript 2
$\sin 2\Omega t$ term	subscript 3
$\cos 2\Omega t$ term	subscript 4

For example the mass matrix is

$$\underline{M} = \underline{M}_0 + \underline{M}_1 \sin \Omega t + \underline{M}_2 \cos \Omega t + \underline{M}_3 \sin 2\Omega t + \underline{M}_4 \cos 2\Omega t \quad (2.8)$$

2.4 Galerkin's approach for one mass point of the rotor structure

Now we can use the modal approach to reduce the number of degrees of freedom. Taking account of n modes of the rotor structure ($n \ll N$) and m modes of the support structure ($m \ll M$) and collecting the modes of the rotating structure, the $(3 \times n)$ modal matrix $\underline{\Phi}_i$ for the point i in the rotor structure can be introduced. We also can introduce the modal translation of the coupling point which is defined by the $(3 \times m)$ matrix $\underline{\Psi}_1$ and the modal rotation of the coupling point which is defined by the $(3 \times m)$ matrix $\underline{\Psi}_2$. Assuming now, that the displacement of each point of the rotor structure can be approximated by a linear combination of the modes, we obtain

$$\underline{\rho}_i(t) = \underline{\Phi}_i \underline{q}_R(t) \quad (2.9)$$

For the supporting structure the displacement and rotation of the coupling point can be approximated by

$$\underline{\alpha}_i(t) = \underline{\Psi}_1 \underline{q}_F(t) \quad \underline{\alpha}_i(t) = \underline{\Psi}_2 \underline{q}_F(t) \quad (2.10)$$

The $(n \times 1)$ vector \underline{q}_R is the generalised displacement vector for the rotor structure and the $(m \times 1)$ vector \underline{q}_F is the generalised displacement vector for the supporting structure. This approximation is called the Galerkin's approach or the reduced modal approach. If all modes are taken into account, the method is exact but has no advantages to the direct solution. In all practical cases, a selection of modes is made and the approximation is as bad or as good as the modal selection is made. This aspect will be discussed in more detail later in the text. We now can define the $(9 \times n+m)$ modal matrix \underline{X}_i for the point i of the rotor structure and the following relationship

$$\underline{X}_i = \begin{bmatrix} \underline{\Psi}_1 \\ \underline{\Psi}_2 \\ \underline{\Phi} \end{bmatrix} \quad \underline{g}_i = \underline{X}_i \underline{q} \quad \underline{q} = \begin{bmatrix} \underline{q}_F \\ \underline{q}_R \end{bmatrix} \quad (2.11)$$

2.5 Equation of motion and Galerkin's approach for the complete rotor structure

Applying the procedure to all mass points N in the rotor structure we obtain the equation of motion for the complete rotor structure. The system matrices then have the dimension $(9N \times 9N)$. The equation of motion of the rotor structure is then

$$\underline{M} \underline{\ddot{g}} + [2\Omega(\underline{C} + \underline{D})] \underline{\dot{g}} + [\Omega^2(\underline{Z} + \underline{K}_g) + \underline{K}] \underline{g} = \underline{f} \quad (2.12)$$

with:

$$\underline{g} = \begin{bmatrix} \underline{g}_1 \\ \underline{g}_2 \\ \vdots \\ \underline{g}_N \end{bmatrix} \quad (2.13)$$

We now can define the $(9N \times m+n)$ modal matrix \underline{X} for the complete rotor structure as

$$\underline{X} = \begin{bmatrix} \underline{X}_1 \\ \underline{X}_2 \\ \vdots \\ \underline{X}_N \end{bmatrix} \quad (2.14)$$

The Galerkin's approach for the complete rotor structure is

$$\underline{g} = \underline{X} \underline{q} \quad (2.15)$$

Inserting equation (2.15) in the equation of motion (2.12) and multiply the equation with \underline{X}^{-1} from the left side we obtain the generalised equation of motion for the complete coupled rotor structure

$$\underline{M} \underline{\ddot{q}} + [2\Omega \underline{C} + \underline{D}] \underline{\dot{q}} + [\Omega^2(\underline{Z} + \underline{K}_g) + \underline{K}] \underline{q} = \underline{\bar{f}} \quad (2.16)$$

The system matrices have now the dimension $(m+n \times m+n)$ and are super matrices of the following form

$$\underline{M} = \begin{bmatrix} \underline{M}^{FF} & \underline{M}^{FR} \\ \underline{M}^{RF} & \underline{M}^{RR} \end{bmatrix} \quad (2.17)$$

Again each sub matrix consist of a constant, a $\sin \Omega t$, a $\cos \Omega t$, a $\sin 2\Omega t$ and a $\cos 2\Omega t$ term.

The mass and the stiffness matrix of the supporting structure can now be added to the constant terms of the matrices \underline{M}^{FF} and \underline{K}^{FF} .

All matrices are described in detail in /1/.

The right hand side of the equation of motion are the generalised external aerodynamic forces. The aerodynamic forces acting on the rotor blade are described in the next chapter.

3. AERODYNAMIC MODEL

The generalised external forces in equation (2.16) are defined as

$$\underline{\bar{f}} = \underline{X}^{-1} \cdot \underline{f} \quad (3.1)$$

where \underline{f} are the aerodynamic forces acting on the rotor blades. In GAROS the aerodynamic strip theory is used. The following data for the aerodynamic calculations are necessary

- blade grid points defining the main blade line and blade grid points defining the aerodynamic twist
- the position of the 1/4 chord with respect to the main blade line
- aerodynamic constants like rotational velocity, air density, hub height etc.
- aerodynamic lift, drag and moment coefficients for all used profiles
- position of the used profiles

At each time step the physical displacement and velocity of the coupling point as well as for each aerodynamic blade element is calculated. Using the equation (2.3) for the total displacement and the derivation with respect to time for the total velocity, the real position and velocity of the deformed blade can be calculated. Also the blade twist angle is calculated. Now this displacement and velocity can be transformed to the aerodynamic blade element co-ordinate system as well as the inflow wind velocity.

If selected by the user, the induced velocity is calculated for each aerodynamic blade element. Different methods are available:

- Glauert's method for wind energy converters or for helicopters in auto rotation
- Glauert's method for propellers
- Lissaman and Wilson
- Hütter

If selected by the user effects due to tower shadow, wind gradient and turbulence are accounted for. Also a tip loss correction according to Prandtl can be selected. Changes of horizontal and vertical wind direction can be accounted for.

When the true wind velocity and angle of attack of an aerodynamic blade element have been evaluated, the aerodynamic force and moment for this element can be calculated. With the notations C_l , C_d , C_m as the lift, drag and moment coefficients, α as the angle of attack, v as the relative wind velocity to the blade element, dr as the length of the blade element, c as the chord length and ρ as the density of air, the following forces and moment can be introduced:

$$\text{lift force} \quad L = \frac{\rho}{2} v^2 c \, dr \, c_L(\alpha) \quad (3.2)$$

$$\text{drag force} \quad D = \frac{\rho}{2} v^2 c \, dr \, c_D(\alpha) \quad (3.3)$$

moment about the quarter chord

$$M = \frac{\rho}{2} v^2 c^2 \, dr \, c_M(\alpha) \quad (3.4)$$

The forces and moment are distributed to the blade grid points of the finite element model.

This procedure is quite time consuming. The CPU time is unlike other analysis steps, not only dependent on the modes used in the analysis, but also dependent on the size of the physical rotor model.

In the following paragraphs some of the mentioned aerodynamic effects will be described in detail.

3.1 Tower shadow

The tower shadow is assumed to have a 1-cos form. The velocity is calculated according the equation

$$v = v_\infty \left[\left(1 - \frac{v^*}{2} \right) - \frac{v^*}{2} \cos \left(\frac{\pi y_b}{r_t} \right)^{\text{exp}} \right] \quad (3.5)$$

for $|y_b| \leq r_t$

with

$$v^* = 1 - \frac{v_{\min}}{v_\infty}$$

v_∞ steady wind velocity

v_{\min} minimal wind velocity

y_b y-distance from actual blade element to tower axis

r_t tower radius

exp shape factor for tower shadow

3.2 Wind gradient

For the wind gradient an exponential-law in the form

$$v = v_{hub} \left(\frac{h}{h_{hub}} \right)^\alpha \quad (3.6)$$

is used in the calculations.

3.3 Discrete gust

For extreme load calculations the user can define a discrete gust according to the equation

$$v = v_\infty + \frac{v_{gust}}{2} \left[1 - \cos \left(\frac{2\pi t}{T_{gust}} \right)^{\text{exp}} \right] \quad (3.7)$$

with v_∞ steady wind velocity

v_{gust} gust peak velocity above steady wind

T_{gust} time for gust to pass through rotor

t time

exp gust shape factor

3.4 Turbulence

If selected by the user, a three dimensional turbulent wind field can be taken into account in the calculations. The turbulent wind fields for a certain amount of time steps are calculated with another program in advance according to the method from Jan and Shinozuka /3/. The turbulence spectrum and coherence function used in the calculation of the turbulent wind fields are according to the IEC 1400-1 regulation.

GAROS uses a linear interpolation in time between the turbulent wind fields. The turbulence option is usually only used to calculate fatigue loads.

4. SOLUTION METHODS

The generalised equation of motion for a rotor with constant rotor speed is

$$\overline{\underline{\underline{M}}} \ddot{\underline{q}}(t) + \overline{\underline{\underline{D}}} \dot{\underline{q}}(t) + \overline{\underline{\underline{K}}} \underline{q}(t) = \overline{\underline{\underline{f}}}(t) \quad (4.1)$$

with the total damping matrix $\underline{\underline{D}}$ and the total stiffness matrix $\underline{\underline{K}}$. This equation of motion of second order with the dimension $(m+n)$ can be transformed in an equation of first order with the dimension $(2(m+n))$ in the form

$$\begin{bmatrix} \overline{\underline{\underline{M}}} & \underline{\underline{0}} \\ \underline{\underline{0}} & \overline{\underline{\underline{M}}} \end{bmatrix} \dot{\underline{q}} + \begin{bmatrix} \underline{\underline{D}} & \overline{\underline{\underline{K}}} \\ -\overline{\underline{\underline{M}}} & \underline{\underline{0}} \end{bmatrix} \underline{q} = \begin{bmatrix} \overline{\underline{\underline{f}}} \\ \underline{\underline{0}} \end{bmatrix} \quad (4.2)$$

by adding the trivial equation

$$\underline{\underline{M}}\underline{\underline{\dot{q}}} - \underline{\underline{M}}\underline{\underline{\dot{q}}} = \underline{\underline{0}} \quad \text{with} \quad \underline{\underline{\dot{q}}} = \begin{bmatrix} \dot{q} \\ \underline{q} \end{bmatrix} \quad (4.3)$$

In the dynamic analysis we want to calculate the generalised displacements \underline{q} for a given force $\underline{\bar{f}}$ or we want to calculate the eigenvalues of the homogeneous equation. The solution methods used for this problems will not be the main subject in this report, so only a short overview will be given here.

4.1 Eigenvalue analysis

If the structure can be modelled as a system without periodic terms the direct solution method can be used. This is the case for uncoupled rotor structures (analysis without supporting structures) or for a rotor with isotropic support (vertical axis wind turbine). The solution is straight forward and can be found in many text books.

The most general problems with periodic coefficients cannot be solved by the classical direct eigenvalue analysis methods. In GAROS the Floquet method is used to solve these problems. This method is based upon the eigenvalues of the transition matrix. The transition matrix is a matrix built up of the columns of the response vectors of all generalised degrees of freedom when the system is excited in each mode by the independent initial conditions, and integration is performed over one period. A detailed description of this method is given in /2/.

If the periodicity of the system can be regarded as "weak", the azimuth angle can be frozen at different values during the solution phase. The system matrices can be assembled by adding the periodic terms for the actual azimuth angles to the constant terms. This method is also known as the "snap-shot" method. Then, the linear quadratic eigenvalue problem can be solved by the direct method. Because this method is approximate, it must be handled with care if the system shows to be of strong periodic nature.

4.2 Time response analysis

The time integration of the equation of motion (4.2) can be performed for periodic and non-periodic system matrices. A fourth order Runge-Kutta method with variable time step size is used. If the integration will not converge, the program will reduce the time step by a factor of two and try again. If there is still no convergence after halving the time steps 16 times, the integration is aborted with an error message.

4.3 Limitations of the modal approach

The modal approach is very nice and convenient, because the number of degrees of freedom is reduced considerably. However, some important limitations will be discussed here.

A sufficient number of modes should be taken into account in order to calculate the structural deformation properly. There exist no guideline who the modal selection has to be done. One method is to reduce the number of mode step by step and check the influence of the deleted modes on the results.

The structure described by the modes must be linear because otherwise the superposition principle will not be valid.

To calculate the generalised force correctly there must be modes presenting the applied force. A typical example is the centrifugal force of a rotor blade without coning. In this case, the forces act perpendicular to the deflection of the bending modes. The only modes leading to a generalised centrifugal forces are the extension modes, which usually have high frequencies and are normally not calculated. Therefore the centrifugal loads should be calculated by a separate static analysis.

5. ROTOR-MODEL

To establish a finite element model of a rotor blade the user can use the pre-processor MBROT. The finite element model will be build up with beam elements. The blade input data as a function of the rotor radius for the pre-processor MBROT are

- EI-flap
- EI-lag
- GJ-torsion
- EA
- chord
- mass per unit length
- torsion mass moment of inertia
- offset main blade line - centre of mass
- offset main blade line - shear centre
- offset main blade line - aerodynamic reference point
- angle of principle axis
- aerodynamic twist

The rest of the rotating substructure like blade bearings, hub, gear box, generator and coupling have to be added by the user afterwards. The degree of sophistication depends on the information the user has about this parts of the machine. In an early state of design the hub may be assumed to be rigid, whereas in the final state of the design a complete finite element model of the hub could be introduced in the rotor model. The same is valid for the drive train. The user can start with a very simple stiff model of the drive train and can improve this model step

by step. It is possible to add concentrated springs and dampers as well as concentrated masses and inertia. Even a complete FEM-model of a gear box or a pitch mechanism can be added in the drive train model. Figure 2 shows a rotor model established by MBROT.

For pitch controlled machines there are different pitch controllers available, from a simple PD-controller with constant control parameters to a more sophisticated PD-controller with adaptive parameters. Also pitch and torque controller for a variable speed control are available.

The generator system is usually modelled with the so called Kloss equation

$$s_k = \frac{M_k s_n}{M_n} \pm \sqrt{\left(\frac{M_k s_n}{M_n}\right)^2 - s_n^2} \quad (5.1)$$

with

M_n	generator nominal moment
s_n	generator nominal slip
M_k	generator pull-out moment
s_k	generator pull-out slip

6. TOWER MODEL

To build up the FE-model of the supporting structure any available FE pre-processor can be used. The tower can be a lattice tower, a tubular steel tower or any other possible structure. There is, as in the case of the rotor model, no restriction to the degree of sophistication. The machine bed for example could be established with stiff beam elements or as a complete FEM model. Figure 3 shows a FEM model of a lattice tower.

7. RESULTS

I now will present some GAROS results in frequency and time domain. The results are from a WEC in the MW-range.

Figure 4 shows the Eigenfrequencies of the coupled structure obtained with the snap-shot method. This is usually the first step to check whether resonances can occur in the structure. Figure 5 shows the modal participation of mode 3 of the coupled structure. The arrows in the figure represent the modes of the two uncoupled substructures. In this case mode 1 to 8 are the first 8 tower modes and the rest are rotor modes. In mode 3 of the coupled structure you see the coupling between the tower torsion mode (mode 3) and the first anti metric flapping modes of the rotor (modes 10 and 11). This is a very useful tool to study the participation of different tower and rotor modes in the coupled fixed-rotating structure.

The figures 6 and 7 show the results of a time domain simulation. In both cases the tower top shear force

perpendicular to the wind direction is plotted. In figure 7 the deformation perpendicular to the wind direction is constrained whereas in figure 6 the fully articulated tower model is used. This is one simple example how the number of degrees of freedom of the tower model is influencing the results.

8. VALIDATION OF RESULTS

The mechanical model of GAROS has been validated for some simple problems without aerodynamic forces. This has been done for a rotating discrete mass, a rotating disk, a rotating shaft and a simple coupled fixed-rotating rotor model /1/. For all mentioned problems an analytical solution is known. The agreement between the analytical and the GAROS results in frequency and time domain are very good. Since there are no basic differences between these simple problems and a more sophisticated rotor model, GAROS is suitable to handle coupled fixed-rotating elastic structures.

The results of the aerodynamic modules are compared with other validated programs and the agreement is good. Since the coupling between the mechanical and the aerodynamic calculation, the aeroelastic calculation, is very extensive, the GAROS program system is suitable to solve coupled fixed-rotating aeroelastic problems.

9. REFERENCES

- /1/ A. Vollan, "Analysis of Rotating Structures with MSC/NASTRAN and GAROS", Mac Neal Schwendler-Seminar, June 1990, Rome
- /2/ M. Roseau, "Vibrations non linéaires et théorie de la stabilité", Springer Tracts in Natural Philosophy, Vol. 8, 1966
- /3/ M. Shinozuka, C. M. Jan, "Digital Simulation of Random Processes and its Applications", Journal of Sound and Vibration, 1972, Vol. 25, pp. 111 - 128

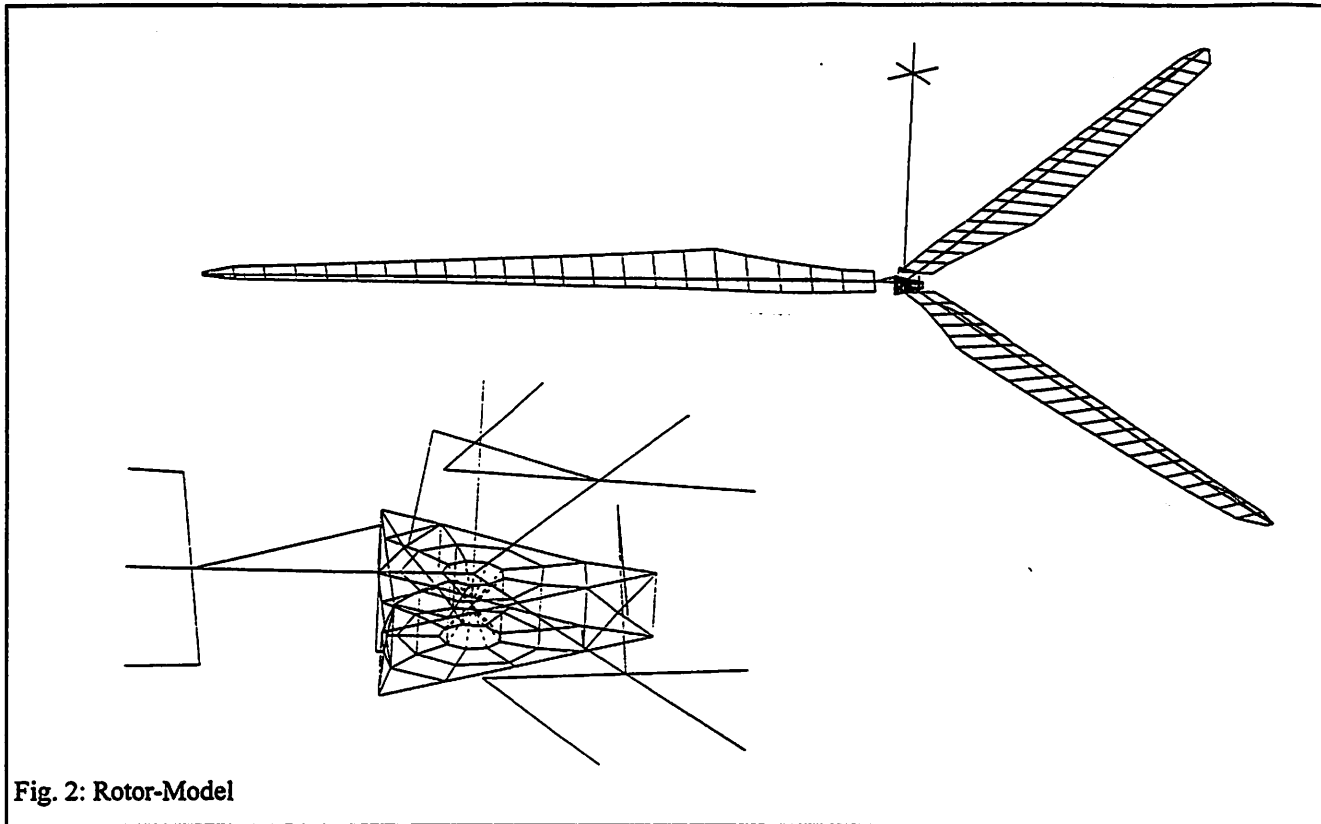


Fig. 2: Rotor-Model

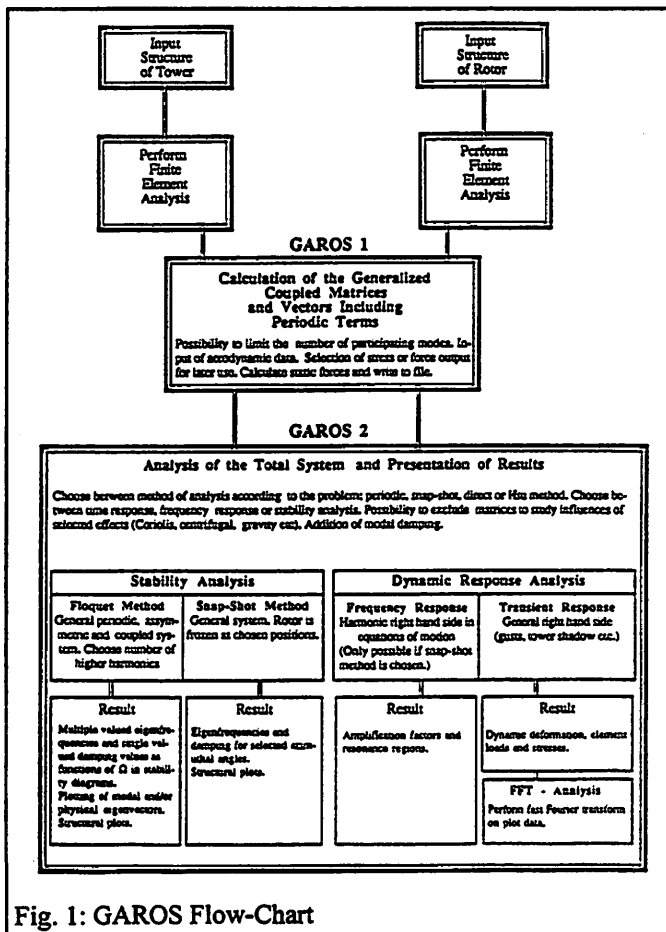


Fig. 1: GAROS Flow-Chart

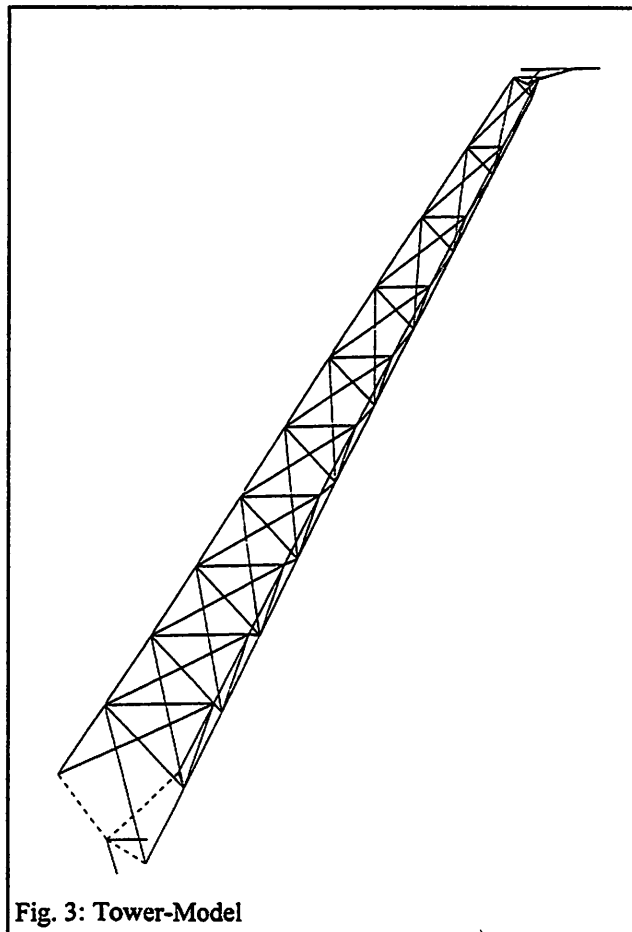


Fig. 3: Tower-Model

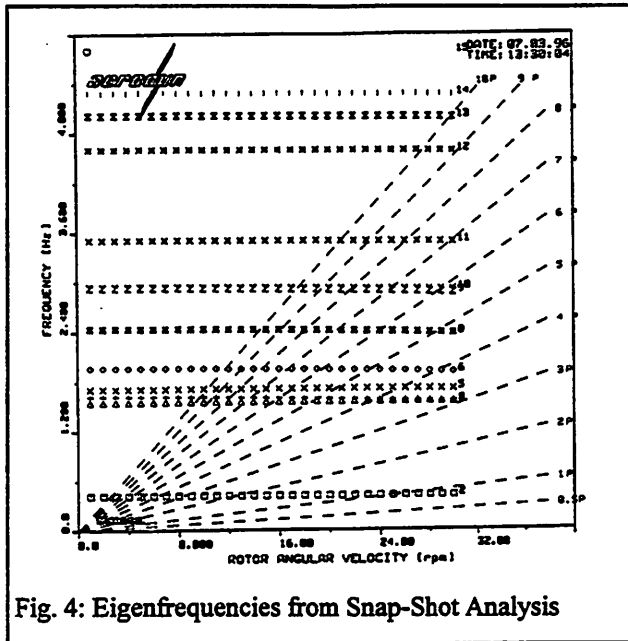


Fig. 4: Eigenfrequencies from Snap-Shot Analysis

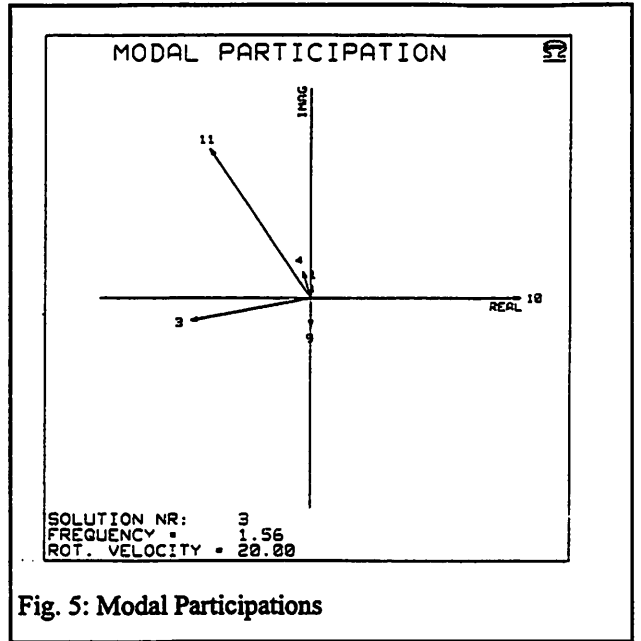


Fig. 5: Modal Participations

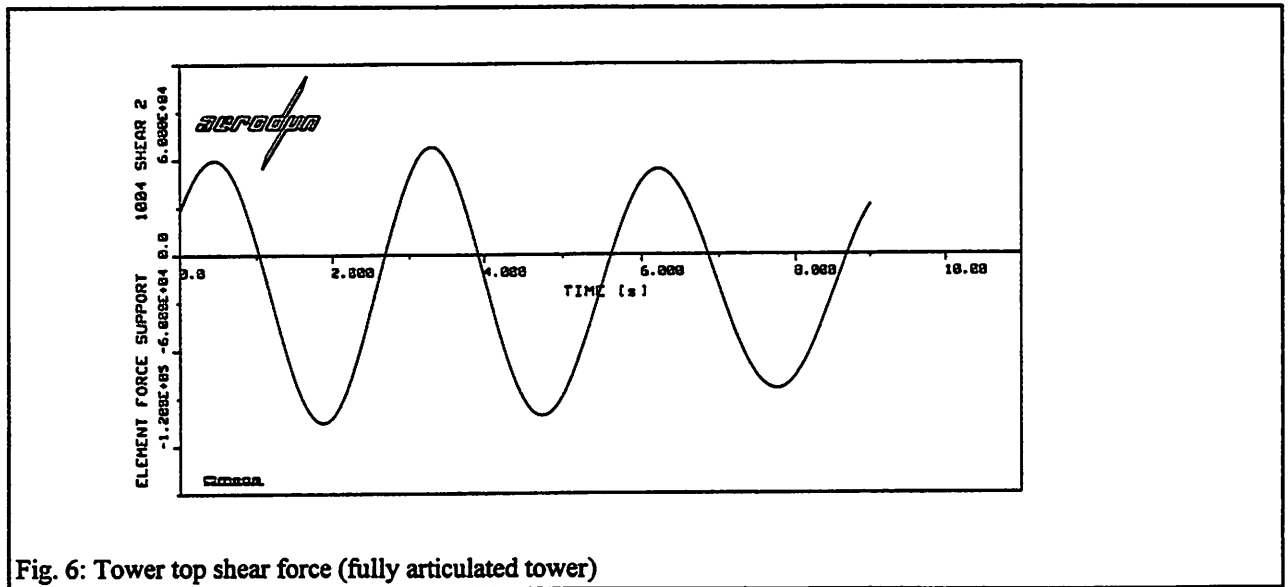


Fig. 6: Tower top shear force (fully articulated tower)

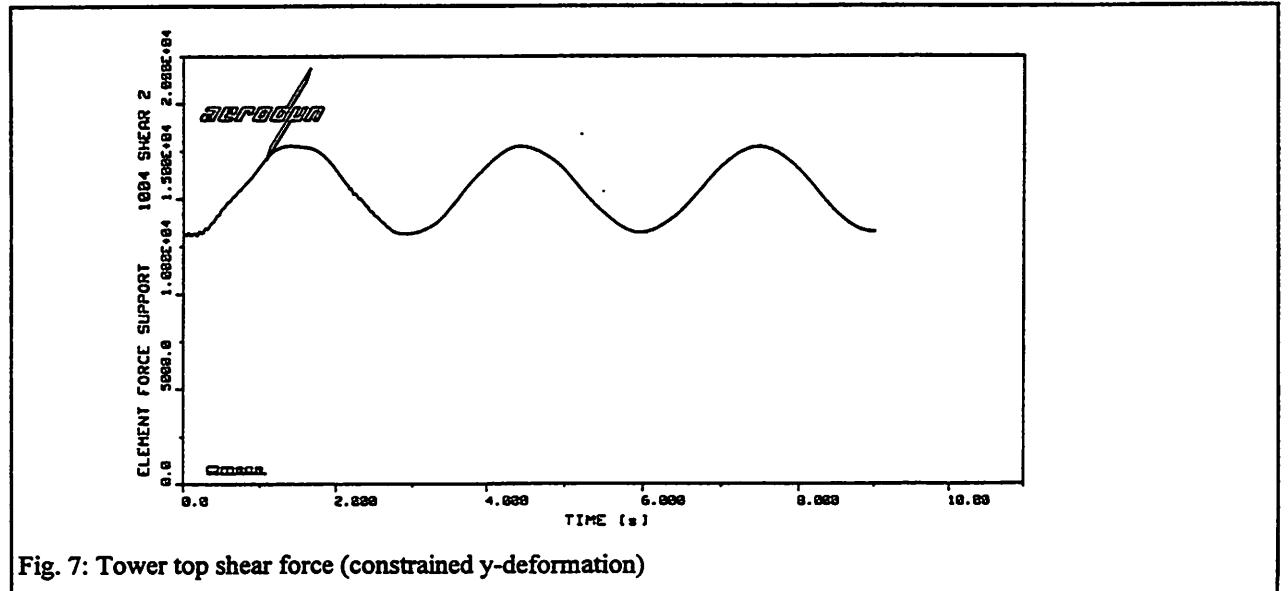


Fig. 7: Tower top shear force (constrained y-deformation)

**AEROELASTIC MODELLING WITHOUT THE
NEED FOR EXCESSIVE COMPUTING POWER**

by

David Infield**CREST****(Centre for Renewable Energy Systems Technology)
Department of Electronic and Electrical Engineering
Loughborough University****email: d.g.infield@lut.ac.uk****ABSTRACT**

The aeroelastic model presented here was developed specifically to represent a wind turbine manufactured by Northern Power Systems which features a passive pitch control mechanism. It was considered that this particular turbine, which also has low solidity flexible blades, and is free yawing, would provide a stringent test of modelling approaches.

It was believed that blade element aerodynamic modelling would not be adequate to properly describe the combination of yawed flow, dynamic inflow and unsteady aerodynamics; consequently a wake modelling approach was adopted. In order to keep computation time limited, a highly simplified, semi-free wake approach (developed in previous work) was used.

A similarly simple structural model was adopted with up to only six degrees of freedom in total. In order to take account of blade (flapwise) flexibility a simple finite element sub-model is used.

Good quality data from the turbine has recently been collected and it is hoped to undertake model validation in the near future.

MODELLING APPROACH

AERODYNAMICS:

- convecting semi-free wake analysis**
- intrinsically includes induction lag effect**
- includes wake expansion and skewing**
- simple representation of tower shadow**
- simple lifting line model**
- can use 2D aerofoil data corrected to 3D**

STRUCTURAL MODELLING:

- low order model for fast solution**
- finite element sub-model of blade bending**

MODELLING OBJECTIVES:

- simplified model for design applications**
- limited demands on computer power**
- adequately represent passive pitch control**
- cope with flexible blades**
- include teeter motions (with delta-3 coupling)**
- calculate steady state characteristics**
- calculate transient response to gusts**

A REFERENCE DATA SET:

Detailed measurements specifically for validation of aeroelastic codes made at RAL on 9 m diameter, 2 bladed turbine from Northern Power Systems.

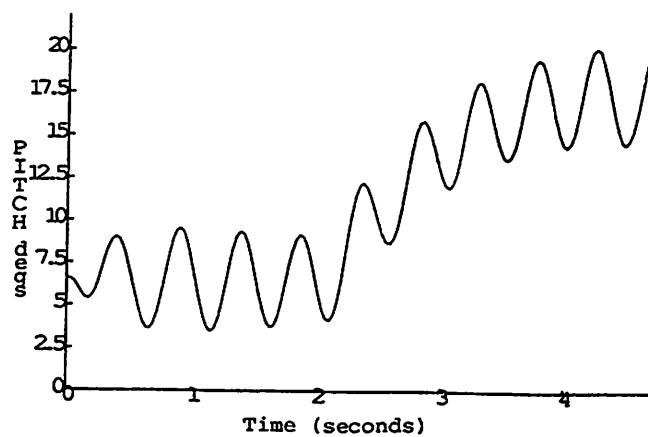
Parameters available include:

- blade pitch angle**
- teeter angle**
- pitching force/moment**
- rotor angular position**
- generator angular position**
- yaw error**
- wind speed at 1R and 3D upstream**
- electrical power output**

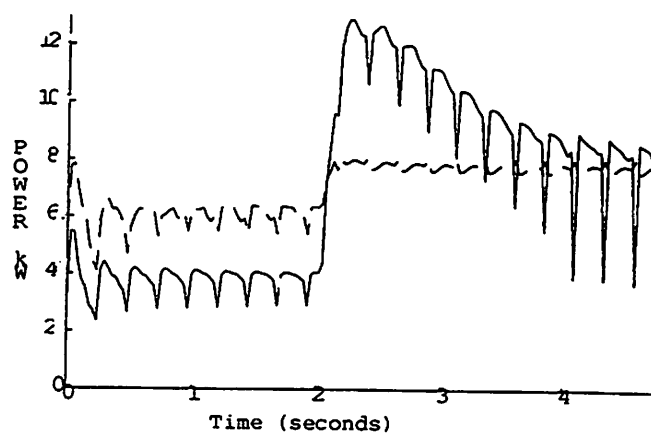
REFERENCES:

- 1. Zhong S and Infield DG; Prediction of wind turbine performance in axial and non-axial flows by a prescribed wake model. Proc BWEA 13.**
- 2. Naryshkin S and Infield DG; Aeroelastic modelling of a horizontal axis wind turbine with passive pitch control. Proc BWEA 14.**
- 3. Mahmud F, Dutton AG and Infield DG; Aeroelastic investigation of a passive pitch controlled wind turbine. Proc BWEA 17.**
- 4. Final report to EPSRC from RAL; Modelling dynamically active wind turbines.**

PRESENTATION TO 28th IEA TOPICAL EXPERTS MEETING ON AEROELASTICS

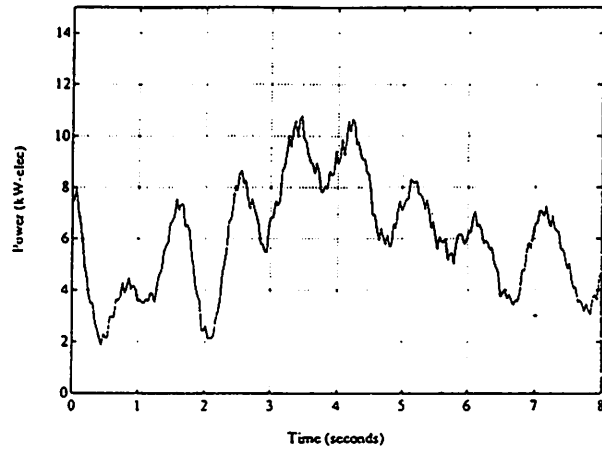


Pitch response to wind speed step

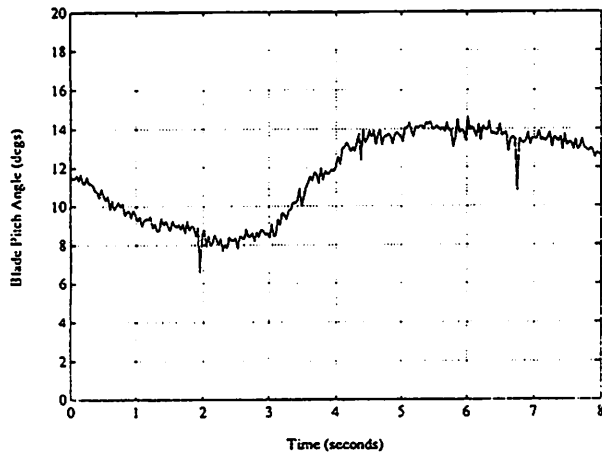


Power response to wind speed step

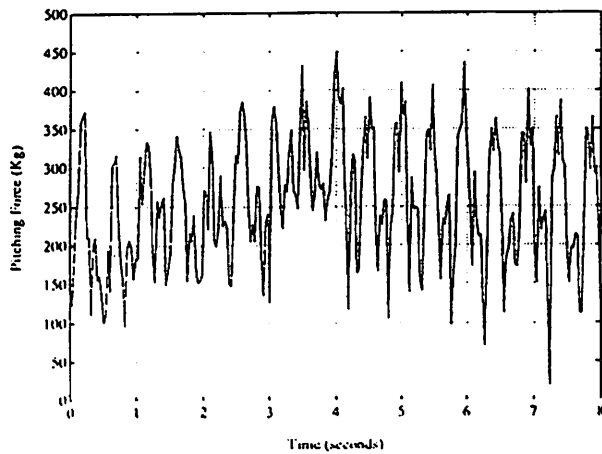
PRESENTATION TO 28th IEA TOPICAL EXPERTS MEETING ON AEROELASTICS



Measured power during gust



Measured pitch during gust



Measured pitching force during gust

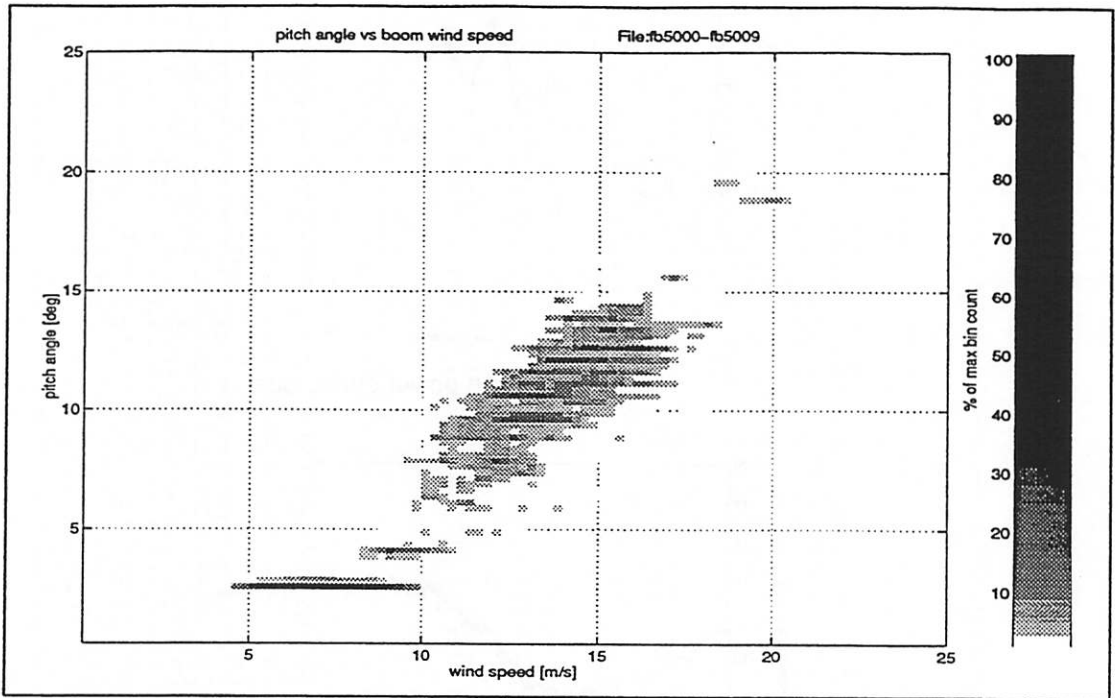


Fig. 3 : Measured distribution of pitch angle v boom wind speed

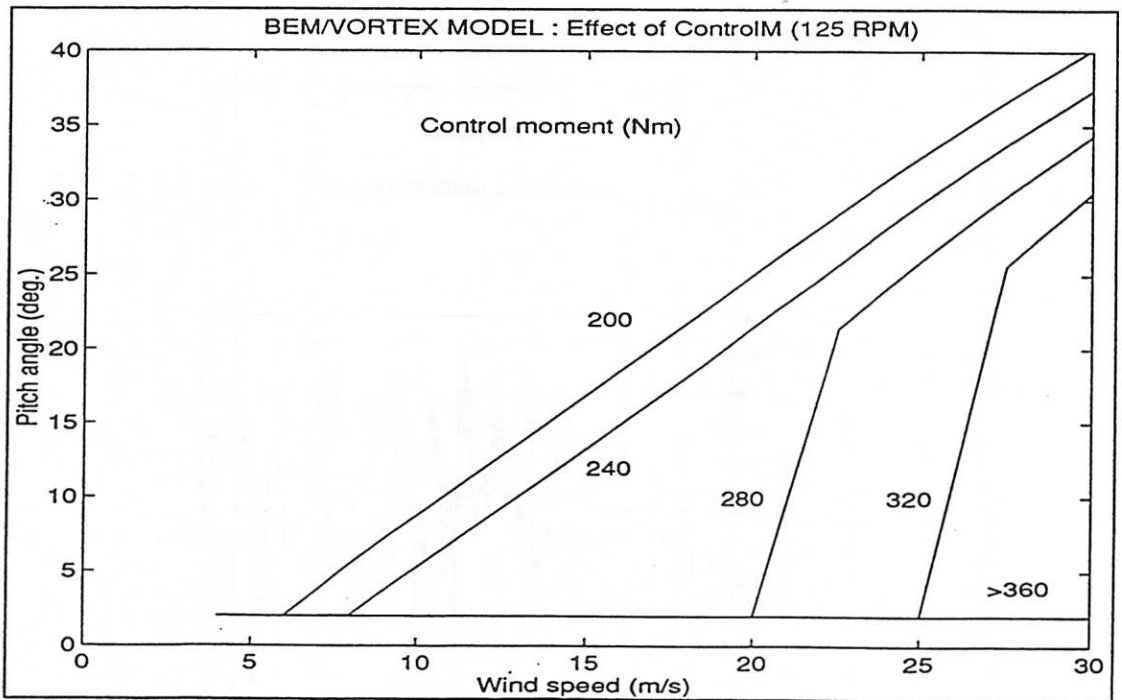
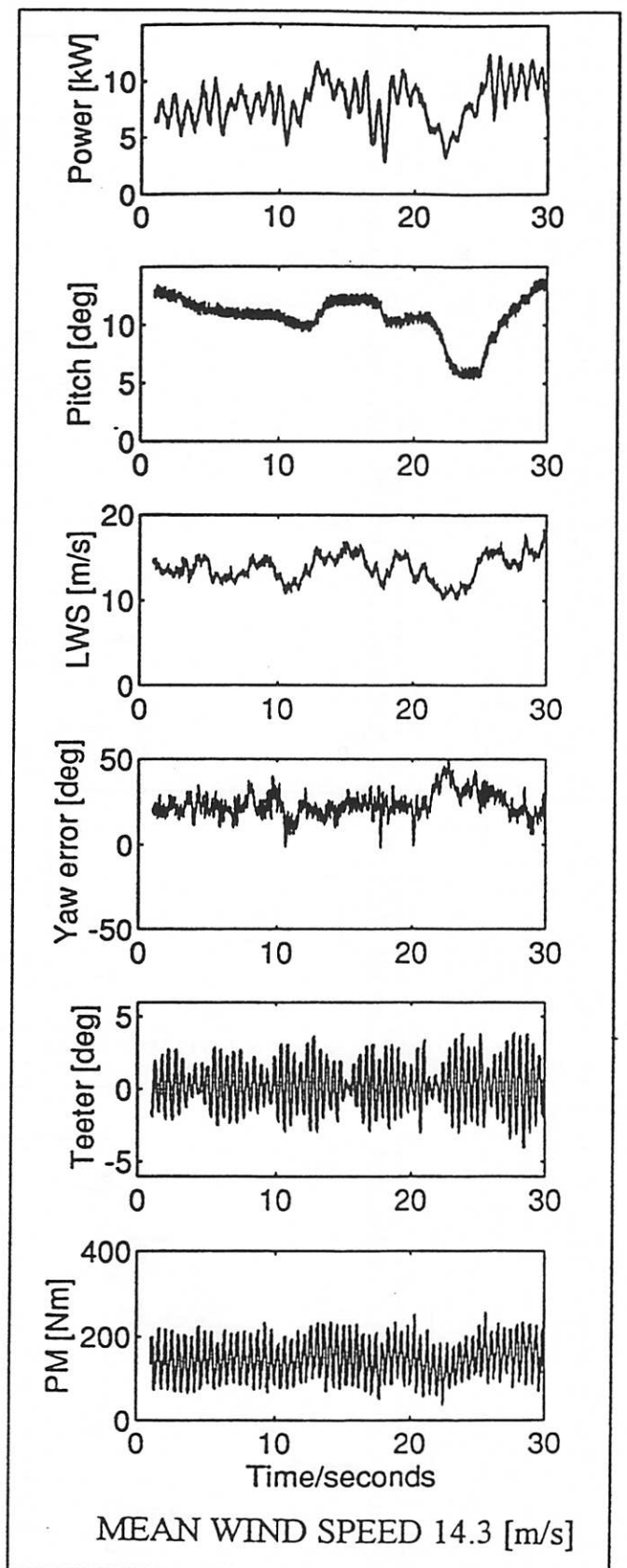
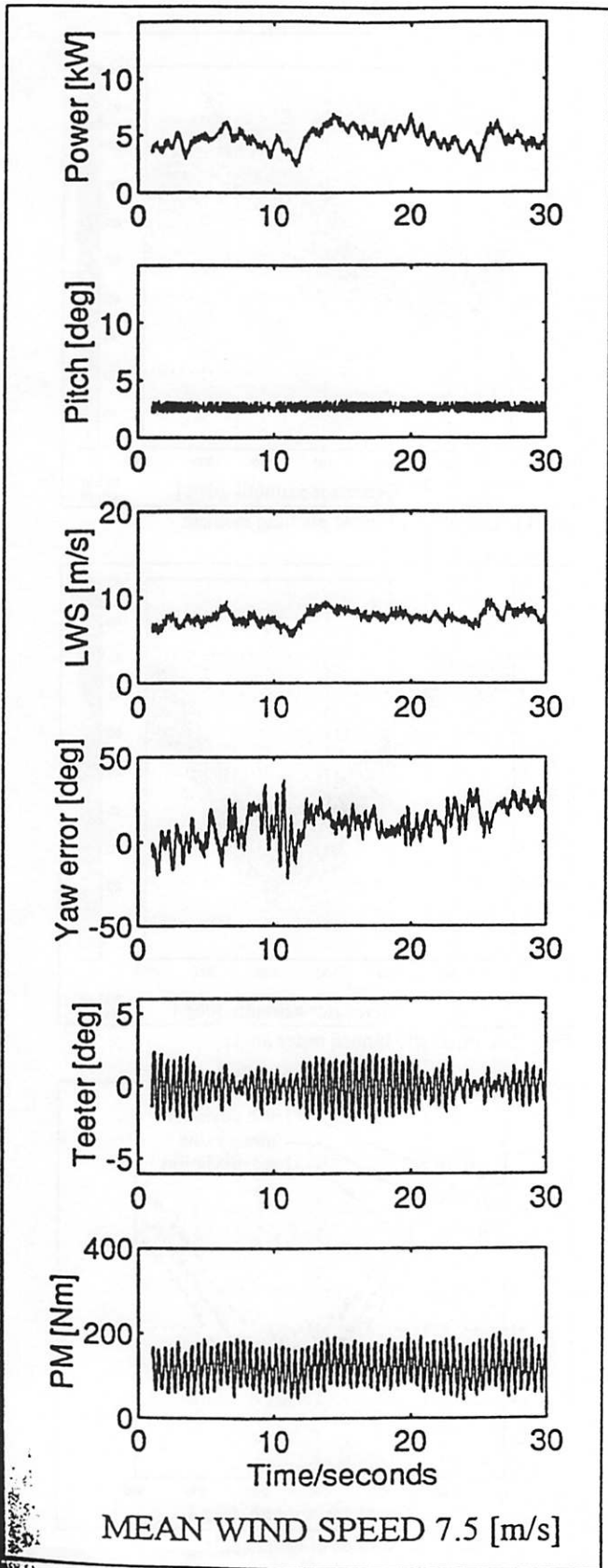


Fig. 4 : Pitch angle v wind speed characteristics for varying control moment in the aeroelastic model

PRESENTATION TO 28th IEA TOPICAL EXPERTS MEETING ON AEROELASTICS



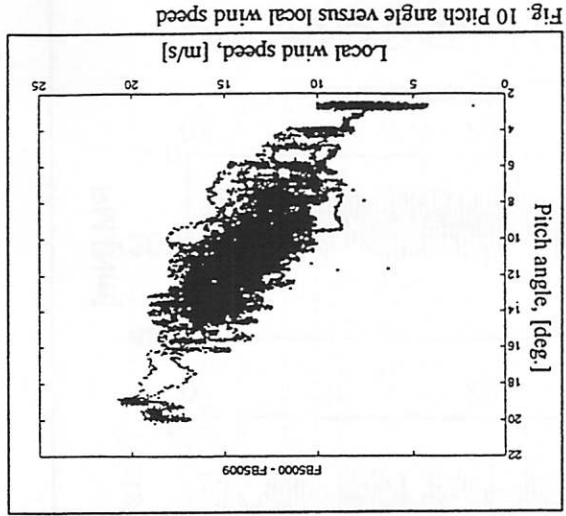


Fig. 10 Pitch angle versus local wind speed

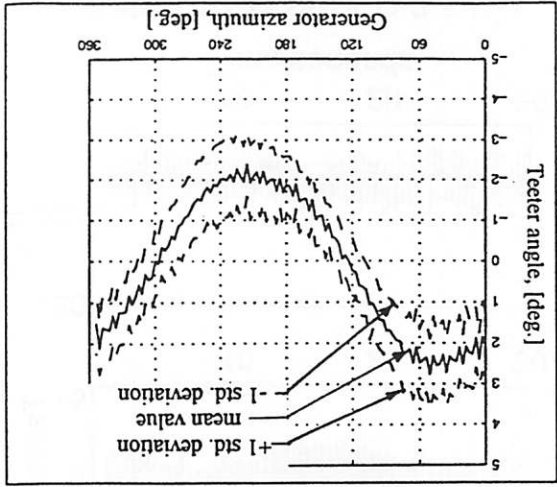


Fig. 13 Deterministic value of teeter angle

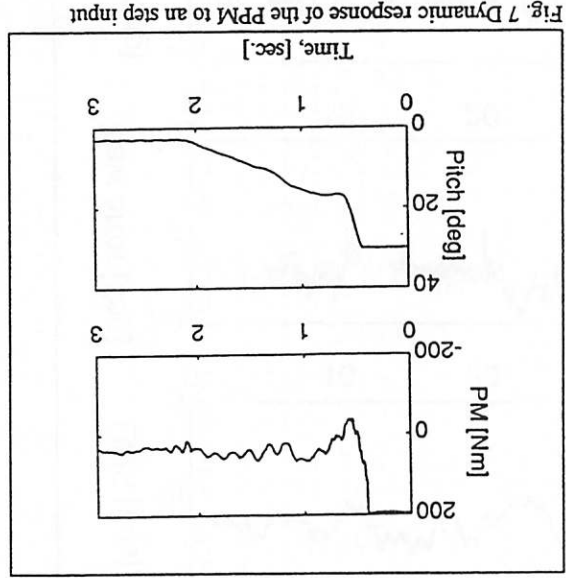


Fig. 7 Dynamic response of the PPM to an step input

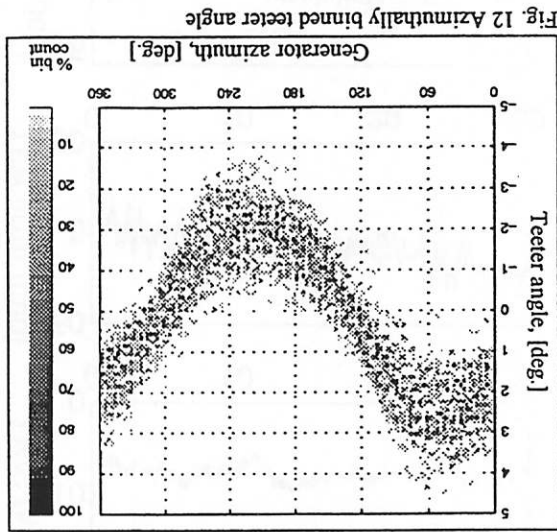


Fig. 12 Azimuthally binned teeter angle

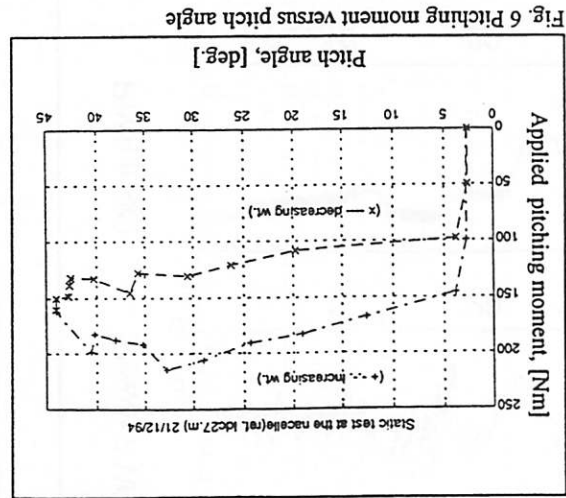


Fig. 6 Pitching moment versus pitch angle

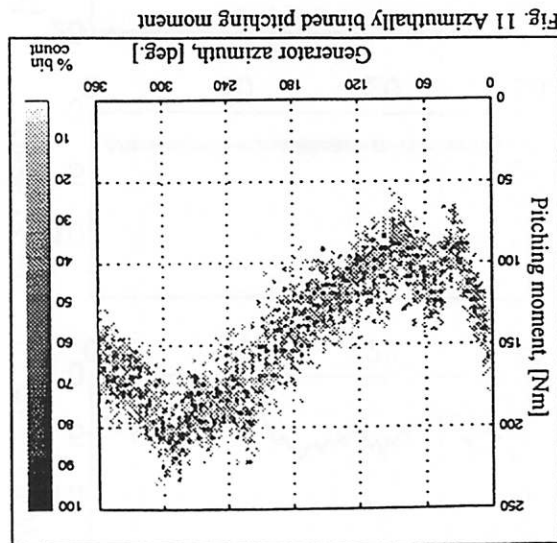


Fig. 11 Azimuthally binned pitching moment

Allan Kretz

RISØ

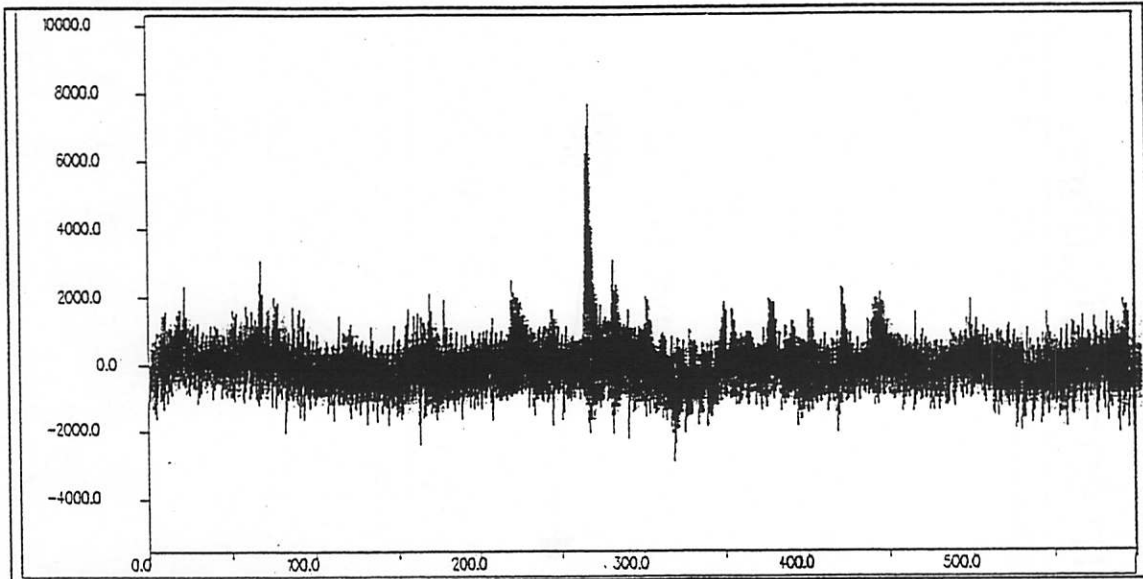
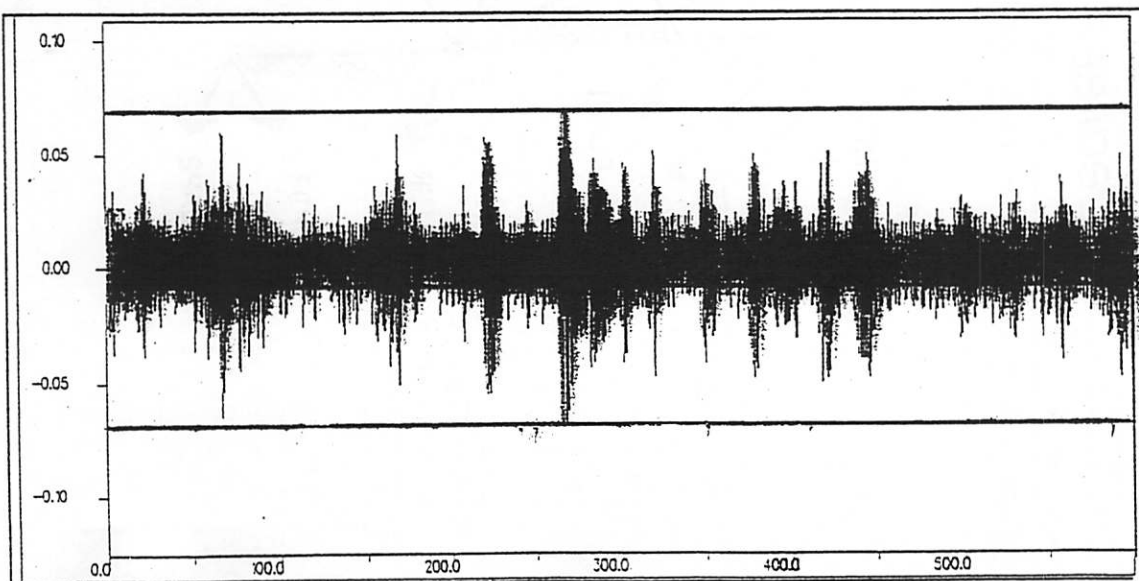
Denmark

WINDANE-12 WINDTURBINE

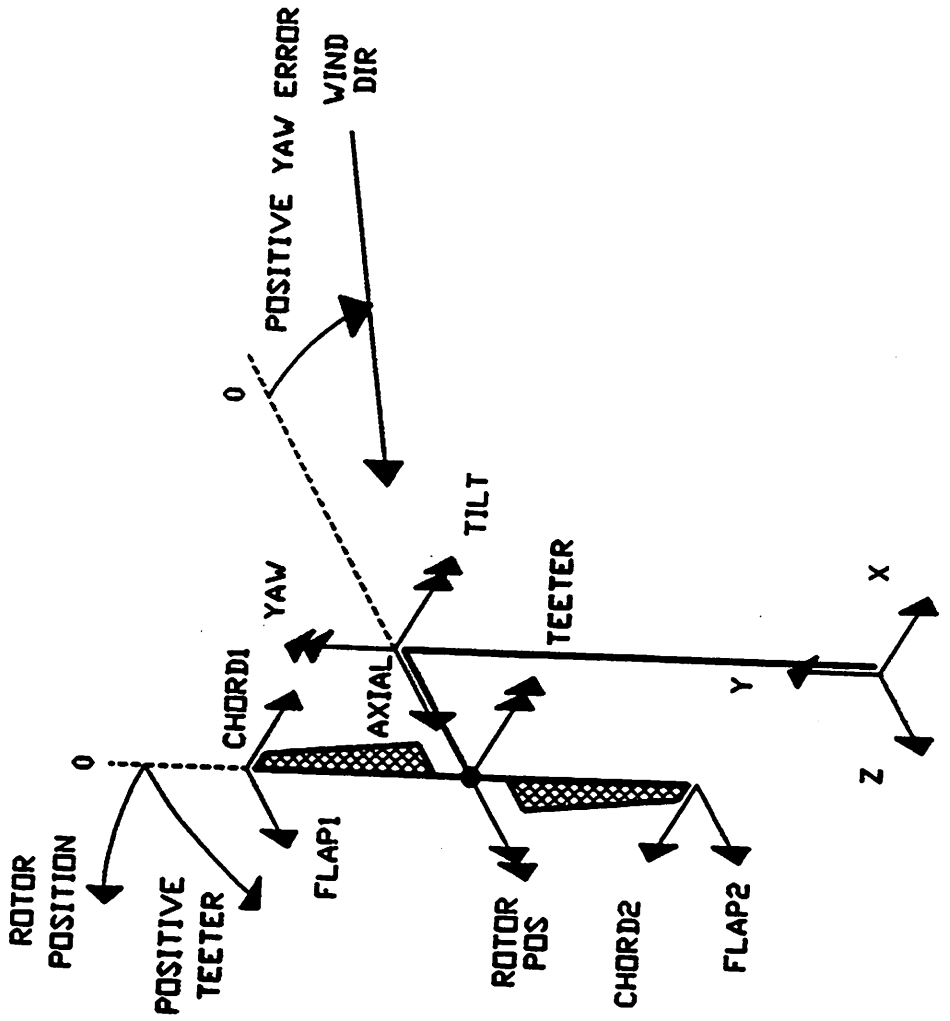


MAIN DATA FOR THE WINDANE-12

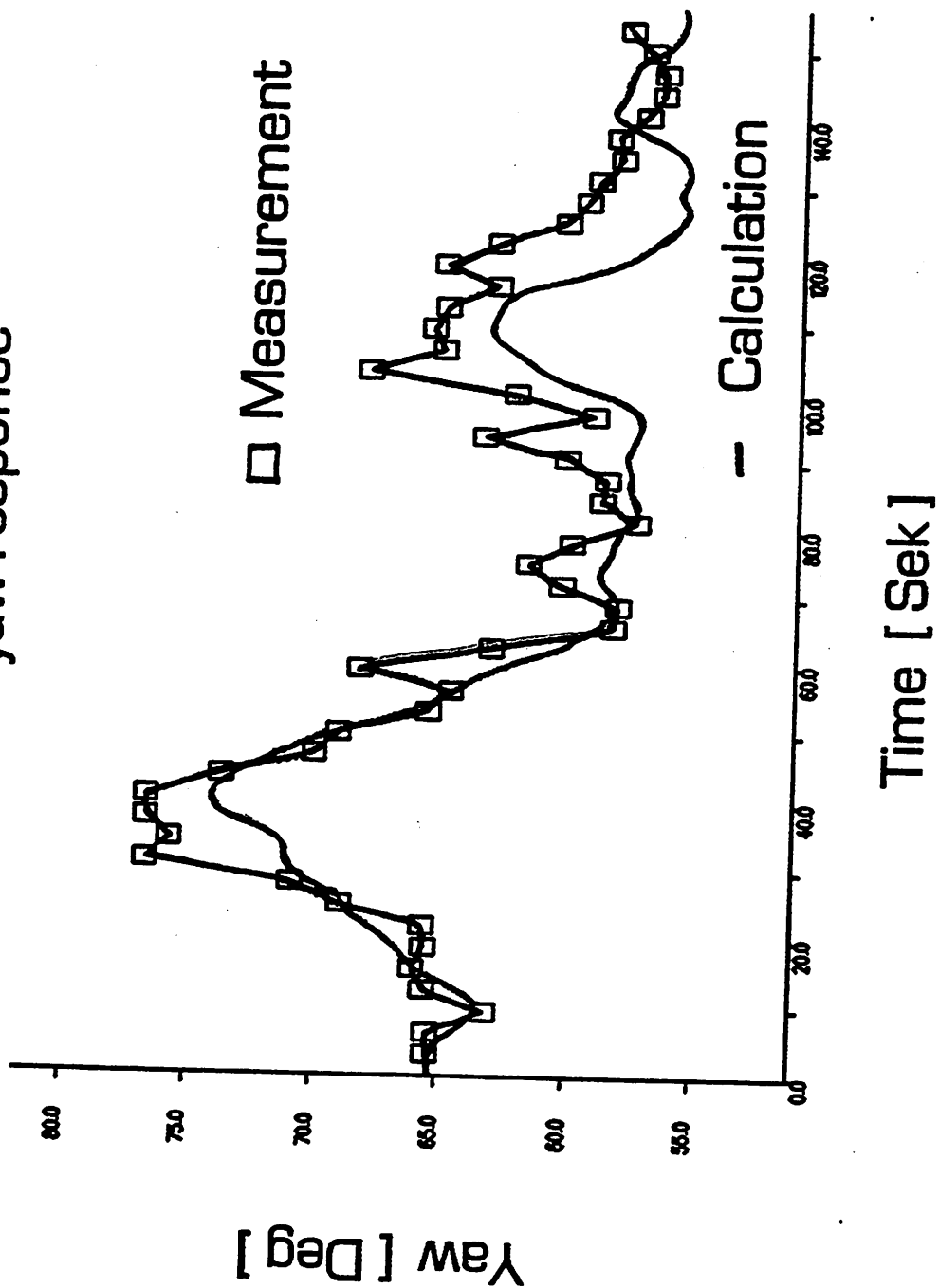
TOWER _{HEIGHT}	15.5	m
TILT _{ANGLE}	0.0	deg.
TOWER-HUB _{LENGHT}	1.24	m
FREE TEETER _{ANGLE}	0.6	deg.
MAXIMUM TEETER _{ANGLE}	4.0	deg.
CONE _{ANGLE}	5.7	deg.
PITCH _{ANGLE}	-2.0	deg.
DELTA ₃	0.0	deg.
ROTOR _{DIAMETER}	12.0	m
ROTATIONAL _{SPEED}	74.0	rpm
PROFILE _{SERIES}	NACA 4412-24	
POWER _{OUTPUT}	22.0	kW

EXTREME LOADS IN HIGH WIND 15 [m/s]TILT MOMENT [Nm]TEETER ANGLE [rad]

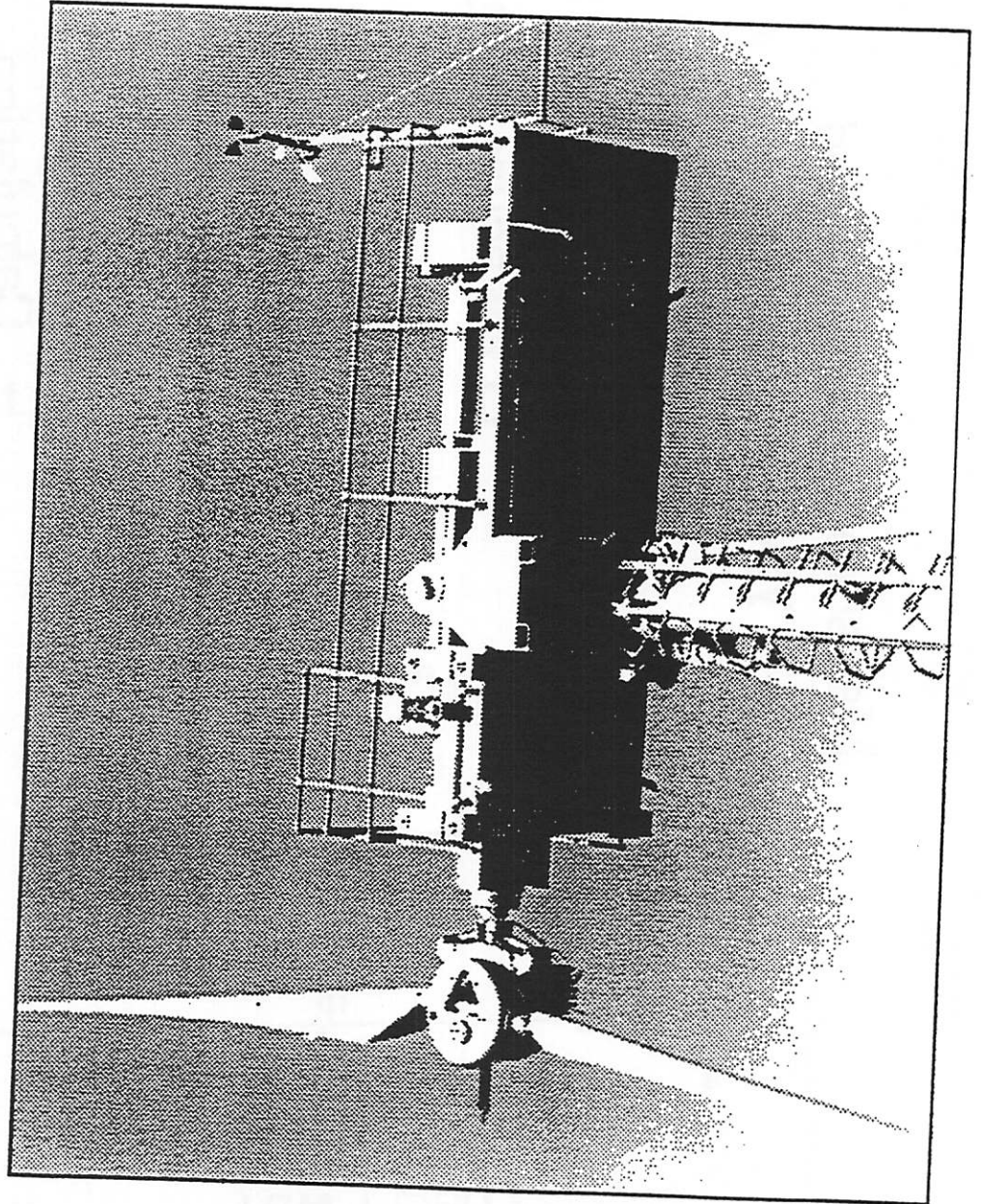
Degrees of freedom and definitions



Measured and calculated yaw response



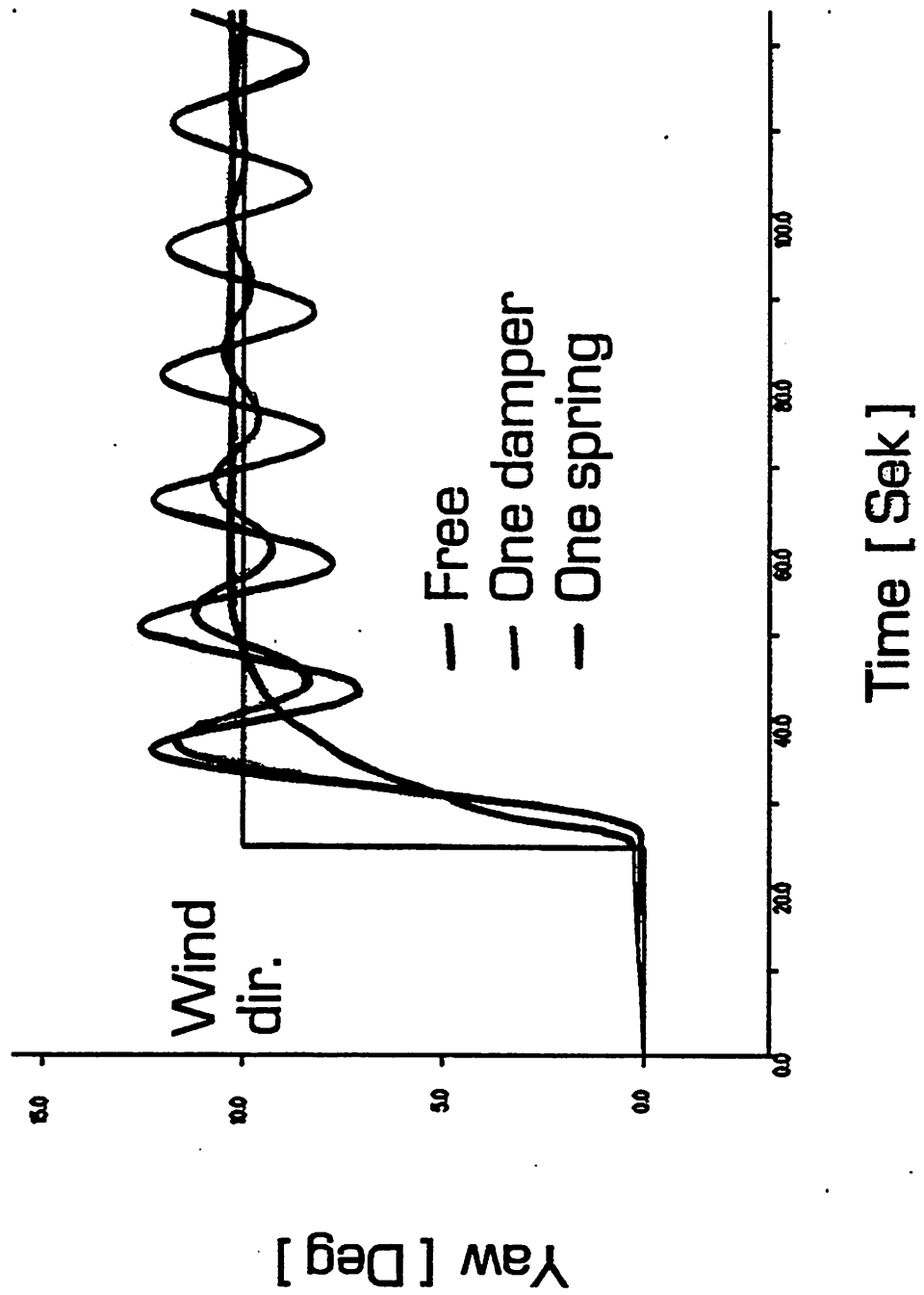
**CLOSE-UP OF THE RESEARCH TURBINE
MOUNTED WITH THE WINDANE 12 ROTOR**



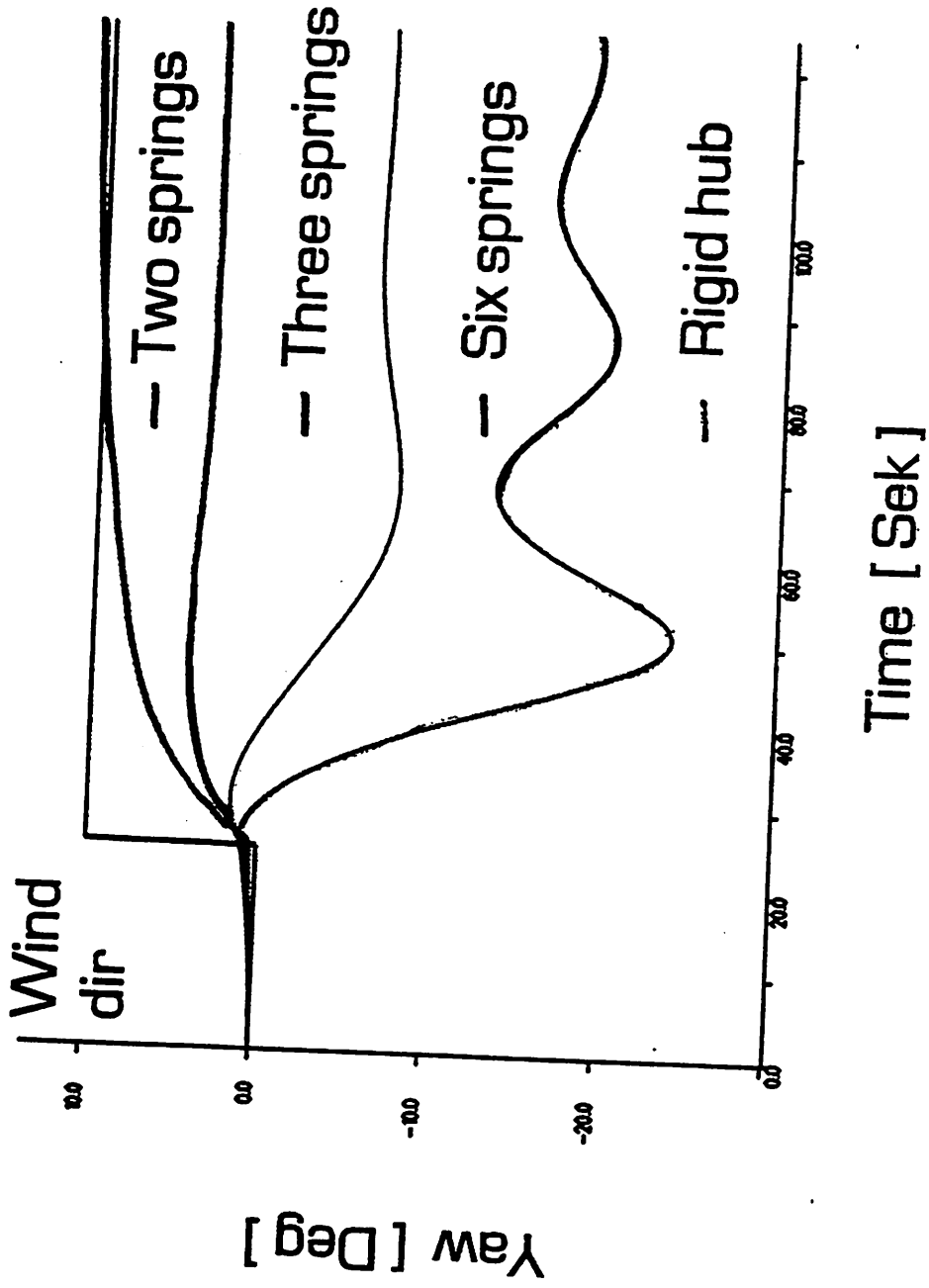
**MEASURED AND CALCULATED YAW ERRORS
AS FUNCTION OF TEETER CONFIGURATION**

teeter configurations	measured yaw error [deg]	calculated yaw error [deg]
F-free	+2.1	+0.1
1S-one spring	+1.7	+0.3
1D-one damper	+1.1	+0.1
2S-two springs	+1.0	+0.7
3S-three spr.	+0.6	-6.7
6S-six spr.	no space	-16.6
RH-rigid hub	-32.4	-28.9

Predicted yaw response
(10 Deg wind dir. step)



Predicted yaw response
(10 Deg wind dir. step)



GENERALIZED YAW MOMENT

$$Q_{yaw} = \int_0^R Q_{yaw}(r) dr$$

$$\begin{aligned}
 Q_{yaw}(r) = & [\sin(P_{azi})(r+hk) + \cos(P_{azi})l][F_{flap1}(r) - F_{flap2}(r)] \\
 & + \cos(P_{azi})[h+rk-n+P_{axial}][F_{edge1}(r) - F_{edge2}(r)] \\
 & + \sin(P_{azi})hP_{teeter}[F_{flap1}(r) + F_{flap2}(r)] \\
 & + [\cos(P_{azi})P_{teeter} + P_{ilt}]r[F_{edge1}(r) + F_{edge2}(r)]
 \end{aligned}$$

h - tower-hub length

k - blade coning

l - blade offset

n - teeter hinge offset

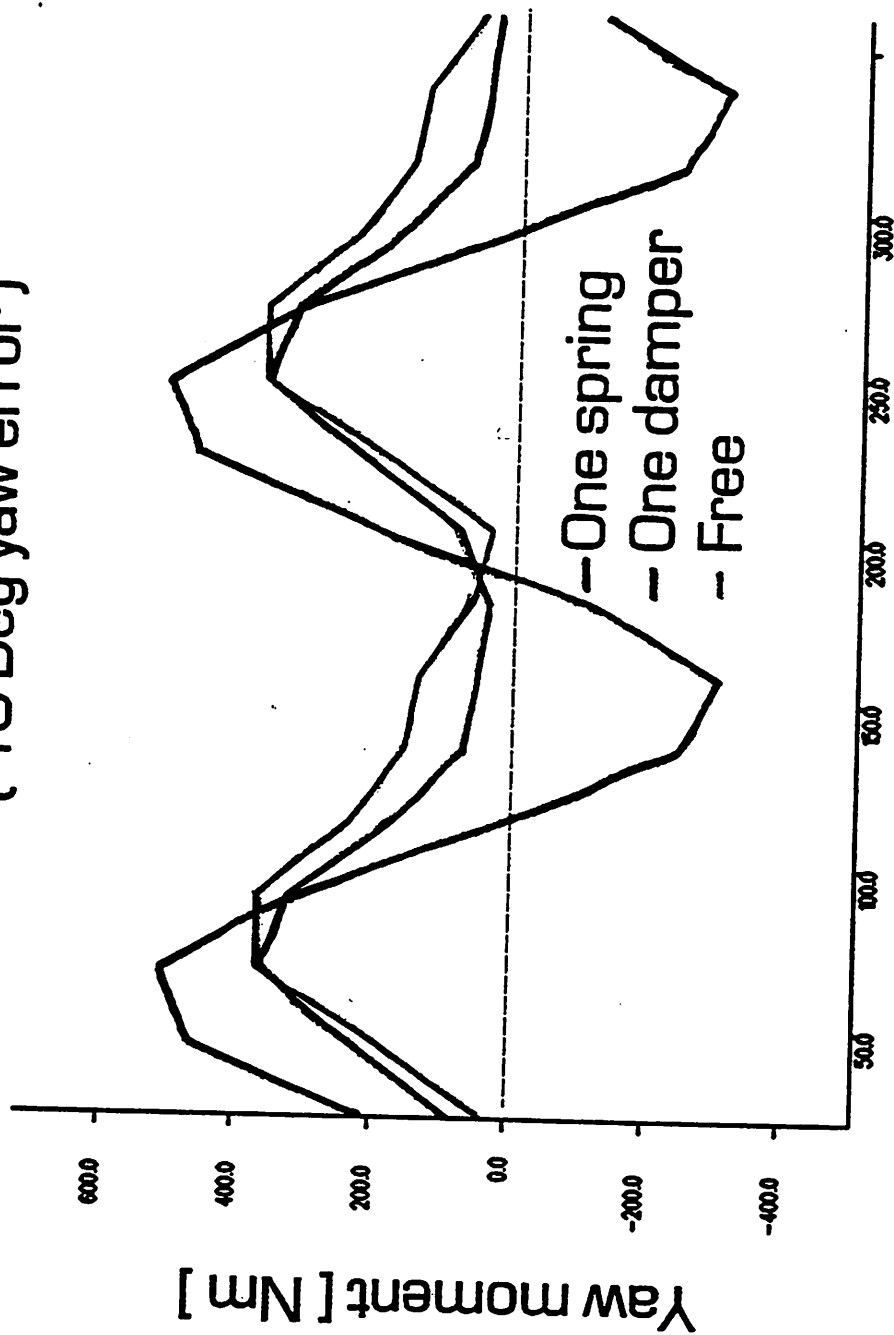
r - radial distance along the rotor

R - rotor radius

**MAJOR TERMS OF THE GENERALIZED YAW MOMENT
(10 DEG YAW ERROR)**

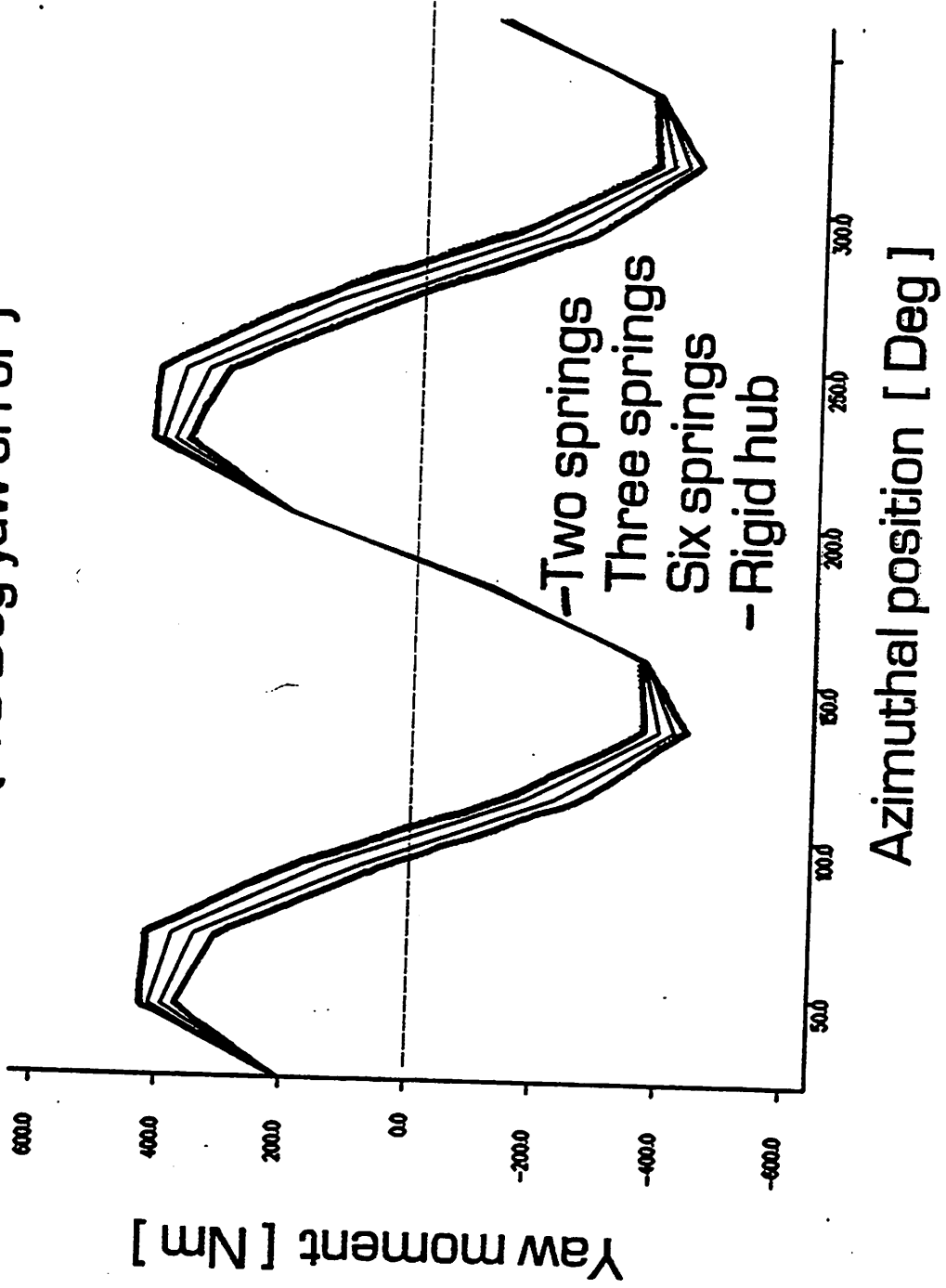
Con- figu- ration	1st term [Nm]	2nd term [Nm]	3rd term [Nm]	4th term [Nm]	Q_{yaw} [Nm]
F	-64.7	21.2	234.7	2.2	193.4
1D	-51.1	9.0	204.9	2.2	165.0
1S	129.9	-42.7	46.3	-27.5	106.0
2S	86.9	-56.3	15.1	-16.3	29.4
3S	70.7	-59.8	7.7	-11.2	7.4
6S	50.8	-62.6	2.6	-5.9	-15.1
RH	30.9	-64.4	0.0	-0.2	-33.7

Predicted yaw moment
(10 Deg yaw error)



Azimuthal position [Deg]

Predicted yaw moment
(10 Deg yaw error)





Paper presented at the 28th IEA Experts Meeting
'*State of the Art of Aeroelastic Codes*'.
11-12 April 1996, Technical University of Denmark, Lyngby

The Aeroelastic Code HawC – Model and Comparisons

Jørgen Thirstrup Petersen
The Test Station for Wind Turbines
Risø National Laboratory
DK-4000 Roskilde

April 11, 1996

The Aeroelastic Code HawC – Model and Comparisons

Jørgen Thirstrup Petersen
The Test Station for Wind Turbines
Department of Meteorology and Wind Energy
Risø National Laboratory
DK-4000 Roskilde, Denmark

ABSTRACT

A general aeroelastic finite element model for simulation of the dynamic response of horizontal axis wind turbines is presented. The model has been developed with the aim to establish an effective research tool, which can support the general investigation of wind turbine dynamics and research in specific areas of wind turbine modelling.

The model concentrates on the correct representation of the inertia forces in a form, which makes it possible to recognize and isolate effects originating from specific degrees of freedom. The turbine structure is divided into substructures, and nonlinear kinematic terms are retained in the equations of motion. Moderate geometric nonlinearities are allowed for. Gravity and a full wind field including 3-dimensional 3-component turbulence are included in the loading. Simulation results for a typical three bladed, stall regulated wind turbine are presented and compared with measurements.

1. INTRODUCTION

The continued work with development of wind turbines, which are more optimized with respect to material costs, will inevitably lead to structures being more flexible. To obtain a qualified estimate of the design life for such structures, it is important to establish reliable models and complete aeroelastic codes, which are capable of correctly representing the complex loading in general and the dynamic effects on the turbine in particular.

At present several existing models comply with this demand to a very satisfactory extent, and it has become general practice to use such models in the wind turbine industry during the design process as well as in the research community. The success of the models is closely linked to the level of their verification. Several models have now been continuously in use for about a decade, and their development have been closely connected to measuring programs. The complex validation of the models has thereby reached a rather mature level, and their weaknesses are considered rather well identified.

The majority of the aeroelastic models are based on the modal formulation and a time domain solution. The modal formulation is an effective way of reducing the number of degrees of freedom (DOFs) and thereby reducing the time needed for obtaining a result. These models are primarily well suited for design purposes, but their limitations will often exclude them for research purposes, where the main task usually is to investigate the areas, which the simpler models do not cover.

The present aeroelastic code – HawC (derived from *horizontal axis wind turbine code*) – is primarily considered a research tool. Its development was initiated in a Ph.D. study at Risø in 1986, and the first operational version of the model was ready in 1990 [4]. Since then, the model has been continuously in use, and has been extended in several areas. The development has been accompanied with a continued verification process connected to sev-

eral measurement programs.

The model concentrates on the correct representation of the inertia loads in a form, which makes it possible to identify and isolate the inertia loads according to their origin.

The model is based on the finite element formulation and a simple prismatic beam element is used. The wind turbine is divided into three substructures comprising the tower, the shaft-nacelle and the rotor blades. The substructures are coupled at nodes where important bearing restrained degrees of freedom (DOFs) usually are located. At the tower top node the yaw and the azimuthal rotation takes place. At the shaft end the teeter bearing is located. In the model these bearing rotations are treated as real DOFs, and they enter a general kinematic analysis together with the elastic deformations – translations and rotations – at the tower top and at the shaft end. The kinematic analysis results in the accelerations of the material points on the substructures and subsequently in the inertia loads. The inertia loads are consistently transformed to the nodes resulting in expressions combined of matrices and vectors. The local dependency is expressed through the mass-, Coriolis-, and softening matrices. Due to the kinematic coupling additional inertia terms arise. They can be arranged in the equations of motion (EOMs) as additional matrices of the types above and vectors.

In general, the equations are nonlinear due to product terms of the DOFs. The kinematic analysis provides for the geometric compatibility between the substructures, and the final EOMs are obtained by imposing force equilibrium at the two sets of substructure coupling nodes.

Structural damping is represented as proportional damping. The aerodynamic loading is derived by use of a quasi-steady theory. The influence of the elastic deformations on the aerodynamic force is taken into account. The wind field includes wind shear, tower shadow and simulated turbulence.

Based on the mathematical model a computer program has been developed. The program may be run on a personal computer, but with models having more than say 150 DOFs, a more powerful workstation will usually be needed to keep the answering times within reasonable limits. The nonlinear EOMs are solved in the time domain by use of an implicit Newmark integration scheme in combination with iterations, performed to ensure equilibrium at each time step. When running the program, different levels of linearization and the actual DOFs can be chosen.

Below simulations performed on a three bladed, stall regulated wind turbine are presented.

2. STRUCTURAL MODEL

The discretization of the wind turbine structure is performed by use of prismatic, finite beam elements with two nodes. Each node has 6 DOFs, corresponding to 3 translations and 3 rotations. Coupling between bending and torsion of the element is accounted for. Shear rotations are also included in the equations, but warping is neglected.

The division of the wind turbine in the tower, shaft and blade substructures and the attached coordinate systems are shown in Fig. 1.

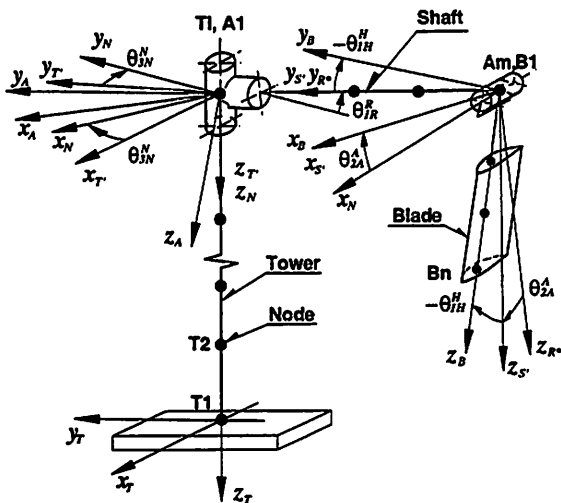


Figure 1. Substructures and coordinate systems. Undeformed state.

An example of division of the substructures in finite elements is also shown in the figure together with the node numbering. The tower nodes are numbered from $T1$ to Tl , the shaft nodes from $A1$ to Am and the blade nodes from $B1$ to Bn . The common node between tower (Tl) and shaft ($A1$) and accordingly the common node between the shaft (Am) and the blades ($B1$) comprise the two substructure coupling nodes.

The angular rotations (θ) are referenced to the coordinate axes with the sign in accordance with the right hand screw rule. The lower indices 1, 2 and 3 refer to the respective axes x , y and z about which the rotation takes

place, and the letter indices refer to the actual coordinate system. Each of the following 3 coordinate systems is rigidly attached to the first node on one of the 3 substructures. The T -system to the tower substructure at $T1$, the A -system to the shaft substructure at $A1$ and the B -system to the blade substructure at $B1$. Within these coordinate systems the substructure models are formed. At the tower top (Tl) a coordinate system (index T') is rigidly attached, following the tower top during deformation. Equivalently, at the shaft end (Am) the S' -system is rigidly attached following the shaft during deformation. The rotations of these two coordinate systems are found as a part of the solution, namely the angular DOFs $\theta_{iTl}^{T'}$ and $\theta_{iAm}^{S'}$ ($i = 1,2,3$ or $i = x,y,z$), respectively. Through the transformation matrices described in Sec. 3, these DOFs enter the kinematic analysis together with the bearing restrained DOFs corresponding to yaw (θ_{3N}^N), azimuthal rotation (θ_{2A}^A) and teeter rotation (θ_{1H}^H). The remaining coordinate systems in Fig. 1 serve to define some intermediate reference positions, corresponding to the undeformed state. The N -system follows the nacelle. The R^* system is stationary in the nacelle but rotated relative to the N -system corresponding to the tilt angle, θ_{1R}^R .

The figure does not reveal the whole truth about the node numbering on the blades and the modelling possibilities for the blades. In the program it is possible to model 2 or 3 blades and any geometry can be represented as long as the beam element is considered adequate. For example coning and pitch are modelled within the blade substructure. The node numbering is accomplished so that the matrices get a banded structure.

The deformations at a node, for example on the blade substructure, are expressed by the 6 component vector

$$\{q_{Bi}^B(t)\} = \left\{ \begin{array}{l} \{u_{Bi}^B(t)\} \\ \{\theta_{Bi}^B(t)\} \end{array} \right\} = \left\{ \begin{array}{l} u_{xBi}^B(t) \\ u_{yBi}^B(t) \\ u_{zBi}^B(t) \\ \theta_{xBi}^B(t) \\ \theta_{yBi}^B(t) \\ \theta_{zBi}^B(t) \end{array} \right\} \quad (1)$$

where u represents translation and θ rotation at the node. The upper index B refers to the coordinate system to which the vector components are referenced and the lower index Bi shows that the components are related to node No. i on the blade substructure. This expresses the general notation used for vectors.

The substructuring has the obvious advantage that the incorporation of the elastic rotations and the bearing restrained rotations in the kinematic analysis is considerably simplified. Further, the substructuring has two other important implications. One is that the rigid body rotations of the substructures are removed from the deformation vectors, and this implies that the limitations on the allowable rotations at the nodes on the shaft and the blade substructures are extended. These limitations arise because finite rotations cannot be expressed as vectors. Another implication is that updating of the geometry in the deformed state, according to the rotations at

the two coupling nodes, is computationally rather cheap and can be easily done during solution of the equations. Thus, only the geometric nonlinearities within a substructure need further consideration, when the structure is deformed. The influence of the axial force on the deformed blade elements is taken into account in a linearized form through a geometric stiffness matrix.

3. KINEMATIC ANALYSIS

The EOMs are derived by use of Newtons direct method. The acceleration of a material point on the substructures is found as the second time derivative of the position vector in the inertial system (T) to the point in question. For example for a blade point we have

$$\{r_{B0}^T\} = \{s_{Tl}^T\} + [T_{T'T}][T_{NT'}][T_{RN}][T_{AR}] \left(\{s_{Am}^A\} + [T_{S'A}][T_{BS'}]\{s_B^B\} \right) \quad (2)$$

where $\{s\} = \{r\} + \{u(t)\}$ is the position vector in the substructure coordinate system in the deformed state. Here $\{r\}$ is constant and reflects the geometry in the undeformed state and $\{u\}$ is the deformation. In Eq. 2 the terms in square brackets are 3×3 transformation matrices, as an example $[T_{T'T}]$ transforms vector coordinates from the T' -system to the T -system. The differentiation with respect to time is carried out directly in Eq. 2 using the chain rule. When differentiating, for example

$$[T_{T'T}] = \left[T_{T'T} \left(\{ \theta_{Tl}^T(t) \} \right) \right] \quad (3)$$

the time dependency of the matrices must be kept in mind. The result for the acceleration is combined of matrix and vector cross products and is a rather complicated expression which, in spite of that, can be identified as representing terms equivalent to the terms of the well known four term expression for a single rotating coordinate system, i.e. translational acceleration, centrifugal acceleration, Coriolis acceleration and acceleration due to nonuniform rotation. The result is not represented in the present context.

An intermediate result of the kinematic analysis is the velocity of points on the blade substructure, which is used in the aerodynamic calculation.

The acceleration expression is evaluated by carrying out the multiplications by use of the algebraic programming system REDUCE [3] and subsequently ordering the terms according to common factors of DOFs and their time derivatives. This ordering is performed by a filtering program written in FORTRAN 77 and specially developed for the purpose. Any directions for linearization are also introduced in the REDUCE program.

For a blade point the form of the resulting acceleration expression is

$$\{\ddot{r}_{B0}^B\} = [A_B]\{s_B^B\} + [B_B]\{\dot{u}_B^B\} + [C_B]\{\ddot{u}_B^B\} + \{a_{Bc}^B\} \quad (4)$$

where the elements in the coefficient matrices $[A_B]$ and $[B_B]$ and in the vector $\{a_{Bc}^B\}$ are functions partly of the system parameters and partly of the DOFs for the structure outside the blade substructure and their time derivatives. $[C_B]$ is the unity matrix. $[B_B]$ is skew-symmetric. The vector $\{a_{Bc}^B\}$ is after the filtering written as

$$\{a_{Bc}^B\} = [D_B]\{\ddot{u}_{Tl}^T\} + [E_B]\{\dot{\theta}_{Tl}^T\} + [F_B]\{\ddot{\theta}_{Tl}^T\} + [G_B]\{u_{Am}^A\} + [H_B]\{\dot{u}_{Am}^A\} + [R_B]\{\ddot{u}_{Am}^A\} \quad (5)$$

where still the coefficient matrices generally are functions of system parameters and DOFs.

4. EQUATIONS OF MOTION

According to the principle of virtual displacements, the inertia loads are consistently transformed to the nodes. After having performed the volume integral for an element, the 12×1 vector of inertia node loads can be written (still with the blade substructure as an example)

$$\{F_B^E\} = -[M_B]\{\dot{q}^E\} - [C_{BC}]\{\dot{q}^E\} - [K_{BI}]\{q^E\} - \{F_{4B}^E\} - [F_5][T_{EB}]^T[A_B]\left(\{r_2^B\} - \{r_1^B\}\right) - [F_6][T_{EB}]^T\left([A_B]\{r_1^B\} + \{a_{Bc}^B\}\right) \quad (6)$$

where now the material and local geometry dependency are inherent in the expression. In Eq. 6 the following is noted about the terms: Index E refers to local finite element coordinate system, the $[T_{EB}]$ matrix transforms vectors from the local element coordinate system to the blade substructure system, upper index T indicates the transpose, $[M_B]$ is the mass matrix, $[C_{BC}]$ is the skew-symmetric Coriolis matrix originating from the $[B_B]$ matrix mentioned in Sec. 3, $[K_{BI}]$ is the softening matrix originating from the $[A_B]$ matrix, $\{F_{4B}^E\}$ is a vector being a rather complex function of the $[A_B]$ matrix and material and geometric parameters, $[F_5]$ and $[F_6]$ are functions of geometry and material parameters, $\{r_1^B\}$ and $\{r_2^B\}$ are substructure position vectors to element node 1 and node 2, respectively.

The two last lines of Eq. 6 can be rewritten by extracting DOFs from the $[A_B]$ matrix according to the following decomposition

$$[A_B]\{r_j^B\} = [T2_j]\{\ddot{\theta}_{Tl}^T\} + [T1_j]\{\dot{\theta}_{Tl}^T\} + [S2_j]\{\ddot{\theta}_{Am}^A\} + [S1_j]\{\dot{\theta}_{Am}^A\} + [S0_j]\{\theta_{Am}^A\} + \{H2_j^B\}\ddot{\theta}_{1H}^H + \{H1_j^B\}\dot{\theta}_{1H}^H + \{C0_j^B\} \quad (7)$$

where $j = 1$ or $j = 2$. These terms result in additional mass-, Coriolis- and softening matrices.

Further, it is possible to decompose $\{F_{4B}^E\}$ as a matrix product. This will not be shown in the present context. After substitution of the decomposed results in Eq. 6 and equating the resulting inertia force with the elastic deformation force, the undamped, homogeneous, dynamic element equilibrium equation is obtained, for the moment neglecting the boundary conditions. The subsequent steps in establishing the system EOMs are

- the element structural damping is introduced
- the distributed external forces (gravity and aerodynamic force) are consistently transformed to the element nodes
- the element equations are coupled to the substructure equations by imposing displacement compatibility and force equilibrium at the nodes
- the substructure equations are coupled to the system equations by imposing force equilibrium at the coupling nodes
- the boundary conditions at the tower foundation are introduced

The structural damping is taken into account as proportional damping, i.e. the damping matrix is a linear combination of the mass- and the stiffness-matrix. The deterministic wind field includes logarithmic or user-defined shear and tower interference, which is modeled as a potential flow. Turbulence is simulated, either by use of the Sandia model [5] or the Mann model [2], giving a 3-dimensional and 3-component turbulence field, which is added vectorially to the deterministic wind field. The aerodynamic load is calculated by use of the well known quasi-steady blade element theory and momentum balance. A model for dynamic stall is included as well as the possibility for applying pitch regulation.

The solution of the EOMs is carried out by means of the Newmark implicit integration scheme in combination with Newton-Raphson iterations, performed to ensure equilibrium of the nonlinear equations at each time step [1], thus preventing the accumulation of errors.

The natural frequencies and the modeshapes can be calculated and illustrated by animation.

5. SIMULATION RESULTS

Results from simulation with HawC have been compared with measurements on the three bladed, stall regulated, 500 kW Nordtank NTK-500/37 wind turbine, which has been intensively tested at the homogeneous Risø test site. The finite element model consists of 5 elements on the tower, 2 on the shaft and 7 on each blade, resulting in a total of 168 DOFs. The main data and the fundamental frequencies for the turbine, corresponding to stand still, are listed in Table 1.

The mean wind speed is close to 10 m/s and the turbulence intensity close to 14%.

Table 1. Main data for Nordtank 500 kW.

Rotor diameter:	37.0 m
Tower height:	33.8 m
Tower design:	Tapered, tubular, steel
Rotational freq. (1P):	0.50 Hz
1 st tower bending freq.:	0.81 Hz
Shaft tors. freq.:	1.08 Hz
Rotor yaw freq.:	1.63 Hz
Rotor tilt freq.:	1.72 Hz
1 st blade flapwise freq.:	2.07 Hz
1 st blade edgewise freq.:	3.43 Hz

In general, good agreement is found between the measured and the simulated results. Examples of the power spectral density (PSD) of selected moments and the electrical power are shown below. The covered time period is 600 seconds, and the sample frequency is 32 Hz. The spectra have 8 statistical degrees of freedom. In all plots the effect of rotationally sampling of turbulence is revealed as peaks at multiples of the rotor rotational frequency (1P) indicating that the representation of the turbulence in this homogeneous case is satisfactory

In Fig. 2 the flapwise blade root bending moment is shown. The distribution on the frequencies show that the dynamics is well represented. The differences in energy levels may all be contributed to the statistical uncertainties.

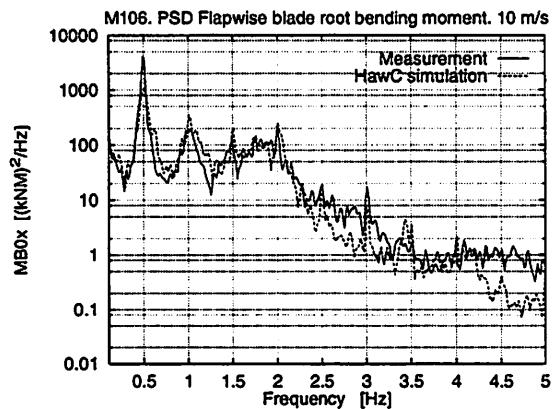


Figure 2. Comparison of PSDs of blade flapwise bending moment.

The PSD of the edgewise blade root moment is shown in Fig. 3. A rather pronounced discrepancy is observed in the range from 2P-4P. A reason for this might be a cross-coupling between the flapwise and edgewise strain-gauges. If the measured response is correct, then it must have its origin in a symmetric rotor mode, as the discrepancy is not observed outside the rotor, as can be seen on the later PSDs e.g. of the shaft torsional moment in Fig. 6.

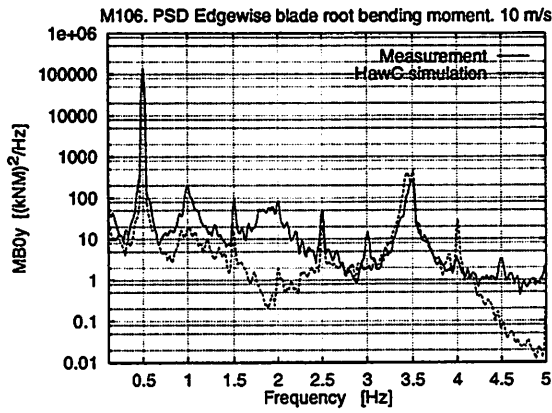


Figure 3. Comparison of PSDs of blade edgewise bending moment.

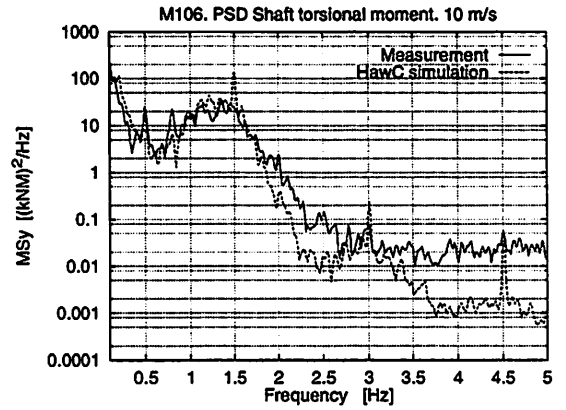


Figure 6. Comparison of PSDs of shaft torsional moment.

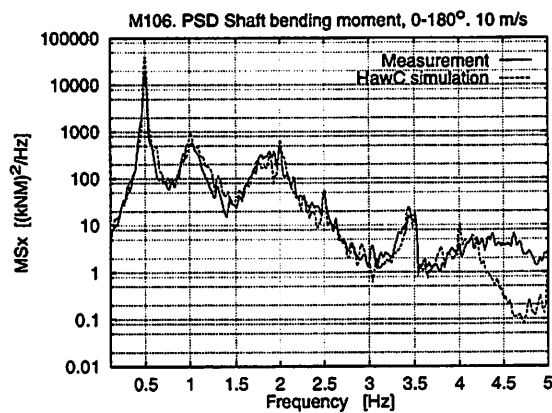


Figure 4. Comparison of PSDs of main shaft bending moment. Rotating.

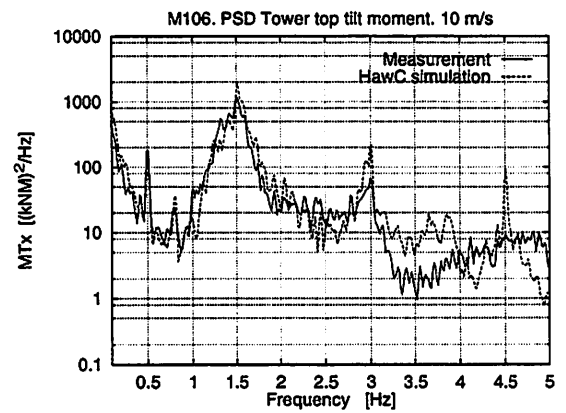


Figure 7. Comparison of PSDs of tower top tilt moment.

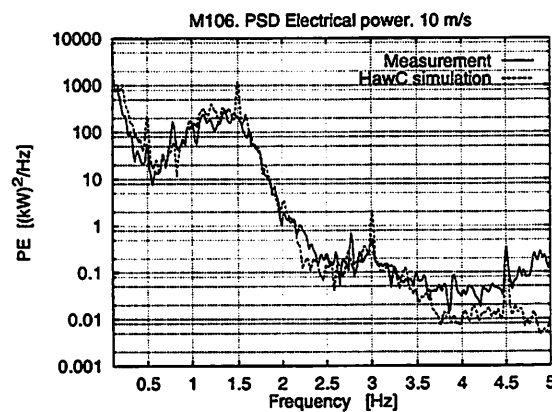


Figure 5. Comparison of PSDs of electrical power.

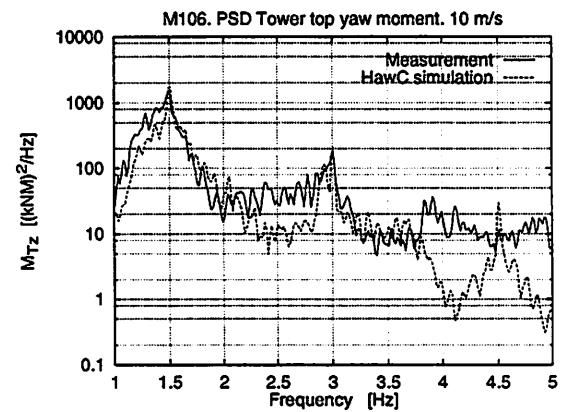


Figure 8. Comparison of PSDs of tower top yaw moment.

6. CONCLUSION

A model for simulation of the dynamic response of horizontal axis wind turbines has been presented. The model is rather general as regards representation of inertia loads. It is primarily intended to be a research tool for use when the influence of specific dynamic effects are investigated and further to support the development of models well suited for parametric studies.

The presented comparisons show that the model is well behaved with respect to dynamics of a typical Danish stall regulated wind turbine in homogeneous terrain. This behaviour is representative for all turbines of comparable design flexibility.

The above mentioned validation process is continued and will consecutively reveal the weaker areas of the aeroelastic model relative to the actual need, which is identified mainly by the industry but also by research work, where the aim is to be ahead of the present stage of industrial development.

Usually, the improvements of the structural parts of the model is straight forward and basically a matter of investing the time needed, because well established techniques can be applied. The situation is a little different with respect to the description of the flow, both the atmospheric flow and the aerodynamics, because these areas cover research representing new knowledge.

In short the development areas of most concern at the moment is listed without priority. Areas related to structure have been omitted for the reasons mentioned above. The following areas are considered important candidates for improvement and/or implementation:

- Validated models for dynamic stall.
- Models for atmospheric flow in complex terrain.
- Models for flow in wake and park conditions.
- Models for yawed flow.

REFERENCES

- [1] Bathe, K.-J. *Finite Element Procedures in Engineering Analysis*. Prentice-Hall, Englewood Cliffs, New Jersey, 1982.
- [2] Mann, J. and Krenk S. *Fourier Simulation of a Non-Isotropic Wind Field Model*. Paper no. 117/3/27. In Proceedings of the 6th International Conference on Structural Safety and Reliability, ICOSSAR'93, Innsbruck, Austria, 9-13 August, 1993.
- [3] Hearn, A.C. *Reduce User's Manual*. Version 3.3, RAND Publication CP78 (Rev. 7/87). The RAND Corporation. Santa Monica, California, 1987.
- [4] Petersen, J.T. *Kinematically Nonlinear Finite Element Model of a Horizontal Axis Wind Turbine*. Ph.D. thesis. Dept. of Meteorology and Wind Energy. Risø National Laboratory. Roskilde, Denmark, 1990.
- [5] Veers, P. *Three-dimensional wind simulation*. Sandia report. SAND88-015. Sandia National Laboratories. Albuquerque, New Mexico, 1988.

**IEA-Symposium on
State of the Art of Aeroelastic Codes for Wind
Turbine Calculations,
Lyngby April 11-12, 1996**

Design Basis 2.

Gunner Larsen and Poul Sørensen

Risø National Laboratory, Roskilde, Denmark

April 1996

1 Introduction.

Design Basis Program 2 (DBP2) is comprehensive *fully coupled* code which has the capability to operate in the time domain as well as in the frequency domain. The code was developed during the period 1991-93 and succeed Design Basis 1, which is a *one-blade model* presuming stiff tower, transmission system and hub.

The package is designed for use on a personal computer and offers a user-friendly environment based on menu-driven editing and control facilities, and with graphics used extensively for the data presentation. Moreover in-data as well as results are dumped on files in Ascii-format. The input data is organized in a in-data base with a structure that easily allows for arbitrary combinations of defined structural components and load cases.

2 The model

Basically DBP2 is a fully integrated model of a *horizontal axis* turbine with all essential couplings between tower, transmission system, generator and blades taken into account. At present the model is limited to standstill situations and to normal operation of the turbine. *Constant rotational speed* is assumed, which does not prevent modelling of the small induction generator slip, but it do prevent modelling of inverter connected variable speed wind turbines with a large rotor speed range. Moreover, the number of blades is *presumed* larger than two in order to ensure rotational symmetry of the rotor. The last assumption is closely related to the decomposition of the harmonics in the frequency domain [2].

The structure of the model is illustrated in Figure 1.

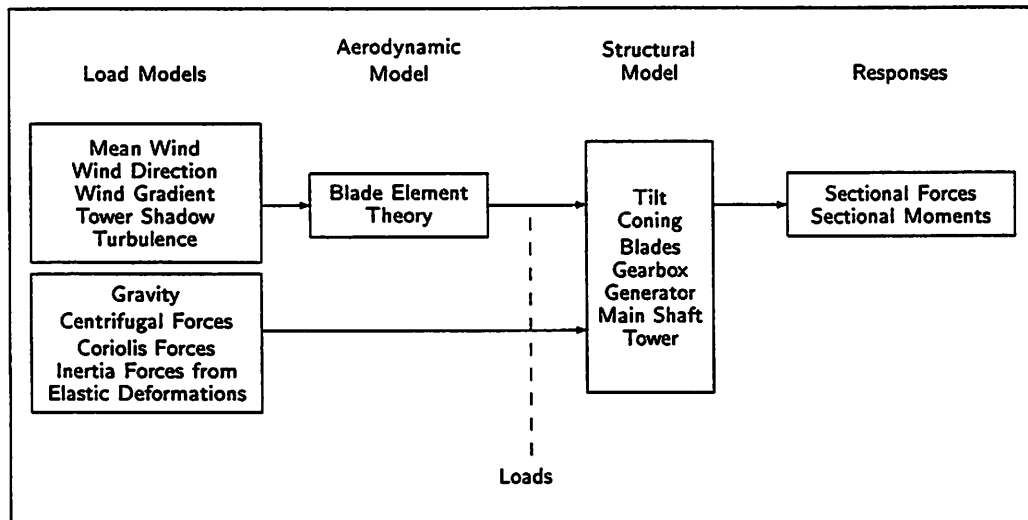


Figure 1. Elements of the model.

The *load models* comprise volume forces (gravity-, centrifugal-, Coriolis forces, and inertia forces due to elastic deformations of the structure) and surface forces caused by the wind field. The wind field contains a deterministic as well as a stochastic component, thus inducing elastic deformations comprising both a deterministic and a stochastic part. Taking into account geometric stiffness and weakening contributions in the structural model, all the volume forces comprises a deterministic as well as a stochastic load part.

The *wind load* due to the mean wind (including wind shear, tower influence, yaw error, and inclination of the ground) comprises the deterministic part of the wind, whereas the temporal wind variation caused by turbulence is introduced in terms of a stochastic process model.

The *tower shadow model* is based on a simple two dimensional potential flow field solution, and is applicable only for upwind-type turbines with tubular towers. However, in the case of a lattice tower, an approximate tower effect can be obtained by specifying a equivalent fictitious tubular tower diameter.

The *turbulence model* (used in the time domain approach) is based on the Sandia method [3]. The algorithm generates wind turbulence time series at a chosen number of points in a plane perpendicular to the mean wind direction and propagates the time series in the mean wind direction at the mean wind speed (i.e. Taylor's frozen turbulence hypothesis is assumed valid). Only the turbulence component perpendicular to the rotor plane is considered in this context, and the method ensures correct modelling of both the single point power spectral densities of the wind speed and the correlation between wind series at two arbitrary points (assuming homogeneous turbulence in the cross wind plane).

The *aerodynamic model* is used to transform the wind flow field to loads on the structure. Here an extended version of the two-dimensional blade element theory has been applied. Inclination of ground surface, tilt, yaw-error, and coning can be taken into account.

The basic assumptions for the blade element theory are that the flow is stationary and laminar. Although the basic assumptions to some degree are violated, the load derivatives with respect to the wind speed components (influence coefficients), as predicted by the theory, are used to handle the unsteady wind loading. This linearization is crucial for the frequency domain solution. In performing this linearization the *equilibrium wake* approach is adopted, where the induced velocities in the rotor plane takes values related to the instantaneous wind speeds in the gradient estimate. Consequently, the approach requires that the up- and downstream conditions to be instantaneously adjusted in accordance with momentum theory; this is believed to be best fulfilled for relatively slow variations and is in agreement with the conception of the structure as a low pass filter. Within the present concept, the application of a detailed non-linear stall hysteresis model is excluded, and the gradient approximation is also used for calculations in the stall regime.

In formulating the *structural model*, the wind turbine is idealized as a structure composed of four main component types - tower, generator, transmission system, and blade. Tower, transmission system, and blades are modelled as one dimensional beams, and here the common small-deformation assumption is adopted. The mechanical behaviour of the generator is described only in terms of damping and inertia quantities.

In the present context the *tower* component is the elastic structure extending from the foundation to the point of intersection between the axis of rotation of the rotor (referring to a undeformed structure), and a vertical line through the centre of the base. The tower component thus include the elastic behaviour of the nacelle structure. The foundation is presumed as being fully rigid, and consequently the tower boundary conditions at the base end are zero deflection and zero slope. However, the inclusion of a suitable elastic element close to the ground will approximate other characteristics of fundation.

The *generator* is modelled as an asynchronous generator with the mechanical moment linearly related to the generator slip. The transmission system is the designation for the rotating elastic structure extending from the tower top to the centre of the rotor, and the blade is the elastic structure between the centre of the rotor and the blade tip.

A complete structural model of the wind turbine can now be obtained by combining a tower component, a generator component, a transmission system component, and a number (larger than or equal to three) of blade components as illustrated in Figure 2.

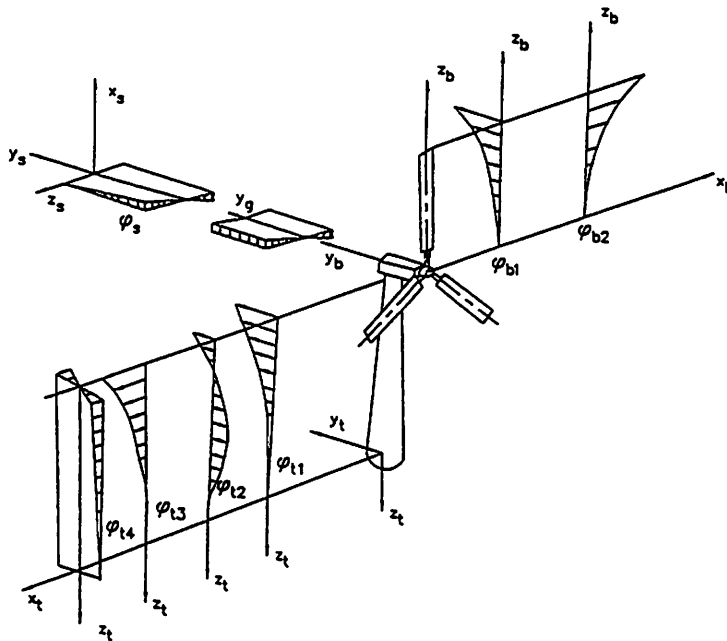


Figure 2. Degrees of freedom and component coordinate systems.

As indicated in Figure 2, a right-handed Cartesian coordinate system is attached to each of the component types, with generator and transmission system using the same system. Note, that in coordinate systems related to beam structures, the coordinate directions perpendicular to the beam axis are always directed along principal axis, and for the tower the y-axis is moreover directed along the mean wind direction. A lower coordinate index t refers to tower, whereas indices s and b refers to shaft and blade, respectively.

The *principal axis* are assumed to have identical orientation in all cross sections of a particular structural component, thus excluding the possibility of structural

modelling of pretwist in the blade structure. Consequently the user of the code has to compromise by selecting a single *structural pitch angle* which is considered to be representative for the entire blade.

In formulating the dynamic equilibrium equations the modal decomposition technique is adopted for the components tower, transmission system and blades. Thus, the resulting equations are formulated with a mixture of generalized coordinates (modal amplitude functions) and physical coordinates as the unknowns. The degrees of freedom in question are illustrated in Figure 2, with the φ 's denoting the actual mode shape functions. As with the coordinate directions, the lower indices attached to the mode shape functions refer to tower, shaft and blades, respectively.

To improve clarity in the figure, the blade mode shapes have only been given for one of the blades. As appears, a blade is presumed to bend in the flap- and edgewise directions in its fundamental modes, whereas a torsional deformation is excluded.

The shaft is limited to elastic deformation in its fundamental torsion mode and no bending deformation is accepted. The tower is free to bend around the tower x- and y-axis, and to twist around the tower z-axis. The tower deformations are formulated in terms of the fundamental modes in all three coordinate directions supplemented by the second bending mode in the tower y-axis direction.

Generally, the dynamic equations are formulated in the undeformed coordinate systems. However, concerning normal forces in the beam elements (typically arising from centrifugal forces and gravity), the impact from deformation of the structure on the equation of motion has been accounted for by including the moments arising from those as geometric stiffness and geometric weakening contributions.

Based on the small-deformation assumption, the equations of motion are linearized in the elastic variables.

3 Solution strategy

In the time domain, the resulting differential equations describing the deformations are solved in an iterative manner using the *Newmark method*, which has been proven successful with respect to accuracy and stability. Note, that appropriate time steps must be able to resolve the relevant natural frequencies of the compound structure.

However, basically the stochastic turbulence components are described in the frequency domain, and a more direct and much faster way of obtaining the system response is to transform the system of equilibrium equations to the frequency domain. Thus, in this situation the dynamic system is transformed to a *transfer function* which directly determine the frequency output from the frequency input and which in addition provides a direct qualitative understanding of the dynamic system behaviour.

The basic principle in obtaining the frequency domain solution is to decompose the structural variables into sums of harmonics in the (constant) angular frequency

of the rotor. Doing that, the nonlinear relations¹ between the structural variables are transformed into linear relations between the amplitudes of the harmonics of the variables. These linear relations are in turn easily transformed to the frequency domain and solved there. Thus the derivation of the amplitudes of harmonics of the response is founded on conventional frequency domain methods applied to the relations between the amplitudes of harmonics. Finally, the responses are determined uniquely from their respective amplitudes of harmonics.

The main advantage of the frequency domain view is the calculation speed (approximately a factor of 100 faster than a similar time simulation) which facilitate optimization and parameter studies in the preliminary design phase. The drawbacks are that strong non-linear phenomenon (transients etc.) cannot be described.

4 Output

Basically, the results comprises power curve, thrust curve, and performance analysis (including the distribution of the production on wind speeds presuming the mean wind speed to be Weibull-distributed), and structural responses in arbitrarily selected cross sections. The structural response include three sectional forces, three sectional moments, and modal amplitudes related to the relevant mode shapes. The output form of the response depend (of course) on whether a time domain or a frequency domain calculation is specified. In case of a frequency domain modelling, the the deterministic part of the responses are presented as an azimuthal mean, whereas the stochastic part are given in terms of power spectral densities. The response result from a time simulation is given as time series.

In order to facilitate parametric studies related to the model structure, a number of toggle functions have been integrated in the package. These control a possible elimination of degrees of freedom and allow for certain modifications in the aerodynamic algorithm concerning tip loss and rotor interference on the undisturbed mean wind field. Moreover, a number of quantities related to the solution strategy of the equations (time domain/frequency domain, convergence thresholds, sample frequency, etc.) are available to the user, giving the possibility of ensuring convergence to the "true" solution and to minimize the computer time consumption.

5 Demonstration example

In the present section, measurements have been compared with simulations obtained both with the time domain- and the frequency domain approach. The demonstration include two turbines of different size - the 2MW Tjæreborg wind turbine and a 300kW Nordtank NTK300F wind turbine. The main load parameters for the Tjæreborg turbine were : mean wind speed 11.17 m/s, turbulence intensity 12.4%, turbulence length scale 3000 m, rotor speed 22.2 RPM, and yaw error -7.8 deg.. The main load parameters for the Nordtank turbine were : mean

¹The only non-linearity is the essential kinematic non-linearity originating from the rotation of the blades relative to the tower.

wind speed 6.96 m/s, turbulence intensity 16.9%, turbulence length scale 600 m, rotor speed 39.5 RPM, and yaw error -4.2 deg.

As for the time simulations and the measurements, the deterministic- and stochastic parts of the response are separated by an azimuthal binning. Thus the deterministic part is determined as the azimuthal mean. Subsequently, the stochastic part is simply determined by subtracting the deterministic part from the total response.

In Figures 3 and 4 the deterministic- and stochastic responses, related to blade root bending moment of the Tjæreborg turbine, are shown. Figures 5 and 6 shows similar results for the Nordtank base tower bending moment.

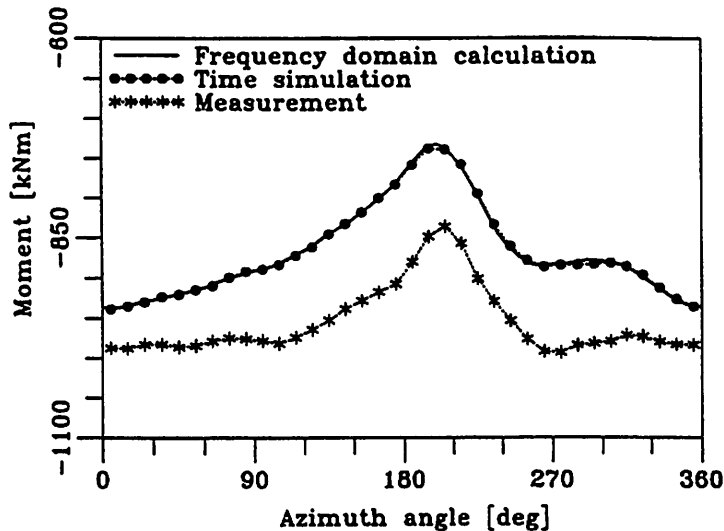


Figure 3. Deterministic response of Tjæreborg root bending moment.

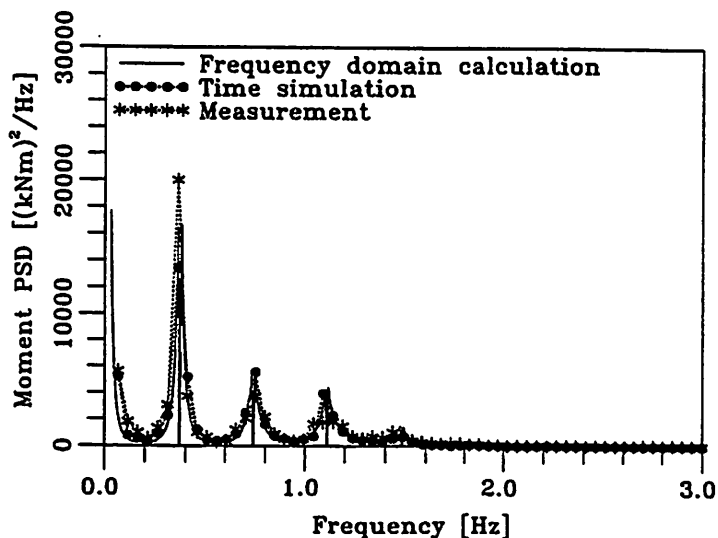


Figure 4. Stochastic response of Tjæreborg root bending moment.

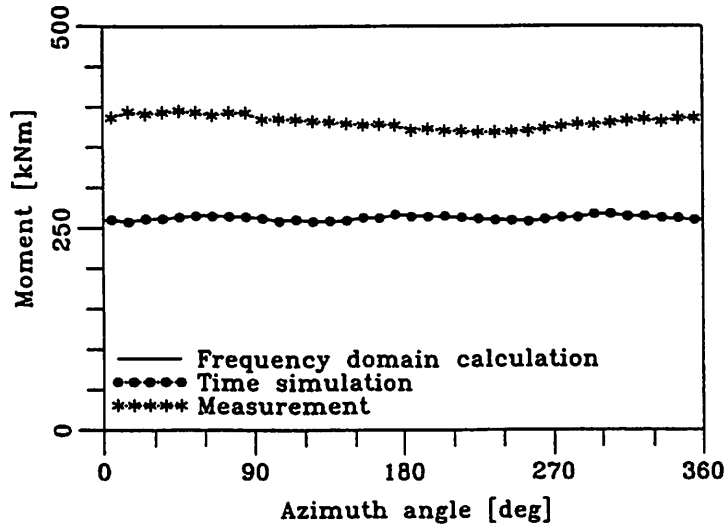


Figure 5. Deterministic response of Nordtank base bending moment.

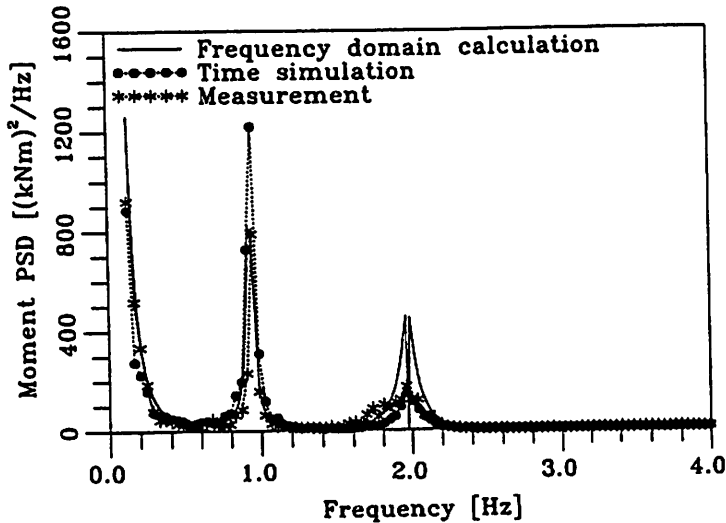


Figure 6. Stochastic response of Nordtank base bending moment.

The examples shows that measurements, frequency domain simulations, and time domain simulations are in very good agreement, both concerning the deterministic- and the stochastic response. However, the frequency domain simulations displays "dips" in the power spectral densities at harmonic frequencies. This is caused by the choice of coherence function (coherence equal to one for zero frequency). The lack of these "dips" in the time domain formulation is due to the too rough frequency resolution.

Note furthermore, that the predicted energy at relative high harmonics is less with the time domain solution than with the frequency domain solution. This is caused by the limited number of grid points in the turbulence field generation for the time domain solution causing a poor resolution in the rotational sampling of the blades in the wind field.

6 Conclusion

The time domain simulation and the frequency domain simulation has been demonstrated to give very similar results within the framework of the present model.

Generally speaking, each of the methods have their advantages and drawbacks, and they complement each other in an exelent manner. The main anvantages of the frequency domain approach are

- that it provides a direct qualitative understanding of the dynamic system behaviour,
- fast calculation speed, which faciliate parameter studies (in the preliminary design phase) and mathematical multipoint optimization,
- that considerations conserning the time steps in relation to solution stability and reliability is avoided,
- that problems with poor resolution of higher harmonics due to unsufficient spatial resolution in the turbulence grid is avoided.

The drawbacks are that strong non-linear phemenon (transients, variable rotational speed, etc.) cannot be described, and that the fatigue estimation cannot at present be based on the frequency domain response. However, the future perspective is an inclusion of a fatigue calculation, based directly on the frequency domain results.

7 References

- [1] Larsen, G.C. and Sørensen, P. (1994). Verification of Design Basis Program 2 - A Coupled Aeroelastic Wind Turbine Model. Risø-R-730(EN).
- [2] Sørensen, P., Larsen, G.C. and Christensen, C.J. (1995). A Complex Frequency Domain Model of Wind Turbine Structures. ASME Journal of Solar Energy Engineering, Vol. 117, pp. 311-317.
- [3] Veers, P.S. (1988). Three-Dimensional Wind Simulation. SAND88-0152. Sandia National Laboratories, Albuquerque, New Mexico.

Word file: Lyngby.doc

The wind turbine response program, called FKA_12 of Stentec, the Netherlands

ir. W. Kuik, Heeg, N601.01.04.96, April 9, 1996

Summary

An introduction to the dynamic response program FKA_12 for wind turbine calculations is given. Some user experience with this very fast code is given and also ideas for new development.

A paper presented at the EC,EIA R&D Wind meeting Lyngby, Denmark, April, 11/12 1996 about the State of the Art of Aeroelastic Codes for Wind Turbine Calculations

contents

1. Stentec, a company profile
2. Aeroelastic computer code
3. User experience
4. New developments
5. References
6. Figures

1. Stentec, a company profile

STENTEC means STromings ENergie TEChnologie

Stentec is specialized in aero-and hydro technology, and software development

Stentec BV is situated in Heeg in the North of the Netherlands

The company consists of 2 departments with around 12 persons

Stentec Windenergie

5 Highly qualified windturbine designers

Independent Windenergy consultant since 1983

Blade and turbine development, and international certification of windturbines

Developing specialized software for the design of horizontal axis windturbines

Dynamic response program, FEM, design spreadsheets, interactive optimisation

Clients: Windturbine and blade manufacturers, and others

Stentec Software

Spin-off of the development of Aeroelastic codes for windturbines

Developing real time simulation software for the PC market since 1990

International sales since 1993 of Sail Simulator, and Laser Match Racing

From Borland Pascal and Intel Assembly for DOS to Borland Delphi for Windows (3.11/95)

Latest development: Sail Simulator 3 (sept 96), and Bird Flight Simulator (sept 97)

Stentec Milestones for the Netherlands

First dynamic response program in 1983

Design of a multiwindturbine with 6 rotors in 1987

First stochastic windfield generator in 1990

First certification in 1986, using the dynamic response code for loadspectrum calculation

Stentec can be contacted via:

Post	Hollingerstr 14, 8621 CA, Heeg, the Netherlands
Telephone	+31 515 443515
Fax	+31 515 443586
E-Mail	Stentec@pi.net

2. **Aeroelastic computer code**

<u>name</u>	FKA
<u>current version</u>	FKA12
<u>description</u>	Time response program for horizontal axis windturbines (1-4 blades)
<u>technique</u>	Differential model, according to bladelement-impuls theory Modeshape input, from FEM, Blade hinge model for flap and lag Advanced postprocessor with Statistics, Rainflow Counting, Markov Matrices and FFT
<u>Options</u>	Stochastic windfield generator according to ESDU Batch calculating and processing View of turbine deformation during calculation
<u>degrees of freedom</u>	Blade pitch, flap, lag (per blade) Rotor Shaft azimuth angle, generator angle Yaw yaw coupling, yawmotor angle Tower 1e and 2e forward modes, 1e sideward mode, and torsional mode
<u>Wake model</u>	Constant axial disturbance factor (a) conform a helicopter model Correction of this factor conform a Glauert model and measurements for oblique flow Time constant U/R used for a dynamic wake effect. Tangential factor (a') directly calculated from the local tangential profile forces, taking the wakerotation into account.
<u>Blade area</u>	Prandtl tip correction on C_l and C_m , taking tip and root effect into account (c/r) dependent correction of airfoil polar, giving higher root C_L values (centrifugal effect) 20 different airfoil polars as input can be used.
<u>Windmodel</u>	All kinds of deterministic shapes or a
<u>Stochastic windfield generator, called EWS_4</u>	$u(y,z,t)$ and $v(t)$, according to ESDU Waves $u(z',t)$ are generated by filtering a white noise. A wave runs in a specific direction in the rotorplane. e.g. from left to right. They have an ESDU length scale and turbulence intensity. The local longitudinal wind speed is the addition of this ESDU waves which are rolling over the rotorplane from 9 different directions (see fig. 7 for principle view).
	advantages of EWS 1. Fast 2. Windfield generation during timeresponse, of infinite length 3. Good results of resulting loadspectra. compared to other spectra and measurements (fig. 2) 4. Easy expandable to $v,w(y,z,t)$ conform ESDU
<u>Output</u>	The dynamic response includes all coupling terms, between tower, rotor and drivetrain In fig. 1 a frequency diagram is given, showing rotor speed where resonance or interaction is possible. Loadspectra for all internal forces (fig. 3), with fatigue reserve factors calculated with standard S-N curves (e.g. NEN 2096)

3. User experience

High Speed Loadspectra generation, due to optimized code and blade hinge model

example Turbine model	3 blades, 12 elements per blade, active pitch, tower 1e side and forward
Wind model	Stochastic windfield generation during simulation
Computer system	Pentium 150 Mhz PC, 1.2 Gbyte HD, 16 Mb RAM
Sum	Fatigue spectrum with 14 * 10 minutes response calculation
Timing	70 minutes for dt = 100 ms > Around one hour
Batchprocessing	around 20 minutes
Printing	10 to 30 minutes
Time factor	2 times more than realtime

Some turbines will run slower, other faster, depending on modelling and size.

Conclusions: Calculations are (more than) Real Time on fast PC's
 One Loadspectrum could be made on Monday morning, including print out.
 Optimization of e.g. pitch control is possible within a couple of days,
 taking the whole loadspectrum into account

Some projects & applications

Verification of the results, comparing to the output of other response codes, like Phatas, with well known turbines (ECN 25 HAT , NEW ECS 45), ECN KRH project (ref.1).

Development of a 2 bladed, free flapping windturbine rotor, with passive pitch control by aerodynamical moments (Cm) , on a flexible tower (Lagerwey 2 bladed LW18, fig.4)

Comparison of calculated loadspectrum and ECN measurement for LW27 (see fig.2, ref. 2)

Design of a lattice tower for India (LW30)

Non linear flutter calculations of the Cm pitch control during high winds (fig.5)

Development of a gearless 3 bladed, 45 m wind turbine, with an active positive pitchcontrol

Development of a stall regulated active pitch turbine concept (Windworld W 4500)

4. New developments and ideas

Fast and big PC's make it possible to make 1 hour fatigue runs in stead of 10 minutes.

In that case the whole turbulence spectrum will be covered (fig. 6).

1 Hour runs will have higher maxima and lower minima, almost covering extreme amplitude and gradient gusts. In stead of 11 classes $U_{wind} = 3,5,7,9,11,13,15,17,19,21,23$ m/s, perhaps 7 classes 3,6,9,12,15,18,21 m/s could be taken, considering the larger overlap.

Stentec will make use of the new Phatas III from ECN for comparative calculations, improving quality and using its advanced dynamical inflow model for special applications.

Phatas runs about 10 to 100 times slower than FKA.

The fast growing loadset size for certification documents makes it almost impossible to handle.

Therefore an output on CDROM (Golden Disk) for certification loadsets will be defined.

On the CDROM a simple postprocessor makes it possible to examine the data, and perhaps see the turbine deformation realtime. The document for certification will be much smaller and contains this CDROM.

Stentec planned to develop a Wind Turbine Sound Simulation program this year. Sound files with the blade outer part and the drivetrain as sources, will be generated in the dynamic response program, during simulation. A special Windows program will show afterwards the perspective view and stereo sound of the windturbine, taking into account ground reflections, and background noise.

Design and verification was planned this year. The Dutch blade manufacturer Aerpac will contribute to this project.

There is an older version FKA10 for use on a HP system, which works with discrete blade bending elements, like PHATAS. In this program a teeter hub and flexible support can be activated. These techniques will be implemented in the future FKA versions, leading to slower but more precise prediction of fatigue loads in the blades.

An interesting idea is to take out the axial and tangential disturbances factor (a and a'), taking wake effect according to impulse theory into account, and replace them with a model where free vortices will be shed off between the blade elements and the tip, trailing downstream in the stochastic windfield.

In principle this model can cover all the wake effects including oblique flow and dynamics and 3D airfoil data. Each timestep the new position of the end of a vortex line element must be calculated, for each blade element, to a certain depth. Besides the induced velocities on the 2D profile polar of the blade elements must be calculated. The wake spirals which influence each other, could be made visible on the screen.

This process is expected to slow down the calculations a factor 2-4, depending on the vortex wake length.

If the realization of this idea is commercially interesting is the question.

This leads me to an other important point.

Comparison with measurements shows that modern computer code can predict the loadspectrum reasonably well. For certification loadfactors must be used, e.g. 1.35 for fatigue (NEN 6096).

Improved code will sometimes introduce higher loads than the older code, giving problems to prove the strength using conventional loadfactors. Together with improving the codes, the loadfactors must be re-defined by the certification institutes, initiated by the windturbine designers.

As an example the 4P excitation due to turbulent dynamic shear of the lag mode of the blade.

This dynamic effect calculated with a new code is giving a 12% reduced and insufficient margin for fatigue strength of the bladeroot. Because this 12% is well under the 1.35 loadfactor, it could be treated as be included it the loadfactor.

For certification the old code was used. The new code would lead to redesign and a more expensive blade.

5. **References**

1. Schepers, Grol, Snel Kwalificatie rekenprogramma's horizontale as turbines (KRH), ECN, Petten, June 1989, ECN-89-96
2. Wekken, Vink Resultaten belastingsmetingen aan de Lagerwey LW27/250 te Tjerkwerd Pette, ECN, dec 1994

stationaire run (FKA12/Februari 1996 (c) Stentec)
 Windworld W4500as, Pos. Pitch, Var. Drehzahl

1e mast freq. via GIFTs bepaald

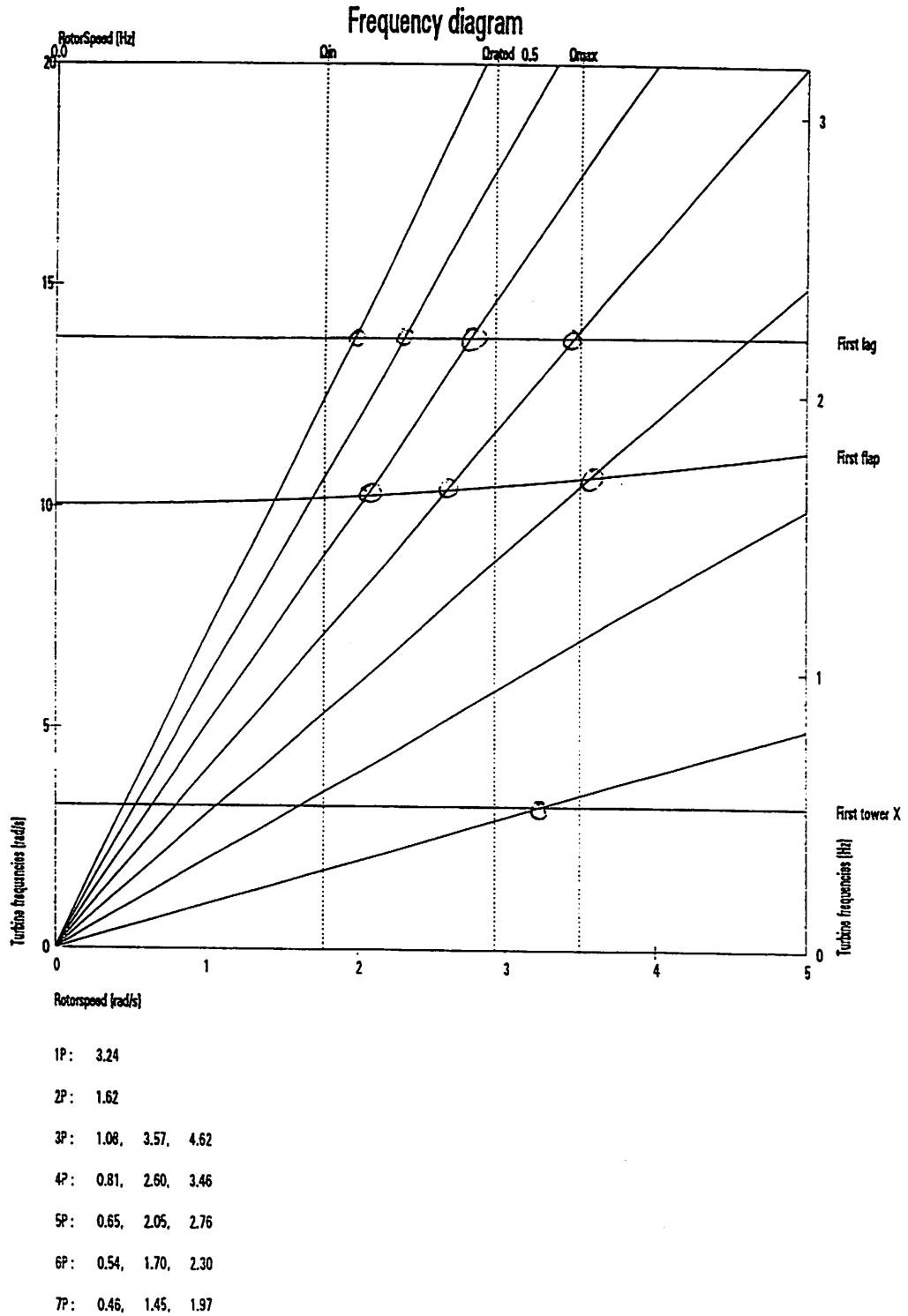


Figure 1: Frequency diagram

L 154 29 / 250

1 1/2% Turbulence
during measurements

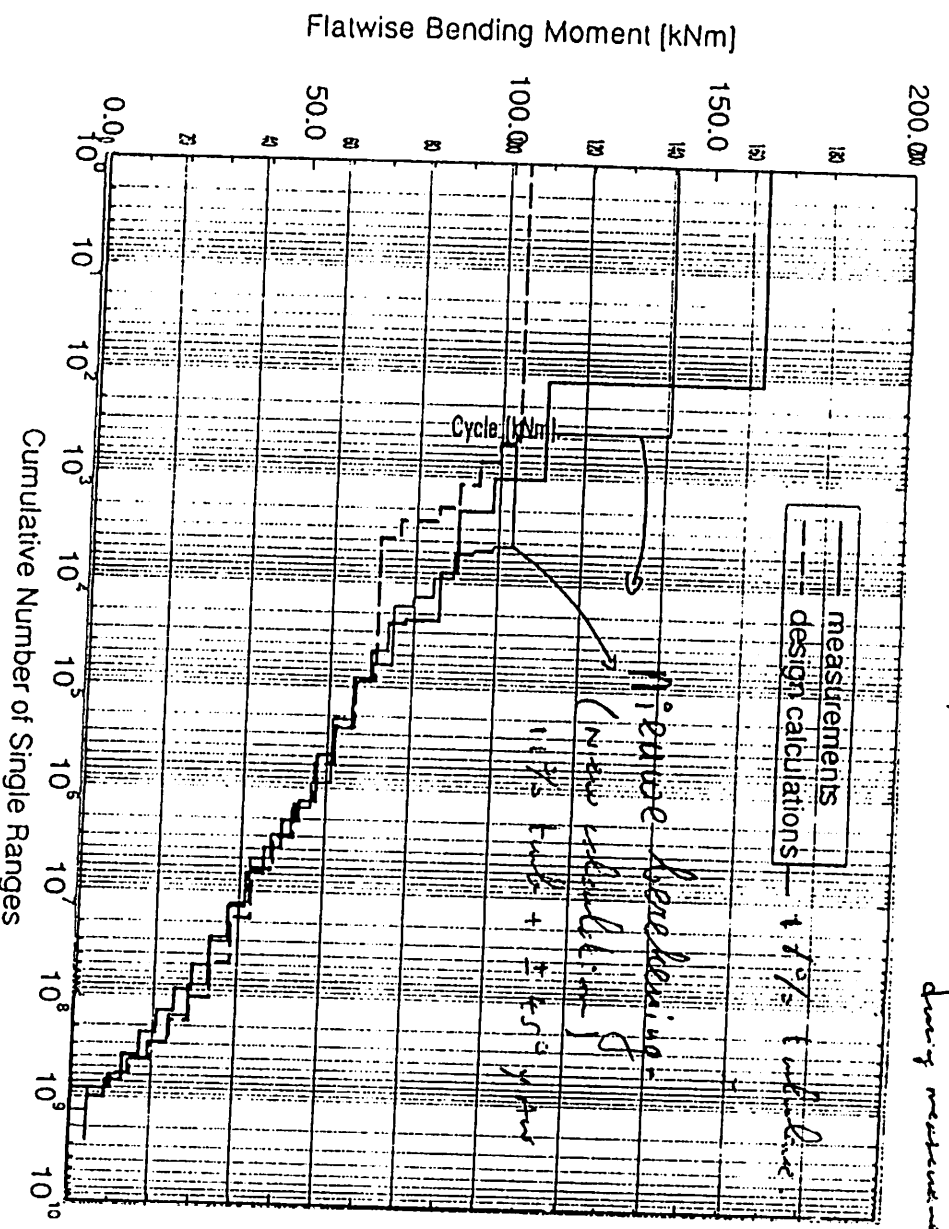


Fig. 12. Vergelijking van het ontwerp en gemeten klappelastingsspectrum. De spectra zijn opgesteld voor rotorstraal R=1,1 m en representatief voor 20 jaar bedrijf.

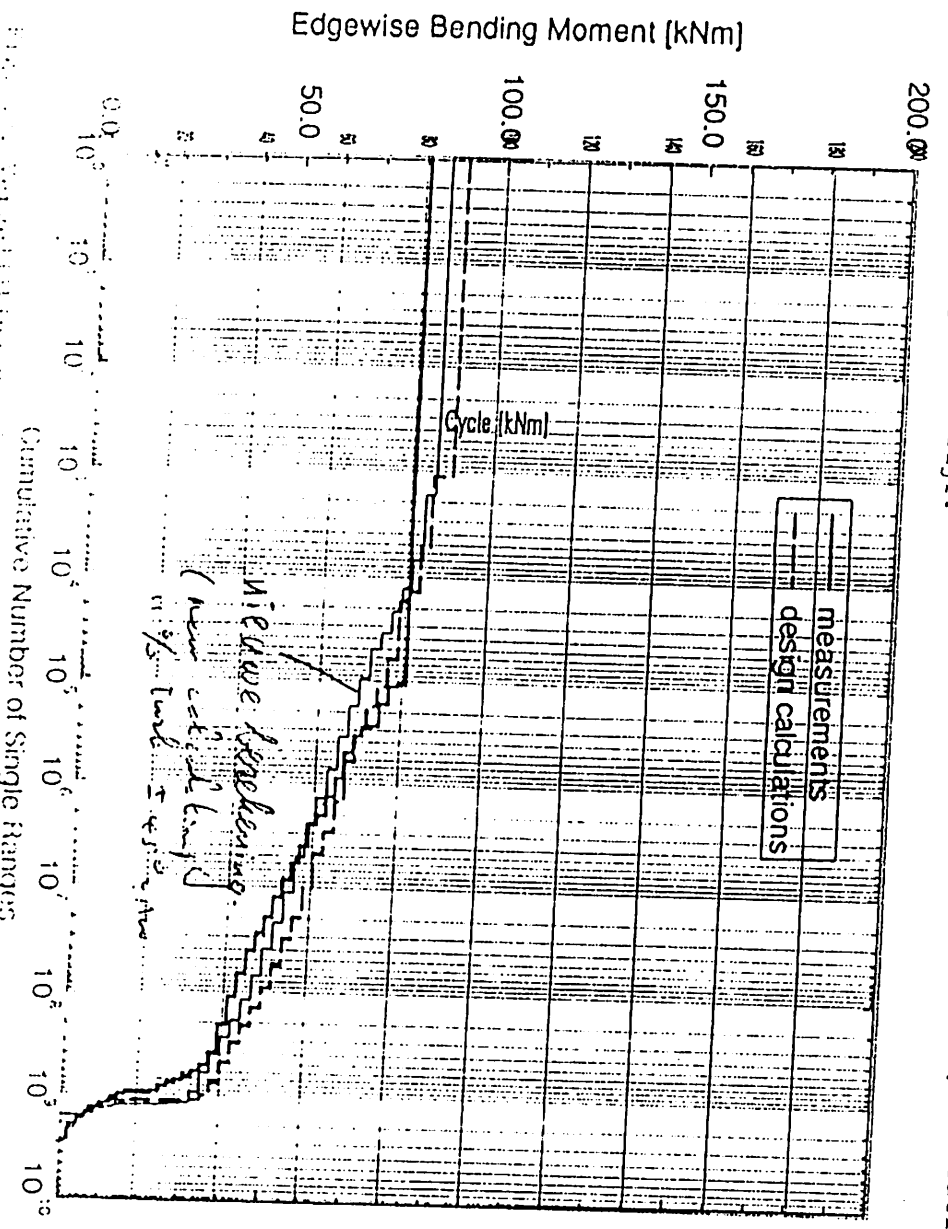


Fig. 12. Comparison of the design and measured flap loading spectrum. The spectra were set up for a rotor radius R=1.1 m and representative for 20 years of operation.

FKAll-plot Monday, Apr 3rd 1995 12:15 (c) 1993 Stentec B.V.
 Lagerwey Windturbine type : LW27/280
 buismast, blad volgens ATV7
 tbv. verificatie metingen Tjerkwerd

COMMENT:

Signal : Inplane-moment(k) kNm

Location	Frequency	Repetition (per)	Minimum	Mean	Maximum	Last Mean Square	Damage %	
Stations	0.0000	k/c	600.000	-19.592	13.864	42.386	17.490	0.000
F0	11.7619	%	600.000	-19.638	0.100	19.823	13.601	0.000
F1	17.8403	%	600.000	-20.242	1.943	24.711	13.791	0.000
F2	19.7910	%	600.000	-20.393	5.208	33.070	14.260	0.144
F3	17.6857	%	600.000	-19.672	10.042	43.832	14.858	2.437
F4	13.1846	%	600.000	-16.276	15.549	50.234	15.491	13.463
F5	8.3281	%	600.000	-16.585	17.283	53.015	15.934	26.066
F6	4.4911	%	600.000	-18.442	17.003	52.530	16.310	24.141
F7	2.0754	%	600.000	-20.532	16.516	55.023	16.660	17.016
F8	0.8233	%	600.000	-25.371	16.200	62.840	17.142	10.539
F9	0.0821	%	600.000	-33.073	15.742	72.010	18.405	1.929
FA	42.0000	/year	200.000	-24.325	10.683	42.102	15.765	0.000
FB	42.0000	/year	200.000	-21.315	6.936	42.227	17.119	0.000
FC	0.0200	%	600.000	-4.437	3.608	7.881	1.811	0.000
FD	6.0000	/year	200.000	-31.847	11.413	55.181	17.699	0.000
FE	6.0000	/year	200.000	-22.088	8.006	53.536	18.801	0.000
FF	0.5500	%	600.000	-21.538	14.244	54.473	18.921	4.141
E1A	1.0000	k/c	200.000	-23.789	6.039	56.650	21.047	0.000
E1B	1.0000	k/c	200.000	-33.992	11.494	58.800	17.941	0.000
E2A	1.0000	k/c	600.000	16.213	17.845	18.631	0.365	0.000
E2V	1.0000	k/c	600.000	19.866	22.697	29.017	1.066	0.000
E3R	1.0000	/year	200.000	-24.192	0.111	24.005	15.362	0.000
E3M	1.0000	/year	200.000	-27.241	1.636	27.386	15.333	0.000
E5	1.0000	k/c	200.000	-27.334	0.103	37.806	15.230	0.000

Rainflow resolution = 1.325 kNm
 Number of years = 20

Cycles [kNm]	Frequency
103.352 - 106.002	0
100.702 - 103.352	0
98.052 - 100.702	0
95.402 - 98.052	0.5E+0002
92.752 - 95.402	2.6E+0003
90.102 - 92.752	3.0E+0003
87.452 - 90.102	4.3E+0003
84.802 - 87.452	6.8E+0003
82.151 - 84.802	7.3E+0003
79.501 - 82.151	2.3E+0004
76.851 - 79.501	4.0E+0004
74.201 - 76.851	0.8E+0004
71.551 - 74.201	1.9E+0005
68.901 - 71.551	3.5E+0005
66.251 - 68.901	4.9E+0005
63.601 - 66.251	1.6E+0006
60.951 - 63.601	3.0E+0006
58.301 - 60.951	5.3E+0006
55.651 - 58.301	0.6E+0006
53.001 - 55.651	1.5E+0007
50.351 - 53.001	2.4E+0007
47.701 - 50.351	3.4E+0007
45.051 - 47.701	4.5E+0007
42.401 - 45.051	6.8E+0007
39.751 - 42.401	9.8E+0007
37.101 - 39.751	1.5E+0008
34.451 - 37.101	1.3E+0008
31.801 - 34.451	2.2E+0007
29.151 - 31.801	6.3E+0006
26.500 - 29.151	3.5E+0006
23.850 - 26.500	3.5E+0006
21.200 - 23.850	4.3E+0006
18.550 - 21.200	4.9E+0006
15.900 - 18.550	1.1E+0007
13.250 - 15.900	2.3E+0007
10.600 - 13.250	4.9E+0007
7.950 - 10.600	7.7E+0007
5.300 - 7.950	1.1E+0008
2.650 - 5.300	1.9E+0008
0.000 - 2.650	4.4E+0008

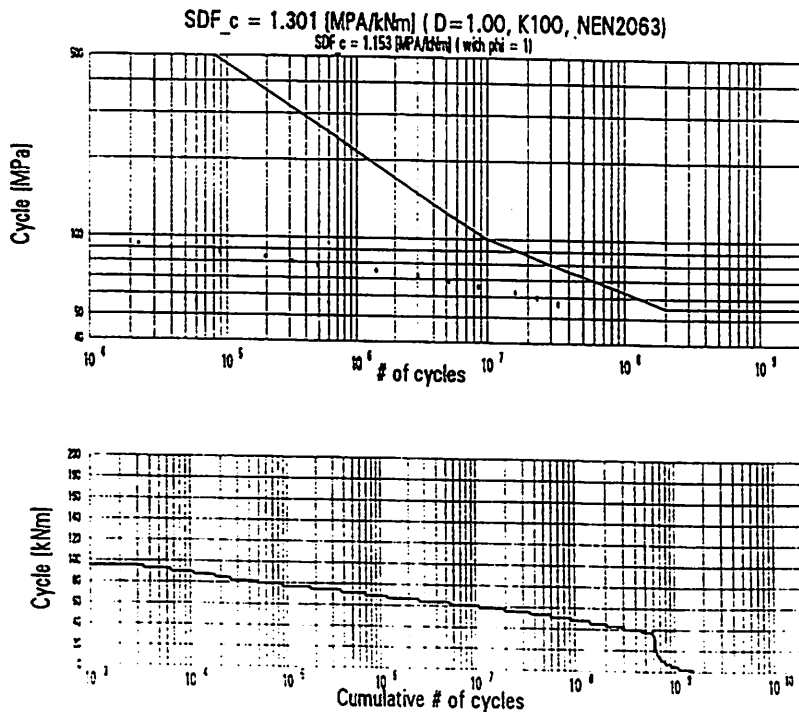


Figure 3: Range spectrum of the Inplane-moment, determination SDF_c factor.

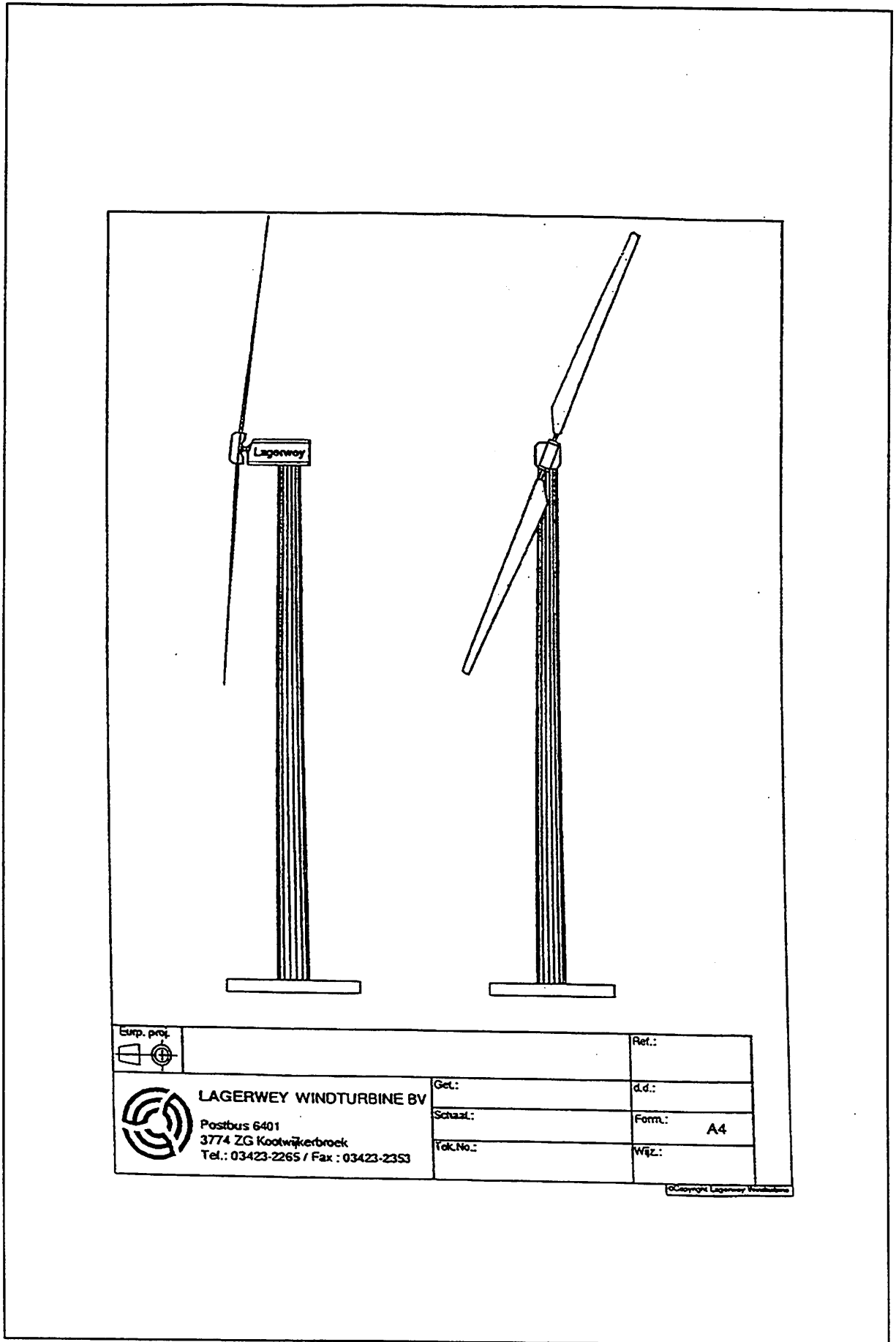


Figure 4: Lagerwey Windturbine: LW18/80.

FKA12-plot Calculation : C3.08.01 (FKA12/November 1995 (c) 1995 Stentec)
 Calculation date : Feb 12th 1996 08:24

39 m mast
 bepaling afkeur criteria

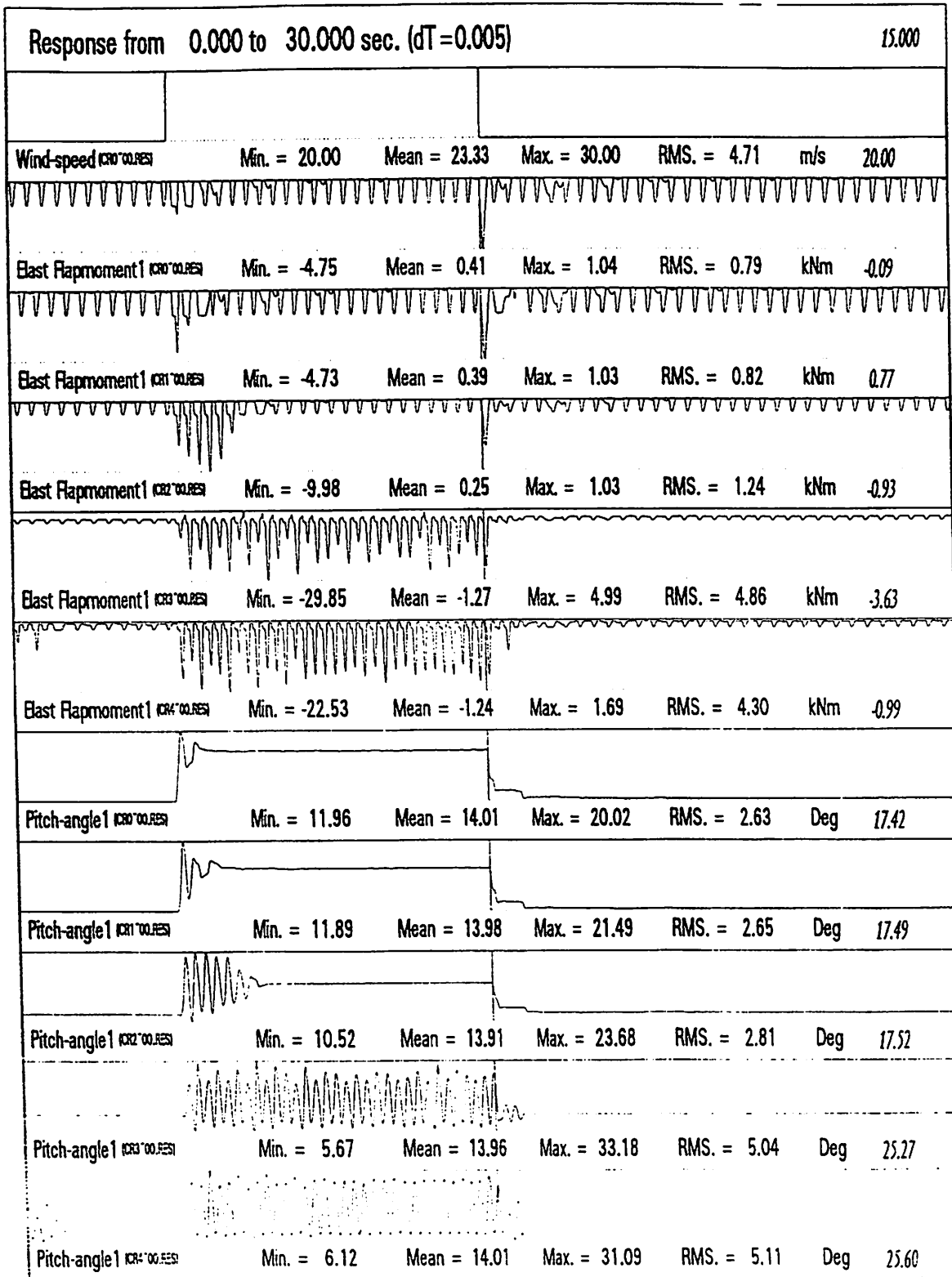


Figure 5: Non-linear flutter calculations of the C_m pitch control during high wind speeds.

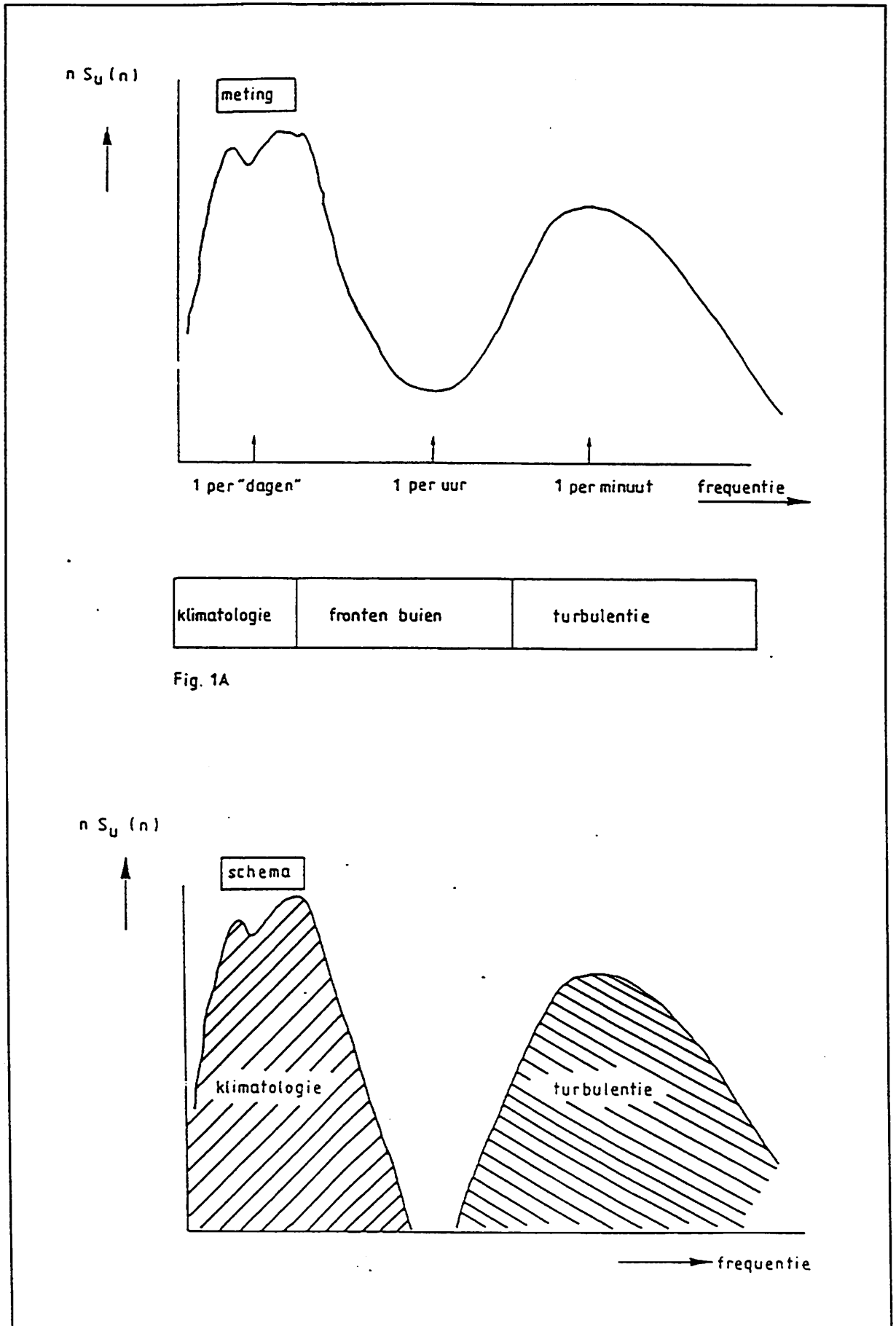
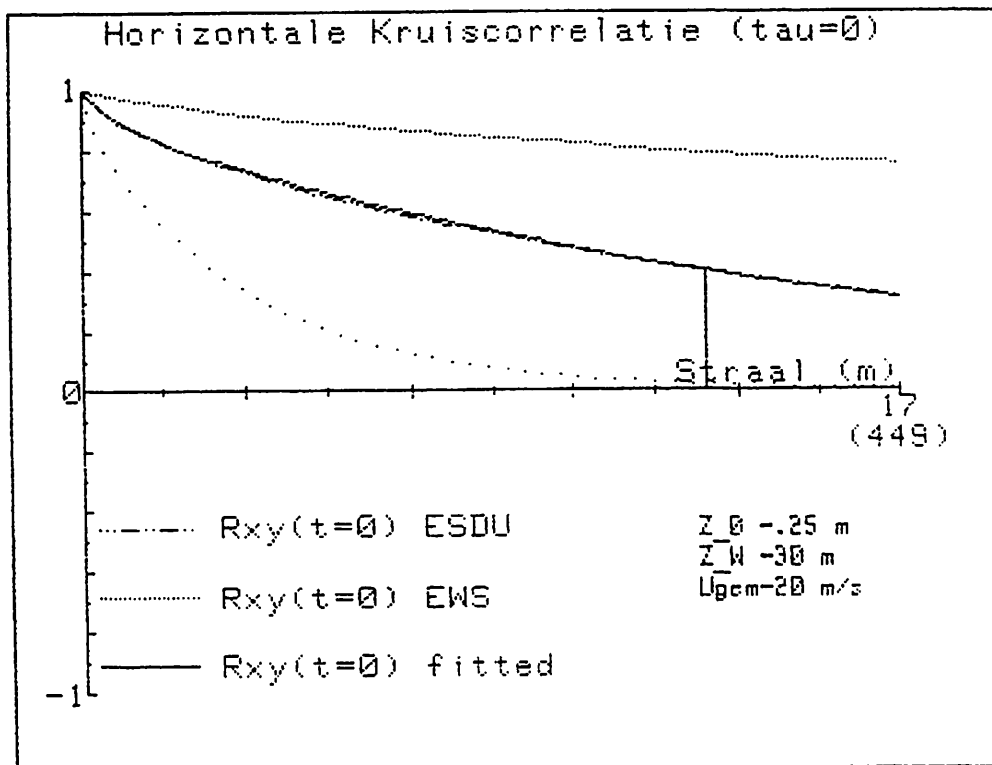


Fig. 1A

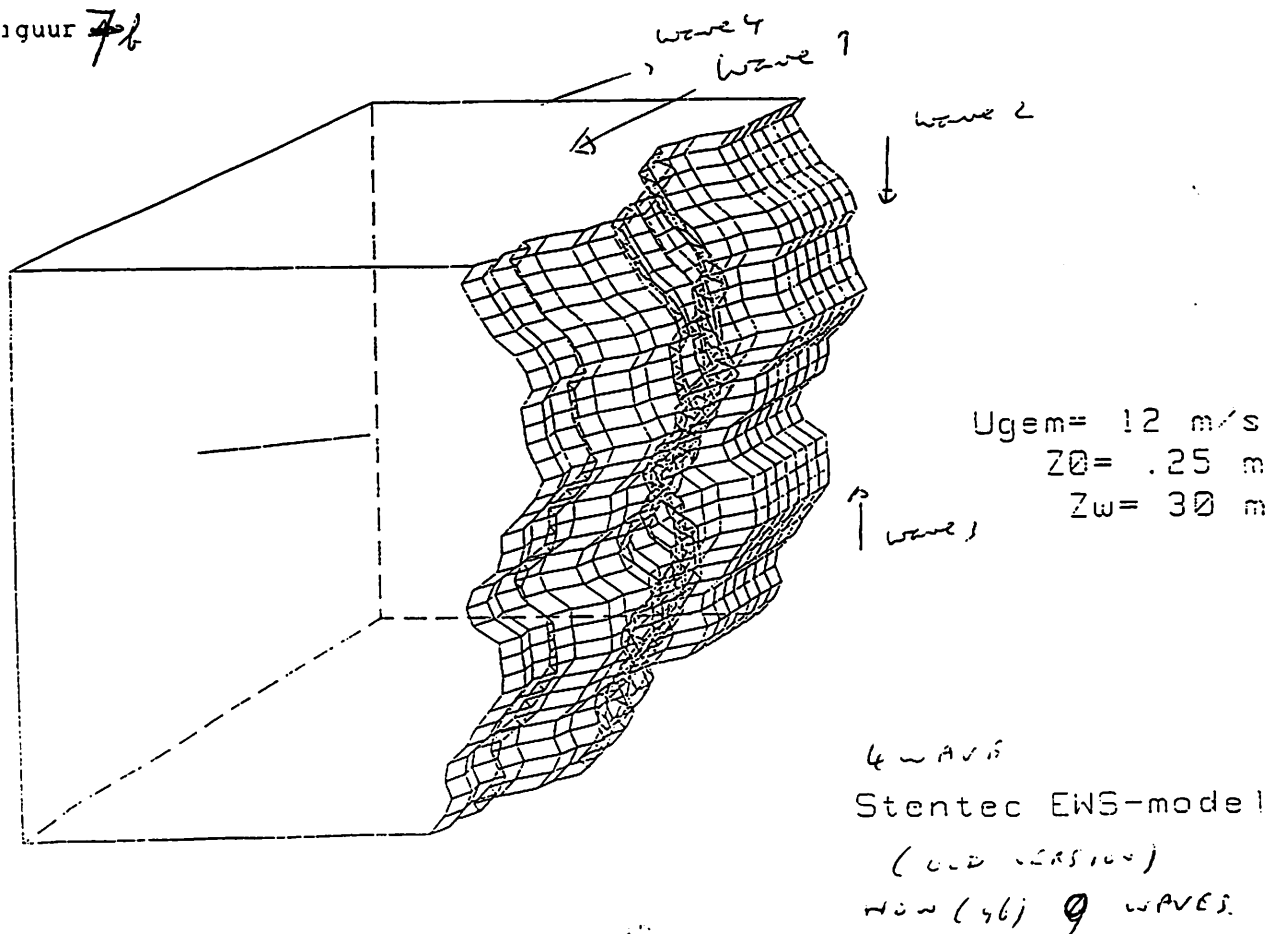
Figure 6: Sketch of wind fluctuations.

M.054.01.12.89

figuur ~~A~~
7



figuur ~~7b~~
7b



28th Topical Expert Meeting:

**State of the art of aeroelastic codes
for wind turbine calculations**

B. Visser
Stork Product Engineering

The aeroelastic code FLEXLAST

Summary

To support the discussion on aeroelastic codes, a description of the code FLEXLAST was given and experiences within benchmarks and measurement programmes were summarized. The code FLEXLAST has been developed since 1982 at Stork Product Engineering (SPE). Since 1992 FLEXLAST has been used by Dutch industries for wind turbine and rotor design.

Based on the comparison with measurements, it can be concluded that the main shortcomings of wind turbine modelling lie in the field of aerodynamics, wind field and wake modelling.

Introduction

The development of the code FLEXLAST started in 1982 when Stork began with the design of the Newecs25 and Newecs45 turbines. Later the code was used for the design of the 25mHAT test facility at ECN and within the FLEXHAT programme, different rotors were designed (e.g. the Flexteeter rotor).

Since 1990 the code has been used for the design and certification by Dutch companies (NedWind, Aerpac and Rotorline) and for certification calculations for foreign companies (Micon, Nordtank, Tacke, and Ecotecnia).

Structural model

Within FLEXLAST, the structural behaviour of a wind turbine is modelled with the following dynamic modes:

- Blade:
first flap and lead lag bending mode by a hinged blade model.
- Hub:
teeter mode by linear spring or stiffness curve.

- first axial and lateral bending mode by a mass spring model.
- Drive train:
 - torsional mode by mass spring model.
- Passive pitching:
 - pitch motion by means of a mass spring model including the coupling between centrifugal force and pitch moment and mass coupling between fixed and pitching part of the blade.

The structural model is shown in figure 1 and 2 (out of plane and in plane dynamics)

The following stationary modes are included:

- Active pitching:
 - pitch motion by definition of pitch speed.
- Active yawing
 - yawing by definition of yaw speed.

The coupling between the dynamic modes include the mass coupling between blades, tower and drive train, and also the coriolis and gyroscopic forces.

Aerodynamic model

The stationary aerodynamics include:

- Rotor forces:
 - blade element theory, conservation of momentum.
- Tip losses:
 - Prandtl correction factor.
- 3-D effects:
 - optional correction (e.g. H. Snel (ECN))
- Tower shadow:
 - dipole model.

The unsteady aerodynamics include:

- Dynamic inflow:
 - first order filter with $t=D/V_{hub}$
- Dynamic stall:
 - Stig Oye model (first order dynamics)

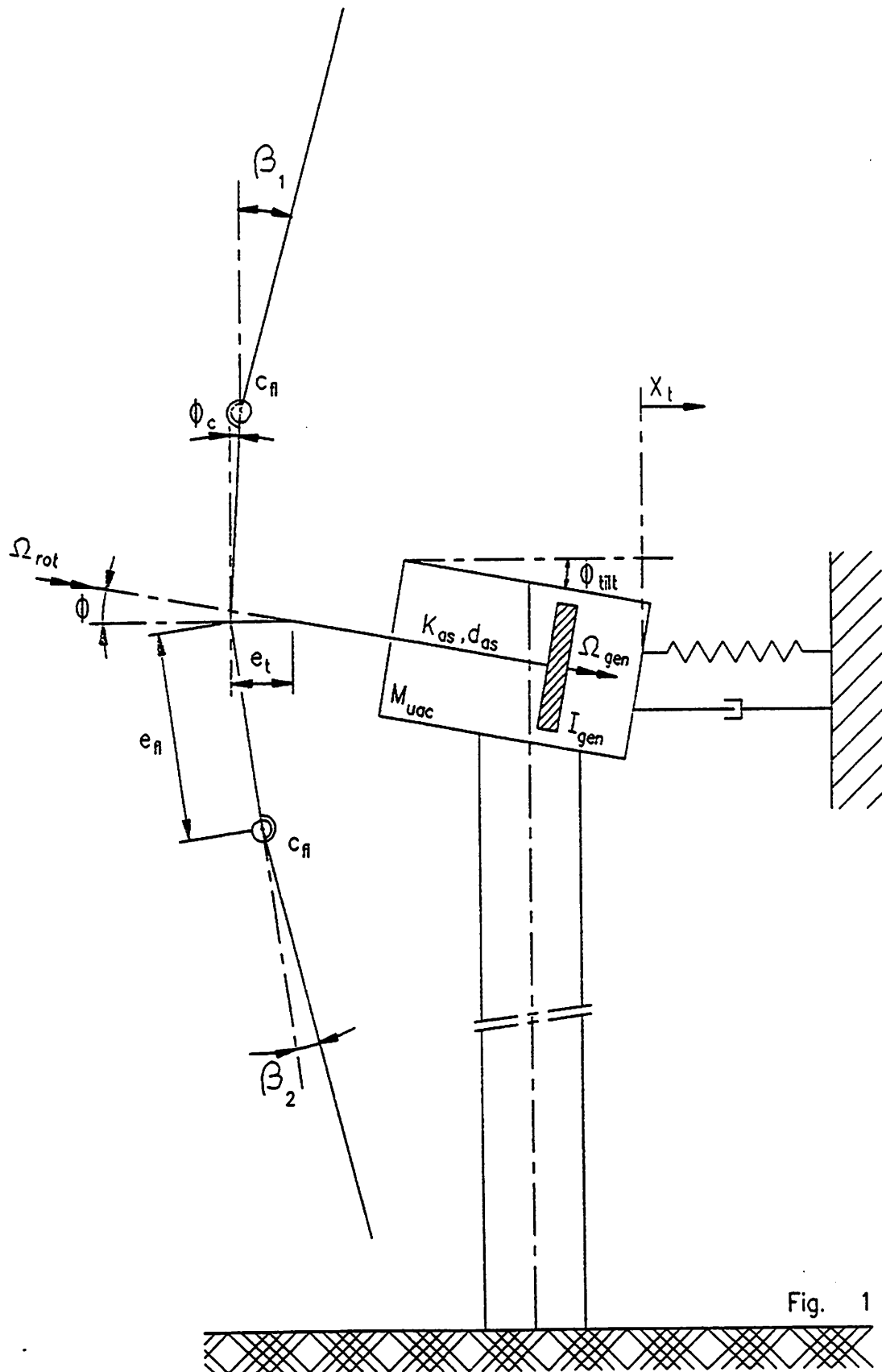


Fig. 1

Figure 1 The physical model and its out of plane degrees of freedom

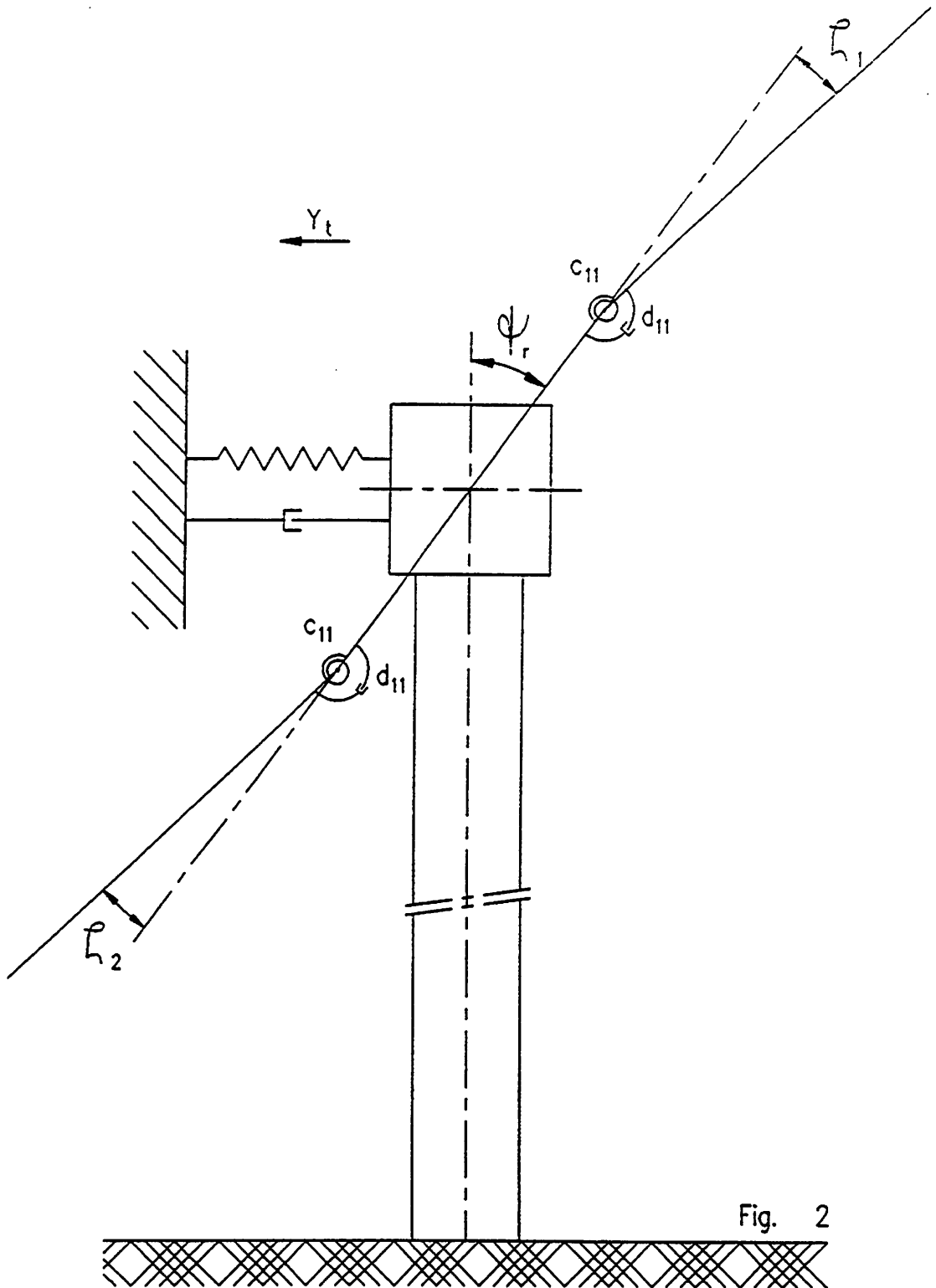


Fig. 2

Figure 2 The physical model and its in-plane degrees of freedom

Validation

The validation of FLEXLAST has been executed within benchmarks and measurement programmes:

- **Bechmarks:**
 - National benchmark 1989, turbine HAT-25, Newecs-45, WEG-MS1.
 - International benchmark 1991, turbine WEG-MS1.
 - Refstress benchmark 1994, turbine Tjaereborg.

- **Measurement programmes:**
 - Newecs-45 1988
 - NedWind 40 1994
 - NedWind 50 1996
 - UNIWEX 1992
 - TIP-1 1990
 - Flexteeter 1993
 - Stall-flexteeter

Also, some comparisons between measurements and calculations were performed for certification of other turbines.

Shortcomings / areas of new research

The shortcomings and areas of new research will be dealt with in two ways: concerning FLEXLAST in particular and in general.

FLEXLAST:

The trend to design flexible rotors leads to the need for a more accurate prediction of blade bending modes and tip deflection. The hinge model, as used in FLEXLAST, has a limited accuracy for these dynamics. For this reason, FLEXLAST will be extended by the application of bending mode shapes or a multiple hinge model. This way, also second blade bending shapes will be included.

General:

The main shortcomings of the modelling of wind turbine behaviour lie in the field of aerodynamics and wind field description:

Stall is still a difficult phenomenon to model. The amount of aerodynamic damping in stall is difficult to predict but very important for the loads on rotor, nacelle and tower.

In order to improve the tuning of dynamic stall models, more reliable 2-D stationary aerofoil data is needed. Especially for inflow angles higher than 20 degrees.

Although 3-D corrections have improved the predictions, it is still difficult to predict the maximum power of a stall turbine.

Although the wake models have improved, a better understanding of phenomena like skewed wake, can lead to significant improvements of the aeroelastic codes.

In case of variable speed turbines with a high constant tip speed ratio, the acoustics of the rotor are a important design parameter. More research in this area can lead to a more optimal turbine design.

An improvement, of wind turbine modelling in general, can be reached by parallel calculations with a second aeroelastic code. This way, mistakes and bug can be excluded.

PRACTICAL ASPECTS OF A FLEXIBLE WIND TURBINE BLADE DESIGN

T. VRONSKY

Wind Energy Group
345 Ruislip Road
Southall
Middlesex UB1 2QX, U.K.

Summary

This paper describes some aspects of flexible blade design and touches briefly on some solution techniques used in practical blade design.

Introduction

Wind turbine loads can be significantly reduced by introducing "well tuned" flexibility into the design. Rotor blades are the main source of loading and can therefore contribute to a substantial load reduction.

The stall-regulated blade structural design is most often driven by either extreme storm loads or by operational fatigue loads. Centrifugal relief plays a significant role in reduction of the blade fatigue loads by reducing both the mean loads as well as variation. It was shown by Rassmussen et. al. (Ref.1) that by having blade natural frequency (at standstill) below 1.5P and by avoiding structural resonancies, fatigue loads can be lowered by up to 50%.

In the stationary storm load case the centrifugal relief is not present. The load can, however be shed from the blades if they are sufficiently flexible, as they deflect away from the wind.

Normal running fatigue loads

Normal running loads are commonly calculated by blade element theory, coupled with modal analysis of the structural response. Three directional turbulent wind models are used for generating fatigue spectra. Single flapping mode is used in the initial design simulations, which makes calculations more efficient, easing design iterations while maintaining a reasonable degree of accuracy.

High wind speed load calculations are very sensitive to the treatment of aerodynamic loads, especially of the dynamic stall model. Beddoe's model of dynamic stall was shown to predict quite well the dynamic behaviour of a free yaw down wind machine, while the prediction of the actual blade loads is believed to be on the conservative side (Ref 5.). The prediction of the correct yaw behaviour is important for tuning the yaw system (e.g. selection of yaw damping), which is required for getting the right balance between the loads imposed on the yaw system and the loads on the blades due to gyroscopic moments during fast yawing response to sudden wind shifts.

Extreme storm loads

Extreme storm loading is very important for a stall regulated machine. It is therefore most desirable to minimise its effects. Blade flexibility allows large coning angles at the blade tip and thus relieves extreme thrust and bending moment on the blade.

Aerodynamic modelling based on the cross-flow drag theory for moderate cone angles near the blade root, and on the slender wing theory for large coning angles towards the blade tip, was shown to give a good prediction of quasi-static loads on a flexible blade. The theoretical predictions of load relief were confirmed by a series of wind tunnel tests on a small model of the blade (1:30 scale). The model was

tested at 15 m/s wind speed. The blade was modelled as a thin plate with the correct aspect ratio and sharp edges, which made the results insensitive to the Reynolds number. Straight blades in a series of oblique angles to the incoming wind were tested, followed by a model blade bent into the predicted shape, with 60 degrees of deflection at the tip. The result was a 47% reduction in the thrust load and 55% reduction in the blade root bending moment, very close to the predictions. The cross-flow theory was satisfactory for angles up to 30 degrees, while the slender body lift theory due to Polhamus (Ref. 2) was in a good agreement with the results for angles above 60 degrees. An empirical transition between the two theories was needed for angles between 30 and 60 degrees.

Calculation of the deflected blade shape under the extreme storm load presents a strongly non-linear problem, the loads acting on the blade being a function of its shape. Initially a standard incremental solution technique with equilibrium correction (Ref. 3) was adopted. This algorithm is stable, but inefficient and not very suitable in the initial design stage. A simplified iteration method was developed, with rapid convergence and fairly good accuracy. The simplicity of the method allows for it to be implemented in a spreadsheet, which is ideal for preliminary design calculations. The method is based on the observation that the slope (i.e. the local coning angle) of the deflected blade shape can be closely approximated by sinusoidal function with the blade root and blade tip coning angle as the only parameters. The actual deflected blade is calculated by a standard integration on beam elements, taking account of the large displacement effects (load followers). The iterations are repeated until the residual mean error between the estimated and calculated slopes is minimised. (It usually takes no more than 5 iterations to achieve error less than 1°, which is a reasonable accuracy).

The effect of the dynamic response to a sudden gust was checked by a simple single-degree-of-freedom dynamic analysis, using a standard assumed mode method (Ref.4 et al.) with the modal shape from the pseudo-static calculations. The simulation predicted only a small dynamic magnification of the aerodynamic loads thanks to the significant effect of load shedding at high deflection angles and aerodynamic damping due to large flapping movements.

References

- [1] *Rasmussen, F. Thomsen, K.* Dynamic Tuning of Three-Bladed Wind Turbines, Proc. EWEC 1993
- [2] *Polhamus, E.C* NASA TN-D-3767, 1967
- [3] *Hinton, E.* Introduction to Non-linear Finite Element Analysis, NAFEMS 1992
- [4] *Craig, R.R.* Structural Dynamics, J. Wiley, 1981
- [5] *Quarton, D. Smith, R.R.* Dynamic Simulations of MS4 Turbine, private correspondence

HOW COMPROMISED IS DESIGN ?

The problem

Uncertainty

-----> redundancy

-----> cost

So.....

WHAT ARE THE IMPORTANT UNCERTAINTIES ?

~ ~ ~ ~ ~

The issues, as usual, boil down to cost. Wind turbines are necessarily over-engineered to allow for uncertainties in the machine loads. These uncertainties arise because of deficiencies in the modelling of the machine and of the input loads to the machine.

Before it is possible to prioritise the uncertainties, it is necessary to define the criteria for judgement. In the context of this meeting the aim was to both agree the uncertainties and to help establish a 'near term' focus for efforts to address those uncertainties. The criteria should therefore include the immediate design difficulties and our near term prospects for impacting on those areas of difficulty.

IAN FLETCHER
ETSU
APRIL 96

FUTURE DEMANDS ?

Pushing to reduce costs

-----> **Reduced mass**

-----> **Reduced loads**

-----> **Flexible machines**

- *Flexible rotors (towers?)*
- *Down-wind*
- *Free-yaw*

~~~~~

The UK wind energy programme is moving as indicated above. This results in a head-on collision with many of the areas of greatest uncertainty and is proving demanding in terms of modelling and design. However, the need to reduce costs must inevitably lead to lighter, more dynamic machines that will in turn require more complex models, place greater demands on computers and have higher development costs.

The table that follows must be considered in the context of the sort of machine given here. The method of separating the importance to design, the prospects for making improvements and the cost benefit is important. This then gives a commercial context that is most likely to yield a reduction in the cost of wind derived electricity.

It is interesting to note that this broader analysis will give a quite different emphasis to that based on the degrees of uncertainty alone.

## Rankings for future focus

| FOCUS FOR FUTURE EFFORT          |                            |                                         |                                              |                                 |        |         |
|----------------------------------|----------------------------|-----------------------------------------|----------------------------------------------|---------------------------------|--------|---------|
|                                  |                            | How important for design optimisation ? | Modelling prospects: Theoretical/Empirical ? | Potential for cost reductions ? | points | RANKING |
| <b>Wind filed description</b>    |                            |                                         |                                              |                                 |        |         |
|                                  | For lifetime fatigue       | 3                                       | 4                                            | 2.5                             | 9.5    | 6       |
|                                  | Complex terrain/wind farms | 3                                       | 3                                            | 3                               | 9      | 7       |
|                                  | Extreme events             | 5                                       | 4                                            | 5                               | 14     | 1       |
| <b>Quasi-steady aerodynamics</b> |                            |                                         |                                              |                                 |        |         |
|                                  | Extreme gust loading       | 5                                       | 3.5                                          | 5                               | 13.5   | 1       |
|                                  | Stalled aerofoil data      | 4                                       | 3                                            | 4                               | 11     | 3       |
|                                  | Longitudinal flow effects  | 3                                       | 2                                            | 3                               | 8      | 9       |
|                                  | Yaw loads & stability      | 3                                       | 4                                            | 3.5                             | 10.5   | 4       |
| <b>Unsteady aerodynamics</b>     |                            |                                         |                                              |                                 |        |         |
|                                  | Aeroelastic stability      | 5                                       | 3                                            | 2                               | 10     | 5       |
|                                  | Stall                      | 5                                       | 1                                            | 3                               | 9      | 7       |
| <b>Structural dynamics</b>       |                            | 2                                       | 4                                            | 2                               | 8      | 9       |
|                                  |                            |                                         |                                              |                                 |        |         |
|                                  |                            |                                         |                                              |                                 |        |         |
|                                  | COLOUR RANKINGS            | 5                                       |                                              | HIGH                            |        |         |
|                                  |                            | 4                                       |                                              |                                 |        |         |
|                                  |                            | 3                                       |                                              | MEDIUM                          |        |         |
|                                  |                            | 2                                       |                                              |                                 |        |         |
|                                  |                            | 1                                       |                                              | LOW                             |        |         |



## On the Aeroelasticity and Dynamics of Wind Turbines

F. Kiessling, M. Rippl - DLR-Institute of Aeroelasticity, Göttingen, F. R. G.

Wind turbines pose a series of dynamic and aeroelastic problems. This holds true especially for modern designs with high tip-speed ratio which require slender blades and large dimensions. Computational and experimental procedures for investigating aeroelastic stability and dynamic response are necessary. Concerning the static aeroelastic stability, the divergence of the rotor blades and the speed characteristics of the complete rotor have to be considered; rotor blade flutter and the dynamic stability of the coupled tower/rotor must be investigated as dynamic aeroelastic problems. Wind turbines are subjected to dynamic loading from a variety of different sources. Wind shear and turbulence cause time-varying inflow which results in unsteady airloads. Tower shadow, upwind turbine wakes, and yaw angles also introduce unsteady inflow to wind turbine rotors. Using only highly sophisticated models, simple relationships may be concealed by effects of minor importance. Therefore problems occurring with components like blades or tower must be identified and adequate analytical models are to be established. With these simplified models parameter variations can be easily performed, followed by the investigation of the aeroelastic system in its entirety, including the generator and control system.

Static aeroelastic problems should not occur with a reasonably designed wind turbine, except in the case of the failure of essential components like the pitch control mechanism. Due to a pitch control mechanism which is not sufficiently rigid, static divergence of the rotorblade may occur. Investigations revealed the dominating influence of the sign of the angle between the blade axis and the pitch axis. A „Divergence of rotational speed“ of the complete rotor may occur in the case of a weak control mechanism, depending on the moment curve of the electrical generator.

A reasonable approach to the dynamic aeroelastic problems of a wind turbine is given when the modal parameters like the eigenfrequencies, eigenmodes and generalized mass of the rotorblades or the tower are known. Common methods to determine the eigenbehaviour are - experimentally - the ground vibration test, and - theroretically - the Finite Element Method. The differential equations of motion describing the bending and torsional deformations of twisted rotating beams have been developed by Houbolt/Brooks. In extension of previous theories there is no restriction concerning the geometrical arrangement of the neutral elastic and mass axes. Additionally, they pay special attention to the coupling terms resulting from the centrifugal forces. By introducing the corresponding expressions into the potential and kinetic energy the mass matrix and stiffness matrix for a finite rotor beam element can be derived. The results of calculated eigenmodes and eigenfrequencies of the rotorblade of a large wind turbine are given. Flutter calculations have been performed based on the calculated eigenbehaviour of the rotor blade. In addition to the rigidity of the pitch control mechanism the flutter stability is influenced by the chordwise position of the center of gravity. Having a rigid pitch control mechanism, the eigenfrequencies of the blades themselves are sufficiently high and flutter does not occur within the range of operation.

To deal with the dynamic behaviour of the complete wind turbine, the equations of motion of the coupled rotor/tower system have to be derived. The amount of time spent deriving the equations of motion increases considerably as more detailed rotor blades and the kinematics of the hub or rotor/body coupling are taken into account. The manual derivation process becomes increasingly tedious and error prone although the procedure is straightforward (e.g. by applying the Lagrange formalism). The general-purpose computer algebra system "REDUCE" has been applied to develop a program which generates literal equations of motion for rotary wing aeroelastic problems, resulting in FORTRAN compatible statements. As an example, the procedure is applied to the problem of a two-bladed wind turbine mounted on an elastic tower. Due to the periodicity of the coefficients, the Floquet method must be applied to solve the equations of motion.

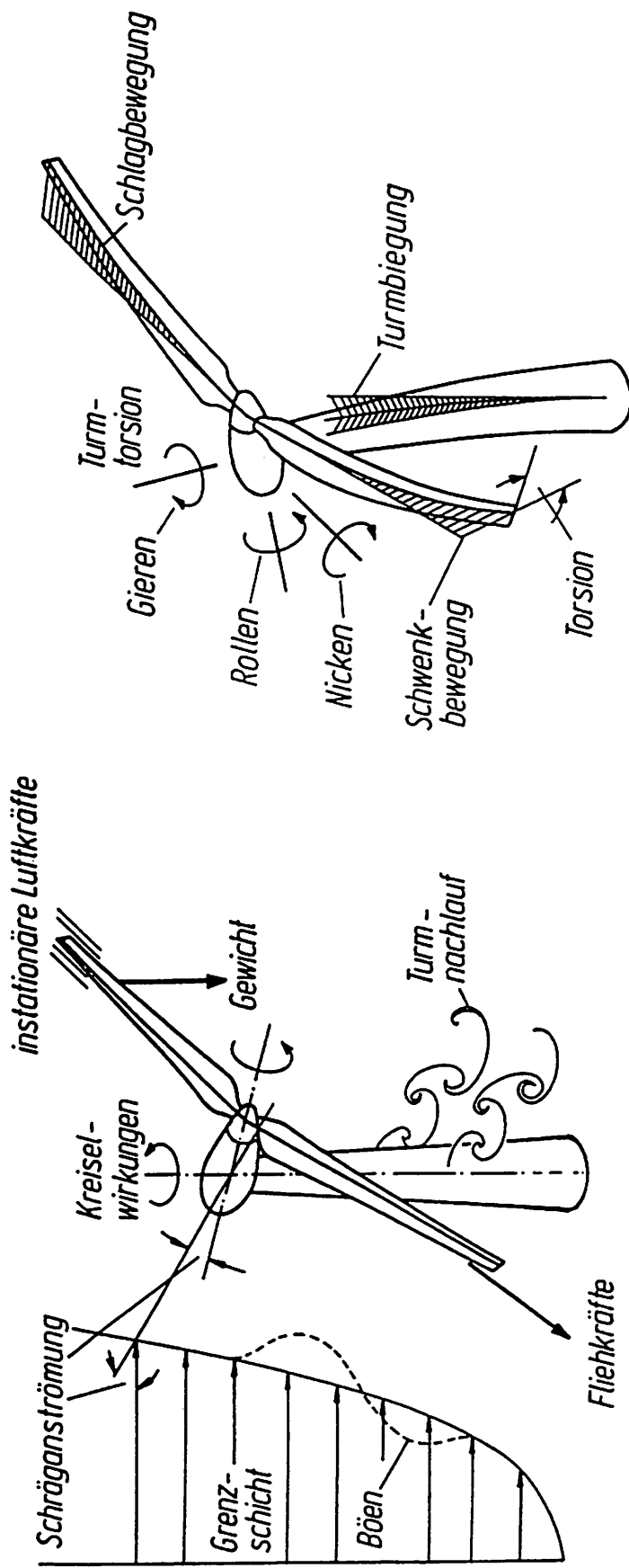
Deutsche Forschungsanstalt für Luft- und Raumfahrt e.V.

# **Aeroelasticity of Windturbines**

**Dr.-Ing. F. Kießling**  
**Dipl.-Ing. M. Rippl**

**DLR -Institute of Aeroelasticity**





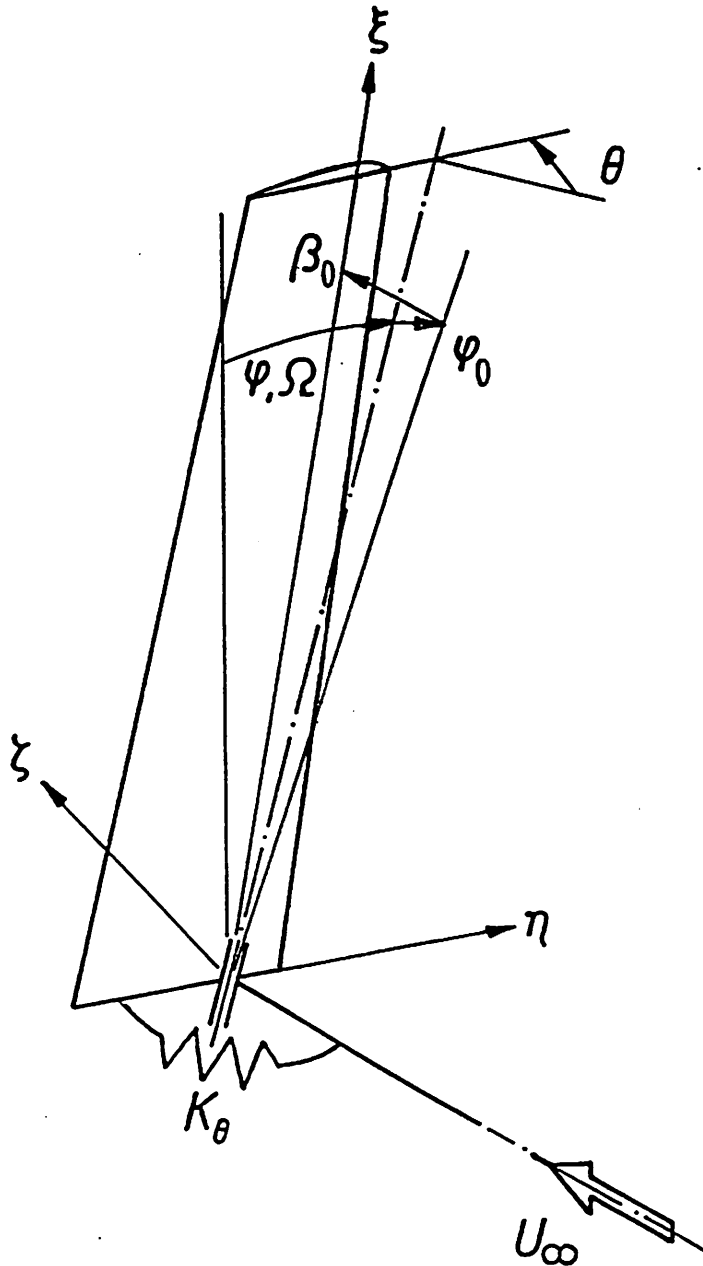
## Forces and deformations of a windturbine

Deutsche Forschungsanstalt für Luft- und Raumfahrt e.V.

## Aeroelastic Stability

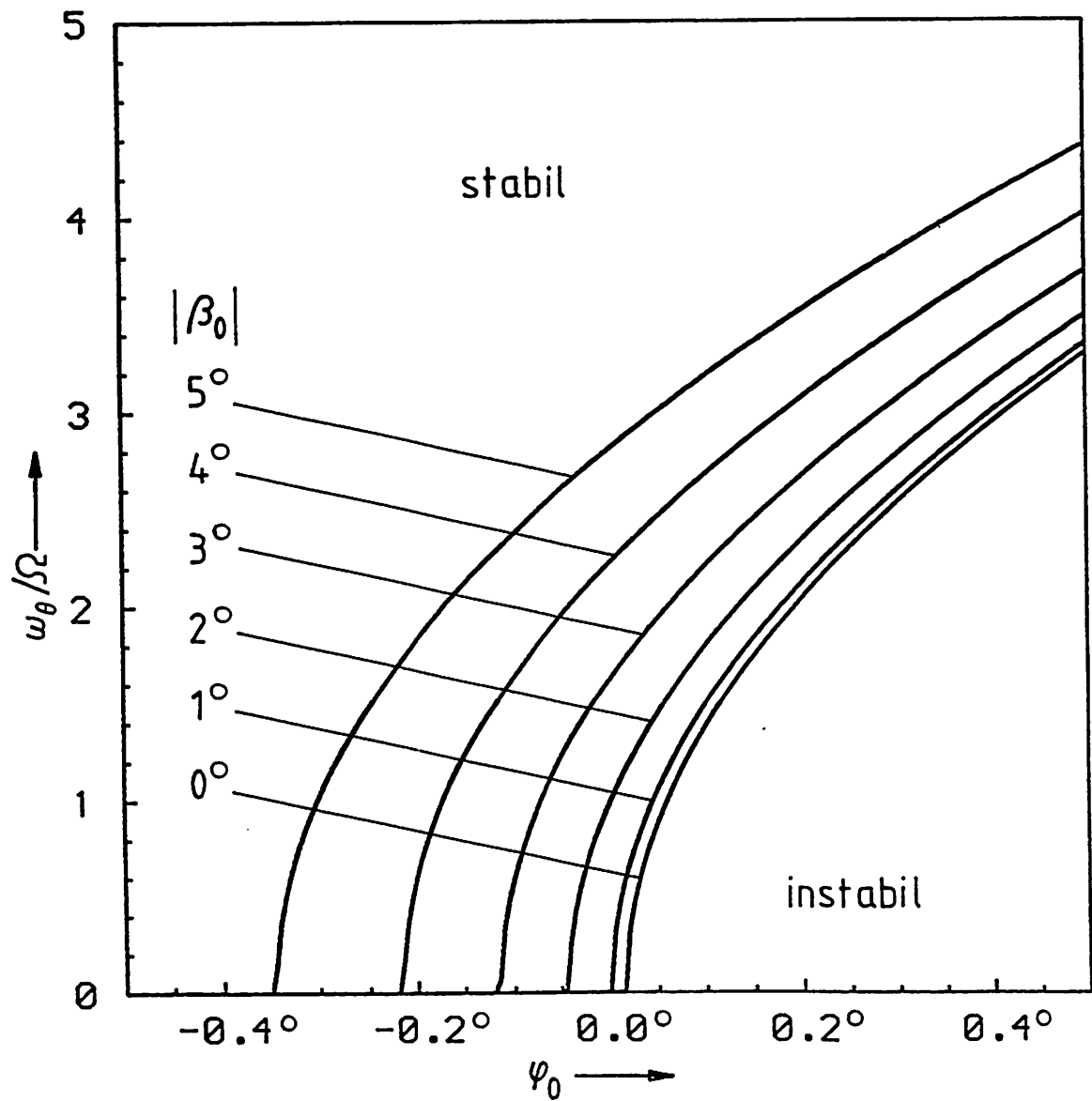
- static aeroelastic problems:
  - single blade divergence
  - rotor overspeeding
- dynamic aeroelastic problems
  - single blade flutter
  - whirl-flutter

Deutsche Forschungsanstalt für Luft- und Raumfahrt e.V.



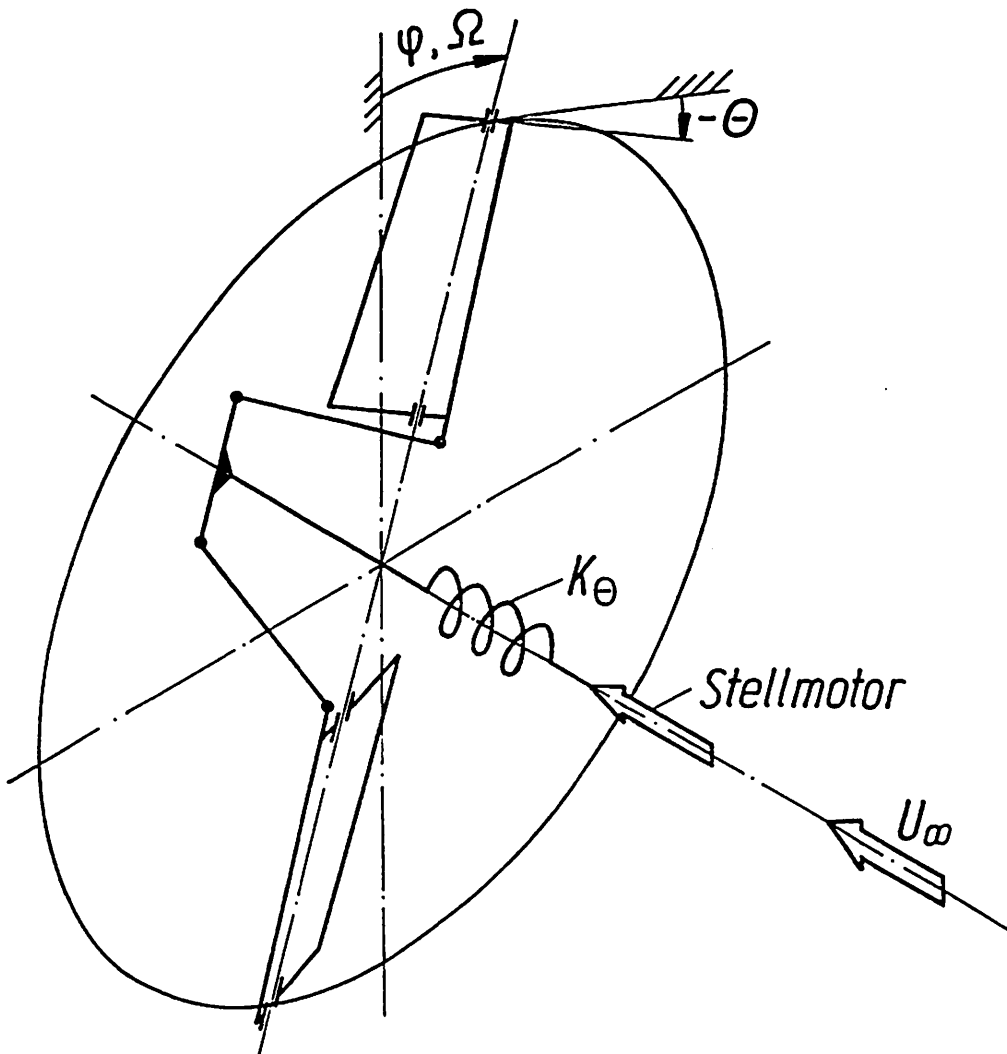
Rotorblade with elastic control mechanism

Deutsche Forschungsanstalt für Luft- und Raumfahrt e.V.



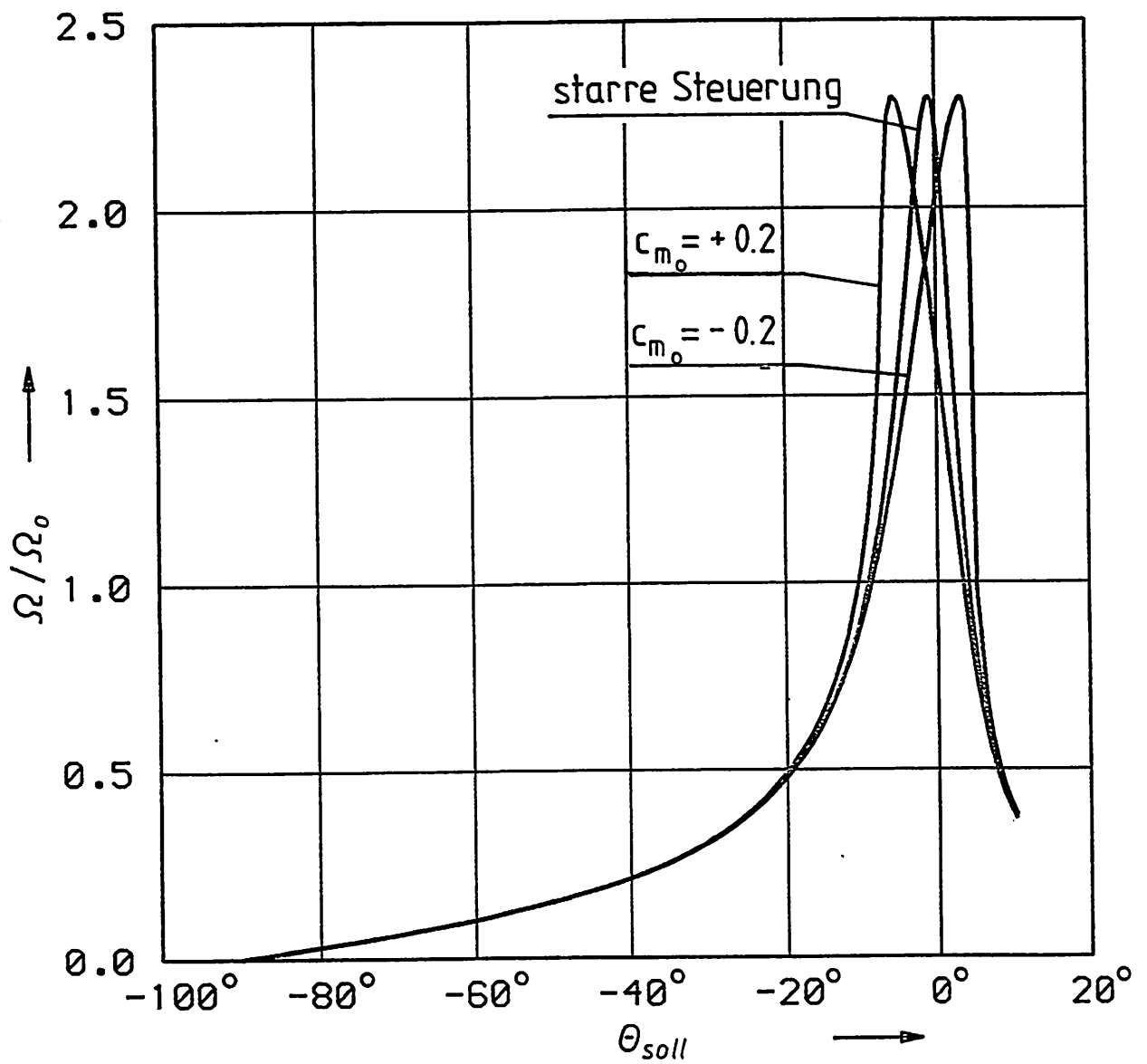
Stability diagram

Deutsche Forschungsanstalt für Luft- und Raumfahrt e.V.



Rotor with elastic control mechanism

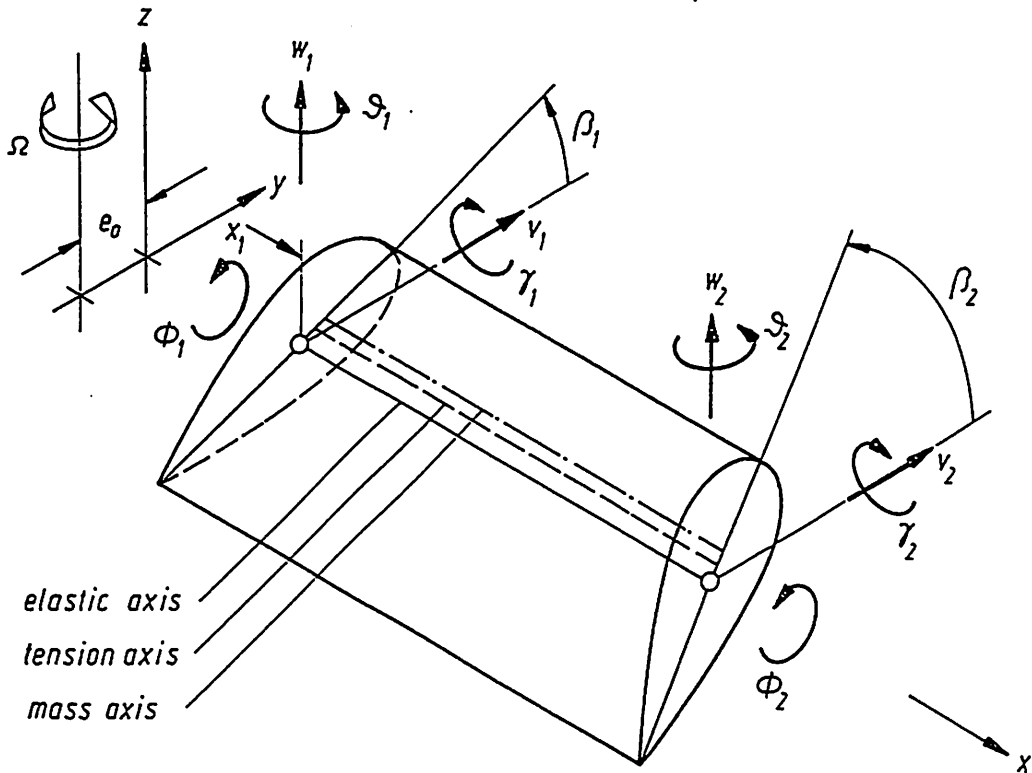
Deutsche Forschungsanstalt für Luft- und Raumfahrt e.V.



Speed characteristics



Deutsche Forschungsanstalt für Luft- und Raumfahrt e.V.



symmetrical cross-section  
 10 degrees of freedom  
 deformations: flapwise bending  
 lagwise bending  
 torsion

## Rotor beam element

Deutsche Forschungsanstalt für Luft- und Raumfahrt e.V.

Displacement functions:

- linear distribution of torsion
- cubic distribution of flapwise and lagwise bending

Masses:

- constant mass distribution
- constant distance between mass axis and elastic axis
- constant mass radii of gyration

Bending and tension:

- constant bending stiffness
- constant distance between area centroid and elastic axis
- constant polar radii of gyration of area centroid
- constant tension stiffness

Characteristics of the rotor beam element

Deutsche Forschungsanstalt für Luft- und Raumfahrt e.V.

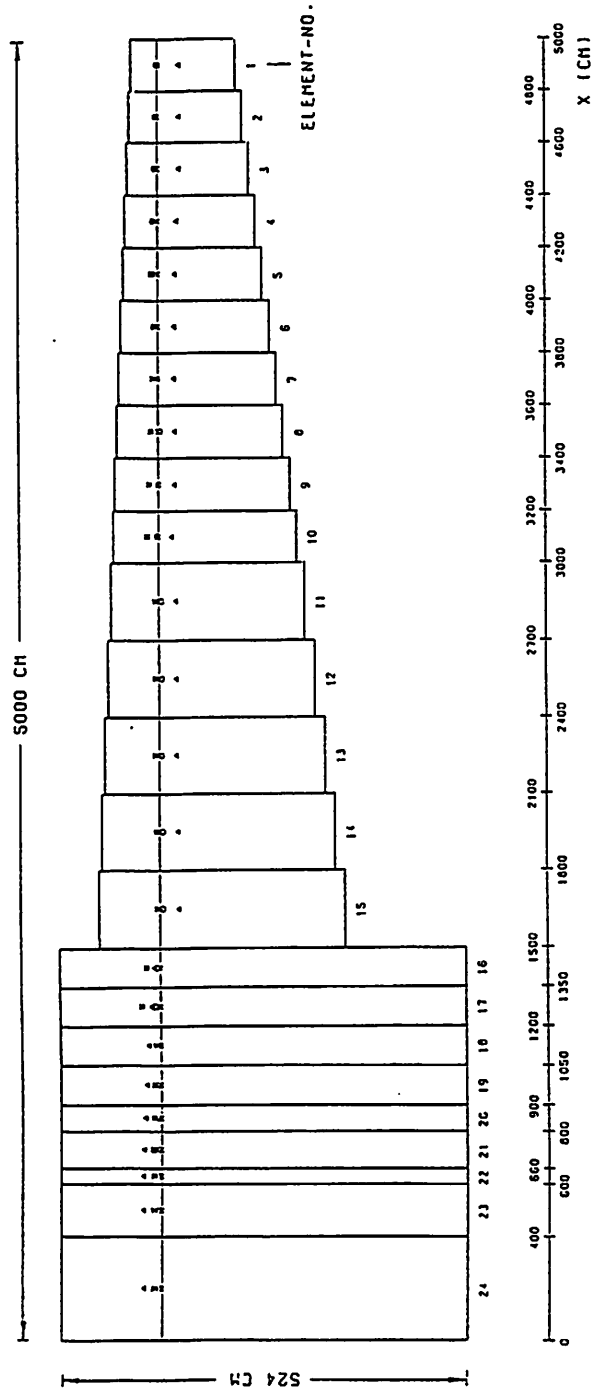
Torsion:

- constant torsional stiffness

Geometry:

- linear distribution of built-in twist
- constant offset between blade elastic axis and rotor axis

Characteristics of the rotor beam element (cont'd)

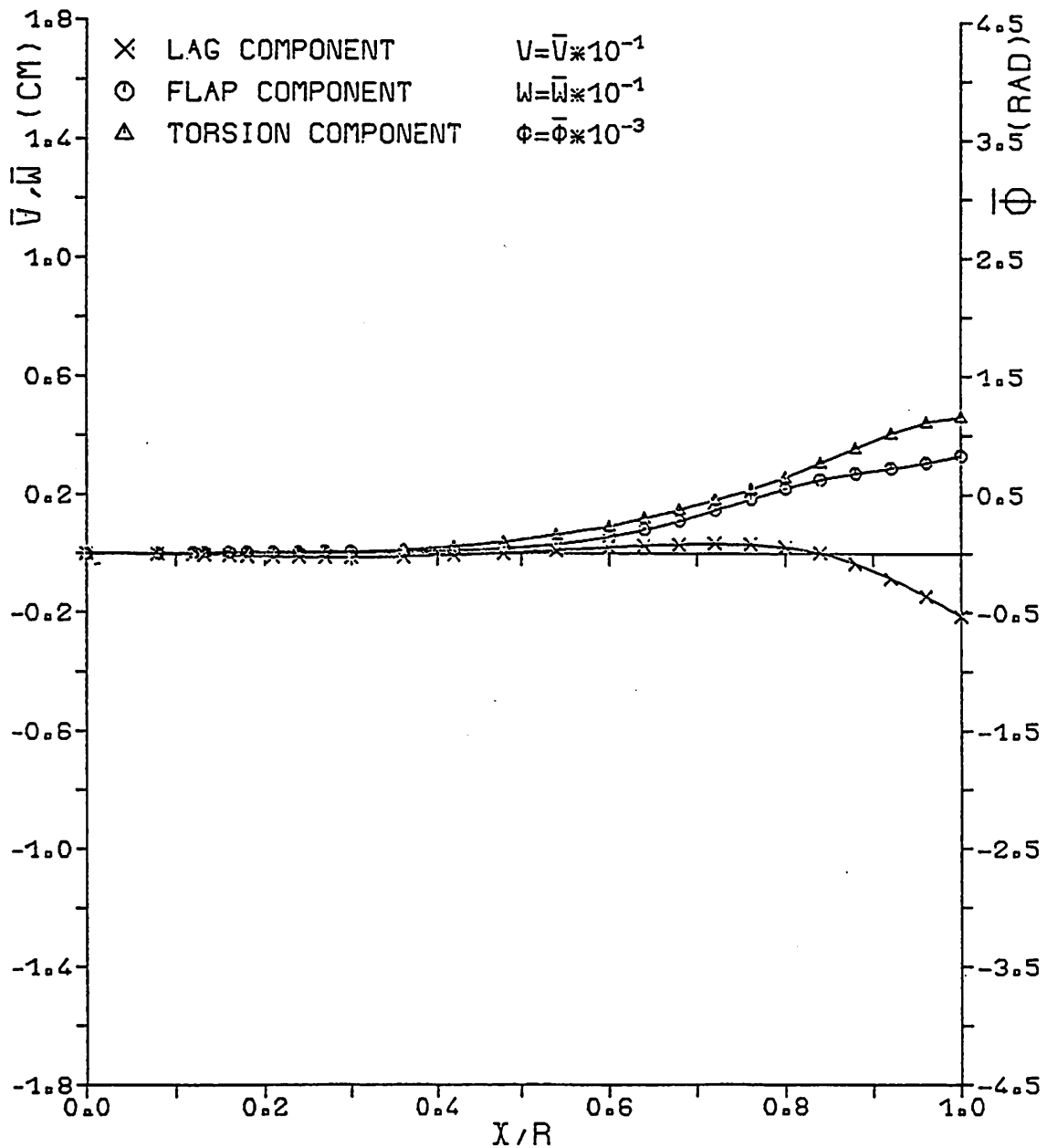


- CENTROID OF CROSS-SECTIONAL AREA EFFECTIVE
- IN CARRYING TENSILE STRESSES
- △ MASS AXIS
- \* ELASTIC AXIS
- x AXIS OF ROTATION

## Finite element model of GROWIAN rotor blade

## Deutsche Forschungsanstalt für Luft- und Raumfahrt e.V.

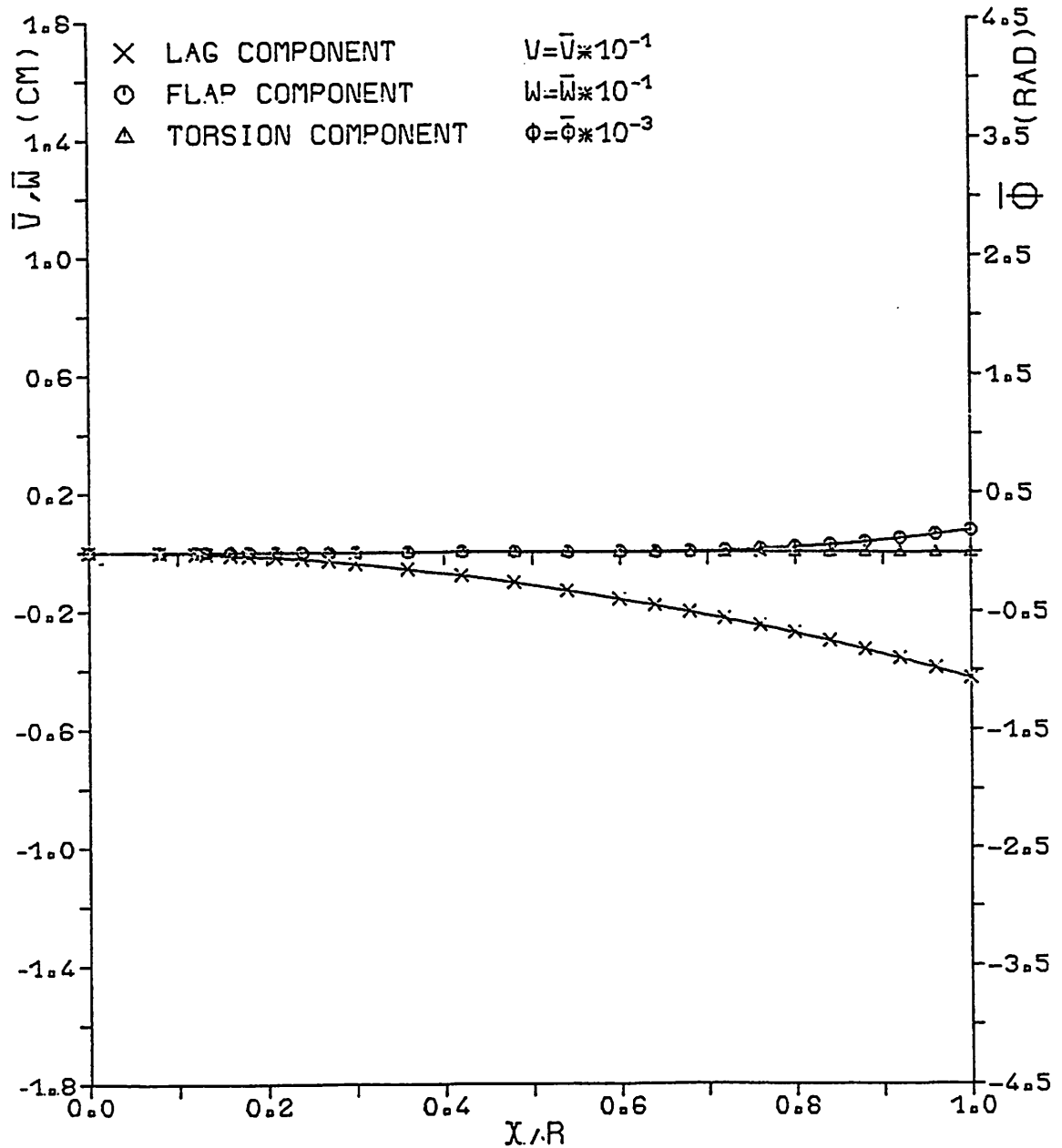
ROTATIONAL FREQUENCY RPM = 18.50 (1/MIN)  
 EIGENFREQUENCY FR = 11.13 (HZ)



Torsional mode for the rotating blade  
 at rated speed

## Deutsche Forschungsanstalt für Luft- und Raumfahrt e.V.

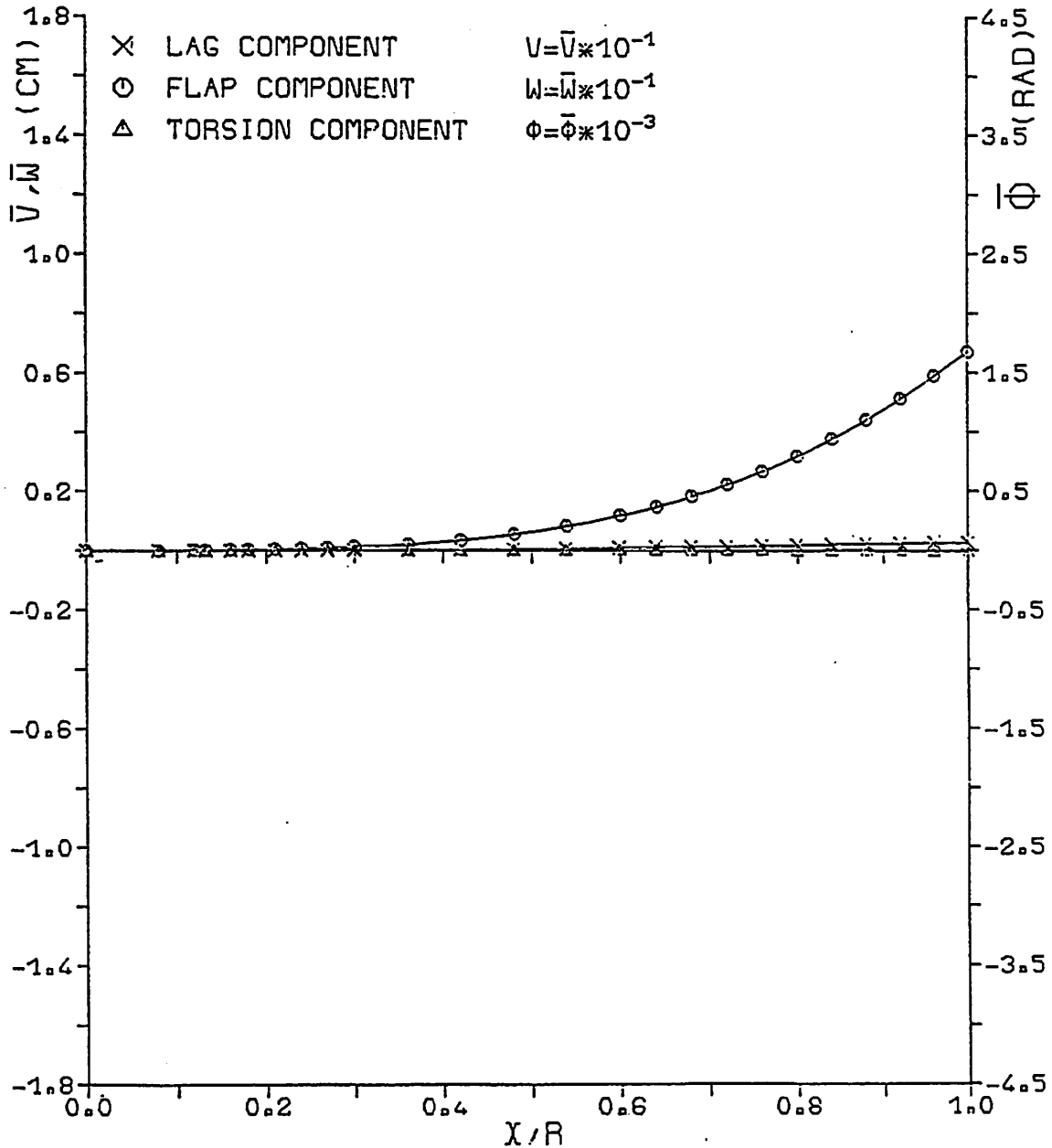
ROTATIONAL FREQUENCY RPM = 18.50 (1/MIN)  
 EIGENFREQUENCY FR = 2.12 (HZ)



Lag mode for the rotating blade at rated speed

Deutsche Forschungsanstalt für Luft- und Raumfahrt e.V.

ROTATIONAL FREQUENCY RPM = 18.50 (1/MIN)  
 EIGENFREQUENCY FR = 1.35 (HZ)



Flap mode for the rotating blade at rated speed

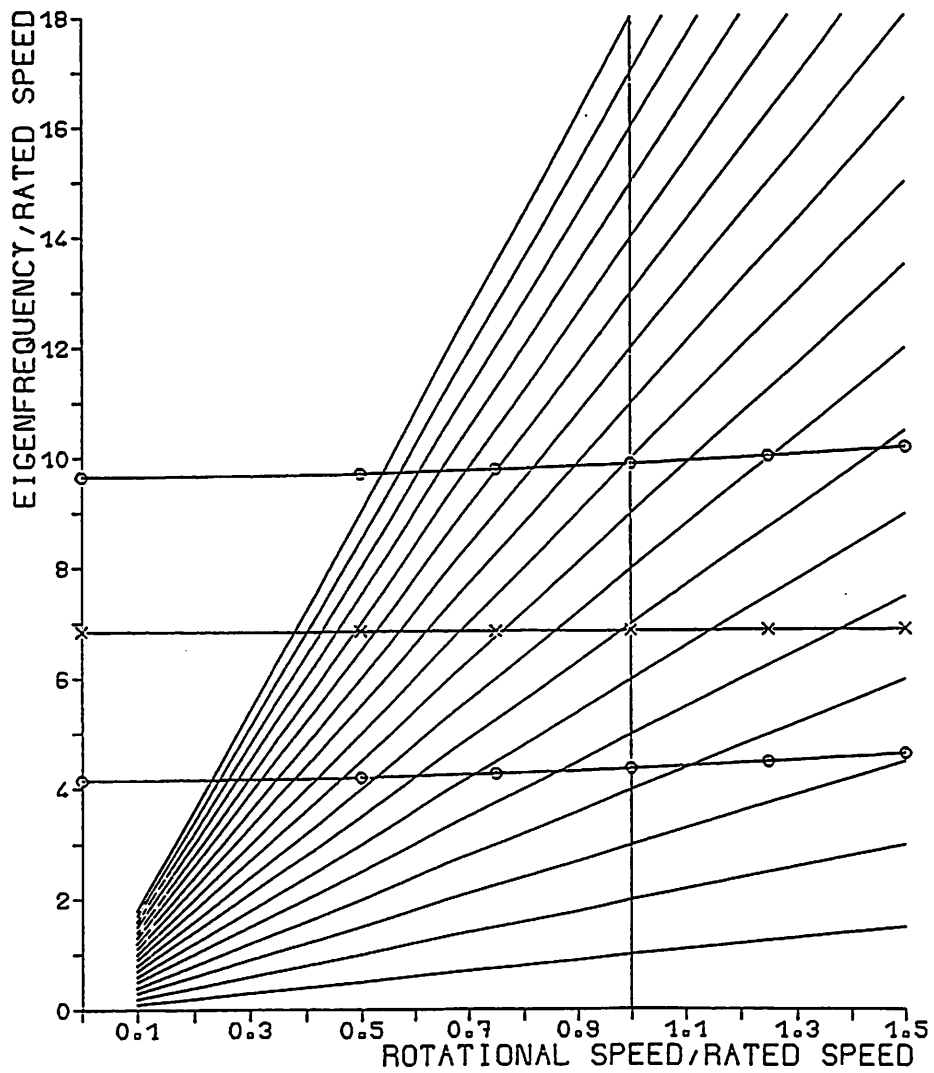
Deutsche Forschungsanstalt für Luft- und Raumfahrt e.V.

FREQUENCY OF RATED SPEED=0.3083(HZ)

○ FLAP FREQUENCY

× LAG FREQUENCY

△ TORSION FREQUENCY



Resonance diagram

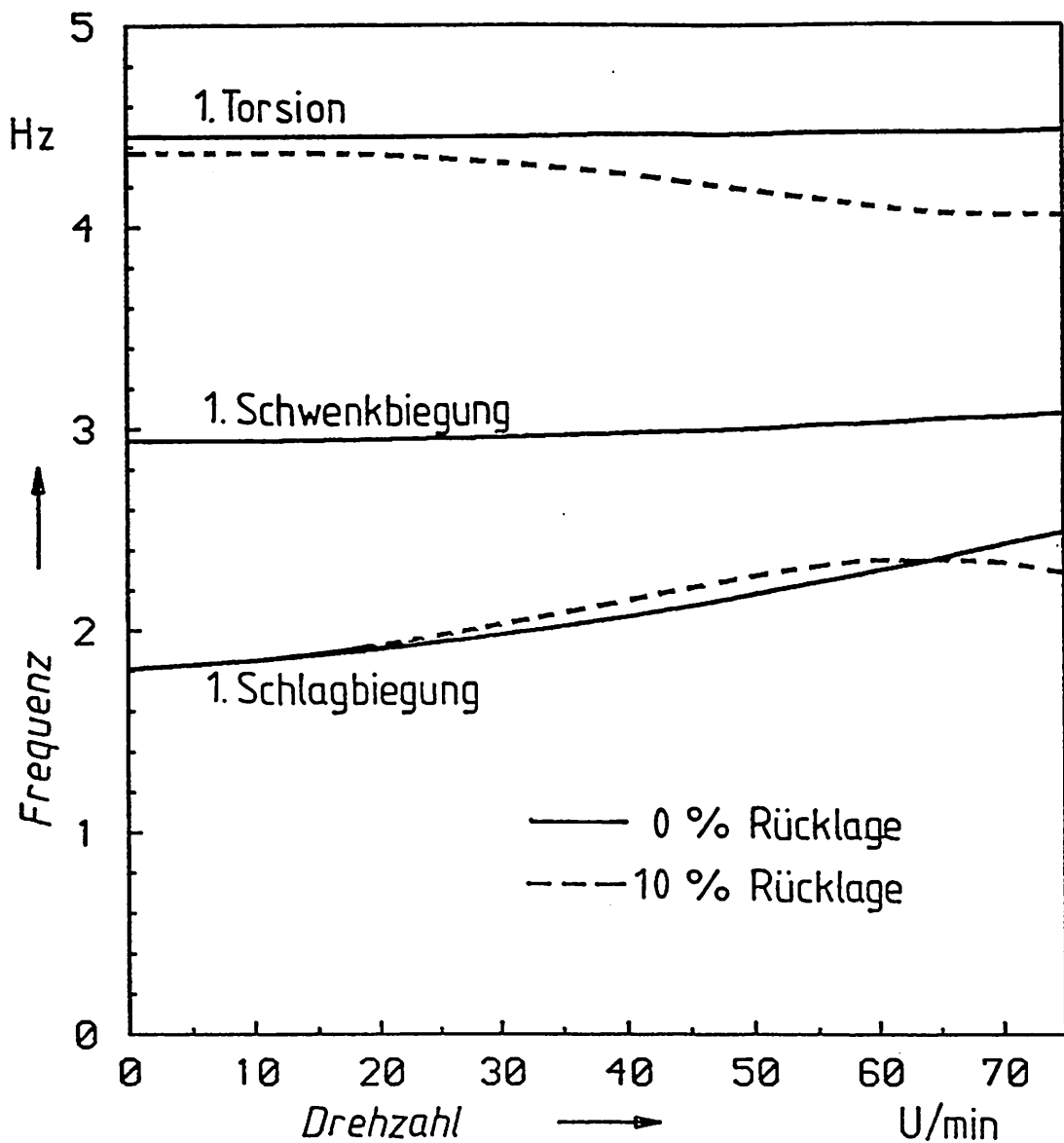


Deutsche Forschungsanstalt für Luft- und Raumfahrt e.V.

- strip theory
- unsteady airloads according KÜSSNER
- modal degrees of freedom  
(from ground vibration test or FE-calculation)
- p-k method for calculating frequency and damping  
(nonharmonic elastomechanical forces, harmonic aerodynamic forces)

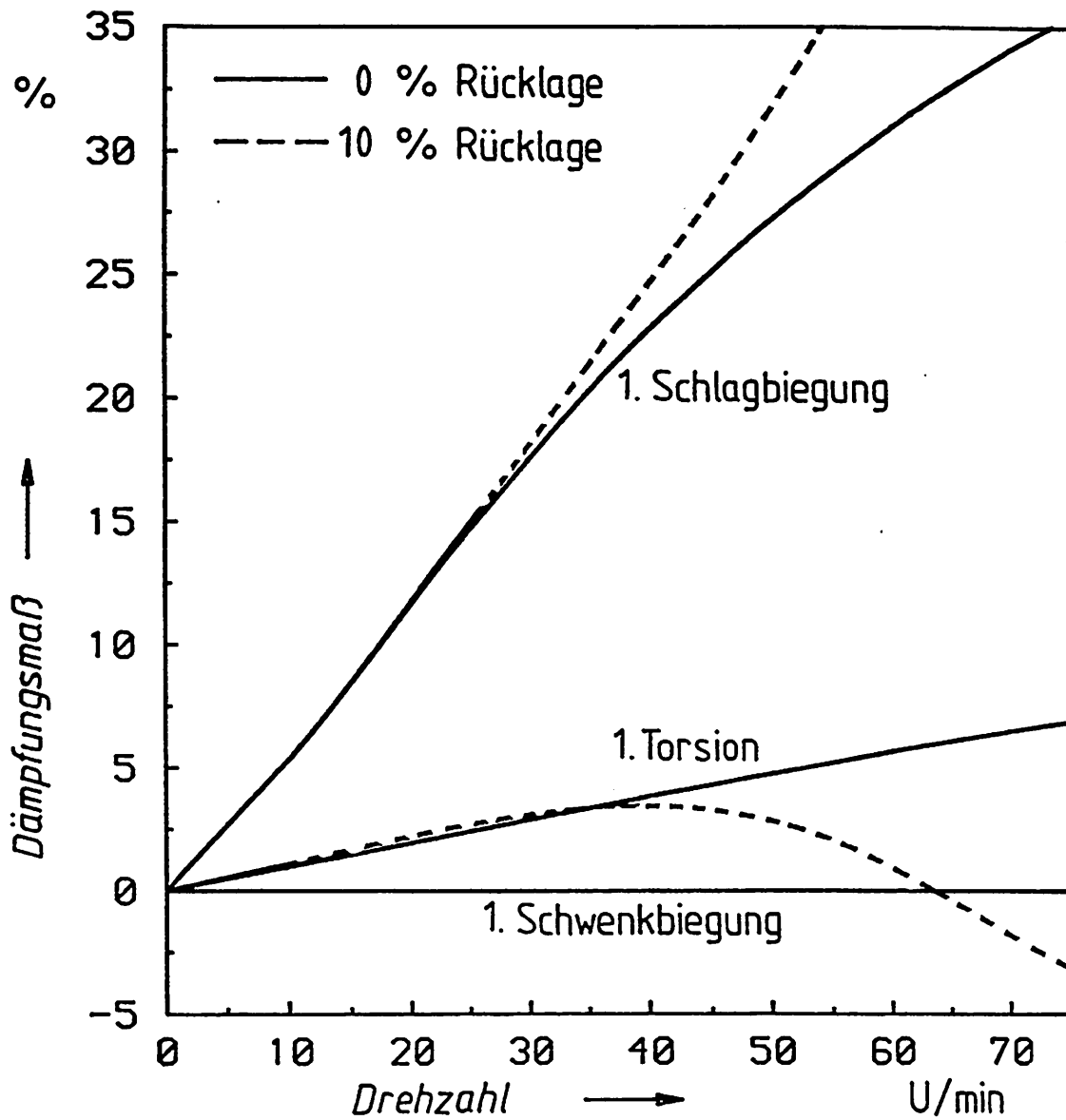
Rotorblade flutter

Deutsche Forschungsanstalt für Luft- und Raumfahrt e.V.



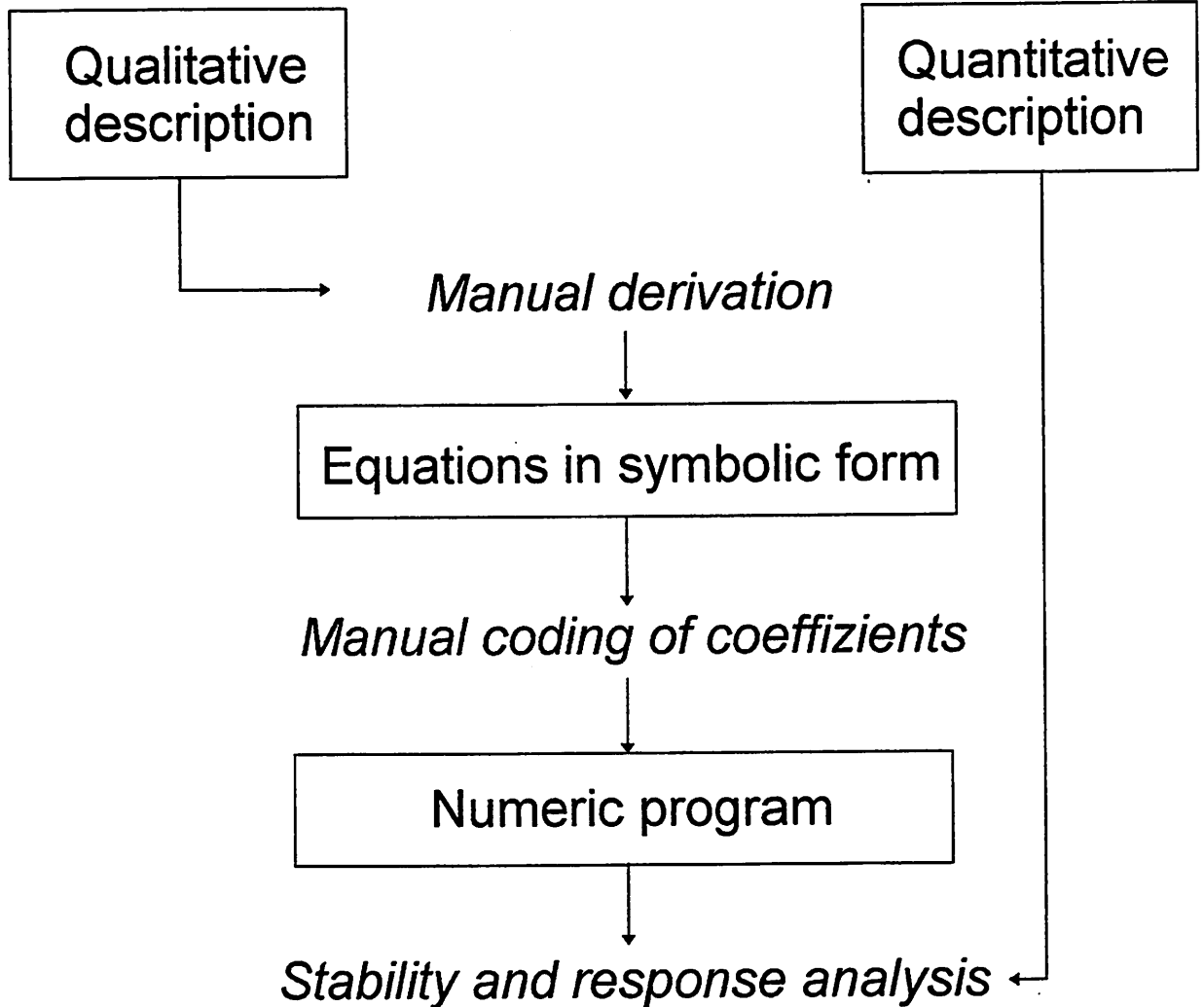
Rotorblade flutter - Frequency

Deutsche Forschungsanstalt für Luft- und Raumfahrt e.V.



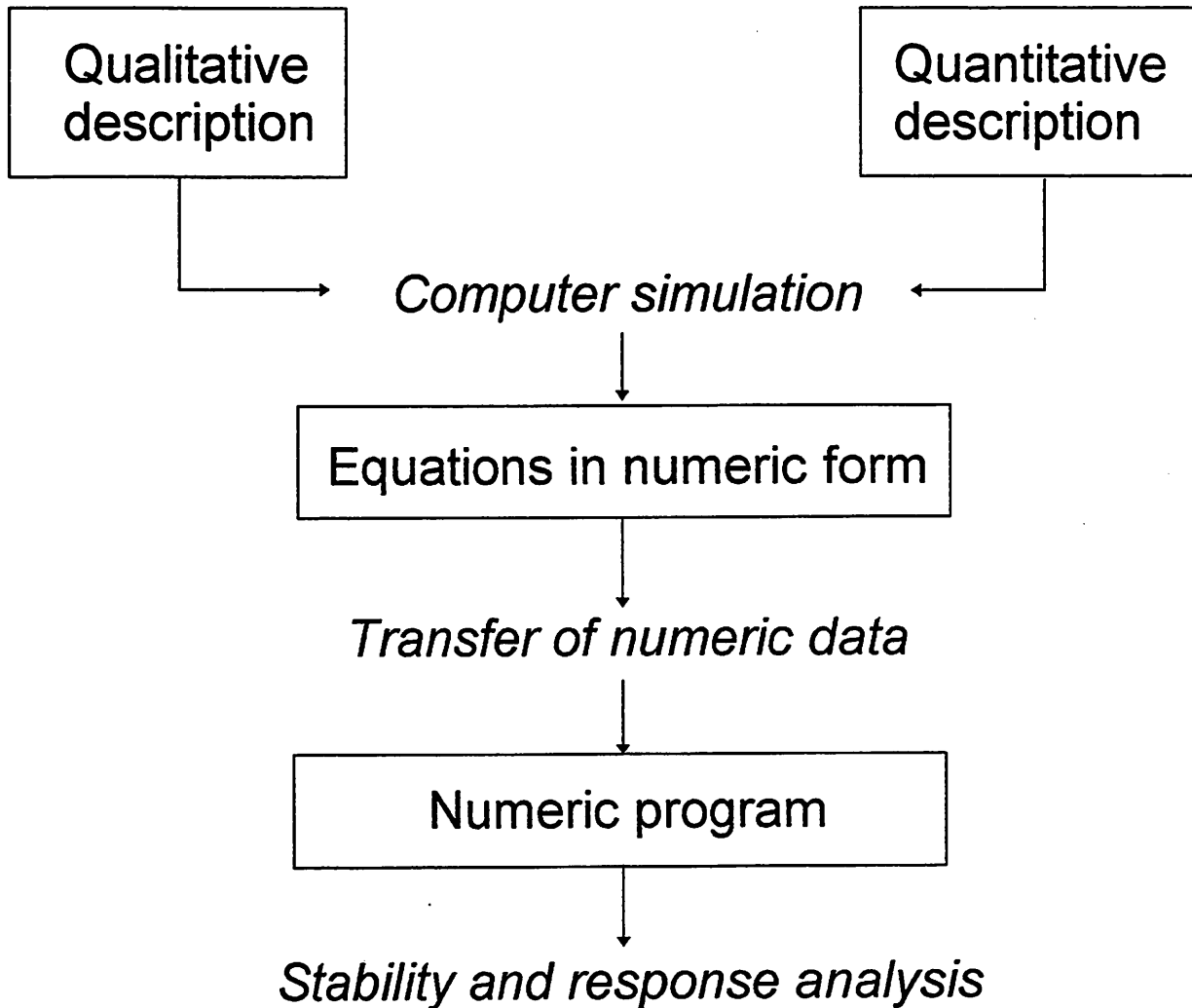
Rotorblade flutter - Damping

Deutsche Forschungsanstalt für Luft- und Raumfahrt e.V.



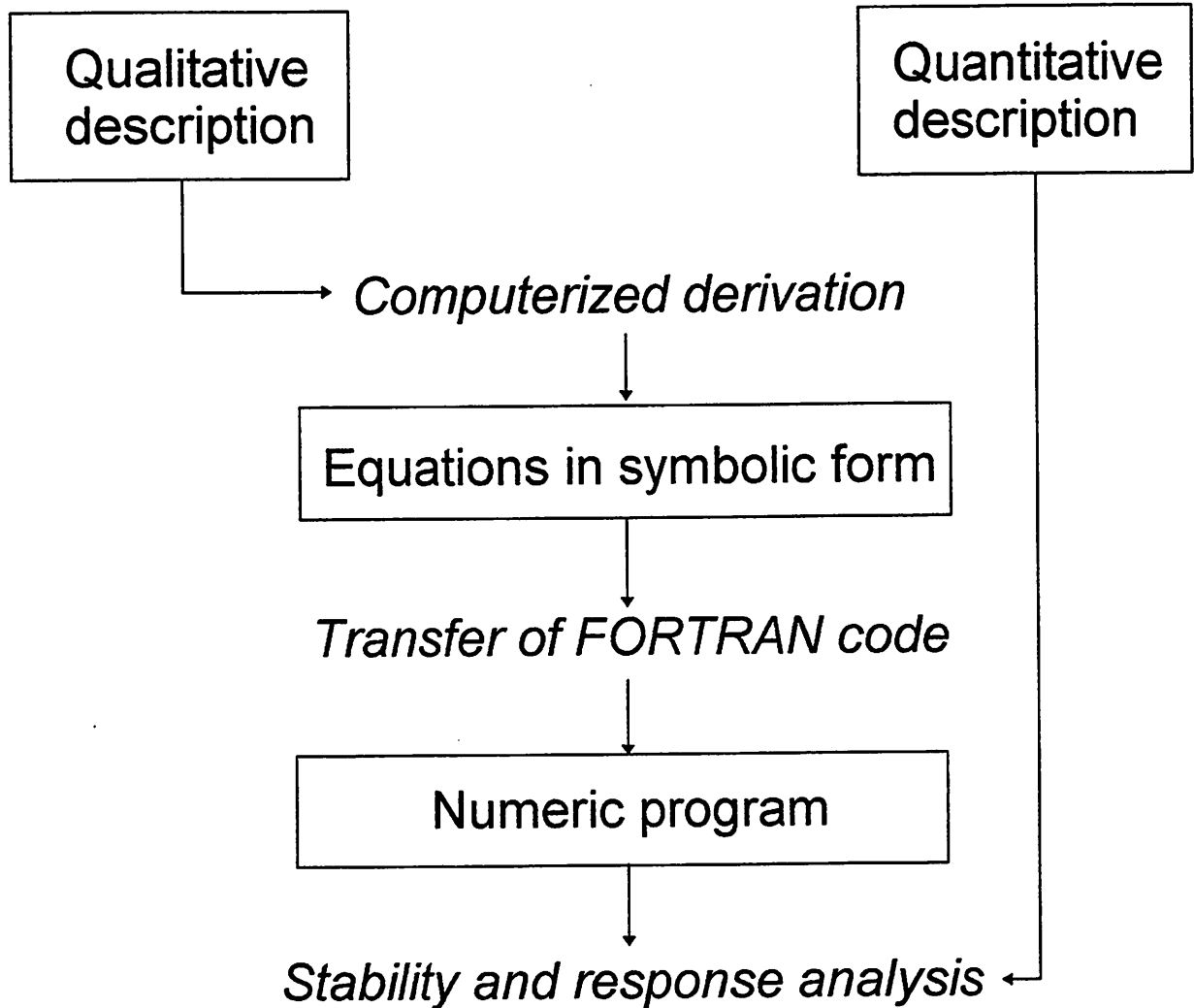
Manual/numeric procedure

Deutsche Forschungsanstalt für Luft- und Raumfahrt e.V.



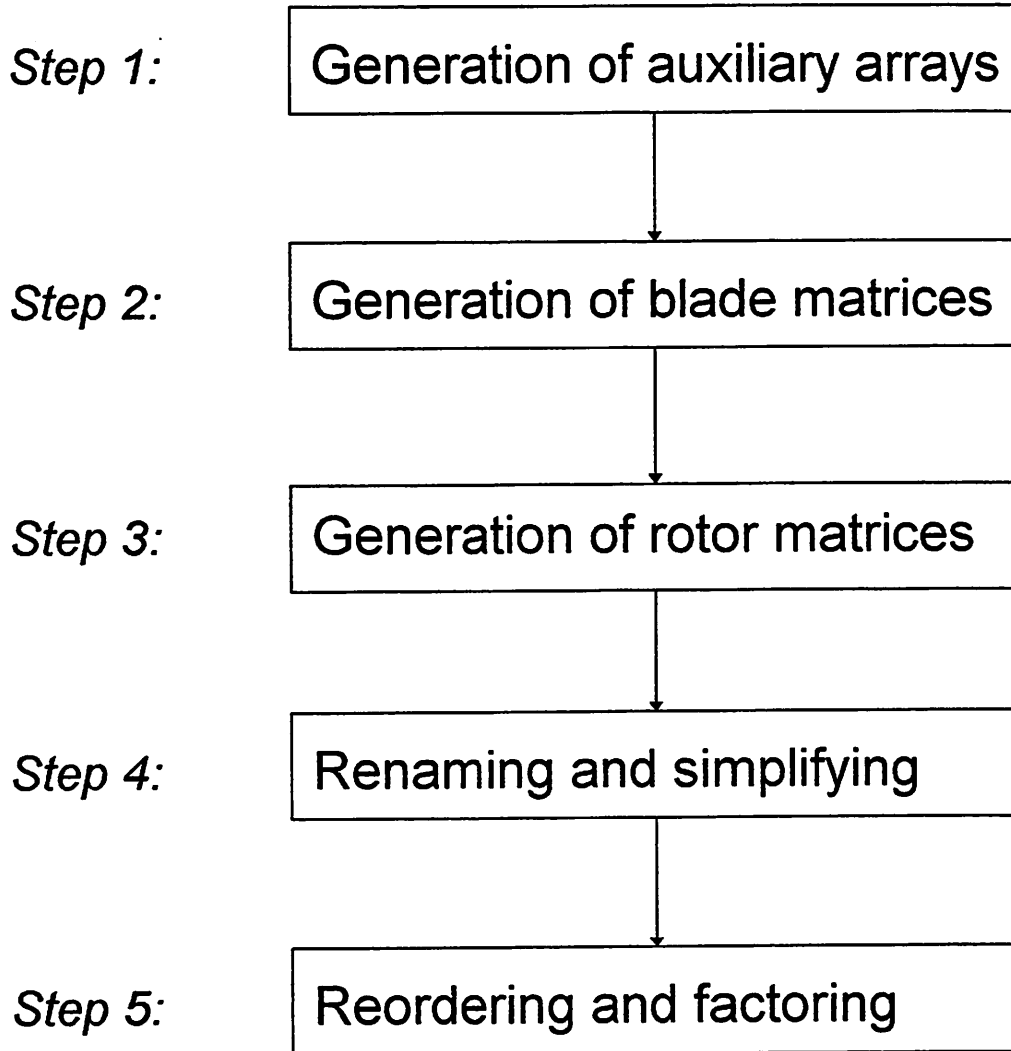
Numeric procedure

Deutsche Forschungsanstalt für Luft- und Raumfahrt e.V.



Symbolic/numeric procedure

Deutsche Forschungsanstalt für Luft- und Raumfahrt e.V.



Program structure

Deutsche Forschungsanstalt für Luft- und Raumfahrt e.V.

| File   | Step |   |   |   |   |
|--------|------|---|---|---|---|
|        | 1    | 2 | 3 | 4 | 5 |
| GLOBI  | *    | * | * | * | * |
| TIME   | *    | * | * |   |   |
| TRIGO  | *    | * |   |   |   |
| WEIGHT | *    | * |   |   |   |
| EVNOM  | *    |   |   |   |   |
| RNMOD  | *    |   |   |   |   |
| DEFMAT | *    |   |   |   |   |
| MATREX | *    |   |   |   |   |
| WIND   | *    |   |   |   |   |
| GRAVI  |      | * |   |   |   |
| AERO   |      | * |   |   |   |
| DEFINT |      | * |   |   |   |
| ROSUM  |      |   | * |   |   |
| RNSIM  |      |   |   | * |   |
| ORDER  |      |   |   |   | * |

Input files



Input (MATREX): Inertial coordinates of a generic element of mass; RN, RA, RX, RQ are (3,1) column matrices and PSN, TEN, PHN, BEK, BEA, DTK, TET are (3,3) elementary rotational transformation matrices defined in input file DEFMAT.

MATRIX RI (3,1)\$

RI := RN + PSN\*TEN\*PHN\*PHK\*BEK\*(RA + BEA\*(RX + DTK\*TET\*(RK + RQ)));

Step 1 result: elements of the Jacobian of RI evaluated at q = 0

JLRI(1,2) := 0\$ JLRI(2,2) := 1\$ JLRI(3,2) := 0\$

JLRI(2,7) := -X\*SIN(QN(1))\*BETA + Y\*COS(QN(2))\*TDEL\*SIN(QN(1))\*BETA  
+Y\*SIN(QN(2))\*TDEL\*COS(QN(1)) - Y\*SIN(QN(2))\*SIN(QN(1)) -  
Z\*SIN(QN(2))\*TDEL\*SIN(QN(1))\*BETA + Z\*COS(QN(2))\*TDEL\*COS(QN(1)) -  
Z\*COS(QN(2))\*SIN(QN(1)) - SIN(QN(1))\*ZA\$

Step 2 result: element of the blade mass matrix

BLKM(7,2) := -BETA\*TDEL\*SIN(QN(2))\*SIN(QN(1))\*IZ +  
BETA\*TDEL\*COS(QN(2))\*SIN(QN(1))\*IY - BETA\*SIN(QN(1))\*IX -  
ZA\*SIN(QN(1))\*I1 + TDEL\*SIN(QN(2))\*COS(QN(1))\*IY +  
TDEL\*COS(QN(2))\*COS(QN(1))\*IZ - SIN(QN(2))\*SIN(QN(1))\*IY -  
COS(QN(2))\*SIN(QN(1))\*IZ\$

REDUCE results

Step 3 result: element of the rotor mass matrix

```
RLKM(7,2) := 2*(TDEL*COS(QN(2))*IZ*COS(QN(1)) +  
TDEL*COS(QN(2))*IY*BETA*SIN(QN(1)) - TDEL*SIN(QN(2))*IZ*BETA*SIN(QN(1)) +  
TDEL*SIN(QN(2))*IY*COS(QN(1)) - COS(QN(2))*IZ*SIN(QN(1)) -  
SIN(QN(2))*IY*SIN(QN(1)) - ZA*I1*SIN(QN(1)) - IX*BETA*SIN(QN(1)))$
```

Step 4 result: element of the rotor mass matrix (renamed variables)

```
RLKM(7,2) := 2*CP*TDEL*CT*IZ + 2*CP*TDEL*ST*IY + 2*SP*TDEL*BETA*CT*IY -  
2*SP*TDEL*BETA*ST*IZ - 2*SP*BETA*IX - 2*SP*ZA*I1 - 2*SP*CT*IZ -  
2*SP*ST*IY$
```

Step 5 result: element of the rotor mass matrix (factored form)

```
RLKM(7,2) := 2*(CP*TDEL*(CT*IZ + ST*IY) + SP*(TDEL*BETA*(CT*IY - ST*IZ) -  
BETA*IX - ZA*I1 - CT*IZ - ST*IY))$
```

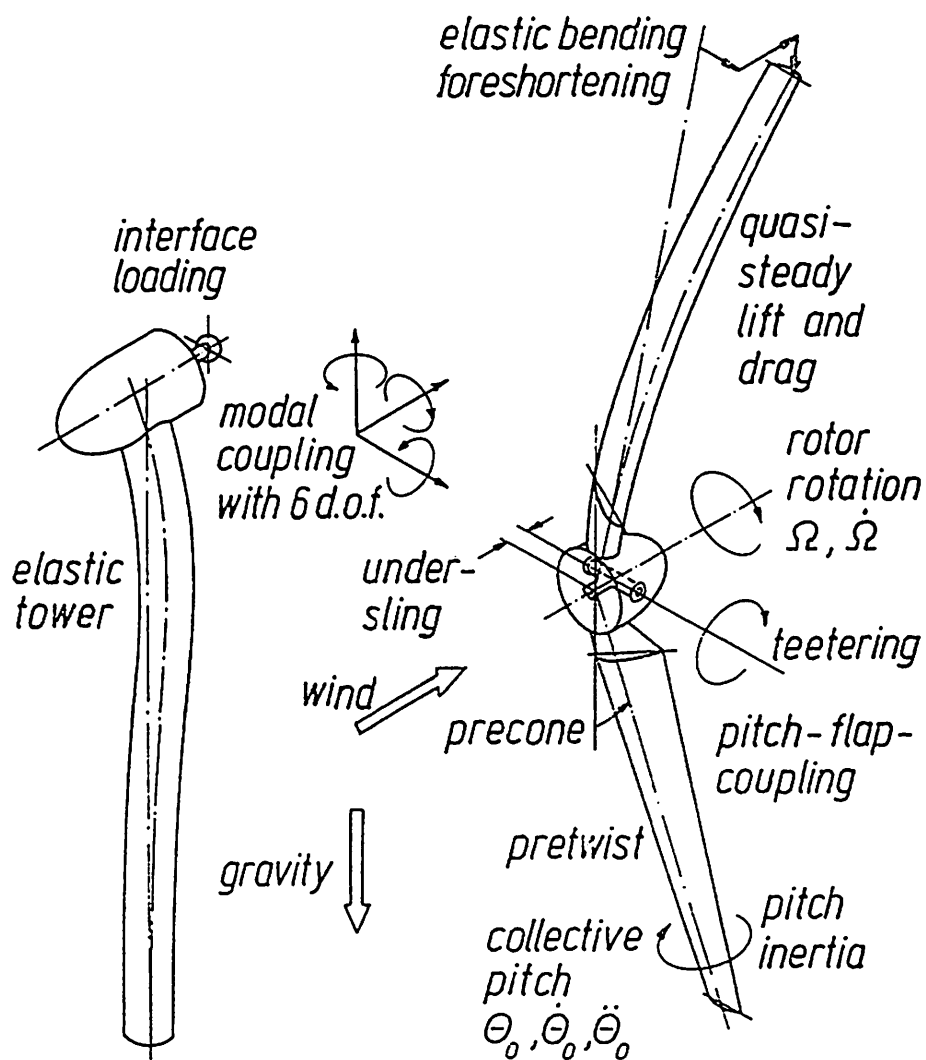
Step 5 result: element of the rotor mass matrix (FORTRAN code)

1234567

```
RLKM(7,2)=2.*(CP*TDEL*(CT*IZ+ST*IY)+SP*(TDEL*BETA*(CT*IY-  
. ST*IZ)-BETA*IX-ZA*I1-CT*IZ-ST*IY))
```

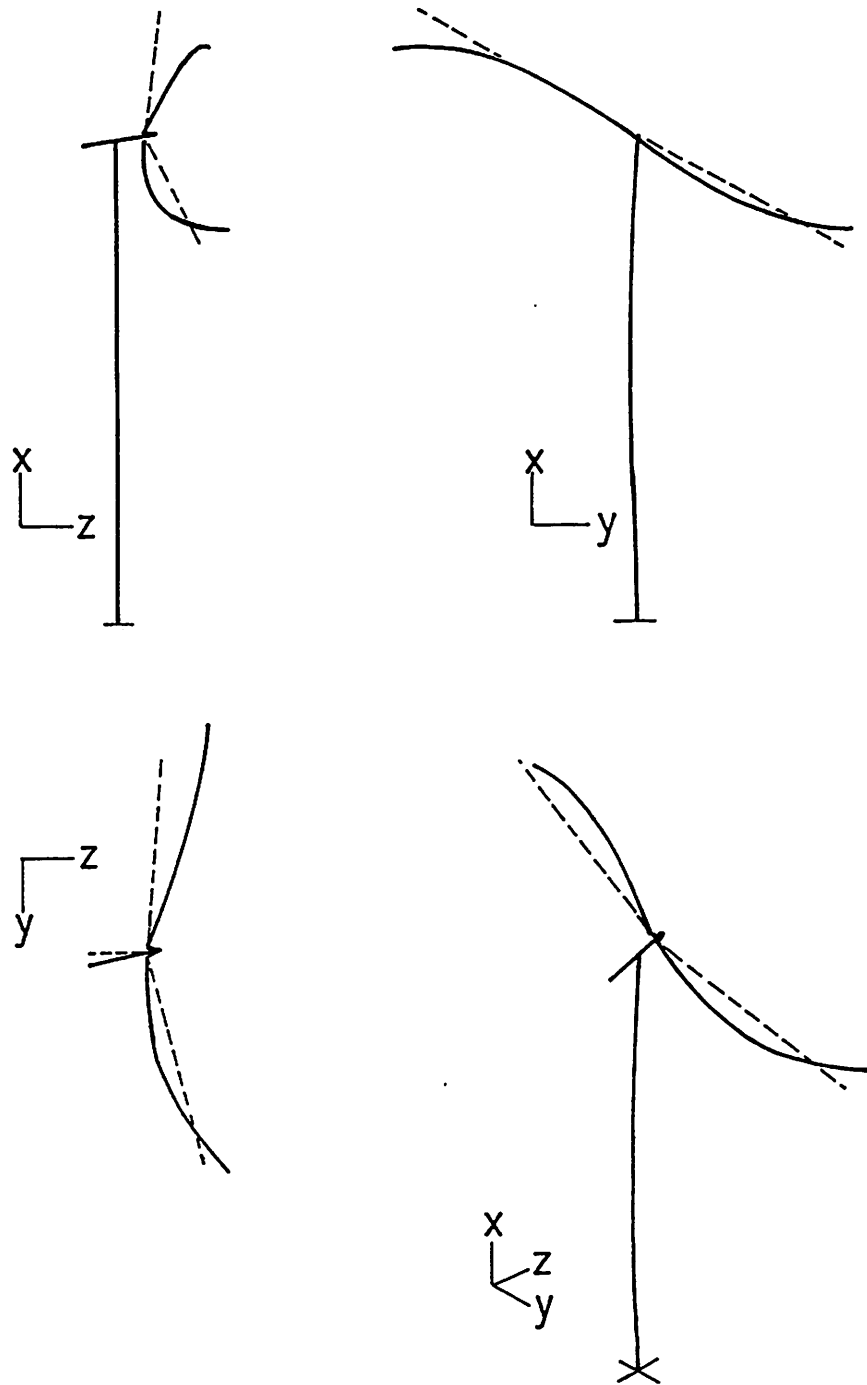
REDUCE results (cont'd)

Deutsche Forschungsanstalt für Luft- und Raumfahrt e.V.



Wind turbine model

Deutsche Forschungsanstalt für Luft- und Raumfahrt e.V.



Time step of Floquet solution

NOTES FROM ROUND-TABLE DISCUSSION.28. EXP. MEETING

Notes taken by David Sharpe.

David Quarton: Posed questions regarding the positioning of wind turbines in wind farms.- This has not been addressed. Neither has the problem of extreme loads. Safety factors used for design should be related to the quality of the design code used.

Wind modelling.

Martin Rippl: Tower shadow is not modelled well.

Vronsky: I agree.

Kuik: Unstable wind conditions should also be included in simulations.

Petersen: There is a lot of data around for many sites which is not generally available. A data base is being assembled for general use.

DQ: Turbulence models are quite well established, but how atmospheric instability can be dealt with is not clear.

Wright: Neil Kelley is working on the problem with relevance to fatigue.

DQ: The turbulence generated in wind farms is also an area which is still unclear.  
Frequency of extreme events needs to be known.

Argyriadis: For areas such as America and Europe there is a lot of data available and has been characterized. In new areas such as India the wind characteristics are not as well understood - Monsoon conditions for example.

Rippl: For the last year in Europe the winds have been unusually from the N-NE , very different wind conditions to previous years as what would have been predicted.

- DQ: Further research into probabilistic analysis for assessing loads on turbines.
- Wilson: Extreme loading cases are associated in some ? behaviour in the wind.
- DQ: Measurement of turbulence over a period may be fitted with some distribution model and extrapolated to the extremes.
- Wilson: I agree, it looks as if you can do this.
- Infield: The models are not yet good enough to do this yet.
- Ganander: Correlating all the various parameters which may accrue to result in an extreme case - phasing of gusts with changes in direction - is essential.
- ?: An emergency stop system may be triggered by freak conditions.
- DQ: Asks about use of turbulence model for predicting extreme conditions.
- Argyriadis: I'm not sure that this is a sensible approach. You cannot be sure that the extreme case will be included in your time history. Deterministic discrete gusts must be applied.
- Vronsky: Discrete gusts do not exist.
- Argyriadis: It's not the reality but probabilistic techniques are not sufficiently advanced.
- DQ: It's an area worthy of further research.
- Larsen: With a special model you can quickly predict the extreme cases without the need for long data gathering runs.
- Lindenburgh: The likelihood of predicting the 50 m/s gust from a 600 sec data run is low.

- Wright: I would wish to see more work done on the understanding of ordinary turbulence.
- Ganander: Using our codes we should try to understand how the turbines? various parameters affect the response to extreme conditions.
- Fletcher: Are my rating points correct then.
- Infield: In the extreme load cases it's the aerodynamics that are important and stall is crucial.
- Vronsky: The extreme stall? loads are still driving designs, not just running fatigue load.

### Stall

- DQ: Must we separate stall hysteresis models from static stall and 3-D effects due to radial flow, but maybe we cannot do this, they are interrelated. For power curve prediction static stall with suitable 3-D effects is adequate but for dynamic loads stall hysteresis models are crucial.
- Visser: Various manufacturers use various models.
- Infield: Heave, surge and pitch motions have different effects on hysteresis.
- Lindenburgh: Even static data shows inconsistencies between data sets.
- Argyriadis: Yes a wide range of blade load variation can be seen between the application of different aerofoil data sets. High angle of attack data is very inconsistent.
- Wilson: With a very flexible blade, measured and predicted results can be as much as  $1/2^\circ$  out.
- DQ: Continued assessment of good quality research work is needed.

- Infield: The choice between blade element and wake aerodynamic models will affect the application of dynamic stall.
- Petersen: What sort of projects should we specify to improve our understanding?
- DQ: Most people are using the Beddoes model, the problem is to tune the model to what happens on wind turbine blades.
- Infield: We need a good generic model.
- DQ: The reason for using a hysteresis model is to introduce sufficient damping to eliminate spurious instability predictions.
- Vronsky: The accuracy of predicting the loads on a flexible machine like the Carter 300 is currently poor.
- Øye: Most data sets lack reliable angle of attack data and so are of limited value. I am more pessimistic than I was a year ago.
- Infield: Some carefully designed 2-D dynamic stall work needs to be done.
- DQ: The most common sections should be concentrated upon.
- Wilson: Is the use of dynamic stall in models to introduce damping in yaw?
- DQ: No. To damp the flapping. To introduce aeroelastic damping.
- Rippl: Structural damping is ? in practice and should be left out of the calculations.
- Øye: Modern blades are so well made, that they have very little structural damping, and that is why the problem of low damping has now arisen. It is a real problem for edgewise bending.



- DQ: The topic of stall is exhausted and we have not made much progress.
- Petersen: A task force to attack the problem is required.
- DQ: Manufacturers must be included. Anybody who is interested should contact Maribo.
- Wilson: Damping itself is also worthy of study and is important. Mainly in edgewise bending modes.
- Ganander: Structural damping is not well understood.
- Kuik: A damper can be introduced if necessary, especially on the large machines.
- Wright: Do we know that flapwise damping is always present?
- Øye: Yes. Measurements have shown this. Structural damping is very temperature dependent.
- Lindenburgh: We plan some tests in which temperature will be monitored.

#### Structural Dynamics.

- Wilson: The problem is deterministic and understood. The complexity of modelling is determined by money.
- DQ: (question to Argyriadis) When these aeroelastic codes are used for certification, do you have any acceptance criteria for the codes themselves?
- Argyriadis: No. They must be validated by measurements, and they should show the influence of certain modes. We use our codes and we look for agreement, but it's not yet a very strict approach. If the power output is wrong then we have a problem. We don't insist on measurement verification as part of the certification procedure.
- DQ: What about the value of safety factors? Can they be reduced if sophisticated codes are used?

- Argyriadis: We are discussing this at the moment.
- DQ: IEC-standards are specified, and there is no provision to reduce them.
- Øye: The safety factors for fatigue calculations are fixed.

Further problems.

- Wright: More validation of codes needs to be done. Is this an issue in Europe?
- DQ: There does not seem to be any money available from the funding agencies at the moment, although the interest is there.
- Wright: It's much the same in the States.
- Infield: There seems to be no consensus on how to deal with yawed flow.
- Wilson: The concensus of the meeting is that it is a very important problem. The yawed static rotor still needs to be better understood.
- Øye: The Glauert approach of using a sinusoidal variation of inflow seems to act well.
- DQ: Beyond 20° the method seems to break down. Dynamic stall is also important for yaw stability.

**28th IEA Experts Meeting, april 11.-12. 1996, Lyngby, Denmark**

## **State of the Art of Aeroelastic Codes for Wind Turbine Calculations**

### **SUMMARY**

**prepared by**

**B.Maribo Pedersen, DTU**

---

This Experts Meeting, the purpose of which is expressed in the introductory note, had gathered 23 participants from 6 different countries. 18 of the participants gave a presentation and although countries with a sizeable wind program, i.e. Italy, Greece and Spain were not present and also not the group at the University of Stuttgart, it is felt that the meeting gave a fair impression of the contemporary state of the art world wide.

6 of the participants came from universities, 7 from national laboratories, 6 from private consultancies, 2 from industry, 1 from a national funding agency and 1 from a certifying company.

10 "complete" codes or packages of codes were presented as well as 6 codes dealing with specific sections of the problem areas.

The "complete" codes all claim to have been validated and given "good" agreement with available experimental data, although few presented evidence to that effect. Details on methods as well as information on accuracy and computing time will in most cases have to be found in the cited references.

Almost all codes solve the equations of motion in the time domain and two codes are claimed to give adequate results with a ratio of computing time to real time of only 2 when run on an up-to-date desk top PC. This seems to indicate that the main draw-back for time domain calculations as compared to calculations carried out in the frequency domain now has been eliminated.

From the written papers in these proceedings one might get the impression that almost all problems have been solved and not much remains to be done. However during the lively discussions which took place during presentations and also from the round table discussion, that impression got tempered by more realistic statements from the authors to the effect that still a number of problem areas need to be better resolved.

These problem areas could be listed as follows:

### ■ Wind Field Modelling

- Turbulence characteristics in wind farms, in mountainous terrain and for unstable atmospheric conditions.
- Extreme wind conditions, i.e. max. wind velocity, extreme rate of change of wind velocity and wind direction, extreme wind shear.

### ■ Rotor Aerodynamics

- better and validated engineering models of 3-D flows and of 3-D "static" and dynamic stall in particular is urgently needed.
- operation under yawed conditions.
- improvement to blade element theory by combination with wake modelling.

### ■ Structural Dynamics

- methods for predicting structural damping.  
With decreased aerodynamic damping when running in stalled condition, the amount of structural damping has turned out to be crucial for edgewise stability for some large machines.
- improvement of codes in order to deal with large deflections (flexible turbines).
- better information on material properties in fatigue.

### ■ Validation

- there still appears to be a need for more complete validations to be carried out. Available experimental data often do not cover the whole operational envelope for the turbine, and in particular it can be very difficult to cover extreme load cases which occur very rarely. Also validation for very flexible machines has only been carried out in a few cases.

With the number of issues as large as listed above, the need for some prioritisation arises. One attempt of putting together a structured and argued priority list was brought forward by Ian Fletcher from ETSU, (see page 169 - 171). The general opinion of the participants was however to give highest priority to a concerted attack on the dynamic stall problem.

David Quarton offered to draft a document which will specify projects most likely to ensure rapid progress towards more general and realistic modelling of this flow regime. When available the document will be circulated to all participants for comments and a final version produced. In this way a solid basis will be available for formulating applications to the relevant funding agencies, national and/or international.

For continued progress towards less conservative designs and hence in the end towards cheaper energy it is vital, that the funding agencies recognize and honour these needs for further research, and that the certification bodies will be willing to accept the results obtained by using the codes, so that current safety factors eventually will be reduced in accordance with the reduction of the uncertainty of the calculations.

**28th IEA Experts Meeting****11-12 April 1996****List of Participants**

| Name               | Address                                                                               | Phone/Fax                                                     |
|--------------------|---------------------------------------------------------------------------------------|---------------------------------------------------------------|
| Mike Anderson      | RES, Eaton Court<br>Maylands Ave<br>Hemel Hempstead<br>UK                             | (44)(0)1442 242222<br>(44)(0)1442 230024                      |
| David Infield      | CREST<br>Loughborough University<br>Loughborough, LE11 3TU<br>UK                      | 44(0)1509 222810<br>44(0)1509 222854<br>d.g.infield@lut.ac.uk |
| David Sharpe       | CREST<br>Loughborough University<br>Loughborough, LE11 3TU<br>UK                      | 44(0)1509 222420<br>d.j.sharpe@lut.ac.uk                      |
| Allan Kretz        | Risø<br>P.O.Box 49<br>DK-4000 Roskilde                                                | (+45)46775091                                                 |
| Jørgen Thirstrup   | Risø National Lab.<br>AMV-762<br>P.O.Box 49<br>DK-4000 Roskilde                       | (+45)46775057                                                 |
| George Giannakidis | Dept. of Aeronautics<br>Imperial College<br>London SW7 2BZ<br>UK                      | (+44)1715945043<br>g.giannakidis@ic.ac.uk                     |
| Bob Wilson         | ME Dept.<br>Oregon State University<br>Corvallis, OR 97333<br>USA                     | (541)737-2218                                                 |
| Alan Wright        | National Renewable<br>Energy Laboratory<br>1617 Cole Blvd.<br>Golden, CO 80401<br>USA | (303)-384-6928<br>(303)-384-6999                              |

| Name             | Address                                                                                            | Phone/Fax                          |
|------------------|----------------------------------------------------------------------------------------------------|------------------------------------|
| C. Lindenburg    | Netherlands Energy<br>Research Foundation<br>Unit Renewable Energy<br>P.O. Box 1<br>1755ZG Petten  | (31)22456 4341<br>(31)22456 3214   |
| Wouter Kuik      | Stentec<br>Hollingerstz 14<br>8621 CA, HEEG<br>Holland                                             | 031-05154-42824                    |
| Bart Visser      | Stork Product Eng.<br>P.O. Box 379<br>1000 AJ Amsterdam<br>Holland                                 | (31)020-5563444<br>(31)020-5563556 |
| Martin Rippl     | Deutsche Forschungsanstalt f.<br>Luft und Raumfahrt<br>Bunsenstr. 10<br>37073 Göttingen<br>Germany | 0551/7092354<br>0051/7092862       |
| Stig Øye         | Dept. of Energy Engineering<br>Fluid Mechanics Section<br>Bldg. 404, DTU<br>DK-2800 Lyngby         | (+45)45254311<br>(+45)45882421     |
| Gunner Larsen    | Risø<br>AMV-762<br>P.O. Box 49<br>DK-4000 Roskilde                                                 | (+45)46775056                      |
| Kimon Argyriadis | Germanischer Lloyd<br>Vorsetzen 32<br>D-20459 Hamburg                                              | (+40)36149-138<br>(+40)36149-1720  |
| Markus Rees      | Aerodyn Energiesysteme<br>Provianthausstr. 9<br>D-24768 Rendsburg                                  | +4331-12750<br>+4331-127555        |
| Hans Ganander    | Teknikgruppen AB<br>Box 21<br>S-19121 Sollentuna<br>Sweden                                         | +468359455<br>+468969987           |
| Tomas Vronsky    | Wind Energy Group<br>345 Ruislip Road<br>Southall                                                  | (+44)1815759365<br>(+44)1815758318 |

| Name               | Address                                                                                   | Phone/Fax                          |
|--------------------|-------------------------------------------------------------------------------------------|------------------------------------|
| Ian Fletcher       | B153<br>ETSU<br>Harwell<br>Oxon OX11 ORA<br>England                                       | (44)1235 433266<br>(44)1235 433355 |
| Flemming Rasmussen | Risø National Lab.<br>Test Station for Wind Turb.<br>4000 Roskilde                        | +45 46775048<br>+45 42372965       |
| Ole Fabian         | Micon A/S<br>Alsvej 21<br>8900 Randers<br>Denmark                                         | +45 89190200<br>+45 89190202       |
| David Quarton      | Garrad Hassan + Partners Ltd.<br>The Coach House<br>Folleigh Lane<br>Long Ashton, Bristol | +44 1275394360<br>+44 1275394361   |
| B. Maribo Pedersen | Dept. of Energy Engineering<br>Fluid Mech. Section<br>Building 404, DTU<br>DK-2800 Lyngby | +45 45932711<br>+45 45882421       |

**IEA R&D WIND - ANNEX XI  
TOPICAL EXPERT MEETINGS**

---

1. Seminar on Structural Dynamics, Munich, October 12, 1978
2. Control of LS-WECS and Adaptation of Wind Electricity to the Network, Copenhagen, April 4, 1979
3. Data acquisition and Analysis for LS-WECS, Blowing Rock, North Carolina, September 26 - 27, 1979
4. Rotor Blade Technology with Special Respect to Fatigue Design Problems, Stockholm, April 21 -22, 1980
5. Environmental and Safety Aspects of the Present LS WECS, Munich, September 25 - 26, 1980
6. Reliability and Maintenance Problems of LS WECS, Aalborg, April 29 - 30, 1981
7. Costings for Wind Turbines, Copenhagen, November 18 - 19, 1981
8. Safety Assurance and Quality Control of LS WECS during Assembly, Erection and Acceptance Testing , Stockholm, May 26 - 27, 1982
9. Structural Design Criteria for LS WECS, Greenford, March 7 - 8, 1983
10. Utility and Operational Experiences and Issues from Major Wind Installations, Palo Alto, October 12 - 14, 1983
11. General Environmental Aspects, Munich, May 7 - 9, 1984
12. Aerodynamic Calculational Methods for WECS, Copenhagen, October 29 - 30, 1984
13. Economic Aspects of Wind Turbines, Petten, May 30 - 31, 1985
14. Modelling of Atmospheric Turbulence for Use in WECS Rotor Loading Calculations, Stockholm, December 4 - 5, 1985
15. General Planning and Environmental Issues of LS WECS Installations, Hamburg, December 2, 1987
16. Requirements for Safety Systems for LS WECS, Rome, October 17 - 18, 1988
17. Integrating Wind Turbines into Utility Power Systems, Virginia, April 11 - 12, 1989



18. Noise Generating Mechanisms for Wind Turbines, Petten, November 27 - 28, 1989
19. Wind Turbine Control Systems, Strategy and Problems, London, May 3 - 4, 1990
20. Wind Characteristics of Relevance for Wind Turbine Design, Stockholm, March 7 - 8, 1991
21. Electrical Systems for Wind Turbines with Constant or Variable Speed, Göteborg, October 7 - 8, 1991
22. Effects of Environment on Wind Turbine Safety and Performance, Wilhelmshaven, June 16, 1992
23. Fatigue of Wind Turbines, Golden Co., October 15 - 16, 1992
24. Wind Conditions for Wind Turbine Design, Risø, April 29 - 30, 1993
25. Increased Loads in Wind Power Stations, "Wind Farms", Göteborg, May 3 - 4, 1993
26. Lightning Protection of Wind Turbine Generator Systems and EMC Problems in the Associated Control Systems, Milan, March 8 - 9, 1994
27. Current R&D Needs in Wind Energy Technology, Utrecht, Sept. 11 - 12, 1995
28. State of the Art of Aeroelastic Codes for Wind Turbine Calculations, Lyngby, Denmark, April 11 - 12, 1996